CRANFIELD UNIVERSITY

COLLEGE OF AERONAUTICS

PhD THESIS

Academic Year 1995-96

H A HINDS

THE APPLICATION OF A MODIFIED STEPWISE REGRESSION (MSR) METHOD TO THE ESTIMATION OF AIRCRAFT STABILITY AND CONTROL DERIVATIVES.

Supervisor: M V Cook

April 1996

ABSTRACT

A programme of research has now been completed in the College of Aeronautics (CoA) at Cranfield University to investigate the use of a Modified Stepwise Regression (MSR) procedure. The technique was applied to data obtained from a small BAe Hawk aircraft model flown in a dynamic wind tunnel facility in order to try to estimate the aerodynamic stability and control derivatives of the model.

A variety of preliminary experiments were performed to enable the static stability of the Hawk model to be evaluated and estimates for a limited number of aerodynamic derivatives were obtained. The initial experiments also allowed data acquisition and processing systems to be developed. Experience of flying and controlling the model in the wind tunnel was gained.

The MSR technique was implemented in the form of a FORTRAN 77 software program. Computer simulations of both the full scale Hawk aircraft and scaled wind tunnel model were written. MSR was found to produce perfect derivative estimates when using noise-free data produced by the aircraft simulations.

Various mathematical models were produced to represent the reduced order small perturbation equations of motion for the Hawk in the wind tunnel. Different methods for re-constructing the perturbation variables were implemented. Although the MSR procedure did not perform optimally with experimental data, some insight into both the MSR method and the practical difficulties associated with using a small dynamic rig has been gained.

ACKNOWLEDGEMENTS

The research which is the subject of this thesis was initiated by MOD(PE), Aerodynamics Department, Defence Research Agency, Farnborough, under the terms of Agreement 2082/192. The support and encouragement of the technical monitor, Dr. A.J. Ross is gratefully acknowledged.

There are many people to thank within the College of Aeronautics who have helped me during both the experimental and writing-up phases of my work, in particular my supervisor Mike Cook, Pete Thomasson, Sandra Fairs, and the Wind Tunnel and Workshop Technicians.

I wish to thank my work colleagues at the Royal Naval College Greenwich, EF2000 Project Office and Trilaterales Programmbüro COBRA for their encouragement and practical support during the writing-up and production of the PhD.

Finally, my family and friends deserve a special mention for their patience and encouragement, especially Jackie, Nick, Chris and Phil.

NOTICE

This thesis was published in a preliminary form as a College of Aeronautics Report, NFP9301, in January 1993. The thesis is a revised version of that report and contains substantial new work.

"The views expressed herein are those of the author alone and do not necessarily represent those of the Institute."

CONTENTS

FIGURES

NOTATION

b	wing span [m]
$b_0,\ldots,b_{n-1}$	stability and control derivatives
$\bar{c}$	wing mean aerodynamic chord [m]
C_l	rolling moment coefficient, $M_X/\bar{q}Sb$
C_m	pitching moment coefficient, $M_Y/\bar{q}S\bar{c}$
C_n	yawing moment coefficient, $M_Z/\bar{q}Sb$
C_X	longitudinal force (ie. drag) coefficient, $F_X/\bar{q}S$
C_Y	lateral force (ie. sideforce) coefficient, $F_Y/\bar{q}S$
C_Z	vertical force (ie. lift) coefficient, $F_Z/\bar{q}S$
$E\{\ \}$	expectation operator
F	F-statistic
F_p	F-statistic used in partial F-test
F_X, F_Y, F_Z	forces along longitudinal, lateral and vertical body axes respectively [N]
g	acceleration due to gravity [ms^{-2}]
H_0, H_1	null and alternative hypotheses respectively
I_x, I_y, I_z	moment of inertia about longitudinal, lateral and vertical body axes, respectively [$kg\text{-}m^2$]
I_{xz}	product of inertia [$kg\text{-}m^2$]
$\bar{l}_T$	horizontal tail arm [m]
$\mathring{L}_v,\mathring{L}_p,\mathring{L}_r,\mathring{L}_\xi,\mathring{L}_\zeta$	dimensional rolling moment derivative due to sideslip, roll rate, yaw rate, aileron and rudder respectively
m	aircraft mass [kg]
M	mach no.
$\mathring{M}_u,\mathring{M}_w,\mathring{M}_{\dot{w}},\mathring{M}_q,\mathring{M}_\eta$	dimensional pitching moment derivative due to forward velocity, vertical velocity, vertical

	acceleration, pitch rate and elevator respectively
M_X, M_Y, M_Z	rolling, pitching and yawing moments respectively [Nm]
n	number of unknown parameters
N	number of data points or number of observation times
$\mathring{N}_v, \mathring{N}_p, \mathring{N}_r, \mathring{N}_\xi, \mathring{N}_\zeta$	dimensional yawing moment derivative due to sideslip, roll rate, yaw rate, aileron and rudder respectively
p	roll rate [rad/s or deg/s]
q	pitch rate [rad/s or deg/s]
$\bar{q}$	kinematic pressure, $0.5\rho V^2$ [Pa]
r	yaw rate [rad/s or deg/s]
r_{jy}	partial correlation coefficient
$r_{jy.1}$	partial correlation coefficient after variable x_1 has been included in the model
R^2	squared multiple correlation coefficient
s	standard error
s^2	estimated residual variance
s_{jy}, s_{jj}, s_{yy}	sum of squares
S	wing area [m^2]
t	time [s]
T	temperature [°C]
U_e	steady component of aircraft velocity along the longitudinal body axis O_z [m/s]
u, v, w	components of velocity [m/s]
u_θ	x-axis velocity component due to pitch response [m/s]
V	total velocity (ie. airspeed) [m/s]

V_e	wind tunnel velocity [m/s]
$\underline{V}_\beta$	covariance matrix of $\underline{\mu}_\beta$
Var{ }	variance operator
w_θ	z-axis velocity component due to pitch response [m/s]
W_e	steady component of aircraft velocity along the vertical body axis O_x [m/s]
$x_1, x_2, \ldots x_{n-1}$	independent variables in the regression equation
$\bar{x}$	mean of an independent variable x
$\mathring{X}_u, \mathring{X}_w, \mathring{X}_{\dot{w}}, \mathring{X}_q, \mathring{X}_\eta$	dimensional axial force derivatives due to forward velocity, vertical velocity, vertical acceleration, pitch rate and elevator respectively.
$\underline{X}$	N x n matrix of independent variables
y	dependent variable in regression equation
y(t)	resultant coefficient of aerodynamic force or moment dependent variable in regression equation
y^*	dependent variable used in intermediate step of stepwise regression
$\bar{y}$	mean of dependent variable
$\mathring{Y}_v, \mathring{Y}_p, \mathring{Y}_r, \mathring{Y}_\xi, \mathring{Y}_\zeta$	dimensional sideforce derivative due to sideslip, roll rate, yaw rate, aileron and rudder respectively
Y	N x 1 matrix of dependent variables
z	independent variable used in intermediate step of stepwise regression
$\mathring{Z}_u, \mathring{Z}_w, \mathring{Z}_{\dot{w}}, \mathring{Z}_q, \mathring{Z}_\eta$	dimensional normal force derivatives due to forward velocity, vertical velocity, vertical acceleration, pitch rate and elevator respectively.

α	angle of attack, $\tan^{-1}(w/u)$ [rad or deg]
α_e	trimmed aircraft angle of attack [rad or deg]
α_f	inclination of fuselage datum to air stream [rad or deg]
α_p	confidence level with F-statistic
β	angle of sideslip, $\sin^{-1}(v/V)$ [rad or deg]
$\beta_0, \ldots, \beta_{n-1}$	estimates of stability and control derivatives
$\underline{\beta}$	parameter vector
γ	angle between direction of flight and horizontal reference (equal to 0 in the wind tunnel)
$\varepsilon(i)$	equation error at time t_i (measurement noise)
ζ	rudder control surface deflection [rad or deg]
η	elevator control surface deflection [rad or deg] rudder respectively [rad or deg]
θ	pitch attitude angle [rad or deg]
Θ_e	angle between trimmed aircraft axes and horizontal reference ($= \gamma + \alpha_e$) [rad or deg]
μ	mean value of a variable
$\underline{\mu}_\beta$	parameter vector known from prior information
ν_1, ν_2	degrees of freedom for numerator and denominator of F-statistic, respectively
ρ	air density [kg/m^3]
σ	standard deviation
σ^2	variance (of measurement noise)
ξ	aileron control surface deflection [rad or deg]
ϕ	roll attitude angle [rad or deg]
ψ	yaw attitude angle [rad or deg]
Ψ	covariance matrix of the observation errors

Longitudinal Mass Matrices and Derivatives:

$$M = \begin{pmatrix} 1 & -\mathring{X}_{\dot{w}} & 0 & 0 \\ 0 & (1-\mathring{Z}_{\dot{w}}) & 0 & 0 \\ 0 & -\mathring{M}_{\dot{w}} & 1 & 0 \\ 0 & 0 & 0 & 1 \end{pmatrix} ; \qquad M^{-1} = \begin{pmatrix} 1 & \mathring{X}_{\dot{w}}/(1-\mathring{Z}_{\dot{w}}) & 0 & 0 \\ 0 & 1/(1-\mathring{Z}_{\dot{w}}) & 0 & 0 \\ 0 & \mathring{M}_{\dot{w}}/(1-\mathring{Z}_{\dot{w}}) & 1 & 0 \\ 0 & 0 & 1 & 0 \end{pmatrix} ;$$

where:

$$\mathring{x}_u = \mathring{X}_u/m ; \quad \mathring{x}_{\dot{w}} = \mathring{X}_{\dot{w}}/m ; \quad \mathring{x}_w = \mathring{X}_w/m ; \quad \mathring{x}_q = \mathring{X}_q/m ; \quad \mathring{x}_\eta = \mathring{X}_\eta/m.$$

$$\mathring{z}_u = \mathring{Z}_u/m ; \quad \mathring{z}_{\dot{w}} = \mathring{Z}_{\dot{w}}/m ; \quad \mathring{z}_w = \mathring{Z}_w/m ; \quad \mathring{z}_q = \mathring{Z}_q/m ; \quad \mathring{z}_\eta = \mathring{Z}_\eta/m.$$

$$\mathring{m}_u = \mathring{M}_u/I_y ; \quad \mathring{m}_{\dot{w}} = \mathring{M}_{\dot{w}}/I_y ; \quad \mathring{m}_w = \mathring{M}_w/I_y ; \quad \mathring{m}_q = \mathring{M}_q/I_y ; \quad \mathring{m}_\eta = \mathring{M}_\eta/I_y .$$

$$X_u = \left(\frac{\mathring{x}_{\dot{w}} \mathring{z}_u}{(1-\mathring{z}_{\dot{w}})} + \mathring{x}_u \right) ; \qquad X_w = \left(\frac{\mathring{x}_{\dot{w}} \mathring{z}_w}{(1-\mathring{z}_{\dot{w}})} + \mathring{x}_w \right) ; \qquad X_q = \left(\frac{(U_e + \mathring{z}_q)\mathring{x}_{\dot{w}}}{(1-\mathring{z}_{\dot{w}})} + (\mathring{x}_q - W_e) \right) ;$$

$$Z_u = \left(\frac{\mathring{z}_u}{1-\mathring{z}_{\dot{w}}} \right) ; \qquad Z_w = \left(\frac{\mathring{z}_w}{1-\mathring{z}_{\dot{w}}} \right) ; \qquad Z_q = \left(\frac{U_e + \mathring{z}_q}{1-\mathring{z}_{\dot{w}}} \right) ;$$

$$m_u = \left(\frac{\mathring{m}_{\dot{w}} \mathring{z}_u}{(1-\mathring{z}_{\dot{w}})} + \mathring{m}_u \right) ; \qquad m_w = \left(\frac{\mathring{m}_{\dot{w}} \mathring{z}_w}{(1-\mathring{z}_{\dot{w}})} + \mathring{m}_w \right) ; \qquad m_q = \left(\frac{(U_e + \mathring{z}_q)\mathring{m}_{\dot{w}}}{(1-\mathring{z}_{\dot{w}})} + \mathring{m}_q \right) ;$$

$$x_\eta = \left(\frac{\mathring{x}_{\dot{w}} \mathring{z}_\eta}{(1-\mathring{z}_{\dot{w}})} + \mathring{x}_\eta \right) ; \qquad z_\eta = \left(\frac{\mathring{z}_\eta}{1-\mathring{z}_{\dot{w}}} \right) ; \qquad m_\eta = \left(\frac{\mathring{m}_{\dot{w}} \mathring{z}_\eta}{(1-\mathring{z}_{\dot{w}})} + \mathring{m}_\eta \right)$$

Lateral Mass Matrices and Derivatives:

$$M = \begin{pmatrix} 1 & 0 & 0 & 0 & 0 \\ 0 & 1 & -e_x & 0 & 0 \\ 0 & e_z & 1 & 0 & 0 \\ 0 & 0 & 0 & 1 & 0 \\ 0 & 0 & 0 & 0 & 1 \end{pmatrix}; \qquad M^{-1} = \begin{pmatrix} 1 & 0 & 0 & 0 & 0 \\ 0 & 1/E_{xz} & e_x/E_{xz} & 0 & 0 \\ 0 & -e_z/E_{xz} & 1/E_{xz} & 0 & 0 \\ 0 & 0 & 0 & 1 & 0 \\ 0 & 0 & 0 & 0 & 1 \end{pmatrix};$$

where:

$$e_x = I_{xz}/I_x \; ; \qquad e_z = I_{xz}/I_z \; ; \qquad E_{xz} = 1 + e_x e_z$$

$$\mathring{y}_v = \mathring{Y}_v/m \; ; \quad \mathring{y}_p = \mathring{Y}_p/m \; ; \quad \mathring{y}_r = \mathring{Y}_r/m \; ; \quad \mathring{y}_\xi = \mathring{Y}_\xi/m \; ; \quad \mathring{y}_\zeta = \mathring{Y}_\zeta/m.$$

$$\mathring{l}_v = \mathring{L}_v/I_x; \quad \mathring{l}_p = \mathring{L}_p/I_x; \quad \mathring{l}_r = \mathring{L}_r/I_x; \quad \mathring{l}_\xi = \mathring{L}_\xi/I_x; \quad \mathring{l}_\zeta = \mathring{L}_\zeta/I_x.$$

$$\mathring{n}_v = \mathring{N}_v/I_z; \quad \mathring{n}_p = \mathring{N}_p/I_z; \quad \mathring{n}_r = \mathring{N}_r/I_z; \quad \mathring{n}_\xi = \mathring{N}_\xi/I_z; \quad \mathring{n}_\zeta = \mathring{N}_\zeta/I_z.$$

$$y_v = \mathring{y}_v \; ; \qquad y_p = (\mathring{y}_p + W_e) \; ; \qquad y_r = (\mathring{y}_r - U_e);$$

$$l_v = \left\{ \frac{\mathring{l}_v}{E_{xz}} + \frac{e_x \mathring{n}_v}{E_{xz}} \right\} ; \qquad l_p = \left\{ \frac{\mathring{l}_p}{E_{xz}} + \frac{e_x \mathring{l}_p}{E_{xz}} \right\} ; \qquad l_r = \left\{ \frac{\mathring{l}_r}{E_{xz}} + \frac{e_x \mathring{l}_r}{E_{xz}} \right\};$$

$$n_v = \left\{ \frac{-e_z \mathring{l}_v}{E_{xz}} + \frac{\mathring{n}_v}{E_{xz}} \right\} ; \qquad n_p = \left\{ \frac{-e_z \mathring{l}_p}{E_{xz}} + \frac{\mathring{n}_p}{E_{xz}} \right\} ; \qquad n_r = \left\{ \frac{-e_z \mathring{l}_r}{E_{xz}} + \frac{\mathring{n}_r}{E_{xz}} \right\};$$

$$y_\xi = \mathring{y}_\xi \; ; \qquad l_\xi = \left\{ \frac{\mathring{l}_\xi}{E_{xz}} + \frac{e_x \mathring{n}_\xi}{E_{xz}} \right\} ; \qquad l_\zeta = \left\{ \frac{\mathring{l}_\zeta}{E_{xz}} + \frac{e_x \mathring{n}_\zeta}{E_{xz}} \right\}$$

$$y_\zeta = \mathring{y}_\zeta \; ; \qquad n_z = \left\{ \frac{-e_z \mathring{l}_\xi}{E_{xz}} + \frac{\mathring{n}_\xi}{E_{xz}} \right\} ; \qquad n_\zeta = \left\{ \frac{-e_z \mathring{l}_\zeta}{E_{xz}} + \frac{\mathring{n}_\zeta}{E_{xz}} \right\}$$

CHAPTER 1

INTRODUCTION

1.0 INTRODUCTION.

Parameter Identification (PID) is the computational process by which the coefficients in a mathematical description of a dynamic system may be estimated from recorded input-output response data. Advanced statistical methods for system identification have been applied to many multiple-input, multiple-output systems. In the case of aircraft PID typical inputs are the control surface angles and typical outputs are the responses in terms of speed, attitude angles and rates. In recent years parameter estimation methods have found extensive use in aircraft applications since it is often difficult to obtain estimates for aerodynamic stability and control (S&C) derivatives by traditional methods with any degree of confidence. Most of the estimation methods make considerable use of statistical techniques and therefore have a degree of uncertainty associated with the results. Thus in order to develop confidence in the methods it is desirable to have as much visibility of the computational process as possible. Clearly this is not always easy to achieve when a complex method is applied to a complex aircraft model.

It is now standard practice to estimate aircraft stability and control derivatives in flight conditions where aerodynamic characteristics can be described in linear terms only and where no significant external disturbances are present. However, interest in high angle of attack, post stall and spin flight conditions has created a need to extend parameter estimation into flight areas where non-linear aerodynamic effects become more pronounced.

Accurate mathematical models of aircraft and flight control

systems are essential to minimize the risks associated with flight control system development. For example, the digital flight control system (FCS) for EF2000 has, in part, been designed using aerodynamic S&C data estimated from wind tunnel experiments. Unlike the Tornado, EF2000 is naturally unstable with no mechanical backup systems and the safety critical FCS was therefore required to function correctly from the very first flight. During the developmental flight test programme, PID techniques are used to confirm, and where necessary correct, the wind tunnel estimates of the S&C data sets. This then enables further development of the aircraft to go ahead, for example in high alpha flight or care free handling, with an increased confidence in the definition of the characteristics of the aircraft.

One of the more recent advances in parameter estimation is the use of the Modified Stepwise Regression (MSR) method. The method was pioneered in the U.S.A. at the NASA Langley Research Center by Klein, Batterson and Murphy (Ref 1). Linear stepwise regression is a technique employed to estimate a functional relationship of a dependent variable to one or more independent variables. It is assumed that the dependent variables can be closely approximated as a linear combination of the independent variables. MSR is based on an ordinary stepwise regression which has been modified by adding a constraint to the parameter selection for the model structure determination. Using only the recorded data as input, the MSR is constructed to force a linear model for the aerodynamic coefficients in the first instance. It then adds significant non-linear terms and deletes insignificant terms from the mathematical model in an iterative process which continues until the best fit of the model output to recorded data is obtained.

An advantage of the MSR method is its relative simplicity in that explicit statistical descriptions of the noise associated with the measured data are not generally required. The method continues to be developed and has been successfully applied to many free flight aircraft and aircraft models.

The MSR method most readily lends itself to aircraft applications where the motion described may result in a non-linear mathematical model. The complexity of such an application arises from the additional non-linear terms in the equations of motion and this introduces the problem of determining how complex the model should be. Although a more complex model can be justified for proper description of aircraft motion the most appropriate relationship between model complexity and measurement information has not always been clear in the past. If too many parameters are sought from an estimate made on the basis of a limited number of data points, a reduced accuracy in evaluated parameters can be expected due to large covariance or unrealistic values of some parameters. Alternatively, attempts to identify all parameters might cause the process to fail altogether. The question which naturally arises is then: "How far can the MSR method be stretched to cope with incomplete model descriptions and a limited number of response variable measurements?". This is the main subject of this research thesis.

1.1 MSR programme and sponsor.

The Defence Research Agency at Farnborough, DRA(F), has supported previous research work on PID at Cranfield University using the dynamic

wind tunnel experimental facility in the College of Aeronautics (CoA). Thus interest in the area of aircraft model complexity resulted in the proposal and setting up of a new programme of research at Cranfield, sponsored by DRA(F), (Ref 2).

Previous aeronautical applications of the MSR method have concentrated on the accurate identification of complex mathematical model structures of aircraft with six degrees of freedom. In such applications the computational complexities of the method can be overshadowed by the complexities of the aircraft model under investigation.

At Cranfield the MSR method was applied to response data obtained from a small aircraft model mounted in a support system which facilitates dynamic wind tunnel testing, see Figure 1 overleaf. The aircraft chosen for this work was the British Aerospace (BAe) Hawk. The Hawk model has four degrees of freedom and only a limited number of the response variables can be measured directly. It was hoped to confirm that the MSR method works equally as well with a simple aircraft model as when it is applied to a more complex model or full scale aircraft. The use of a simple aircraft model was also expected to enhance computational visibility whilst allowing scope for investigating methods of coping with limited data.

In order to control the model in a manner appropriate to the facility it was sometimes found necessary to introduce feedback loops for automatic control; the consequent increase in model complexity provides some additional interest in an area directly related to the problem of applying parameter estimation methods to modern aircraft.

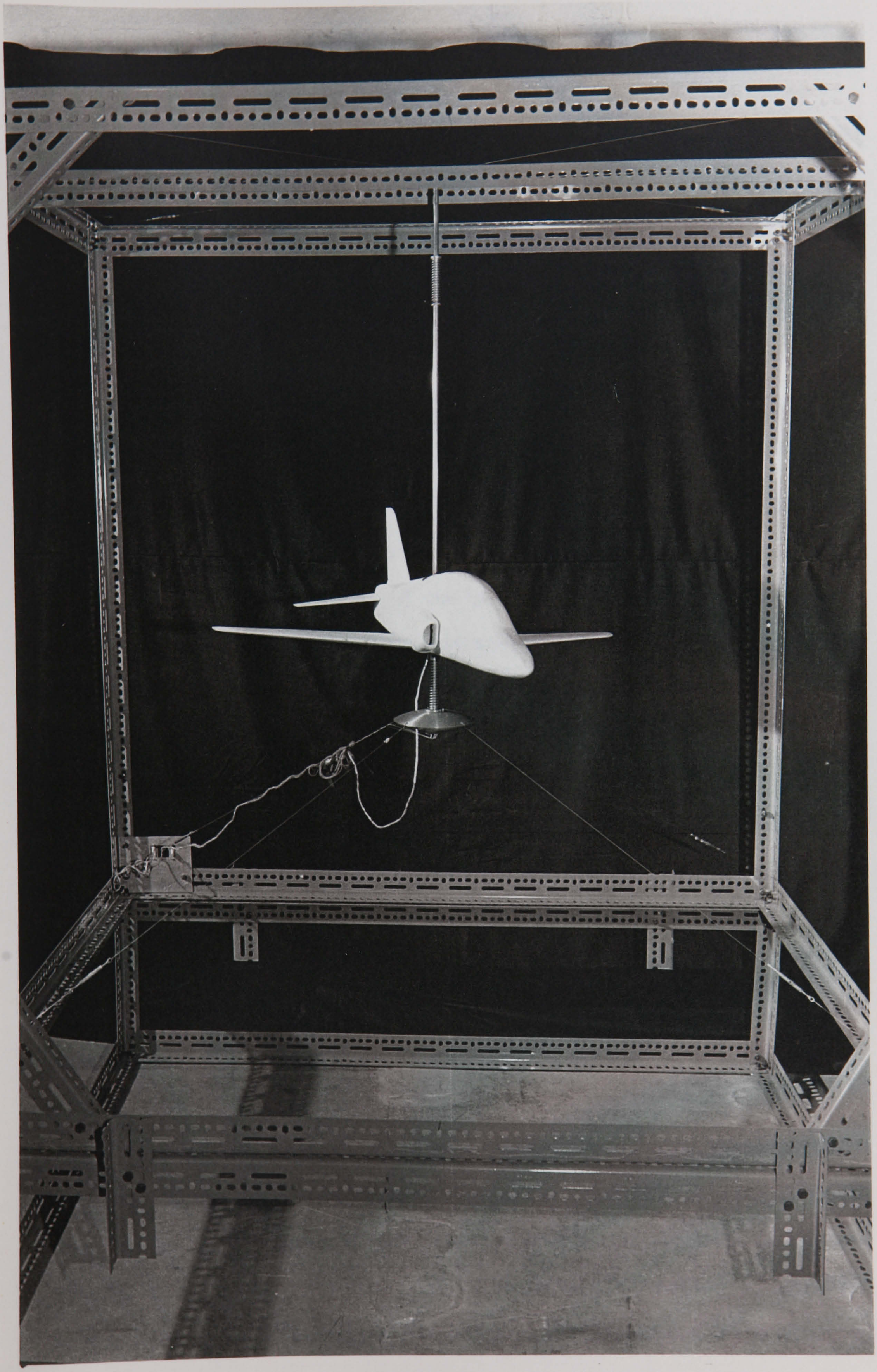

FIGURE 1: DYNAMIC AIRCRAFT MODEL AND SUSPENSION SYSTEM

1.2 Structure of the thesis.

A literature survey was carried out initially to investigate current aircraft parameter estimation techniques and in particular to establish a database of previous MSR research programmes and their results. A brief review of parameter estimation methods is therefore presented in the following chapter.

The various components of the small scale wind tunnel experimental facility in the College of Aeronautics are described. Design parameters for both the full scale Hawk and the 1/12th scale model are defined and S&C derivatives estimated for particular flight conditions. Small perturbation equations of motion for the semi-free flight model aircraft are established and the mathematical modelling and scaling law requirements considered. Alternative representations of the equations of motion in the wind tunnel are evaluated.

A number of preliminary experiments were carried out using the dynamic rig and Hawk model and during the course of this research a number of reports were written and published (Refs 3 to 12). Where necessary, a limited amount of this work is also described in this thesis; for example, calibrations of the model aircraft's control surface angles and estimation of the moments of inertia are reported.

The modified stepwise regression procedure has been implemented on computer in the form of a FORTRAN 77 program. Various digital computer simulations were written in the Advanced Continuous Language (ACSL) and covered the longitudinal and lateral equations of motion of aircraft such as the McDonnell Douglas F-4 Phantom and BAe Hawk. Data produced

by the aircraft simulations were subsequently used to verify the MSR computer program.

A data acquisition system was developed, based on a CED1401 analogue-to-digital converter and the subsequent storage of wind tunnel data on an IBM personal computer. The design and application of digital filters and techniques to facilitate the derivation of various angular attitude rates is explained. The MSR method requires input data (e.g. pitch rate) which cannot be measured directly from the experimental rig.

The experimental work undertaken to record aircraft response data to various inputs and model flight conditions is described. The S&C estimates obtained are compared wherever possible with previous CoA work, theoretical predictions and limited data published on the Hawk. The results obtained when the MSR method was applied to wind tunnel data were somewhat disappointing and this is thought to be mainly due to practical problems in obtaining data from the rig rather than in the method itself. MSR was investigated further using a small set of data for which the iterative stages involved in obtaining the best fit model were well known. MSR was shown to work extremely well using data obtained from digital aircraft simulations.

It is considered that MSR still has potential as an alternative parameter estimation method, especially when more directly-measured input variables are available than is the case with the current experimental facility. The research presented in this thesis thus aims to improve the understanding of the modified stepwise regression technique and its application to aircraft in general.

CHAPTER 2

A REVIEW OF PARAMETER ESTIMATION METHODS

2.0 A REVIEW OF PARAMETER ESTIMATION METHODS.

In November 1988 an on-line literature search of relevant data bases was carried out at Cranfield. This survey was used to compliment literature already held on the subject of parameter identification. A second on-line search was conducted in July 1992. A good proportion of the references found as a result of these searches was obtained and evaluated. It was considered that these were quite comprehensive and provided a sound basis for the research described in this report on the application of a modified stepwise regression.

There are many different parameter estimation techniques used in engineering and scientific fields, flight dynamics being a good example. A variety of parameter estimation methods are discussed later in this chapter. Before this however, various applications of MSR in the aeronautical field are discussed, followed by an introduction to Stepwise Regression and Modified Stepwise Regression. A more rigorous description of the MSR method is presented in Chapter 8 of this thesis.

2.1 MSR research programmes.

Many of the references obtained as a result of the literature search related to work carried out by V. Klein and his colleagues in the U.S.A. This team performed much of the pioneering work in the application of the MSR method to identify aircraft stability and control parameters in the late 1970's (Ref 1).

Other applications of MSR have been concerned with the

identification of the stability and control derivatives of a large-scale free-flying fighter aircraft model. This work was carried out by the RAE and used flight test data obtained from their High Incidence Research Model aircraft, "HIRM2", which was flown in the U.S.A. with NASA assistance (Ref 13). Within the U.K., the DRA at Farnborough and Mulkens at Cranfield (Ref 14) have continued to use the HIRM aircraft for parameter estimation work. There is also some helicopter related parameter identification work being carried out at DRA(Bedford).

2.2 Stepwise regression.

Linear regression is employed to estimate a functional relationship of a dependent variable to one or more independent variables. It is assumed that the dependent variable can be closely approximated as a linear combination of the independent variables. For the system identification of an aircraft operating at low angles of attack, the mathematical model structure for aerodynamic forces and moments is linear and may be written in the form

$$y(t) = \theta_0 + \theta_1 x_1(t) + \theta_2 x_2(t) + \ldots + \theta_{n-1} x_{n-1}(t) \qquad [2.1]$$

where:

$y(t)$ represents the resultant coefficient of aerodynamic force or moment $(C_x, C_y, C_z, C_m, C_l, C_n)$ at time t. These are the dependent variables.

$\theta_1, \theta_2, \ldots, \theta_{n-1}$ are the stability and control derivatives. θ_0 is

the value of any particular coefficient corresponding to the initial steady trimmed flight condition.

$x_1, x_2, \ldots x_{n-1}$ are the independent aircraft state and control variables for example, $(u,v,w,p,q,r,\eta,\xi,\zeta)$ and may also include combinations of these variables at time t.

When a sequence of N observations on both y and x has been made at times $t_1, t_2, \ldots, t_N$, then the measured data can be related by the following set of N linear equations:

$$y(i) = \theta_0 + \theta_1 x_1(i) + \ldots + \theta_{n-1} x_{n-1}(i) + \varepsilon(i) \quad ;i = 1,2,\ldots,N \qquad [2.2]$$

Because [2.1] is only an approximation of the actual aerodynamic relations, the right-hand side of [2.2] includes an additional term, $\varepsilon(i)$, often referred to as the equation error. For N>n the unknown parameters can be estimated from the measurements by a least-squares technique in which the square of the equation error is minimised.

Stepwise Regression is a procedure which inserts independent variables into the regression model one term at a time until the best fit of the regression equation to experimental data is achieved. The order of insertion of the variables is determined by using the partial correlation coefficient as a measure of the importance of variables not yet in the regression equation.

At every step of the regression the variables incorporated into the model in previous stages and the new variable entering the model are re-examined using the F statistic. A variable may be taken out of

the model depending on the value of the partial F_p statistic:

$$F_p = \hat{\theta}_j{}^2/s^2(\hat{\theta}_j) \qquad ;j = 1,2,...n \qquad [2.3]$$

where $\hat{\theta}_j$ is the estimate of the parameter θ_j, and $s^2(\hat{\theta}_j)$ is the variance of estimate $\hat{\theta}_j$.

The process of selecting and checking variables continues until no more variables will be admitted to the equation and no more are rejected. The complete computing scheme for the stepwise regression may be found in Refs 7, 15 and 16.

2.3 Introduction to MSR.

The stepwise regression technique is only changed slightly to obtain the MSR method in that a constraint is applied, hence the name "modified stepwise regression". The MSR constraint is that all the linear terms are entered into the initial model and are examined first. That is, the linear terms are entered into the regression according to their partial correlation coefficients and are kept in the model regardless of the value of F_p. This means that during this part of the procedure no hypothesis testing is applied to reject a term from the model. When all linear terms are included, the non-linear terms postulated are searched and the null hypothesis concerning their significance and the significance of all terms already included in the model is tested.

Selecting parameters which guarantee a good fit to the data does not necessarily mean that the final model selected will be a good

predictor. However, there is a rule known as the "Principle of Parsimony" which may be applied to assist in the final model structure determination. The rule states that given two models fitted to the same data with residual variances which are close to each other, choose the model which involves the smaller number of parameters. MSR uses the prediction sum of squares (PRESS) criterion for the selection of a parsimonious model. The PRESS for the kth model is defined as:

$$\text{PRESS} = \sum_{i=1}^{N} \{ y(i) - y[i|x(1),\ldots,x(i-1),x(i+1),\ldots,x(N)]_k \}^2 \qquad [2.4]$$

The model with the lowest value for the PRESS should be the model with the smallest number of parameters. This would then indicate the model to select as the "best final model".

2.4 An application of MSR.

The MSR method has been applied many times to sets of simulated data and real measured data from an aircraft. In the following example, (Ref 1), a simulated data set was created using a fourth-order Runge-Kutta integration computer program with a step size of 0.001sec. Equations for the aerodynamic model integration were estimated by applying the MSR to flight measurements of a high-angle-of-attack lateral manoeuvre which exhibited longitudinal oscillations due to coupling effects and the model therefore included non-linear terms. When applied to the simulated data, the MSR selected the correct model structure and parameter estimates, thus verifying the MSR in a noise-free environment.

As a measure of the robustness of the MSR, it was also applied to two cases in which both the aerodynamic coefficients C_Y, C_l, C_n and the linear model variables α, β, p and r were corrupted by zero-mean Gaussian noise. The standard deviation of the model variable noise in case 1 was that estimated from the ground calibration of the instrumentation system. In the second case, five times higher noise levels were applied to the same model variables.

With the lower level of noise, the MSR reached a maximum F value with six variables for the side force equation. The F_p's for each of the variables in the regression at a given point can also be examined. If newly added variables have significantly lower F_p's than those already in the model, one should apply the principle of parsimony and pick the less complex model providing its F value is at least equal to the maximum F value.

The parameter estimates in the higher noise level environment deviated slightly for the true values and in some runs the chosen model structures were slightly different from those in case 1. This reflected the lower signal to noise ratio and the effort made by the MSR to fit the noise. Furthermore, the noise in the state variables decreased the uniqueness of the selection in both the F and PRESS criteria.

The modification which constrains the MSR to first fit the linear model is an important feature. For the cases in which noise was added to the model variables, an unconstrained stepwise regression was inconsistent as to which was the best model structure. Also, terms that were not in the simulated model were accepted in certain "best

models" for an unconstrained stepwise regression. Klein and Batterson (Ref 1) concluded that the use of the MSR provided better parameter estimates than an ordinary stepwise regression without constraint.

2.5 Measurements and errors.

In all experimental work it is important to locate the primary source of measurement errors. In flight dynamics there are measurements of time, position, velocity and attitude angles, among others. Errors can exist in each of these, but accurate measurements of speed, for example, are usually much more difficult to obtain than those of time. In such cases the velocity measurements can be assumed to contain the major sources of error or uncertainty.

Assuming that any known systematic effects are removed, such as errors due to calibration or presence of a sensor, then any remaining errors can be considered to be random. These random errors may be described statistically by the standard statistical assumptions below, (Ref 17). These eight assumptions provide a yardstick with which to compare the actual conditions and may or may not all be valid for a particular case. They also provide a basis for selection of estimation criteria (such as minimising a sum of squares) and for statistical statements such as those regarding confidence intervals.

2.5.1 Statistical description of errors:

(i) Errors are additive; that is,

$$Y_i = T_i + \varepsilon_i \qquad [2.5]$$

where, for example,

Y_i is a temperature measurement at time t_i (or position x_i),

T_i is the 'true' temperature at time t_i,

ϵ_i is the random error at time t_i.

A characteristic of additive errors, in contrast to multiplicative errors, is that the errors do not vary greatly with the independent variables such as time and position. It is possible to have both position x_j and time dependence such as in Y_{ji}, but for simplicity only the i dependence will be noted in this section.

(ii) The error ϵ_i has a zero mean;

$$E(\epsilon_i) = 0 \qquad [2.6]$$

where

$E(\cdot)$ is the 'expected value operator'.

This equation indicates that the errors average to zero, that is, there is no bias. The expected value of a continuous random variable Y with the probability density function f(y) is given by

$$E(Y) = \int_{-\infty}^{\infty} y.f(y).dy \qquad [2.7]$$

(iii) Errors have a constant variance,

$$V(\epsilon_i) = \sigma^2 \qquad [2.8]$$

where

$V(\cdot)$ is the variance operator and σ^2 denotes the variance of ϵ_i.

The absence of an i subscript on σ^2 means that all the errors have the same variance (i.e. the same variability) on average. The square

root of the variance is the standard deviation, which has the same units as Y_i.

The variance operator is related to the expected value operator by

$$V(\varepsilon_i) = E(\varepsilon_i^2) - E^2(\varepsilon_i) \qquad [2.9]$$

(iv) The errors are uncorrelated,

$$\text{cov}(\varepsilon_i, \varepsilon_j) = 0 \text{ for } i \neq j \qquad [2.10]$$

where

cov(·) is the covariance operator.

This assumption means that, for example, the error at time t_i is uncorrelated with the error at time t_j (for $t_i \neq t_j$).

The covariance operator is related to the expected value operator by

$$\text{cov}(\varepsilon_i, \varepsilon_j) = E(\varepsilon_i \varepsilon_j) - E(\varepsilon_i)E(\varepsilon_j) \qquad [2.11]$$

(v) Errors have a Gaussian i.e. normal probability density function

$$f(x) = \frac{1}{(2\pi)^{1/2}\sigma} e^{-1/2\left(\frac{x-\mu}{\sigma}\right)^2} \quad \text{for } -\infty < x < \infty, \qquad [2.12]$$

where

μ is the mean (equal to 0) and σ is the standard deviation.

In electronic engineering, random noise having a normal distribution is often referred to as Gaussian.

(vi) Statistical parameters such as the variance σ^2 are known.

(vii) The errors are only in the dependent variables.

For the example of temperature measured as a function of time at a given position, the major errors would be in temperature, not in time or position.

(viii) There is no prior information.

If there is prior information regarding the parameters, however, its proper use may improve the parameter estimates.

2.6 Parameter estimation criteria

Estimation criteria can incorporate various statistical aspects. The simplest criterion is the minimisation with respect to the parameters of the sum of squares between the measured values Y and corresponding calculated values, which is denoted by B. The sum of squares is given by

$$S_{OLS} = (Y-B)^T(Y-B) = \sum_{i=1}^{n}(Y_i - B_i)^2 \qquad [2.13]$$

Minimisation of S_{OLS} does not include any statistical assumptions and is the ordinary least squares (OLS) method. The matrix notation of [2.13] can represent a single summation over time, for example, a total of n measurements. It might also represent measurements over time, t_i, and space, x_j, as follows

$$S_{OLS} = \sum_{j=1}^{m} \sum_{i=1}^{n} (Y_{ji} - B_{ji})^2 \qquad [2.14]$$

where m could be the number of sensors and n the number of 'times'.

A more general criterion is the minimisation of

$$S_{ML} = (Y-B)^T \Psi^{-1} (Y-B) \qquad [2.15]$$

The square matrix Ψ in [2.15] is the covariance matrix of the errors. The role of the Ψ^{-1} matrix is to introduce unequal weights for the measurements - the smaller the variability of a given measurement, the greater its weight. This matrix, which has a statistical bias, also includes weighting to compensate for correlation between measurements, since highly correlated measurements do not contribute as much information as uncorrelated ones. For the case of additive mean errors, Ψ is given by

$$\Psi = \begin{bmatrix} \sigma_1^2 & E(\varepsilon_1\varepsilon_2)\cdots E(\varepsilon_1\varepsilon_n) \\ \vdots & \sigma_2^2 \quad \vdots \\ \vdots & \vdots \quad \vdots \\ E(\varepsilon_n\varepsilon_1) & \cdots \quad \sigma_n^2 \end{bmatrix} \qquad [2.16]$$

where

$$\mathrm{cov}(\varepsilon_i,\varepsilon_j) = E(\varepsilon_i\varepsilon_j) - E(\varepsilon_i)E(\varepsilon_j) = E(\varepsilon_i\varepsilon_j) \quad \text{for zero mean errors.}$$

The use of equation [2.14] does not require that the errors have a constant variance or that they be uncorrelated (the third and fourth standard assumptions). The presence of non-zero off-diagonal terms in Ψ indicates that the measurements are correlated.

If the errors are additive and have zero mean and Ψ is known within a multiplicative constant, then the minimisation of [2.15] gives Gauss-Markov estimates. If, moreover, the model is linear in parameters then the criterion gives the minimum variance parameter estimates.

If the first, second, fifth, sixth and seventh standard statistical assumptions are valid (i.e., additive, zero mean, normal errors with known statistical parameters, and errorless independent variables), minimisation of [2.15] yields Maximum Likelihood (ML) estimates.

If the eight standard statistical assumptions are valid, each sum-of-squares criterion reduces to that given for the OLS method, as shown in equation [2.13].

Another criterion of note is one which has a number of interpretations. If all the standard assumptions, except the third, fourth, and eighth, are valid, the Maximum A Posteriori (MAP) criterion is obtained. This criterion includes the effect of prior information. If the prior estimates of the parameters (before the information in the measurement vector Y is used) are such that the prior parameter estimation vector $\underline{\mu}$ has a normal (i.e. Gaussian) probability density with a covariance matrix of $\underline{V}_{\beta}$, the MAP criterion is the minimisation of

$$S_{MAP} = (Y-B)^T \Psi^{-1} (Y-B) + (\underline{\mu}-\underline{\beta})^T \underline{V}_{\beta}^{-1} (\underline{\mu}-\underline{\beta}) \qquad [2.17]$$

where $\underline{\beta}$ is the parameter vector containing p parameters, $\beta_1,\ldots,\beta_p$

The additional second term in S_{MAP} [2.17] compared to S_{ML} [2.15] incorporates the prior information regarding the parameters. By including this term, better than ML parameter estimates can be found if there is enough prior information. The MAP criterion can also be interpreted to provide ridge regression estimates and to introduce regularisation; these two techniques are needed when the OLS and ML criteria give estimates with large parameter variances. A further benefit of the MAP method is that it can be utilised to develop sequential estimation. Sequential estimation is very powerful because it gives insights into the adequacy of the model and the accuracy of the parameters, (Ref 17 contains examples of two sequential procedures, i.e. the direct sequential and matrix inversion lemma methods).

Since the matrix Ψ is used in both [2.15] and [2.17], the measured vector does not have to contain only a single type of measurement, for example temperature, but can also include other measurements such as heat flux. The Ψ^{-1} matrix includes proper weighting for the different types of measurements. Unlike the least squares criterion [2.13], the use of [2.15] and [2.17] yields estimates that are independent of the choice of units. For example, if temperature in $^{\circ}F$ and velocity in ft/s are used instead of temperature in $^{\circ}C$ and velocity in m/s, different β estimates would result for the OLS method, while the same estimates would result for the ML approach.

In actual practice, the Ψ^{-1} matrix is not usually known before the estimation procedure is used and two approaches are possible. The first is to replace Ψ^{-1} by the identity matrix, i.e. use least squares.

The second approach is to estimate the Ψ^{-1} components from measurements. The use of least squares is usually satisfactory if the variances of all the measurement errors are not greatly different from one another, less than a factor of 10 say. If the variances have very different values, such as for diverse types of measurements, then weighted least squares should be used. The ith diagonal element of Ψ^{-1} would be made approximately equal to the reciprocal of the variance of the random measurement error of the ith measurement; the off-diagonal elements of Ψ^{-1} would be set equal to zero. In the second approach, the measurement errors are modelled.

Maximum likelihood methods only work well if errors are already known or can be expressed in some way. The more recent regression methods on the other hand, do not require statistical noise models and can more useful in some applications.

2.7 State of the art.

Kalman filtering is a technique which has become very popular and is now widely used, particularly in control engineering. The dynamic wind tunnel facility at Cranfield has been used in many previous experimental programmes which investigated parameter estimation; Ref 18 details parameter estimation work carried out at this facility by Heydari using the Kalman filtering technique. The reader is referred to his work for a description of the this technique.

Research into formal methods using discrete mathematics is beginning to produce techniques which enable mathematical modelling of

the physical behaviour of digital hardware and software systems (Ref 19). The conventional, continuous mathematics that is used extensively in modelling flight systems is not adequate for accurate modelling of digital control systems. Therefore, the current practice of digital flight control system design has not had the benefits of extensive mathematical modelling which are common in other parts of flight system engineering.

Formal methods research is showing that by using discrete mathematics, very accurate modelling of digital systems is possible. These discrete modelling methods are still in an embryonic stage, but when they are fully developed, they will bring the traditional benefits of modelling to digital hardware and software design. Sound reasoning about accurate mathematical models of flight control systems can be an important part of reducing the risk of unsafe flight control.

The most recent advances in parameter estimation concern the use of Neural Networks which offer interesting learning or adaptive capabilities. For example, Ref 20 details an approach to incorporating artificial neural networks in nonlinear, adaptive control systems. The controller contains three principle elements: a nonlinear inverse dynamic control law whose coefficients depend on a comprehensive model of the system, a neural network that models system dynamics, and a state estimator whose outputs drive the control law and train the neural network. Attention has been focused on the system identification task, which combines an extended Kalman filter with generalized spline function approximation. Other work with neural networks has focussed on determining which networks are suitable for applications in nonlinear aircraft control and to consider how they can

fit into a nonlinear control law, Ref 21. The lack of visibility of the operation of a neural network's decision making processes could however be an obstacle in these applications.

CHAPTER 3:

THE EXPERIMENTAL FACILITY.

3.0 THE EXPERIMENTAL FACILITY.

A relatively simple dynamic wind tunnel test facility has been designed and built at the College of Aeronautics. Work commenced in 1979 and the development of the facility has been the subject of a number of M.Sc. and Ph.D. research topics in the intervening years, (Refs 18, 22, 23 and 24). The photograph overleaf, Figure 2, shows the experimental facility with the Hawk aircraft model suspended in a frame which has been positioned in the wind tunnel. Also shown in Figure 2, are the electronic control unit (ECU) for the model and the wind tunnel controls. The components comprising the facility are described briefly below.

3.1 The Weybridge wind tunnel.

The properties of an available wind tunnel, such as maximum wind speed and working section size, would normally determine the scope of an experimental facility by constraining the model size. However, in this work the 'Weybridge' open jet wind tunnel together with the 1/12th scale Hawk model, dynamic wind tunnel test rig and supporting equipment had to be used as this facility had been used in previous parameter identification work. The Weybridge tunnel is a low-speed open-section tunnel, with a closed return and a maximum wind velocity of 40m/s. The open working section measures 1.5m by 1.1m diameter, so that the aircraft model size must be limited to a maximum wing span of about 0.9m. The flight envelope which can be reproduced depends on the tunnel speed and scaling law requirements and these requirements are presented in Appendix A.

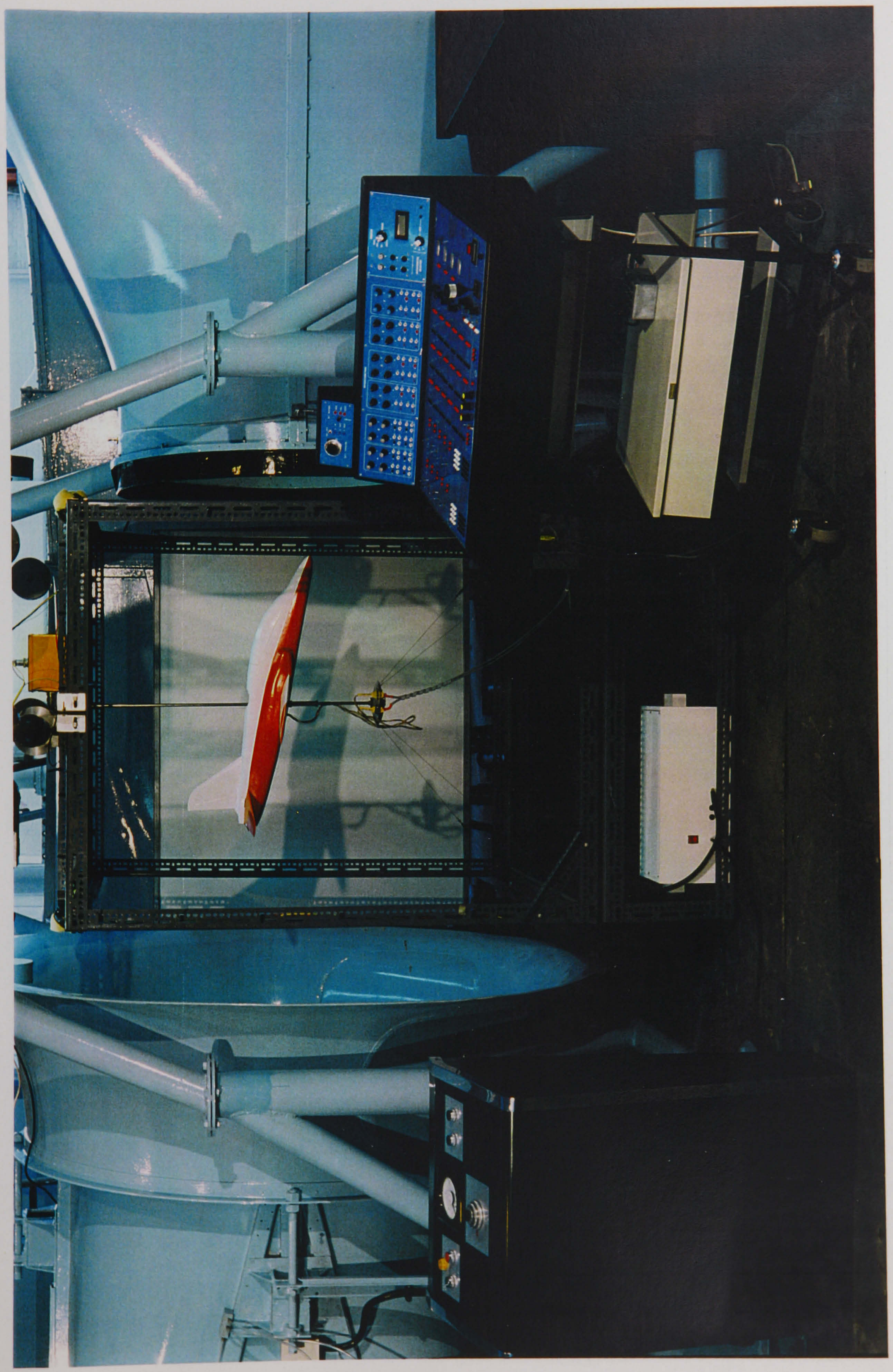

FIGURE 2: THE EXPERIMENTAL FACILITY

3.2 Aircraft models.

During the initial development of the experimental facility (Ref 22) the aircraft model used was based on the BAe Hawk as, when suitably scaled, the model had sufficient internal volume for the suspension and control equipment. Components of the Hawk model are shown in the photograph overleaf, Figure 3. A reasonable amount of performance data was available and when the model was scaled in the ratio 1:12 it had a weight of 3kg. The facility has also been used to evaluate a combat aircraft configuration with forward swept wing (FSW), (Ref 18).

For both the Hawk and FSW models it was necessary to ensure a light-weight structure to allow for the weight of the enclosed equipment and ensure that dynamic scaling requirements were met. The models were constructed using standard aeromodelling techniques and materials which proved quite adequate for the application. The models are controlled by means of a tailplane (Hawk model) or foreplane (FSW model), ailerons and rudder which are all individually driven by small precision servo-actuators. Control signals to and from the model, together with power-supply cables, were grouped together to form a trailing umbilical connection to the control unit.

The Hawk model was also used recently in an M.Sc project by Filmer in which several aspects of the test rig were improved and developed (Ref 24). Chapter 5.0 details some of the development of a vertical height sensor system as well as previous experimental programmes which have used the aircraft models.

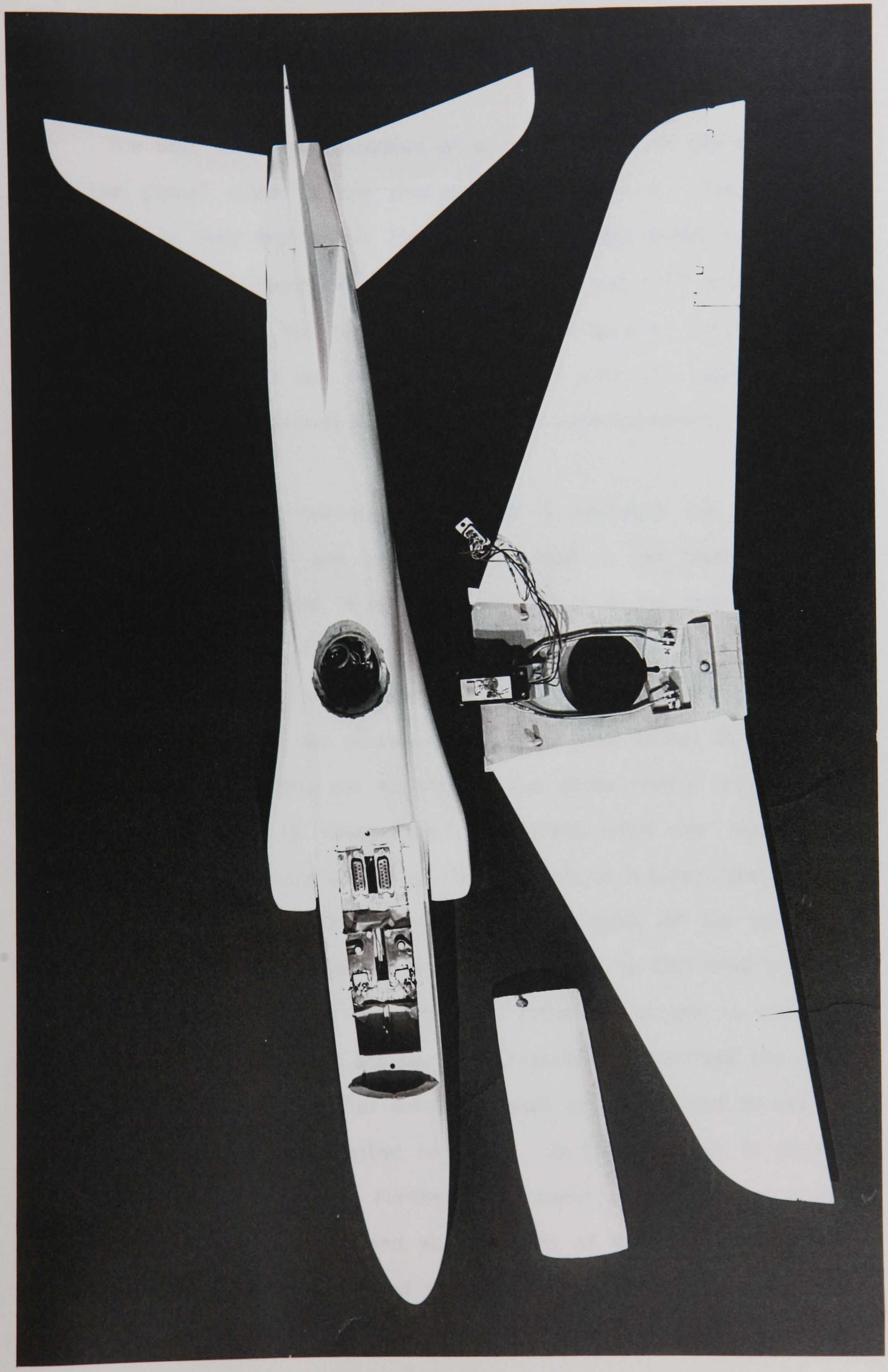

FIGURE 3: HAWK AIRCRAFT MODEL COMPONENTS SHOWING CONTROL SERVOS

3.3 Model suspension system.

The Hawk model is suspended on a vertical rod in the wind tunnel by the gimbal shown in the photograph at Figure 4. The gimbal is designed so that when it is fixed in the aircraft model's frame, any perturbed angles recorded by the yaw, pitch and roll potentiometers correspond directly to the Euler Angles, see Figure 5. Thus linear and rate transformations may be applied directly with the required angles ψ, θ and ϕ being measured directly from the potentiometers.

The suspension system consists of a vertical rod mounted in bearings at its upper and lower ends, so that it can rotate about its vertical axis. The rod is supported, by means of its bearing mounting plates, in a large transportable Dexion framework to which it is rigidly attached by wire bracing, Figure 1. The whole assembly, complete with model, can be removed from the wind tunnel as a unit. A sleeve is keyed to the rod so that it can slide freely in a vertical sense. The rod is constrained to rotate with the sleeve thus transmitting any yawing motion of the aircraft to a potentiometer which measures yaw angle. The sleeve also forms part of the suspension gimbal which is mounted in the model. The model is thus free to rotate in pitch and roll about the sleeve. Rotation in yaw is about the vertical axis of the rod and vertical translation involves the sleeve sliding on the rod. Angular motion in each axis is sensed by means of potentiometers and is limited to $\pm 30^{\circ}$. Vertical motion is possible over approximately 0.75m. Further development allowed the sensing of the vertical position (h) and velocity ($\dot{h}$) of the model. The model degrees of freedom are depicted in Figure 6.

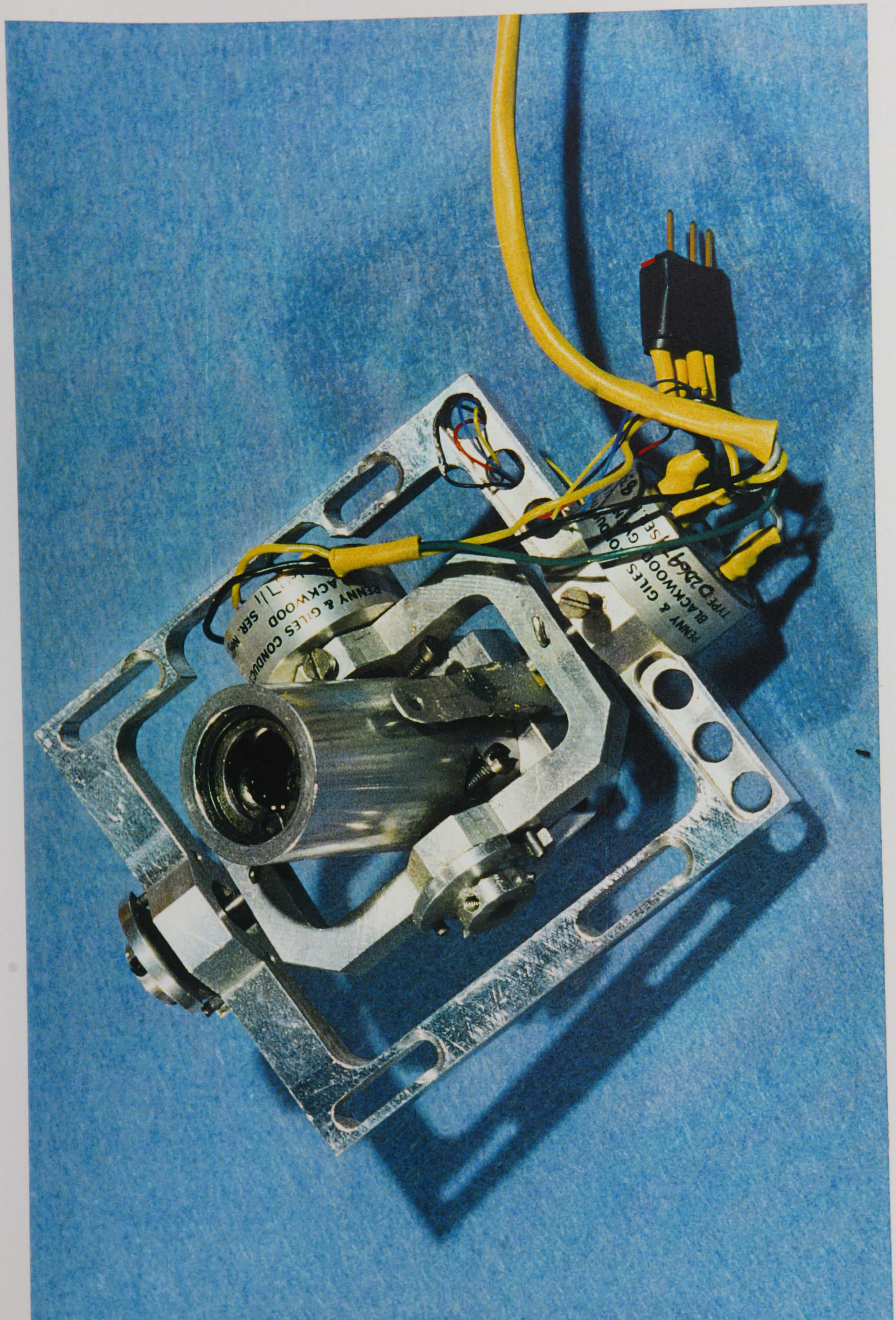

FIGURE 4: MODEL GIMBAL

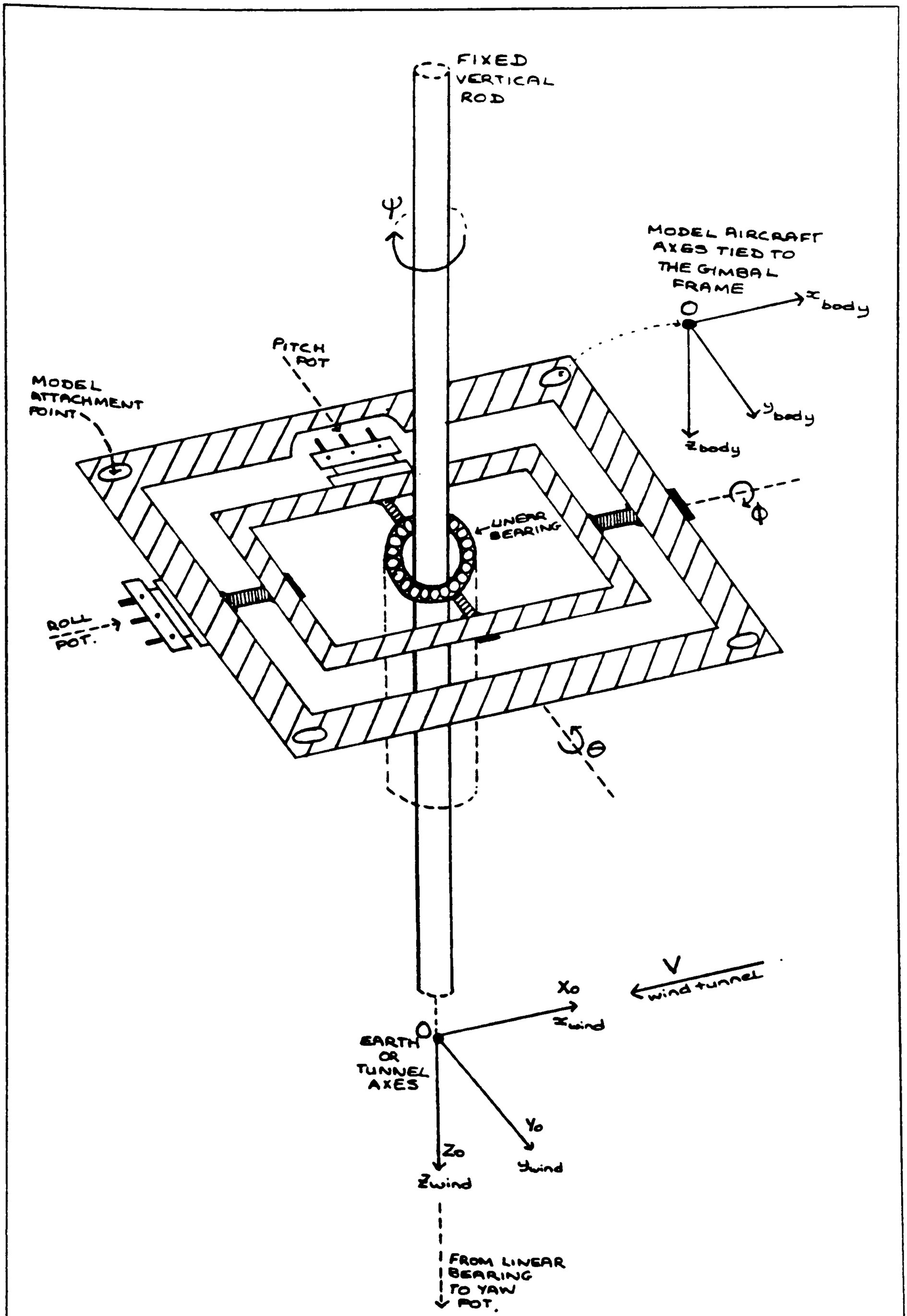

FIGURE 5: MODEL GIMBAL AND AXES SYSTEMS

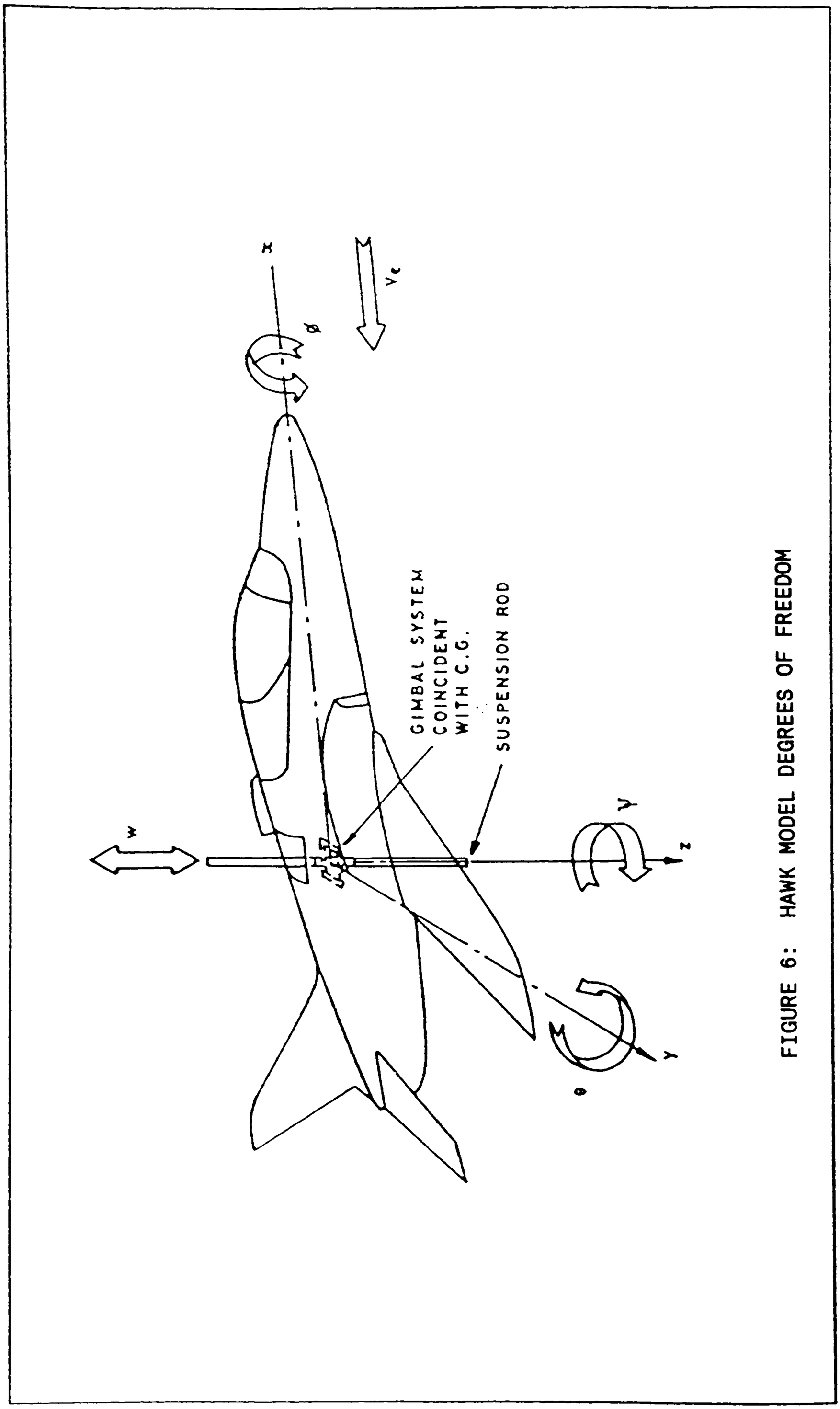

FIGURE 6: HAWK MODEL DEGREES OF FREEDOM

3.4 Electronic control unit.

The electronic control unit (ECU), shown in the photograph at Figure 7, was designed and built as a small, self-contained, transportable console which, for simplicity, employs analogue circuitry throughout. An umbilical from the model connects its various actuators and servo mechanisms to the control panel. Construction of the control unit is highly modular, to facilitate functional changes, and it provides the following facilities:

(i) electrical power supplies;

(ii) input and output interfaces with the model;

(iii) primary control of the model;

(iv) programmable analogue computer elements for feedback purposes;

(v) output signal interfaces for recording and display;

(vi) input and output interfaces to an external computer.

3.5 Recording of data.

Analogue to digital conversion of data from the experimental rig is carried out using a Cambridge Electronics Design (CED) interface, the CED1401. Controlled via software programs on the IBM host computer, up to 8 channels may be simultaneously recorded in separate data files on the host computer. Using CED software it is possible to immediately examine recorded data to asses noise levels and to see whether a usable short period aircraft response has been captured. The ECU is an integral part of the Data Acquisition System (DAS) and further details of this system are given in Chapter 11.

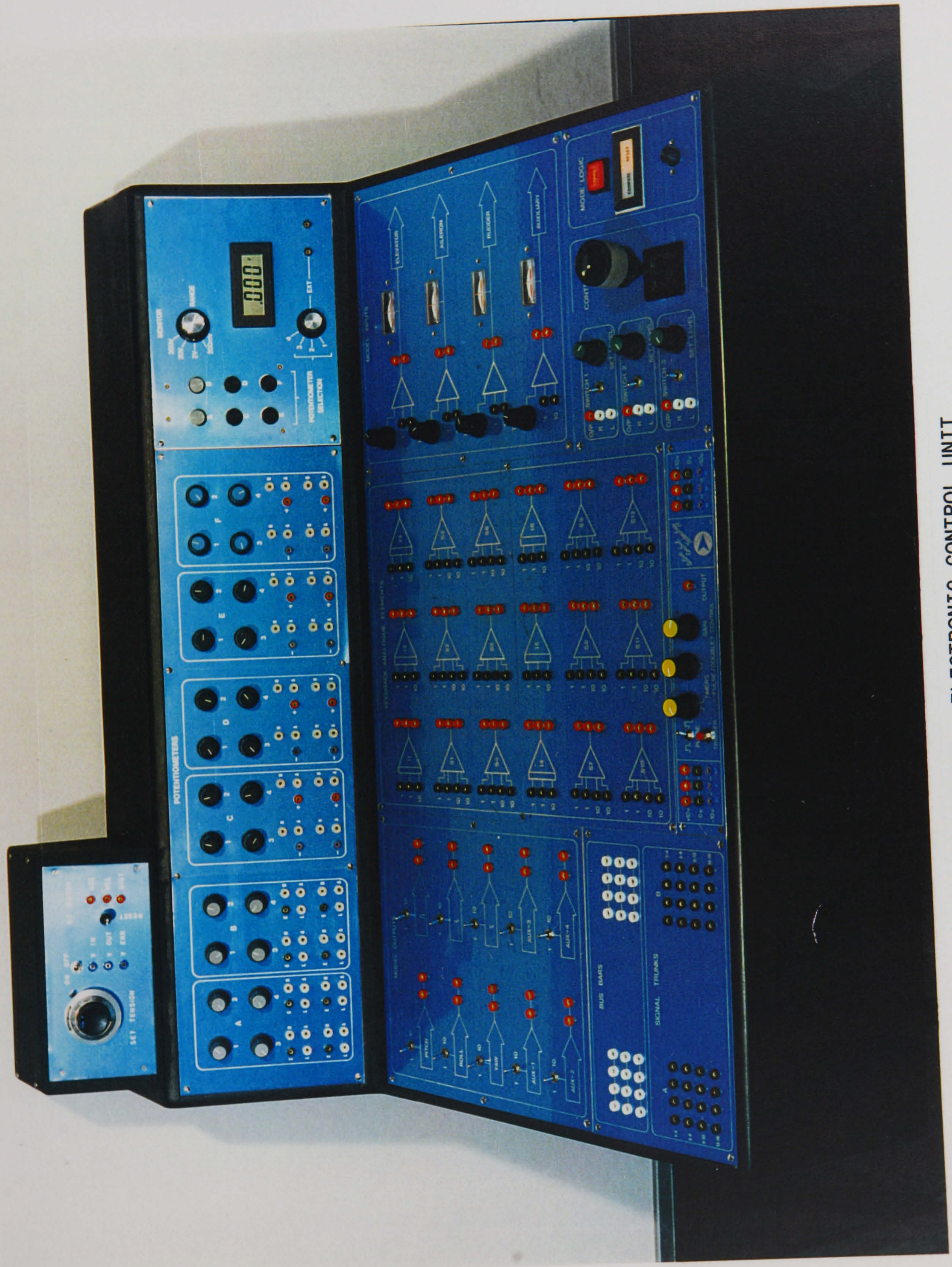

FIGURE 7: ELECTRONIC CONTROL UNIT

CHAPTER 4

MATHEMATICAL MODELLING

4.0 MATHEMATICAL MODELLING.

One aim of this research programme was to develop a mathematical model representative of the model aircraft in the dynamic wind tunnel. There was some evidence to suggest that the form of the mathematical model used in previous experimental programmes was not the most suitable, Ref 25. It was decided to re-examine and change the existing models to reflect the experimental application more precisely.

A good mathematical model is required firstly, to provide a structure for the regression equations and secondly, to form the basis for computer simulations of the aircraft. Data processing algorithms have been developed to convert the recorded experimental data into a format suitable for input to the Modified Stepwise Regression program. Chapter 10 details the statistical theory behind MSR which was developed as far as necessary for the current application.

The standard small perturbation equations of aircraft motion are used as a starting point in this application as it is this type of motion that the dynamic test facility was designed to reproduce. Furthermore, as small perturbations are assumed, it is possible to decouple the equations of motion and to consider the longitudinal and lateral equations separately.

The following sections detail the equations of motion for both a full scale aircraft and a wind tunnel model. An alternative representation of wind tunnel motion is given in Chapter 14, based upon an aircraft in gusts, in which the fluid and inertial components of motion are represented by separate terms in the mathematical equations.

4.1 Longitudinal equations of motion.

The "free flight" general dimensional equations of longitudinal symmetric motion for small disturbances (when referred to body axes) may be written as shown below in [4.1]. The matrix equation coefficients are defined in the form of the normalised stability and control derivatives. (The derivation of [4.1] is given in Appendix B.)

$$\begin{pmatrix} \dot{u} \\ \dot{w} \\ \dot{q} \\ \dot{\theta} \end{pmatrix} = \begin{pmatrix} X_u & X_w & X_q & -g \\ Z_u & Z_w & Z_q & 0 \\ m_u & m_w & m_q & 0 \\ 0 & 0 & 1 & 0 \end{pmatrix} \begin{pmatrix} u \\ w \\ q \\ \theta \end{pmatrix} + \begin{pmatrix} X_\eta \\ Z_\eta \\ m_\eta \\ 0 \end{pmatrix} (\eta) \qquad [4.1]$$

4.1.1 Wind tunnel longitudinal equations of motion.

Assuming no longitudinal and lateral coupling, small perturbations and a constant speed in the wind tunnel, the equations of longitudinal motion for the dynamic wind tunnel model aircraft may be written in the reduced order form below, as shown in Appendix B.

$$\begin{pmatrix} \dot{w} \\ \dot{q} \\ \dot{\theta} \end{pmatrix} = \begin{pmatrix} Z_w & Z_q & 0 \\ m_w & m_q & 0 \\ 0 & 1 & 0 \end{pmatrix} \cdot \begin{pmatrix} w \\ q \\ \theta \end{pmatrix} + \begin{pmatrix} Z_\eta \\ m_\eta \\ 0 \end{pmatrix} (\eta) \qquad [4.2]$$

where

$$z_w = \left(\frac{\overset{\circ}{z}_w}{1-\overset{\circ}{z}_{\dot{w}}}\right); \qquad z_q = \left(\frac{u_e+\overset{\circ}{z}_q}{1-\overset{\circ}{z}_{\dot{w}}}\right); \qquad z_\eta = \left(\frac{\overset{\circ}{z}_\eta}{1-\overset{\circ}{z}_{\dot{w}}}\right);$$

and

$$m_w = \left(\frac{\overset{\circ}{m}_{\dot{w}}\overset{\circ}{z}_w}{(1-\overset{\circ}{z}_{\dot{w}})} + \overset{\circ}{m}_w\right); \quad m_q = \left(\frac{(u_e+\overset{\circ}{z}_q)\overset{\circ}{m}_{\dot{w}}}{(1-\overset{\circ}{z}_{\dot{w}})} + \overset{\circ}{m}_q\right); \quad m_\eta = \left(\frac{\overset{\circ}{m}_{\dot{w}}\overset{\circ}{z}_\eta}{(1-\overset{\circ}{z}_{\dot{w}})} + \overset{\circ}{m}_\eta\right).$$

4.2 Lateral equations of motion.

The "free flight" general dimensional equations of lateral asymmetric motion for small disturbances (when referred to body axes) may be written as shown below. The derivation of this particular format of the equations is also given in Appendix B.

$$\begin{pmatrix}\dot{v}\\ \dot{p}\\ \dot{r}\\ \dot{\phi}\\ \dot{\psi}\end{pmatrix} = \begin{pmatrix} y_v & y_p & y_r & g & 0\\ l_v & l_p & l_r & 0 & 0\\ n_v & n_p & n_r & 0 & 0\\ 0 & 1 & 0 & 0 & 0\\ 0 & 0 & 1 & 0 & 0\end{pmatrix}\begin{pmatrix}v\\ p\\ r\\ \phi\\ \psi\end{pmatrix} + \begin{pmatrix} y_\xi & y_\zeta\\ l_\xi & l_\zeta\\ n_\xi & n_\zeta\\ 0 & 0\\ 0 & 0\end{pmatrix}\begin{pmatrix}\xi\\ \zeta\end{pmatrix} \qquad [4.3]$$

4.2.1 Wind tunnel lateral equations of motion.

Assuming small perturbations, no longitudinal and lateral coupling and a constant speed in the wind tunnel, the equations of lateral motion for the dynamic wind tunnel model aircraft may also be written in a reduced order form, given below.

$$\begin{pmatrix}\dot{v}\\ \dot{p}\\ \dot{r}\\ \dot{\phi}\\ \dot{\psi}\end{pmatrix} = \begin{pmatrix}0 & w_e & -u_e & 0 & 0\\ l_v & l_p & l_r & 0 & 0\\ n_v & n_p & n_r & 0 & 0\\ 0 & 1 & 0 & 0 & 0\\ 0 & 0 & 1 & 0 & 0\end{pmatrix} \cdot \begin{pmatrix}v\\ p\\ r\\ \phi\\ \psi\end{pmatrix} + \begin{pmatrix}0 & 0\\ l_\xi & l_\zeta\\ n_\xi & n_\zeta\\ 0 & 0\\ 0 & 0\end{pmatrix} \begin{pmatrix}\xi\\ \zeta\end{pmatrix} \qquad [4.4]$$

where

$$l_v = \left\{ \frac{\mathring{l}_v}{E_{xz}} + \frac{e_x \mathring{n}_v}{E_{xz}} \right\} ; \qquad l_p = \left\{ \frac{\mathring{l}_p}{E_{xz}} + \frac{e_x \mathring{l}_p}{E_{xz}} \right\} ; \qquad l_r = \left\{ \frac{\mathring{l}_r}{E_{xz}} + \frac{e_x \mathring{l}_r}{E_{xz}} \right\} ;$$

$$n_v = \left\{ \frac{-e_z \mathring{l}_v}{E_{xz}} + \frac{\mathring{n}_v}{E_{xz}} \right\} ; \qquad n_p = \left\{ \frac{-e_z \mathring{l}_p}{E_{xz}} + \frac{\mathring{n}_p}{E_{xz}} \right\} ; \qquad n_r = \left\{ \frac{-e_z \mathring{l}_r}{E_{xz}} + \frac{\mathring{n}_r}{E_{xz}} \right\} ;$$

$$l_\xi = \left\{ \frac{\mathring{l}_\xi}{E_{xz}} + \frac{e_x \mathring{n}_\xi}{E_{xz}} \right\} ; \qquad l_\zeta = \left\{ \frac{\mathring{l}_\zeta}{E_{xz}} + \frac{e_x \mathring{n}_\zeta}{E_{xz}} \right\} ;$$

$$n_z = \left\{ \frac{-e_z \mathring{l}_\xi}{E_{xz}} + \frac{\mathring{n}_\xi}{E_{xz}} \right\} ; \qquad n_\zeta = \left\{ \frac{-e_z \mathring{l}_\zeta}{E_{xz}} + \frac{\mathring{n}_\zeta}{E_{xz}} \right\} ;$$

$$E_{xz} = 1 + e_x e_z$$

and the inertia ratios are,

$$e_x = I_{xz}/I_x ; \qquad e_z = I_{xz}/I_z .$$

4.3 Mathematical regression model formulation.

The equations of motion are quoted in the state space form where the general state equation is

$$\dot{\underset{\sim}{x}} = A\underset{\sim}{x} + B\underset{\sim}{u} \qquad [4.5]$$

The object of the parameter estimation process is to estimate values for the elements in the state matrix A and input matrix B using recorded input and response data. The recorded data represents the state vector $\underset{\sim}{x}$ and the input vector $\underset{\sim}{u}$. Clearly, the reduced order dynamic model will allow the estimation of a limited number of matrix elements only which reduces the estimation problem to an almost trivial level. However, practical constraints mean that not all of the motion variables can be sensed as would be required in an ideal situation. This introduces a considerable difficulty which is compounded by a requirement to extend the equations of motion to include model feedback control laws. Feedback is sometimes employed to assist in controlling the Hawk model when flying in the wind tunnel

The equations of motion comprising the mathematical model are concerned with small perturbation transient motion relative to a stable trimmed equilibrium flight condition. Consequently the resulting linear equations of motion may be decoupled into a longitudinal group and a lateral group as appropriate. The linear mathematical model structure for the aircraft aerodynamic forces and moments may therefore be written in the form shown below:

$$y(t) = b_0 + b_1.x_1 + b_2.x_2 + \ldots + b_{n-1}.x_{n-1} \qquad [4.6]$$

where:

y(t) represents the resultant coefficient of aerodynamic forces or moments. These are the measured dependent variables.

$b_1, b_2, \ldots, b_{n-1}$ are parameters to be estimated and b_0 is the value of a particular coefficient corresponding to the initial steady flight condition.

$x_1, x_2, \ldots x_{n-1}$ are the independent state and control variables and may also include combinations of these variables at time t, although in this particular application only linear forms of the mathematical model are considered.

The MSR procedure is implemented computationally by disassembling the equations of motion into a set of linear simultaneous equations. Each equation, representing one degree of freedom, is reformatted to comply with the mathematical model format required for the regression analysis. This is best shown by the following example which is taken from the longitudinal equations of motion where the axial force equation may be rearranged and written,

$$\dot{u} = x_0 + x_u.u + x_w.w + (x_q - W_e).q - g + x_\eta.\eta \qquad [4.7]$$

If a sequence of N readings of y (that is $\dot{u}$) and the variables x, (that is u, w, q, η), are taken at times $t_1, t_2, \ldots, t_N$ and denoted by $y(i), x_1(i), x_2(i)$, to $x_{n-1}(i)$ where $i = 1, 2, \ldots, N$ then the experimental response data acquired can be represented by the following set of N linear equations,

$$y(i) = b_0 + b_1.x_1(i) + b_2.x_2(i) + \ldots + b_{n-1}.x_{n-1}(i) + \varepsilon(i) \qquad [4.8]$$

$\varepsilon(i)$ is the equation error which is introduced as [4.8] is only an approximation to the actual aerodynamic relationship.

Equation [4.8] may also be expressed in the form shown below where β_j is the estimate of b_j; that is, $\beta_j = \hat{b}_j$ for $j = 0,\ldots,n-1$:

$$\begin{pmatrix} y_{(1)} \\ y_{(2)} \\ \vdots \\ y_{(N)} \end{pmatrix} = \begin{pmatrix} 1 & x_{1(1)} & x_{2(1)} & \cdots & x_{n-1(1)} \\ 1 & x_{1(2)} & x_{2(2)} & \cdots & x_{n-1(2)} \\ \vdots & \vdots & \vdots & & \vdots \\ 1 & x_{1(N)} & x_{2(N)} & \cdots & x_{n-1(N)} \end{pmatrix} \begin{pmatrix} \beta_0 \\ \beta_1 \\ \vdots \\ \beta_{n-1} \end{pmatrix} + \begin{pmatrix} \varepsilon_{(1)} \\ \varepsilon_{(2)} \\ \vdots \\ \varepsilon_{(N)} \end{pmatrix} \qquad [4.9]$$

or alternatively, $$\underline{Y} = \underline{X}.\underline{\beta} + \underline{\varepsilon} \qquad [4.10]$$

The Modified Stepwise Regression procedure may then be applied to obtain the mathematical model which is the best fit to the experimental data. This process is described in Chapter 8 which is concerned with the implementation of the MSR.

4.4 Aircraft axes systems and transformations.

It is convenient to define a set of axes $(Oxyz)_{wind}$ fixed in the aircraft such that the Ox axis is coincident with the resultant total velocity vector $\underline{V}$ in the plane of symmetry of the aircraft. This axis system is referred to as a wind or stability axis system and is equivalent to body axes rotated through the body incidence angle (α_e) about the Oy axis. Figure 8 shows the relationship between body and wind axes.

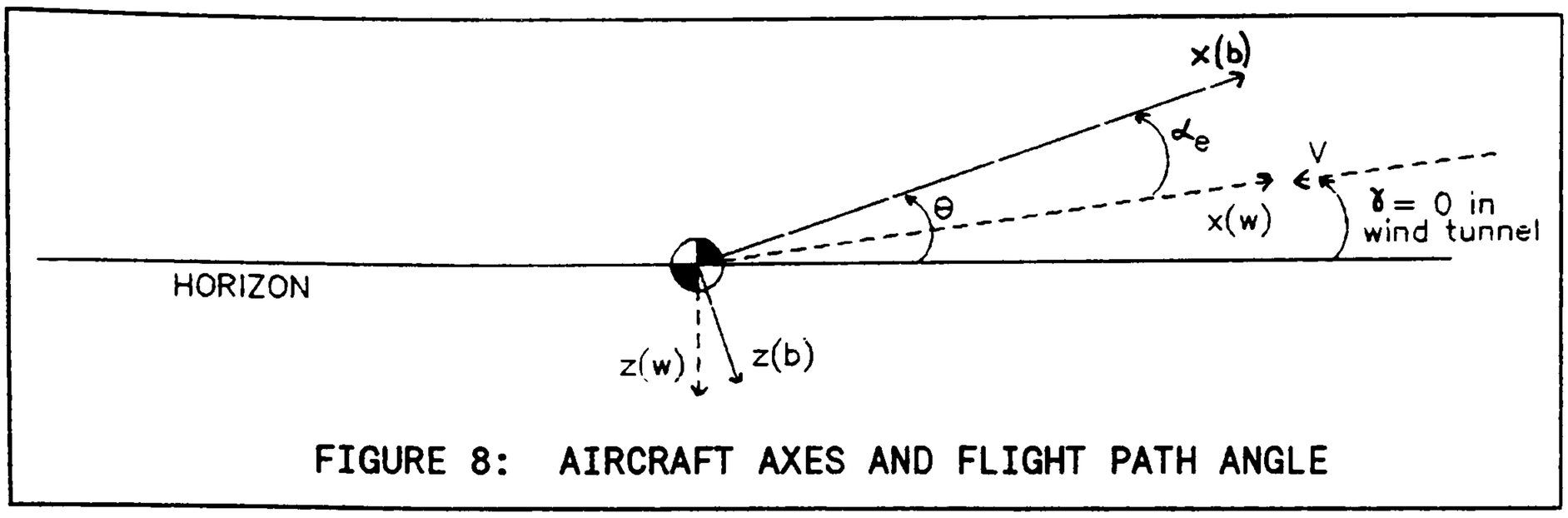

FIGURE 8: AIRCRAFT AXES AND FLIGHT PATH ANGLE

When disturbed the attitude of the aircraft is defined by the orientation of the disturbed body axes ($Oxyz$) with respect to the steady state datum body axes ($Ox_0y_0z_0$). The angular attitude of the aircraft may be established by considering the rotation, about each axis in turn, which is necessary to bring ($Ox_0y_0z_0$) into coincidence with ($Oxyz$). The angles ψ, θ and ϕ define the aircraft attitude with respect to the datum and are called the Euler Angles. These angles are shown in Figure 9.

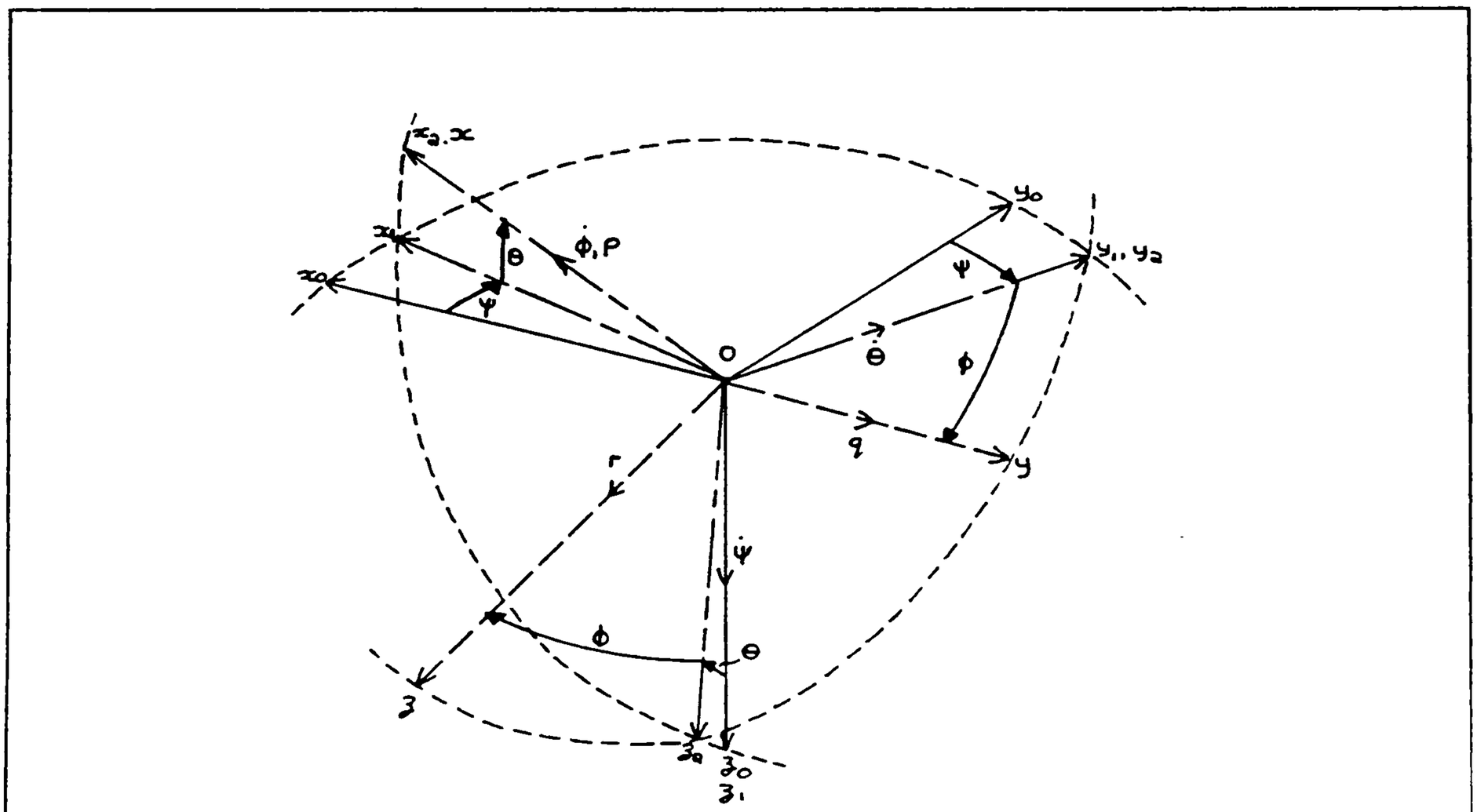

FIGURE 9: THE EULER ANGLES

In order to transform the linear quantities of displacement, velocity and acceleration or force it is usual to consider vector quantities $x_0 y_0 z_0$ in the first axes set ($Ox_0 y_0 z_0$) and to define their angular relationship with the transformed vector quantities xyz in the second axes set ($Oxyz$). Transforming $x_0 y_0 z_0$ by rotations through the yaw angle ψ, the pitch angle θ and then the roll angle ϕ leads to the following transformation relationship, Ref 26,

$$\begin{pmatrix} x \\ y \\ z \end{pmatrix} = \underset{\sim}{A} \begin{pmatrix} x_0 \\ y_0 \\ z_0 \end{pmatrix} \qquad [4.11]$$

where the Direction Cosine Matrix is given by,

$$\underset{\sim}{A} = \begin{pmatrix} \cos\psi\cos\theta & \sin\psi\cos\theta & -\sin\theta \\ \cos\psi\sin\theta\sin\phi - \sin\psi\cos\phi & \sin\psi\sin\theta\sin\phi + \cos\psi\cos\phi & \cos\theta\sin\phi \\ \cos\psi\sin\theta\cos\phi + \sin\psi\sin\phi & \sin\psi\sin\theta\cos\phi - \cos\psi\sin\phi & \cos\theta\cos\phi \end{pmatrix}$$

The transformation matrix for angular perturbation quantities is that which relates attitude rates to body rates. If the angular velocities with respect to earth axes ($Ox_0 y_0 z_0$) are $\dot{\phi}$, $\dot{\theta}$ and $\dot{\psi}$ and the angular velocities of the disturbed body fixed axes ($Oxyz$) are p, q and r, then the following linear relationships between the angular velocities in the two axes systems may be deduced,

$$\begin{pmatrix} p \\ q \\ r \end{pmatrix} = \begin{pmatrix} 1 & 0 & -\sin\phi \\ 0 & \cos\phi & \sin\phi\cos\theta \\ 0 & -\sin\phi & \cos\phi\cos\theta \end{pmatrix} \begin{pmatrix} \dot{\phi} \\ \dot{\theta} \\ \dot{\psi} \end{pmatrix} \qquad [4.12]$$

Note that by assuming small perturbations only the first order approximations $p = \dot{\phi}$, $q = \dot{\theta}$ and $r = \dot{\psi}$ may be made.

4.5 Scaling laws.

Whenever a scaled model is used to investigate the dynamic behaviour of an aircraft it is necessary to be able to correlate the results with the full scale aircraft. To ensure a realistic representation of the full scale aircraft the similarity parameters required are usually found in a non-dimensional form by considering the relevant equations of motion or by the use of dimensional analysis.

Appendix A contains a discussion of the various scaling laws which need to be considered for a successful comparison of the model aircraft to the full scale aircraft. The scaling of derivatives is also discussed in Appendix A. There follows a summary of the similarity laws and although this information is contained in Ref 8 it is repeated here for completeness.

4.5.1 Summary of similarity laws.

For the Hawk model used in this research programme, $\lambda = \frac{1}{12}$. The subscripts '$_m$' and '$_a$' used below refer to model and full scale aircraft parameters respectively.

Optional Parameters	Scale
1. Model Scale	$\frac{l_m}{l_a} = \lambda$
2. Speed	$\frac{V_m}{V_a} = (\lambda)^{1/2}$
3. Density	ρ_m/ρ_a (=1 for Hawk model)

Required Scaling	Relationship
4. Mass	$\frac{M_m}{M_a} = \frac{\rho_m}{\rho_a} (\lambda^3)$
5. Inertia	$\frac{I_m}{I_a} = \frac{\rho_m}{\rho_a} (\lambda^5)$
6. Gravity	$\frac{g_m}{g_a} = \frac{1}{\lambda} \left(\frac{V_m}{V_a} \right)^2$

Analysis of Resultant Motion	Relationship
7. Time	$\frac{t_m}{t_a} = \tau = \frac{V_a}{V_m} \lambda = (\lambda)^{1/2}$
8. Linear Displacement	$\frac{x_m}{x_a} = \lambda$
9. Angular Displacement	$\frac{\theta_m}{\theta_a} = 1$
10. Linear Velocity	$\frac{\dot{x}_m}{\dot{x}_a} = \frac{\lambda}{\tau} = (\lambda)^{1/2}$
11. Angular Velocity	$\frac{\dot{\theta}_m}{\dot{\theta}_a} = \frac{1}{\tau}$
12. Linear Acceleration	$\frac{\ddot{x}_m}{\ddot{x}_a} = \frac{\lambda}{\tau^2}$
13. Angular Acceleration	$\frac{\ddot{\theta}_m}{\ddot{\theta}_a} = \frac{1}{\lambda^2}$

4.5.2 Variation of model gravitation.

A parallel research programme was carried out using the experimental facility and Hawk model by Filmer, Ref 24. The aim of the work was to develop a system capable of altering the gravitational force on the wind tunnel model, i.e. to reduce the effective weight that the model aircraft has to support by generating lift. This implies that gravity for the model must be effectively changed to be less than gravity for the aircraft, i.e. $g_m < g_a$.

If the term $\frac{g_m}{g_a}$ is taken into consideration when model performance is being assessed using the similarity laws, then for a given value of aircraft velocity, V_a, the Froude, Mach, Strouhal and Reynolds numbers will be affected (see Appendix A). In fact all of these numbers will be reduced by a factor of $\left(\frac{g_m}{g_a}\right)^{-1/2}$.

Using data for the Hawk model where $\lambda = \frac{1}{12}$ and considering atmospheric conditions, the Froude number gives a range of model velocities over the span of $0.1 < \frac{g_m}{g_a} < 1.0$. The maximum Weybridge tunnel speed is 35m/s and this produces an upper limit of 0.4 on the mach numbers which can be simulated. Without gravitational variances the normal operating limit is $M = 0.32$. For the same span of $\frac{g_m}{g_a}$, the Reynolds number values provides limits on the low aircraft velocities. In practice the use of an artificial 'g' control system enables g_m to be "adjusted" only over a small range.

Figure 10 is a graphical representation of the way in which the flight envelope could be extended by varying $\frac{g_m}{g_a}$. The combination of Mach number, tunnel speed and Reynolds Number effects on the test area are also shown.

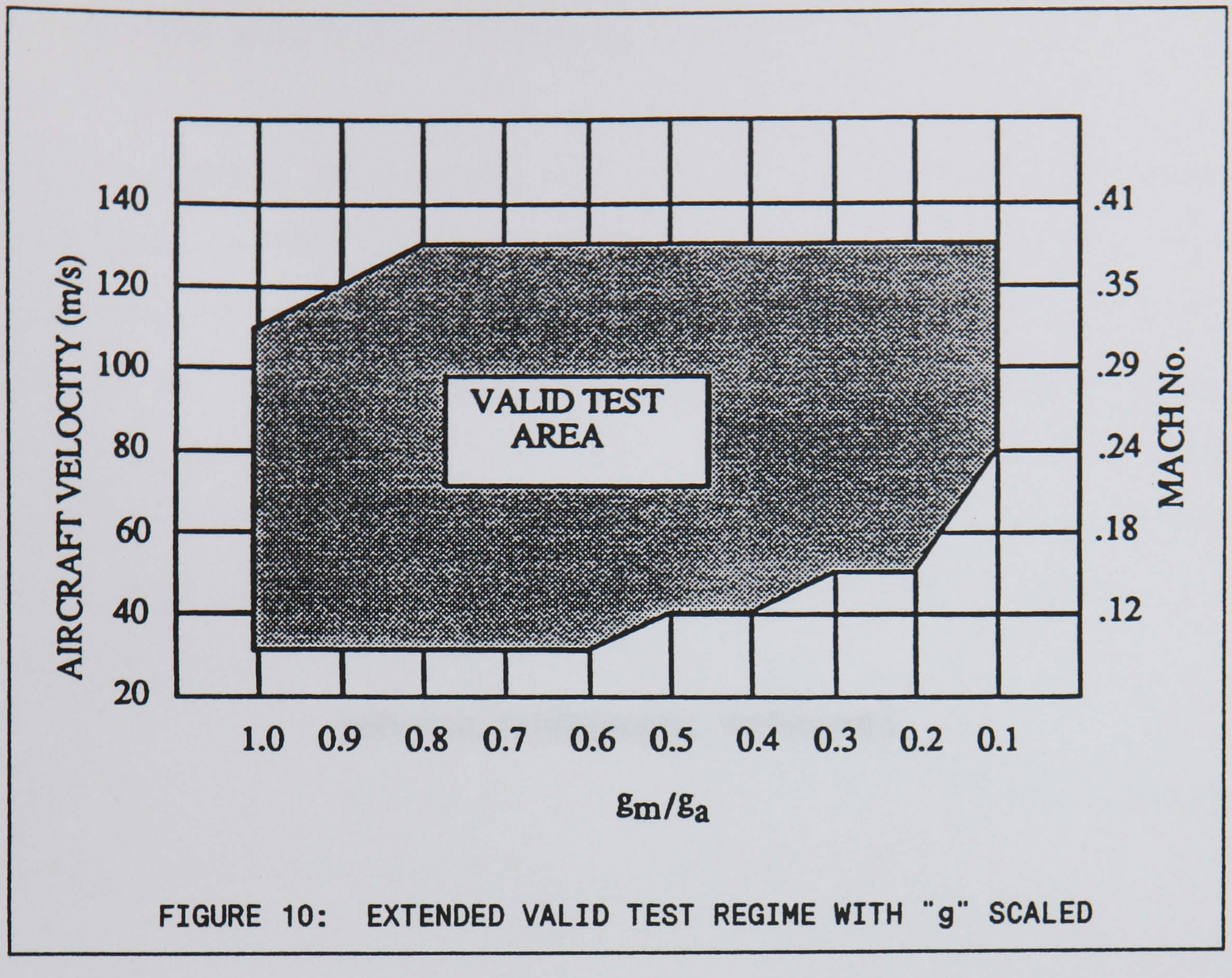

FIGURE 10: EXTENDED VALID TEST REGIME WITH "g" SCALED

CHAPTER 5

PREVIOUS EXPERIMENTAL PROGRAMMES

5.0 PREVIOUS EXPERIMENTAL PROGRAMMES.

The dynamic rig has been the source of many previous experimental programmes in the College of Aeronautics. These programmes were undertaken in order to obtain information on the forms of the mathematical models used to represent the model aircraft dynamics. Furthermore, values of Hawk model derivatives which have been previously estimated or measured are required for comparative purposes. This Chapter briefly describes some of these programmes, starting with the originator of the dynamic facility and ECU.

(i) The Design Development and Evaluation of an Active Control Aircraft Model Wind Tunnel Facility, 1979-1982, Ref 22.

Progress in the field of Active Control Technology (ACT) resulted in an increased interest in dynamic wind tunnel testing for basic research and led to the development of such a facility. This task included the design and construction of a controllable dynamically scaled aircraft model with a suspension system to give the model four degrees of freedom. An electronic control unit was designed to interface with the model and operate the primary control surfaces to facilitate stability augmentation and to provide output signals for measurement purposes.

The dynamic characteristics of the model were recorded for some simulated representative flight conditions and compared with theoretical predictions. The expected characteristics of the model were derived from full-size aircraft data. The use of various stability augmentation functions was investigated to assess the

usefulness of the electronic control unit as a means of providing stability augmentation. The results showed that the system had considerable potential as an ACT Simulator.

(ii) Further Development of a Dynamic Aircraft Wind Tunnel Facility, 1983-1984, Ref 23.

This work made some modifications to the dynamic facility to ease some of the operational difficulties encountered and to achieve a higher degree of reliability. The dynamic characteristics of the Hawk model were obtained and subsequent simulation was found to achieve results to within 15% of theoretical predictions. The use of various stability augmentation techniques was investigated; two different methods were employed to derive the rate signals which were used to augment the basic aircraft dynamics.

(iii) The Estimation of Stability and Control Characteristics of a Generalised Forward Swept Wing Aircraft, 1983-1986, Ref 18.

Advances in composite structures and active control systems made the concept of a forward swept wing aircraft a viable alternative to the more conventional configurations. Research work was carried out on the dynamic behaviour and characteristics of a FSW aircraft having a closely coupled canard. Stability characteristics of the dynamic model were estimated from transient response tests in both longitudinal and lateral modes by means of an Extended Kalman Filter (EKF) statistical method. Simulations of the equations of motion, using estimates of

stability derivatives obtained in this way, closely matched the observed behaviour.

(iv) Artificial 'g' Control System for the Dynamic Wind Tunnel Facility, 1988-1989, Ref 24.

When flown in the wind tunnel the model is very lively, making autostabilisation a prudent addition. Simple feedback loops have been demonstrated and shown to work well. However, the problem of trimming the model to a suitable vertical position in the wind tunnel whilst retaining adequate control over it remained. With this in mind some parallel work was undertaken to design and test a suitable "height hold autopilot". There was also some interest in extending the flight envelope which can be simulated by the dynamic wind tunnel facility.

The main objectives of this programme were thus twofold: Firstly to design and develop a vertical force generation system for the facility capable of applying a constant force on the model during static and dynamic flight phases and with the ability to obtain height data of the model. Secondly, to modify and improve any areas of the facility that would enhance its overall operation.

A servo system for measuring the vertical height, velocity and acceleration of the model on the vertical rod was developed and demonstrated to work satisfactorily. External to the model a servo controlled pulley system situated at the top of the Dexion framework was installed, as shown in the photograph at Figure 11. Additional circuitry for the control panel was also designed and installed. Since the system controls the tension in the vertical cable attached to the

model it was theoretically possible to extend the scale flight envelope slightly by artificially adjusting the weight or apparent "g" acting on the model over a limited range.

Augmentation of height data into feedback loops was attempted to produce a height hold autopilot which would enable greater vertical freedom in the flight testing of the model on the rig. A by-product of this activity was that the equation of motion in the wind tunnel model needed to be extended to include the feedback loops as appropriate. Although the control system appeared to work well in its basic form it needed further adjustment and could not be used in the present research programme. However, sufficient progress was made to indicate that the system looks quite feasible in practice and is a suitable candidate for future development work on the dynamic facility.

A number of other modifications were made to the aircraft model, the support rig and ECU. Changes to the model included a complete strip down to repair damages, inspect control surface hinges and to re-surface the model with an appropriate finish. The number of input and output channels interconnecting the model and rig with the ECU was expanded and the power supplies in the ECU modified to improve overall performance. A good reference manual for the rig was also produced.

(v) Current developments.

Within the College of Aeronautics further development of the artificial 'g' system is planned. Work is also well underway for the replacement of the analogue ECU by an entirely digital system based on a standard 486 personal computer.

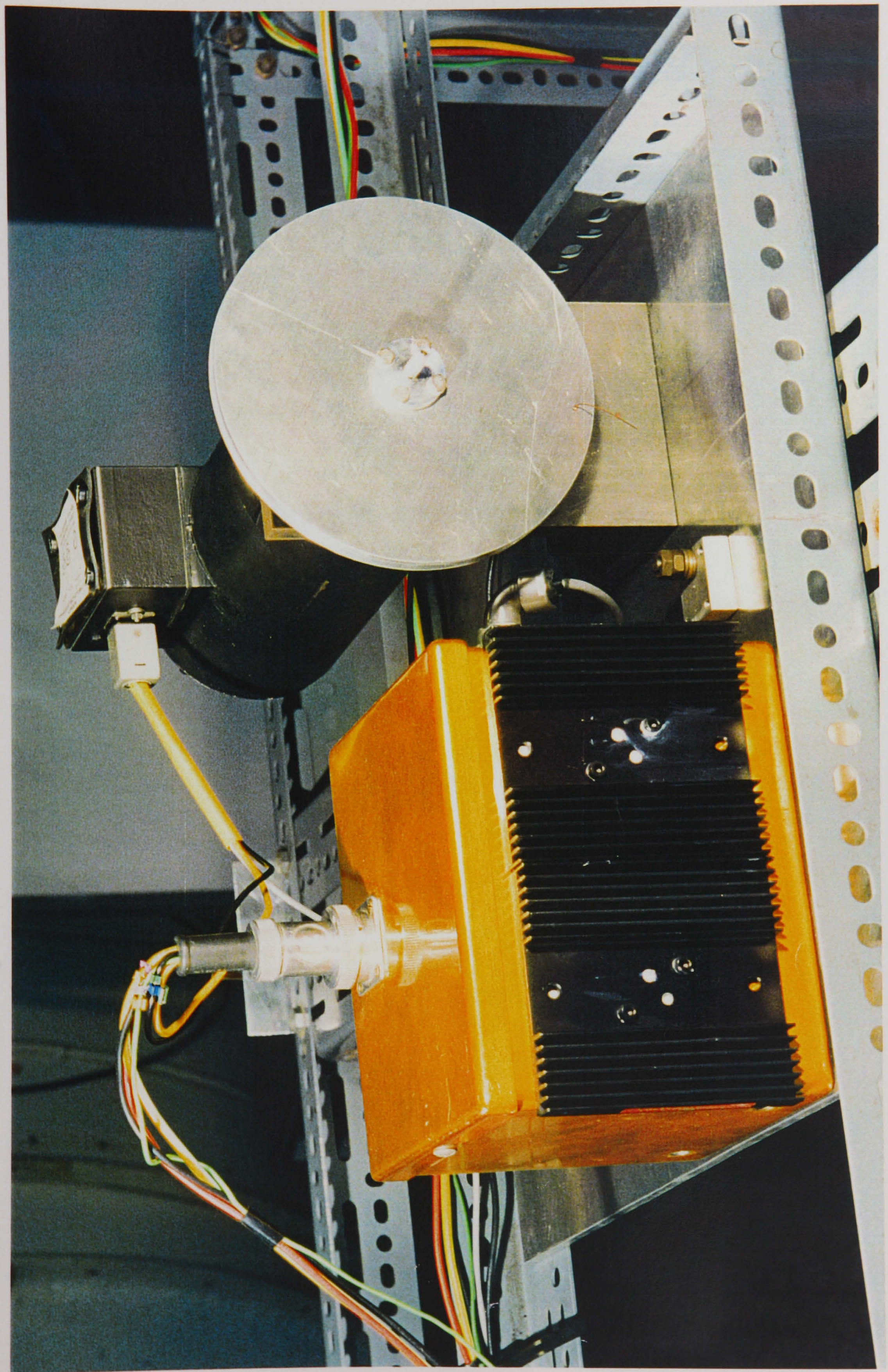

FIGURE 11: SERVO CONTROLLED PULLEY SYSTEM FOR VARYING "g"

CHAPTER 6:

PRELIMINARY EXPERIMENTAL PROGRAMMES

6.0 PRELIMINARY EXPERIMENTAL PROGRAMMES.

This chapter describes the preliminary calibration experiments which were undertaken using the Hawk model, namely control surface and attitude angle calibrations. Longitudinal static stability evaluations and measurements of the moments of inertia of the model were also undertaken; these are described in the two chapters which follow.

6.1 Model control surface calibrations.

The control surfaces of the Hawk model are driven by three electrical servo actuators mounted inside the fuselage. To calibrate the aileron, elevator and rudder control surfaces the model was placed on a level bench with the leading and trailing edges of the wing in a straight and level reference attitude. A pointer was attached to the port aileron and the control surface positioned at various angles with respect to a marked scale drawn on some polar graph paper. For each angle the input and output voltages of the servo were recorded. Due to backlash in the control surface linkages, it was necessary to record two sets of calibration data, one for each direction of movement.

A similar procedure was carried out for the elevator and rudder and calibration graphs were plotted for each control surface, see Figures 12 to 15. It was encouraging to see linear relationships over large proportions of the input and output voltage ranges. Calibration equations were estimated using formulae in the Harvard Graphics software package. (N.B. the non-linear extremes of the servo voltage graphs were ignored when fitting the straight lines.)

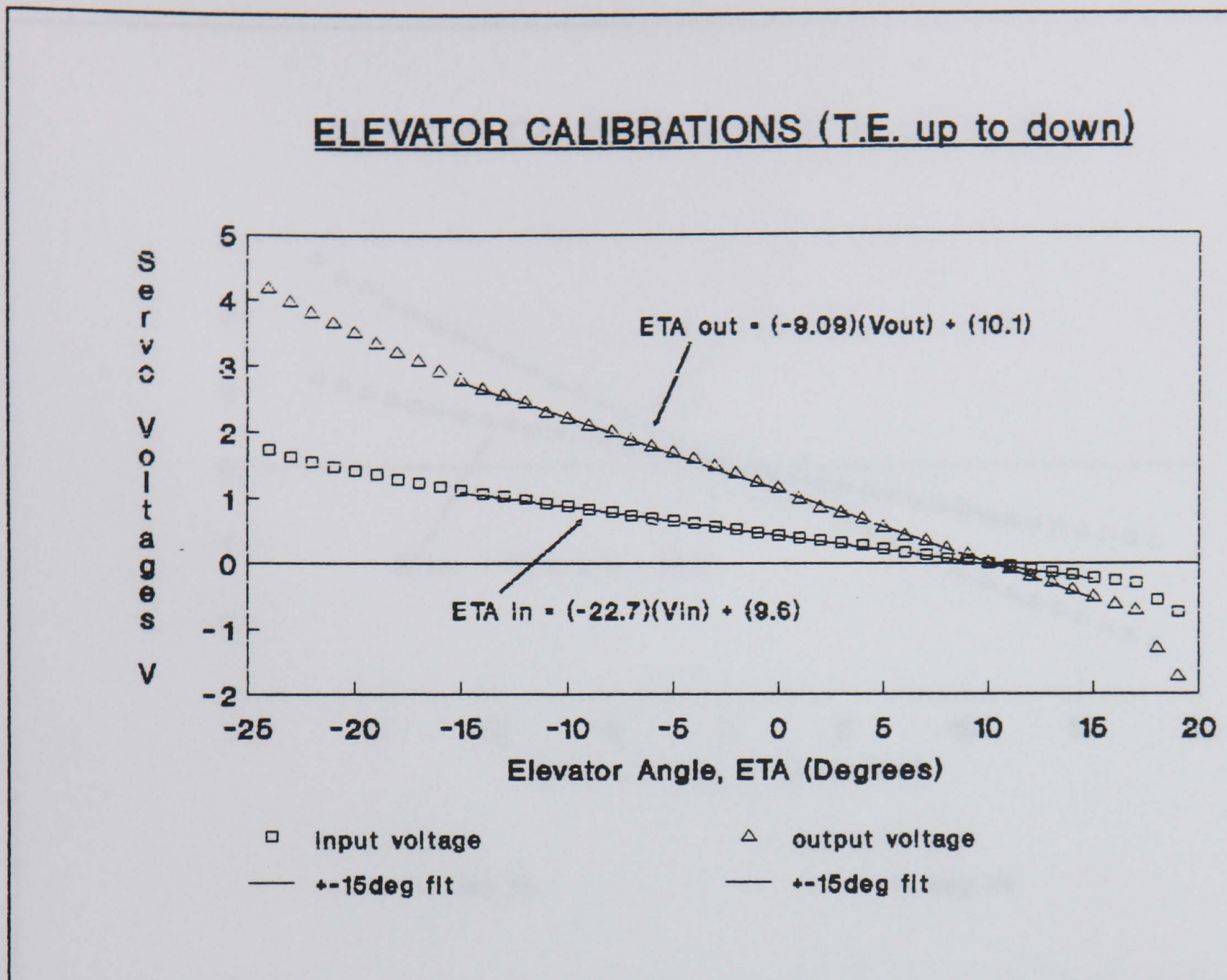

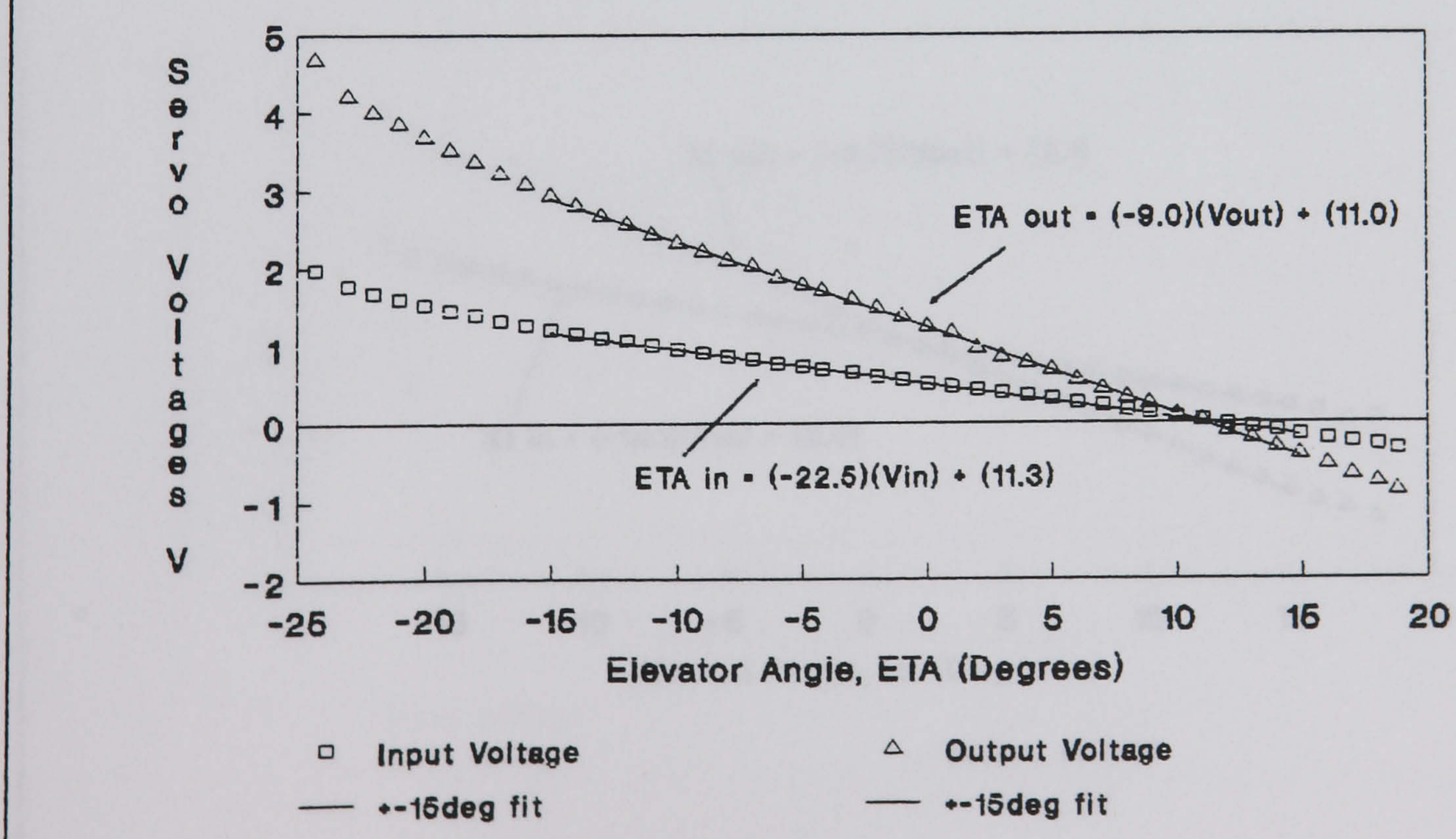

FIGURE 12: ELEVATOR CONTROL SURFACE CALIBRATIONS.

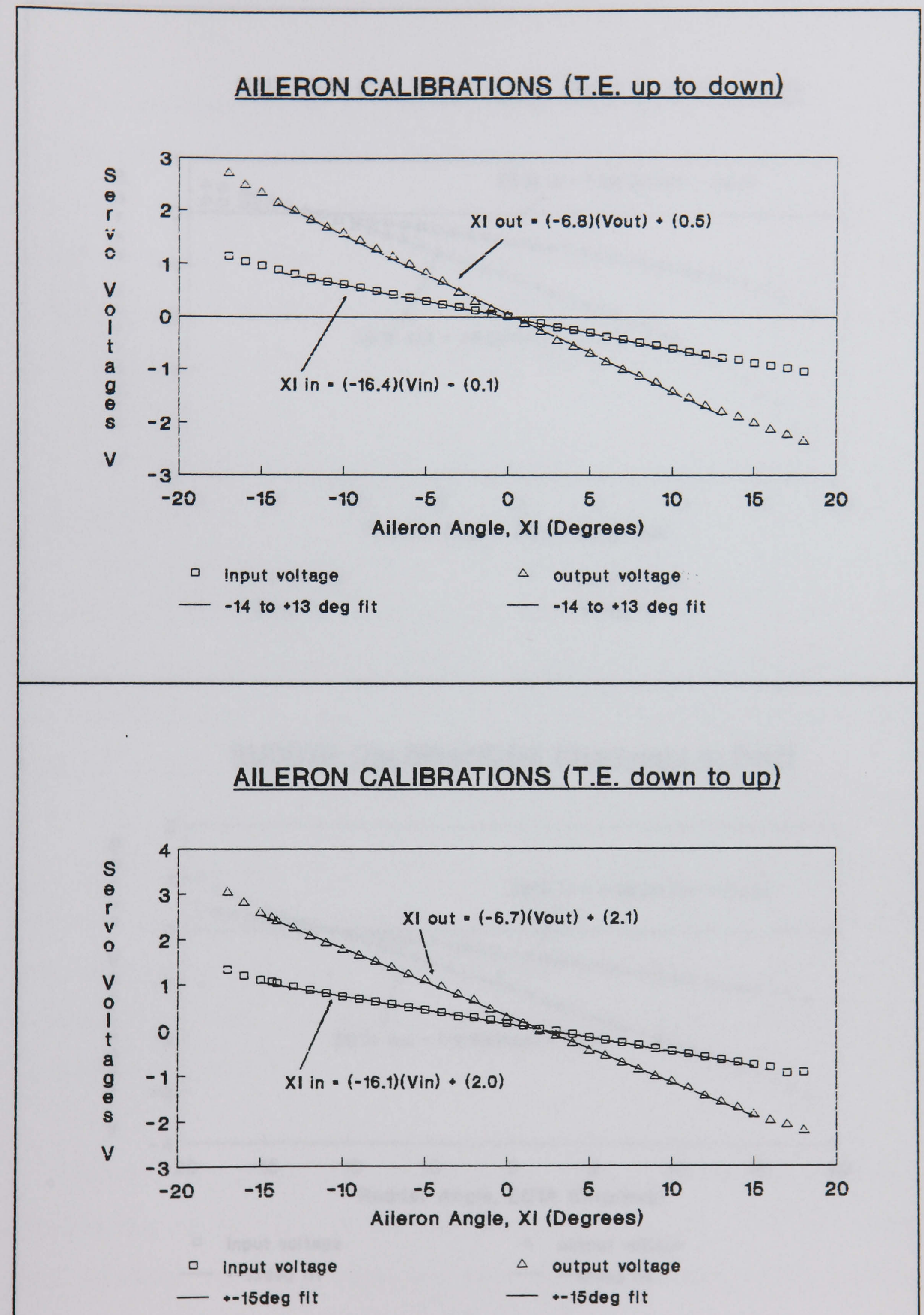

FIGURE 13: AILERON CONTROL SURFACE CALIBRATIONS.

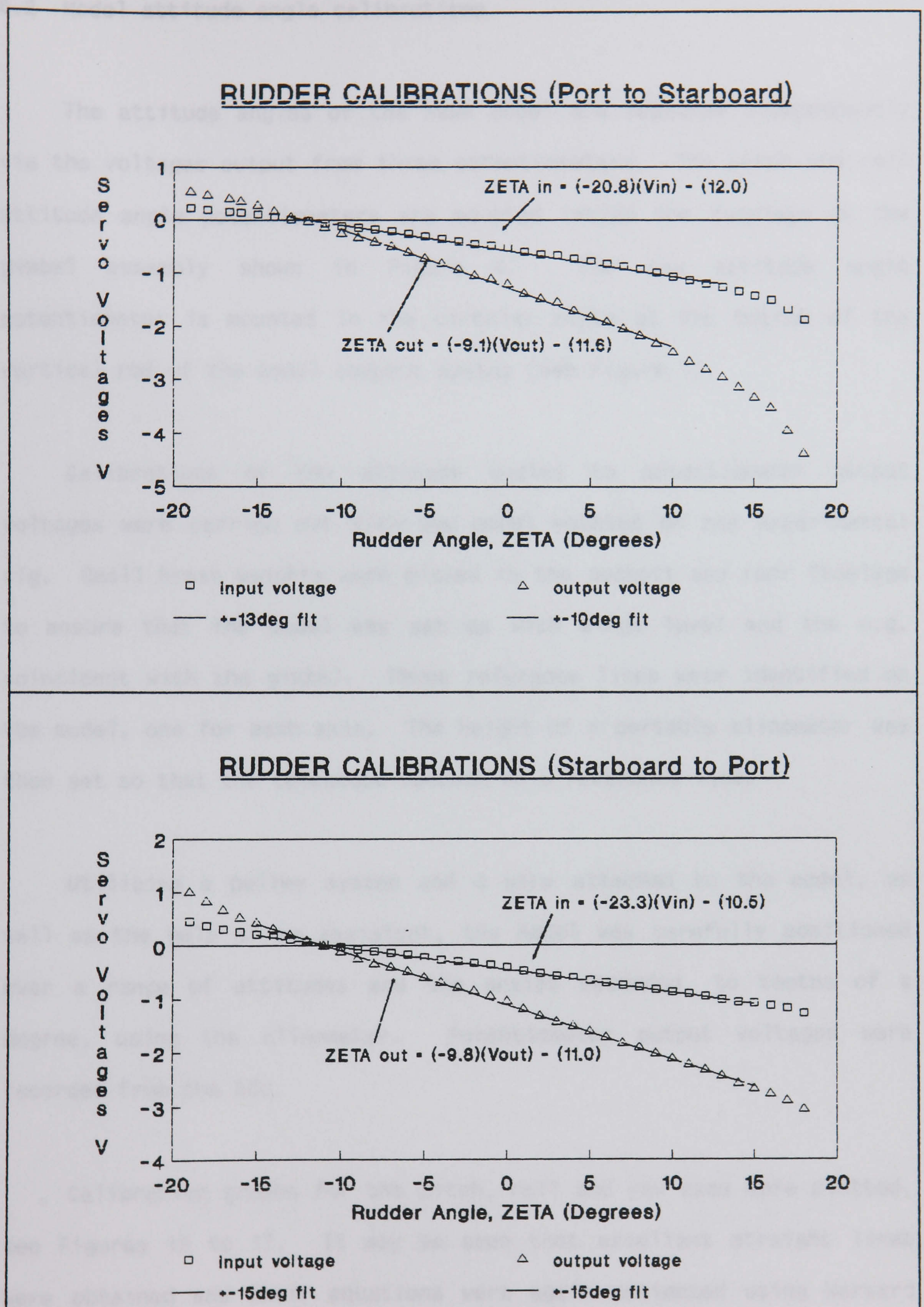

FIGURE 14: RUDDER CONTROL SURFACE CALIBRATIONS.

6.2 Model attitude angle calibrations.

The attitude angles of the Hawk model are measured independently via the voltages output from three potentiometers. The pitch and roll attitude angle potentiometers are mounted inside the fuselage on the gimbal assembly shown in Figure 4. The yaw attitude angle potentiometer is mounted in the circular plate at the bottom of the vertical rod of the model support system (see Figure 1).

Calibrations of the attitude angles to potentiometer output voltages were carried out with the model mounted on the experimental rig. Small brass weights were placed in the cockpit and rear fuselage to ensure that the model was set up with wings level and the c.g. coincident with the gimbal. Three reference lines were identified on the model, one for each axis. The height of a portable clinometer was then set so that the telescope focused on a reference line.

Utilising a pulley system and a wire attached to the model, as well as the help of an assistant, the model was carefully positioned over a range of attitudes and the angles recorded, to tenths of a degree, using the clinometer. Potentiometer output voltages were recorded from the ECU.

Calibration graphs for the pitch, roll and yaw axes were plotted, see Figures 15 to 17. It may be seen that excellent straight lines were obtained and their equations were again estimated using Harvard Graphics.

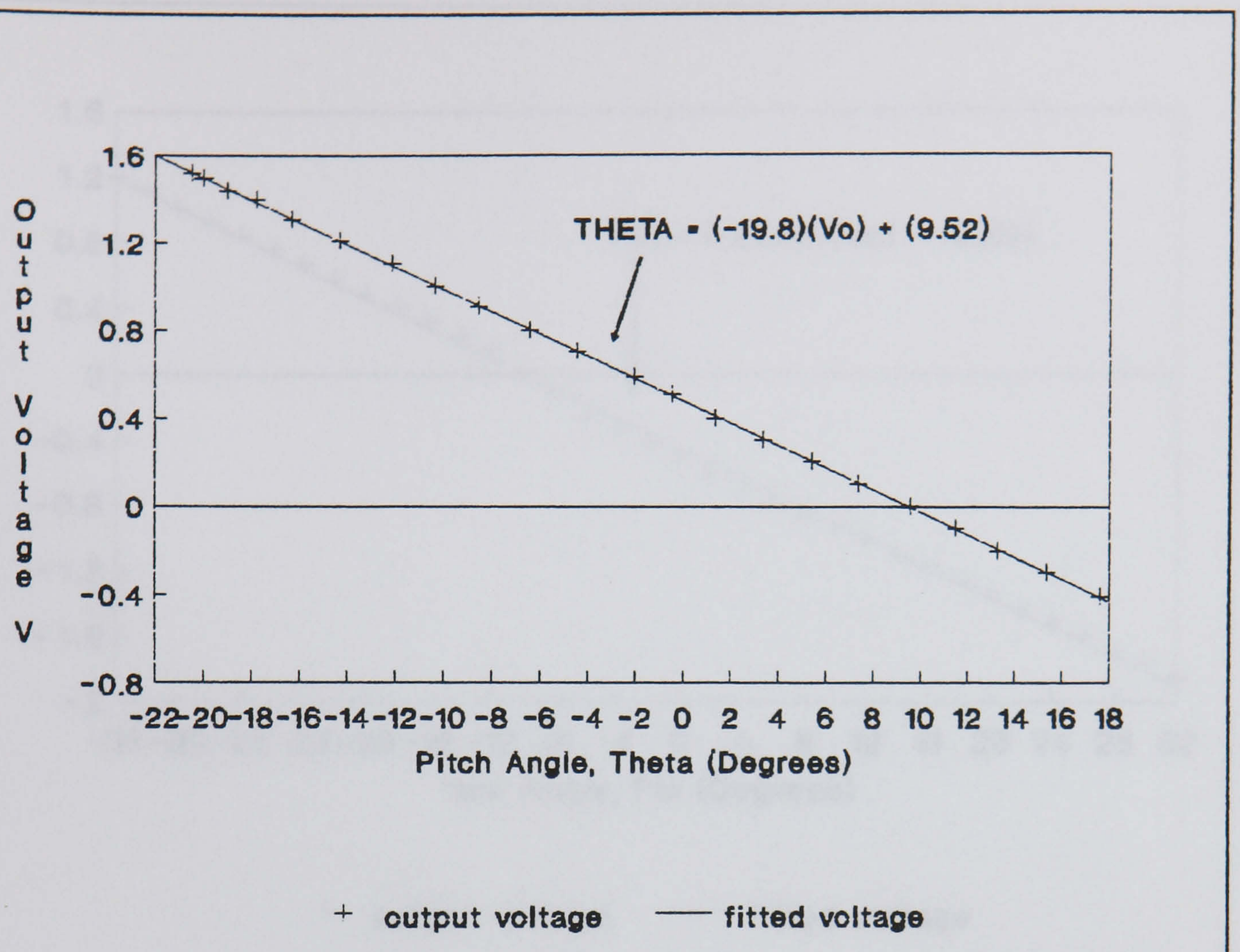

FIGURE 15: PITCH ATTITUDE ANGLE CALIBRATION

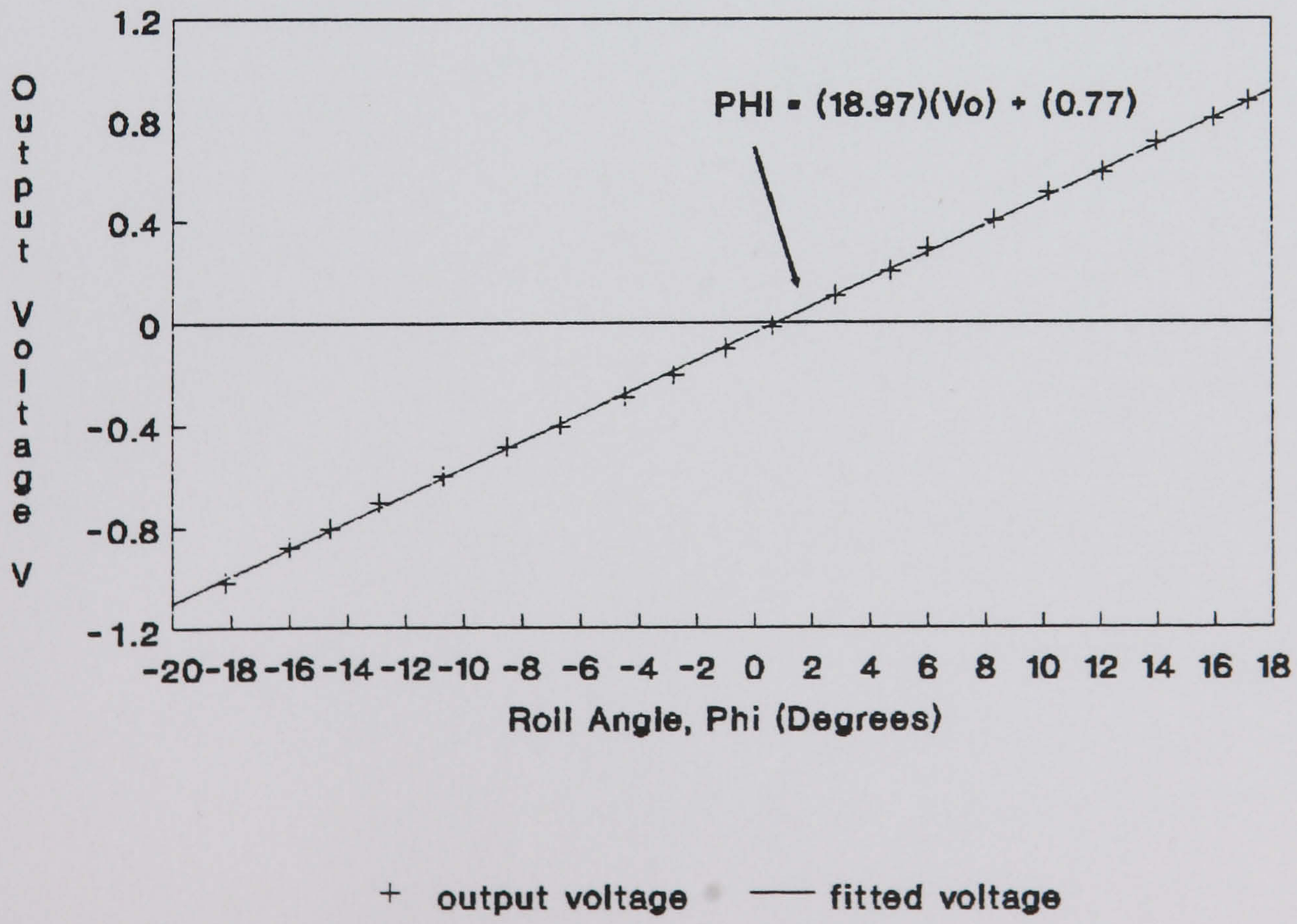

FIGURE 16: ROLL ATTITUDE ANGLE CALIBRATION

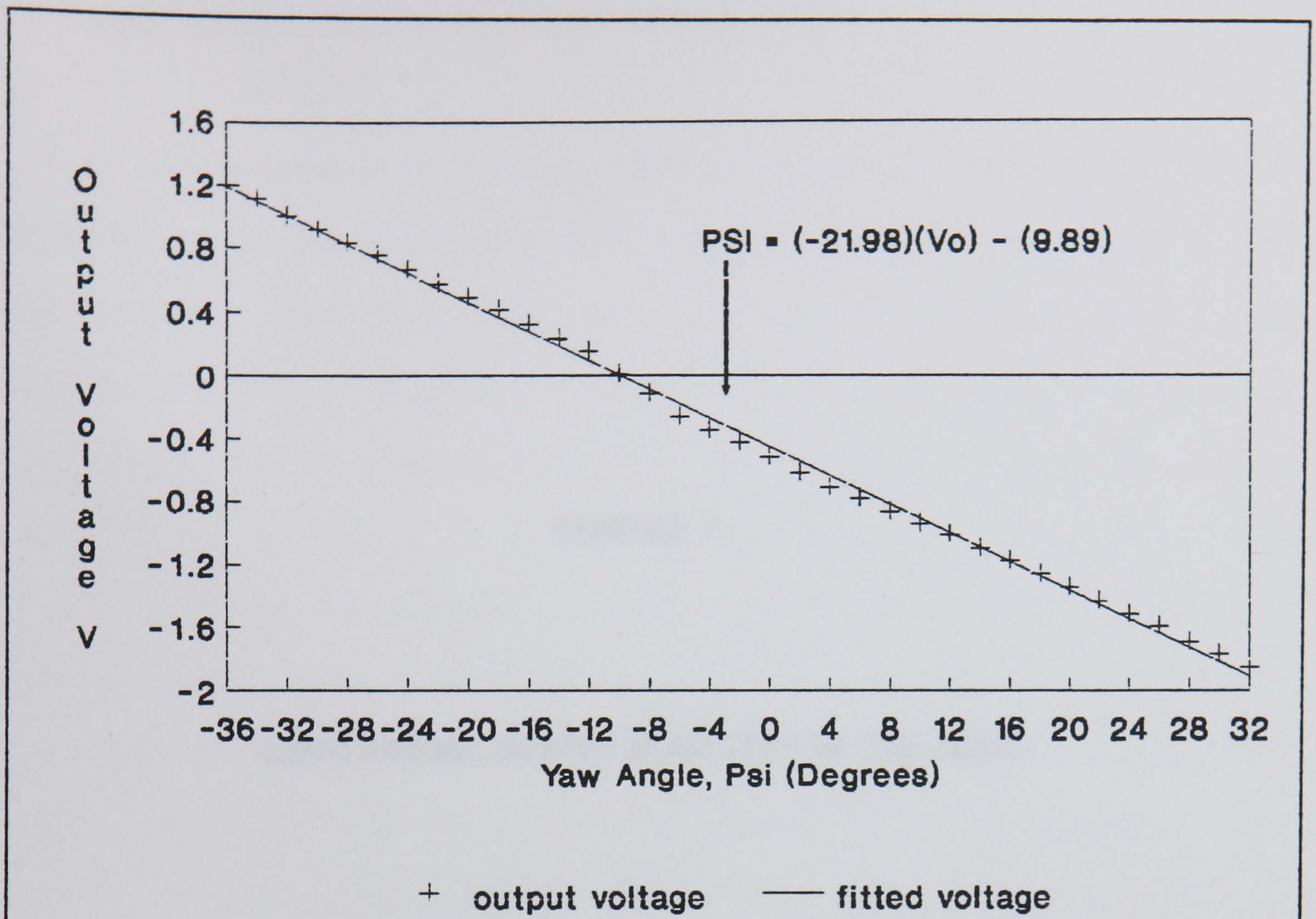

FIGURE 17: YAW ATTITUDE ANGLE CALIBRATION

CHAPTER 7:

LONGITUDINAL STATIC STABILITY OF THE MODEL

7.0 LONGITUDINAL STATIC STABILITY OF THE MODEL

It was necessary to evaluate the longitudinal static stability of the model as it had previously been difficult to trim when flown in the wind tunnel. That fact that the model was difficult to control is somewhat surprising as the full scale BAe Hawk is a stable aircraft and a correctly scaled model should also be stable. Attempts to secure stability of the model by moving the c.g. forward did not help the situation in any way and only changed the tailplane angle required to trim the model. The reason for this stability discrepancy was thought to be due to the gimbal pivot being positioned too far aft in the Hawk model. This suspicion was successfully demonstrated experimentally and details of the analysis of the longitudinal static stability of the model are presented in the following sections.

7.1 Hawk model geometry.

A schematic plan view of the geometry of the wing of the Hawk model is presented in Figure 18. A fixed reference line was taken between the two points where the leading edges of the wing intercept the model fuselage. The geometric mean chord ($\bar{c}$) is assumed to be approximately equal to the aerodynamic mean chord ($\bar{\bar{c}}$). Further, for convenience, the location of the reference line for the measurement of $\bar{\bar{c}}$ was moved forward to start at the leading edge reference line and the distance aft from this will be referred to as $\bar{\bar{c}}_{ref}$ from now on. Definitions of important positions and margins on the Hawk are given in the next section.

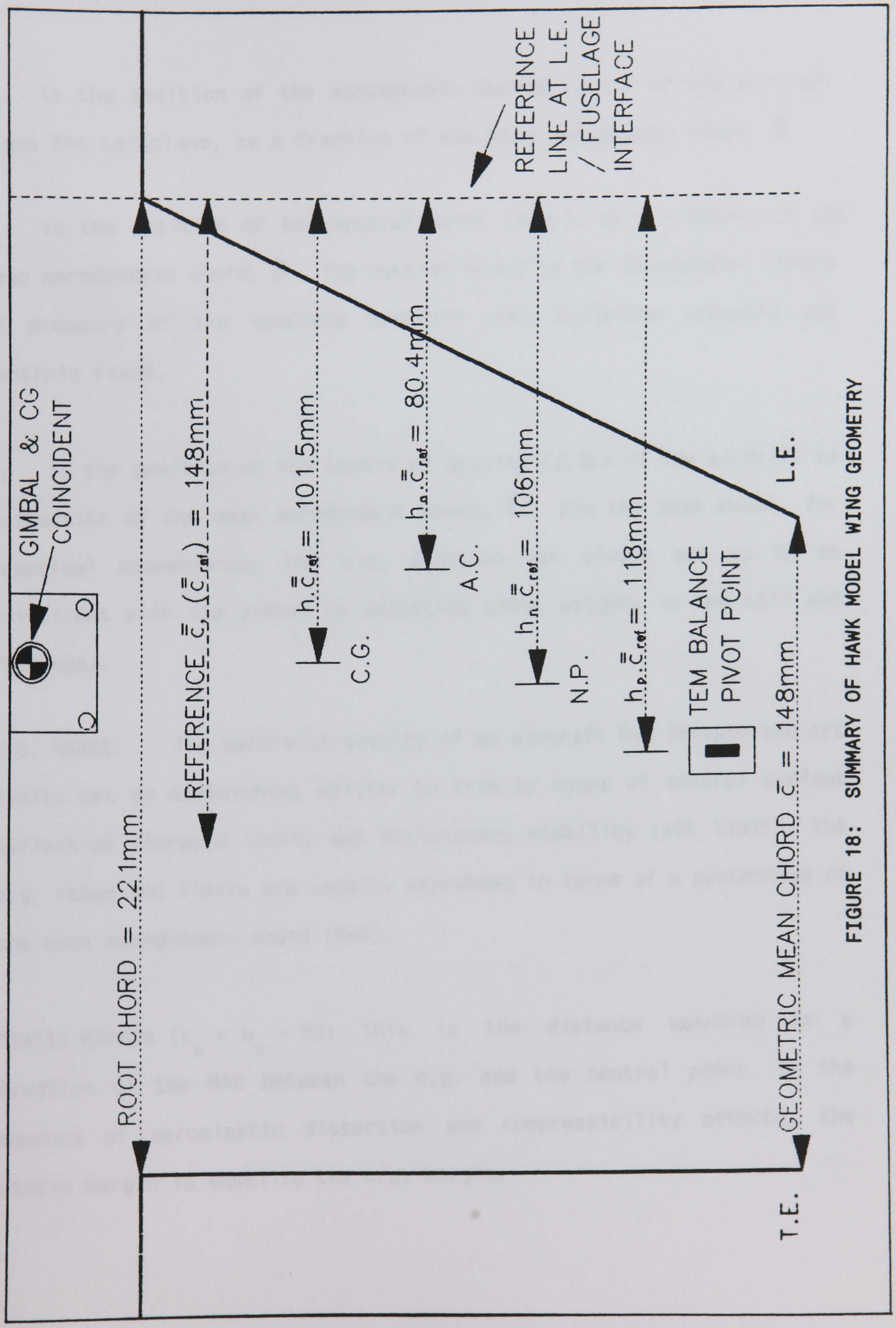

FIGURE 18: SUMMARY OF HAWK MODEL WING GEOMETRY

7.2 Relevant definitions.

h_o: is the position of the aerodynamic centre (*A.C.*) of the aircraft minus the tailplane, as a fraction of the mean aerodynamic chord, $\bar{\bar{c}}$.

h_n: is the position of the neutral point (*N.P.*), as a fraction of the mean aerodynamic chord, $\bar{\bar{c}}$. The neutral point is the aerodynamic centre of pressure of the complete aircraft with tailplane attached and controls fixed.

h: is the position of the centre of gravity (*C.G.*) of the aircraft as a fraction of the mean aerodynamic chord, $\bar{\bar{c}}$. (On the Hawk model, for practical convenience, the c.g. position was always set up to be coincident with the gimbal by adjusting brass weights in the tail and fuselage).

C.G. RANGE: The centre of gravity of an aircraft has forward and aft limits set by diminishing ability to trim by means of control surface deflection (forward limit) and diminishing stability (aft limit). The c.g. range and limits are usually expressed in terms of a percentage of the mean aerodynamic chord (MAC).

STATIC MARGIN ($K_n = h_n - h$): This is the distance measured as a fraction of the MAC between the c.g. and the neutral point. In the absence of aeroelastic distortion and compressibility effects, the static margin is equal to the c.g. margin.

TEM PIVOT POINT: The TEM balance is a piece of equipment used in the measurement of the lift force, drag force and pitching moment of the model. The model is mounted on the balance via three struts which are fixed to the rear fuselage and each wing. The position of the two wing struts are referred to as the TEM pivot point (i.e. $h_p \bar{\bar{c}}$).

7.3 Static stability experiments.

Experiments were undertaken to assess the longitudinal static stability characteristics of the model. The experimental objectives were:

1. To estimate the variation of mean downwash angle at the tailplane with incidence.

2. To estimate the tailplane lift curve slope.

3. To estimate the location of the aerodynamic centre for the wing and body only.

4. To derive the lift trim curve of the model aircraft.

5. To predict the stick fixed static c.g. margin.

6. To establish the relationship between the gimbal centre and stability.

The experiments also provided an opportunity to obtain aerodynamic data from which other useful information could be derived (see Chapter 8).

The position of the c.g. was in front of the TEM pivot and was arranged to coincide with the position of the gimbal centre inside the model fuselage. When experimental readings of the pitching moment were taken they were related to the position h_p of the pivot point of the model on the TEM balance. Therefore, taking moments about the TEM balance pivot point the following expression is obtained:

$$M_p = M_o + L_{WB}(h_p - h_o)\bar{\bar{c}}_{ref} - mg(h_p - h)\bar{\bar{c}}_{ref} - L_T\{l_t - (h_p - h)\bar{\bar{c}}_{ref}\} \qquad [7.1]$$

(M_o: zero lift moment; $L_{WB}(h_p - h_o)\bar{\bar{c}}_{ref}$: wing/body; $mg(h_p - h)\bar{\bar{c}}_{ref}$: aircraft weight moment; $L_T\{l_t - (h_p - h)\bar{\bar{c}}_{ref}\}$: tail contribution)

For the aircraft to be in a trimmed position, the sum of all the moments about the pivot point must be zero, i.e. $M_p = 0$ must be true. This will then give the tailplane angle, η, required to trim the aircraft.

For stability about "$_p$", $dM_p/dC_L < 0$ is required. Equation [7.1], implies that the stability is not influenced by M_o or the term $mg(h_p - h)$. The c.g. position only influences the tailplaneangle required to trim and it is the position of the TEM pivot which is important. A stable trim of the aircraft can only be achieved if the pivot point on the TEM is ahead of the neutral point of the model.

For the tail-less aircraft $$dC_{Mp}/dC_L = h_o - h \qquad [7.2]$$

and for the whole aircraft $$dC_{Mp} / dC_L = h_p - h_n \qquad [7.3]$$

Thus if experiments are undertaken to estimate dC_{Mp} / dC_L and the reference point h_p is known, it is possible to then estimate h_o and h_n. A number of experimental procedures were carried out to calculate the values of the terms in [7.2] and [7.3]. The first requirement was to calibrate the TEM balance, as described in the next section.

7.3.1 Calibration of the TEM balance.

When the model aircraft was mounted on the balance and the wind tunnel run, it was possible to obtain measurements of the lift force (L), drag force (D) and pitching moment (P) of the model in terms of three output voltages. The balance could be adjusted to vary the incidence of the model over the range -10 to 40°. The load ranges of the balance are:

COMPONENT	LOAD RANGE	ACCURACY
Lift	0-10 Kg	25 gm
Drag	0-3.5 Kg	10 gm
Pitch Moment	0-175 gm.m	1.75 gm.m

To calibrate the balance however, the model was removed and a special "T-shaped" bar attached to the balance struts. In three separate experiments to simulate lift and drag forces and pitching moments known weights were hung from the balance using fishing line and the output voltages V_L, V_D and V_P recorded as appropriate.

To discover whether there was any difference in balance readings when the wind tunnel is run, values of the V_L, V_D and V_P output voltages were recorded both before and after a number of wind tunnel runs. The figures were found to drift considerably and if the balance was left for a few minutes after running the tunnel, it appeared that the power supply and transducers of the balance would "warm up" and subsequently change the wind-off values.

To try to minimise the variations in wind-on and wind-off readings, the whole balance was lowered to reduce the proportion of the balance in the wind stream. Also, a large plywood fairing was placed in front of the power supply to try and minimise the cooling effect of the tunnel air stream. These measures led to better before and after wind-off output figures. It was also decided to take wind-off values of the outputs as soon as the air flow stopped after switching off the wind tunnel as these should be closest to the actual "zero" outputs of the balance when readings are taken with the wind on. When the tunnel was switched off, a wand with wool was placed in the air stream to detect when the airflow had stopped.

Lift force calibration:

Increasing numbers of weights were hung midway along the bar connecting the two wing struts to give a negative lift force and V_L recorded. The calibration graph was obtained and found to be linear with a gradient of -213.48 N/V (Figure 19).

Drag force calibration:

Fishing line was run horizontally from the bar between the wing struts and over a pulley at the rear of the balance. Various weights were hung from the rear of the apparatus to simulate the drag force and V_D recorded. The linear calibration graph obtained had a slope of -83.56 N/V (Figure 19).

Pitching moment calibration:

To produce a positive pitch-up moment for the balance, weights were hung 5 cm back along the T-bar from the wing strut connection bar. V_P was recorded for various weights and the pitching moment calculated. The linear calibration graph obtained had a slope of 7.39 Nm/V (Figure 19).

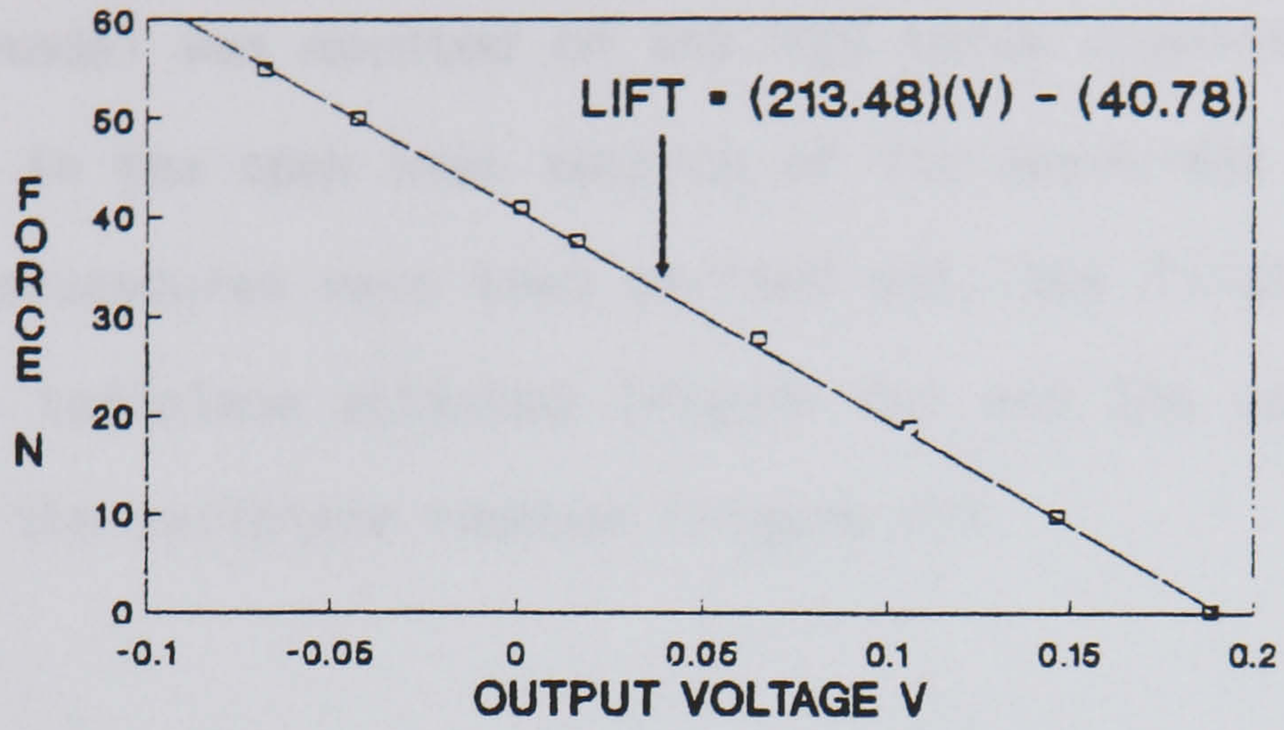

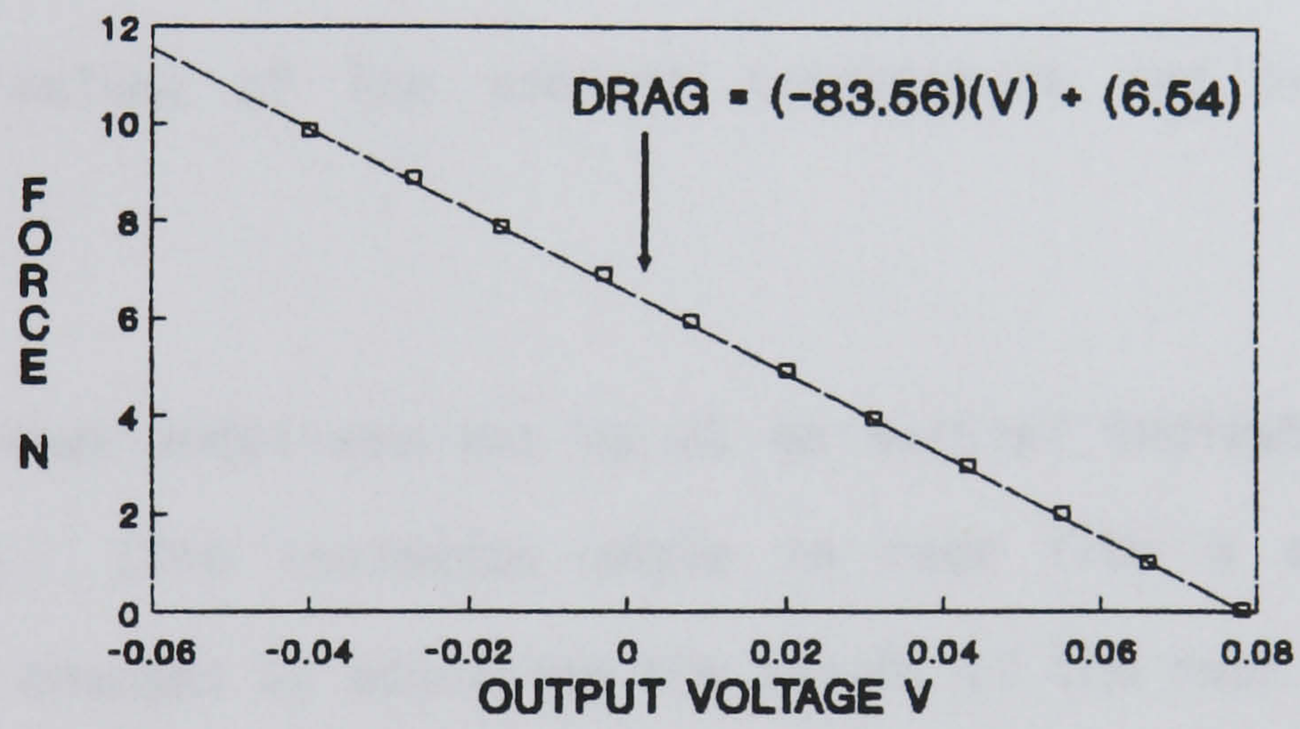

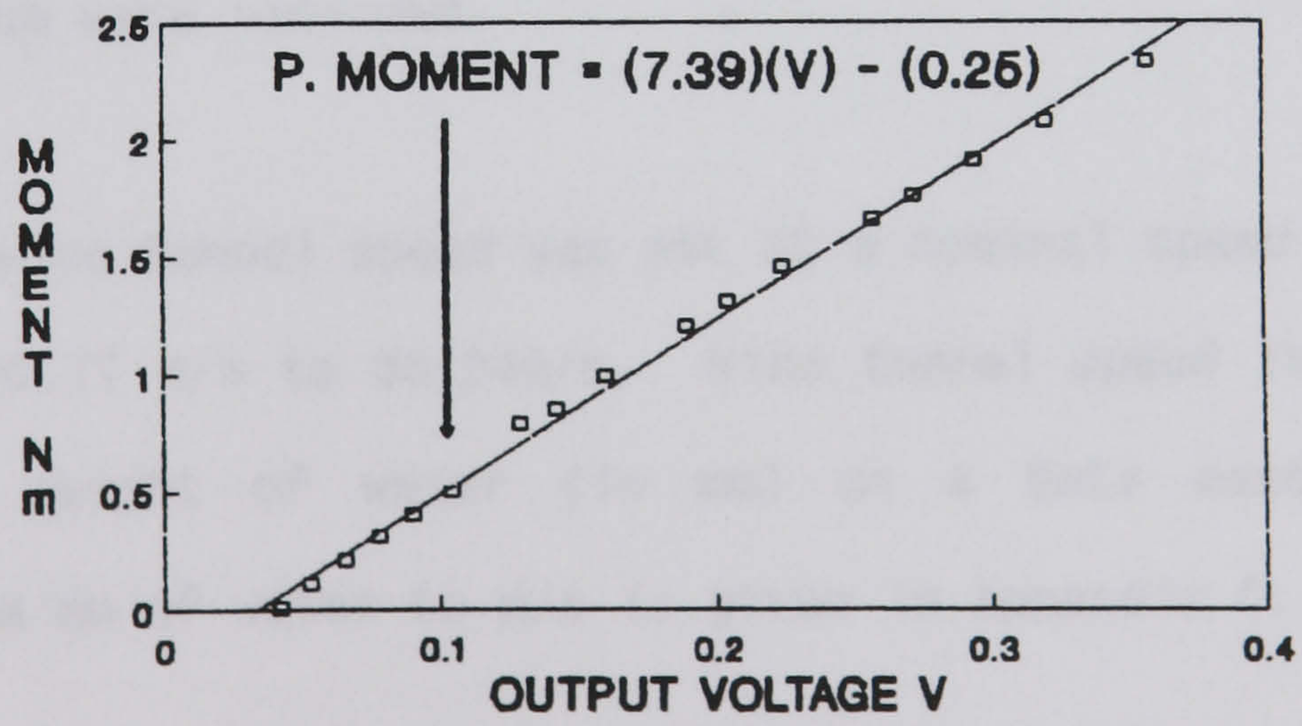

FIGURE 19: TEM BALANCE CALIBRATIONS.

7.3.2 Measurement of Hawk model forces and moments.

The Hawk model was mounted on the TEM three component force and moment balance in the open test section of the Weybridge wind tunnel. The following procedures were then carried out, the first set for the model with the tailplane attached (Figure 20) and the second set for the model with the tailplane removed (Figure 21).

SET 1 - TAIL ON.

Step 1: The values of the ambient temperature and pressure were recorded.

Step 2: The Hawk model was set up at an initial indicated incidence of -4 degrees. (The incidence angle is read from a scale on the balance and is changed by adjusting the height of the rear strut.

Step 3: The wind-off lift, drag and pitching moment voltage outputs from the balance were recorded.

Step 4: The wind tunnel speed was set at a nominal speed somewhere in the range of 30.77 m/s to 33.24m/s. Wind tunnel speed is measured in terms of the height of water (in mm) on a Betz manometer. The conversion from mm of water to m/s is given in Appendix C.

Step 5: The elevator control surface (i.e. the tailplane) was set at angles of -5°, 0°, 2°, 5° and 10° and the values of V_L, V_D and V_P

recorded for each tailplane setting.

Step 6: The wind tunnel was then stopped and the wind-off values of V_L, V_D and V_P recorded again.

Step 7: Steps 3-6 were repeated for a various aircraft incidences ranging from -2° to 14°.

Step 8: Finally, for model incidences of 2° and 4°, values of V_L, V_D and V_P were recorded for a number of tailplane angles which ranged from -14° to $+14^\circ$ in 2 degree steps.

SET 2 - TAIL-OFF

The tailplane of the Hawk model was removed and the following steps carried out:

Step 1: For a range of incidences between -4° and $+14^\circ$, values of V_L, V_D and V_P were recorded for wind tunnel speeds between 30.77 m/s and 33.24m/s

Step 2: The wind-off values of V_L, V_D and V_P were recorded before and after each tunnel run with a particular model incidence.

SET 3 - DRAG TARE CORRECTION.

The drag tare correction for the TEM balance was estimated by removing the model from the balance and connecting each strut support with piano wire. The wind-on value of V_D was then recorded.

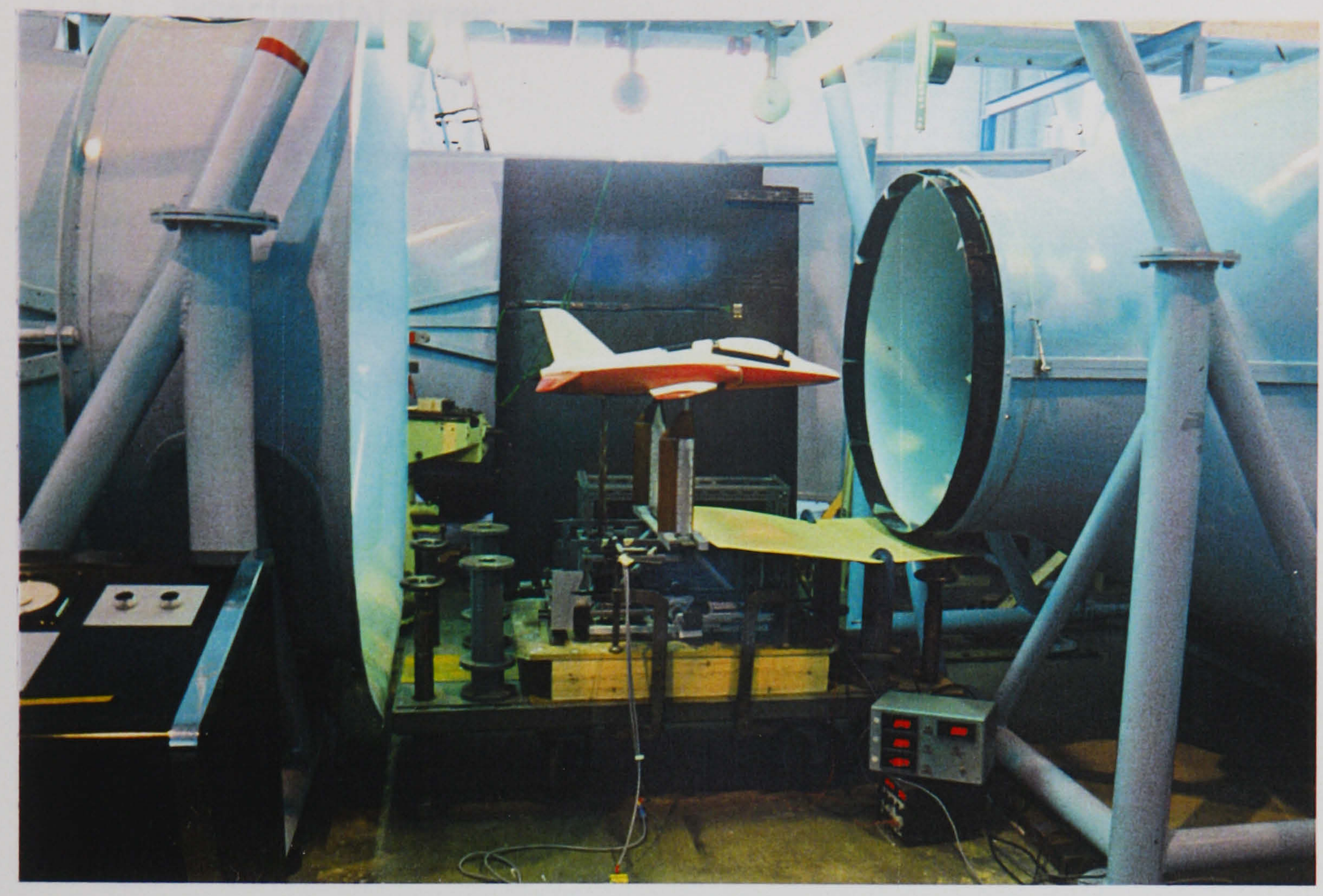

FIGURE 20: HAWK MODEL ON THE TEM BALANCE, TAIL-ON

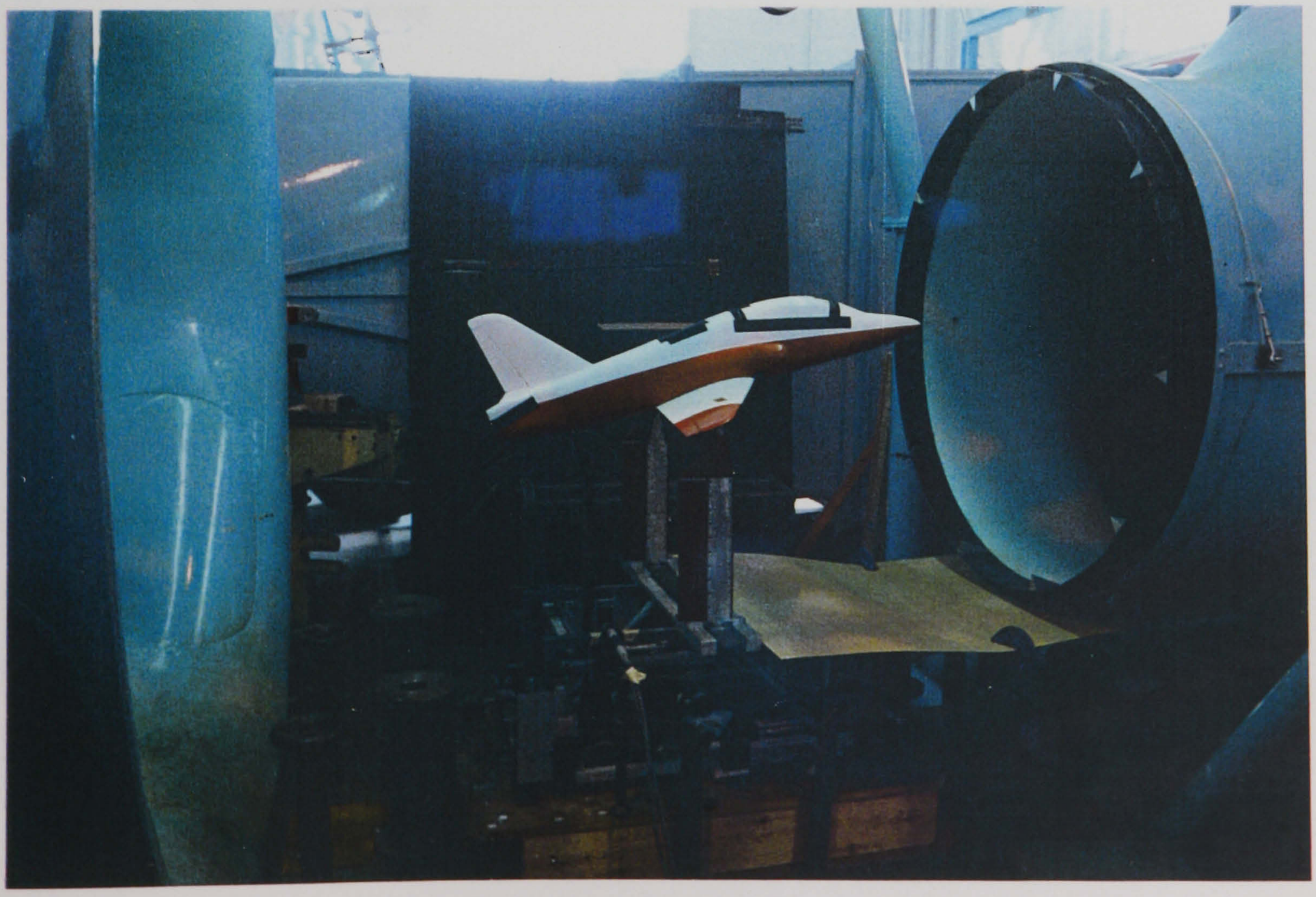

FIGURE 21: HAWK MODEL ON THE TEM BALANCE, TAIL-OFF

7.3.3 Experimental error.

Since the Weybridge tunnel is an open jet facility, the dynamic pressure correction can be assumed to be negligible. However, there were two main sources of experimental error arising in this series of experiments which were considered. The first comprises corrections which should be applied to α and C_D as follows:

(i) $$\alpha_{true} = \alpha_{measured} + \delta\alpha \qquad [7.4]$$

The incidence correction, $\delta\alpha$ is given by

$$\delta\alpha = \sigma.(S/C).C_L \qquad [7.4.1]$$

where

C = cross sectional area of wind tunnel

S = wing area

σ = mean wing interference factor

(ii) $$C_{D_{true}} = C_{D_{measured}} + \sigma.(S/C).C_L^2 \qquad [7.5]$$

The second uncontrollable experimental error arose because the outputs of the TEM balance did not always have the same before and after wind-off readings. Unfortunately the pitch outputs varied the most and often sets of experiments were repeated to try and minimise the difference in outputs and to check for the repeatability of readings.

7.4 Analysis of longitudinal static stability data.

The following sections detail the steps followed in the analysis of the longitudinal static stability of the model. A number of basic assumptions were made for the analysis techniques used. These assumptions, which are only approximately true for the case of an aircraft in a power-off low speed glide, are as follows:

1. The aircraft structure is completely rigid.

2. Compressibility effects are negligible.

3. The non-dimensional lift, drag and pitching moment coefficients are independent of forward speed.

4. There is no vertical displacement of the C.G. from the wing chord line.

5. Tailplane lift is small in comparison with wing lift and the movement of the tailplane centre of pressure is negligible.

6. The flight path is approximately horizontal.

7.4.1 Derivation of C_L, C_D and C_P.

A computer program exists in the College of Aeronautics for the analysis of data from a similar experiment using a 1/22.5 th scale model of the D.H. Dove 104 mounted on the TEM balance. A copy of the program was suitably changed to include relevant Hawk model data (defined in Appendix C) and the new TEM balance calibration information. The program was also changed to allow the tailplane angle

to be entered as well as just the normal aircraft incidence angle. Further changes allowed the balance wind-off output voltage to be entered for every reading taken, instead of the wind-off output being assumed constant throughout the experiment. A later change to the program was also made to allow for the calculation of C_M at different positions on the model. To calculate the lift, drag and pitching moment coefficients, the program carried out the following operations on the balance voltage data:

1. Each reading is corrected for the zero wind-off balance output.

2. The drag tare correction is taken away from each drag voltage.

3. The voltages are converted to the lift (L) and drag (D) forces in Newtons and pitching moment (M) in Newton-metres.

4. The Betz manometer reading is converted from mm H_2O to the wind tunnel speed using the conversion detailed in Appendix C.

5. Finally, the non-dimensional lift, drag and pitching moment coefficients are calculated with reference to the TEM pivot point using the formulae:

$$C_L = L/0.5\rho V^2 S; \qquad C_D = D/0.5\rho V^2 S; \qquad C_M = M/0.5\rho V^2 S\bar{\bar{c}} \qquad [7.6]$$

7.4.2 Mean downwash at tailplane.

The effective angle of incidence of the tailplane is determined by the degree of downwash generated by the main wing. Figure 22 shows that the relationship between the downwash angle ε, tailplane angle of

incidence α_t, tailplane control surface angle η and angle of incidence of the wing α_w may be expressed by:

$$\alpha_t = \alpha_w + \eta - \varepsilon \qquad [7.7]$$

A graph of C_{M_p} vs α_w was plotted for each tailplane angle α_t, Figure 23. On the same graph C_M vs α was plotted for the tail-off configuration. Points of intersection of the tail-on and tail-off graphs correspond to angles of zero tailplane lift. Furthermore, if the tailplane is a symmetrical section, it is aligned to the local flow angle (i.e. $\alpha_t = 0$) and thus gives a measure of the downwash. For each value of α_w the points of intersection of the curves were estimated from Figure 23 and the downwash angle estimated using:

$$\varepsilon = \alpha_w + \eta \qquad [7.8]$$

A plot of ε vs α_w was then made, Figure 24. Assuming a linear relationship, the rate of change of mean downwash angle with incidence was calculated and found to be:

$$d\varepsilon/d\alpha = 0.57 \qquad [7.9]$$

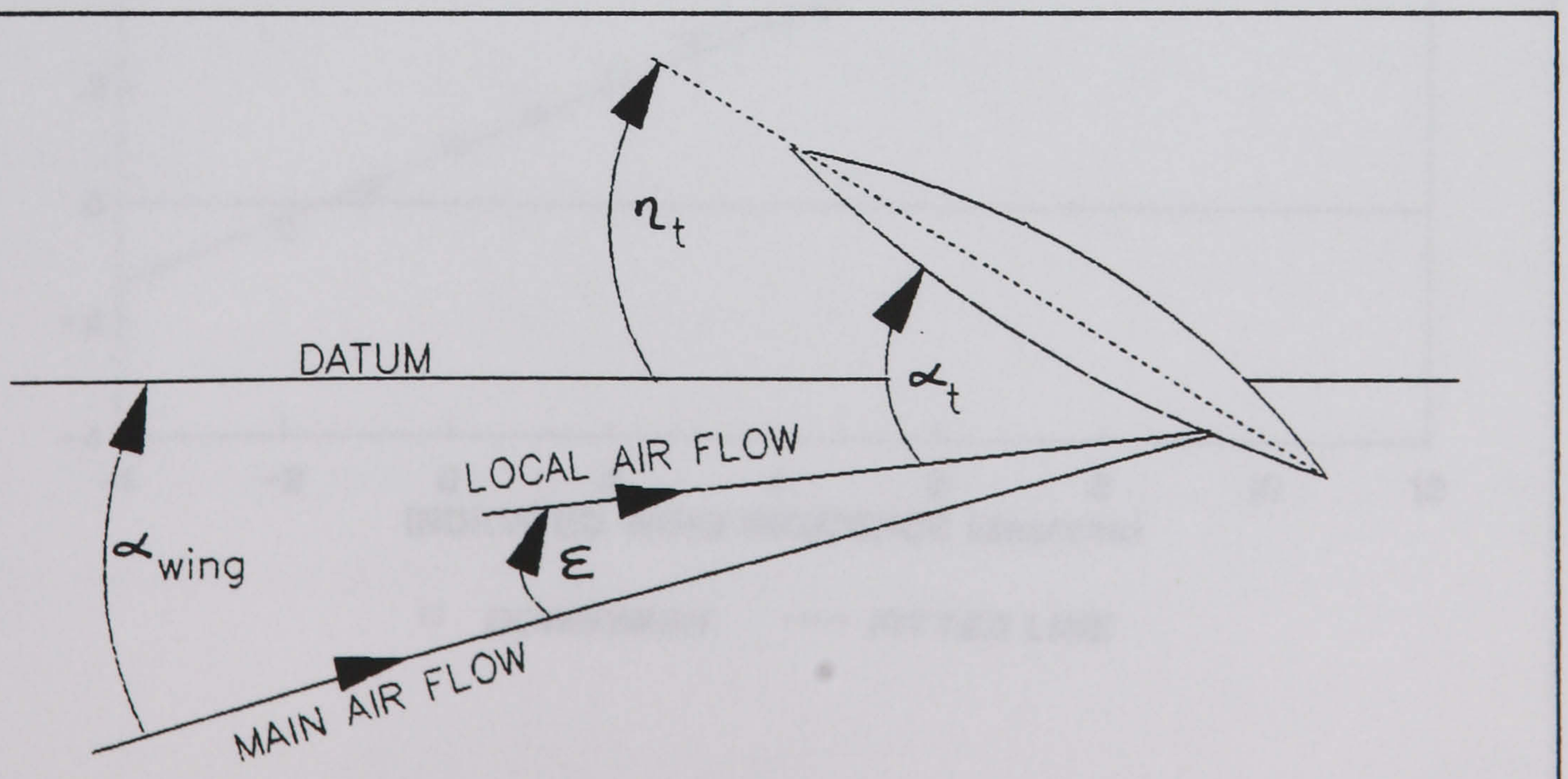

FIGURE 22: TAILPLANE ANGLE OF INCIDENCE AND DOWNWASH

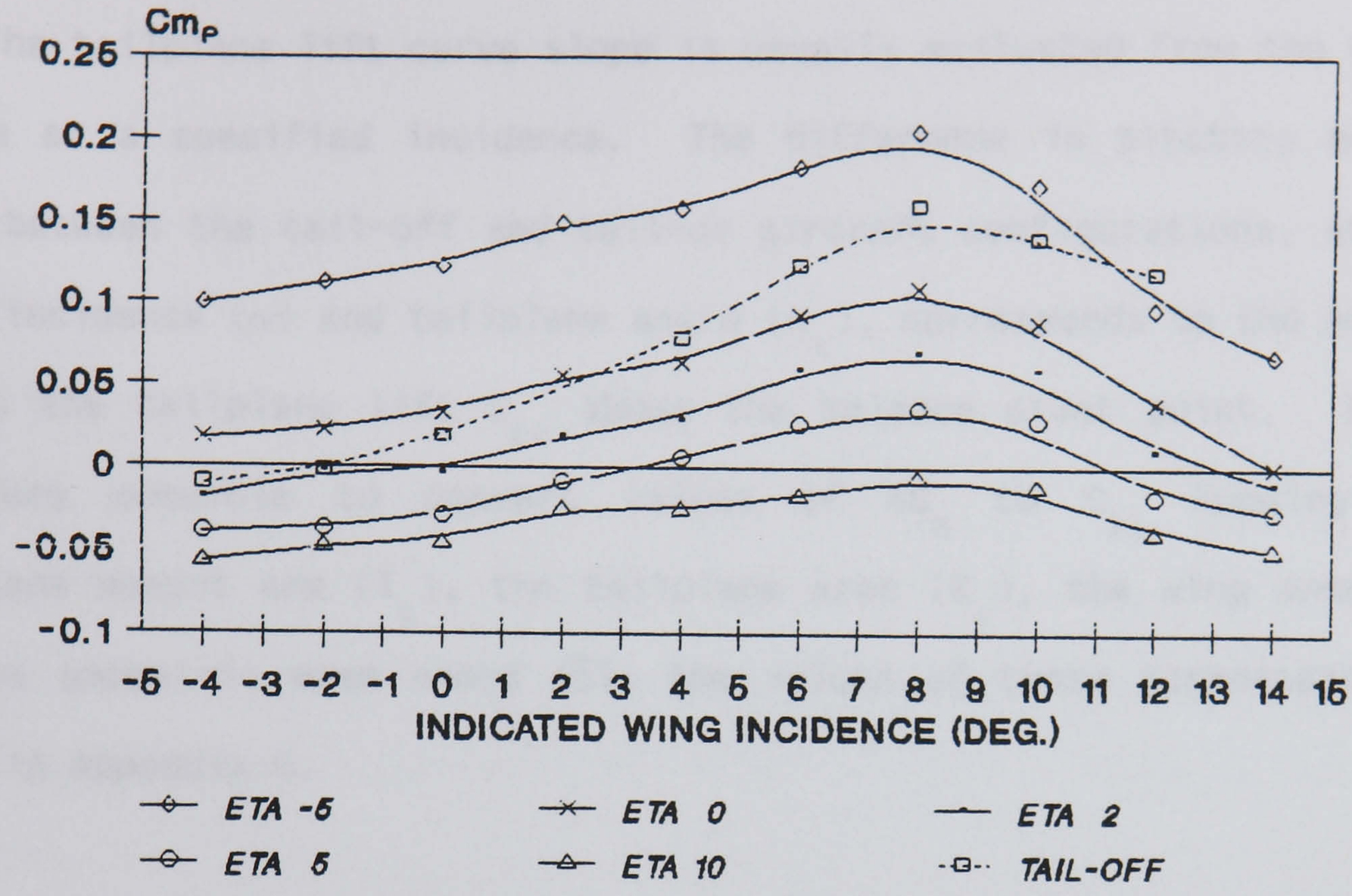

FIGURE 23: C_{M_P} vs α, (TAIL-ON AND TAIL-OFF)

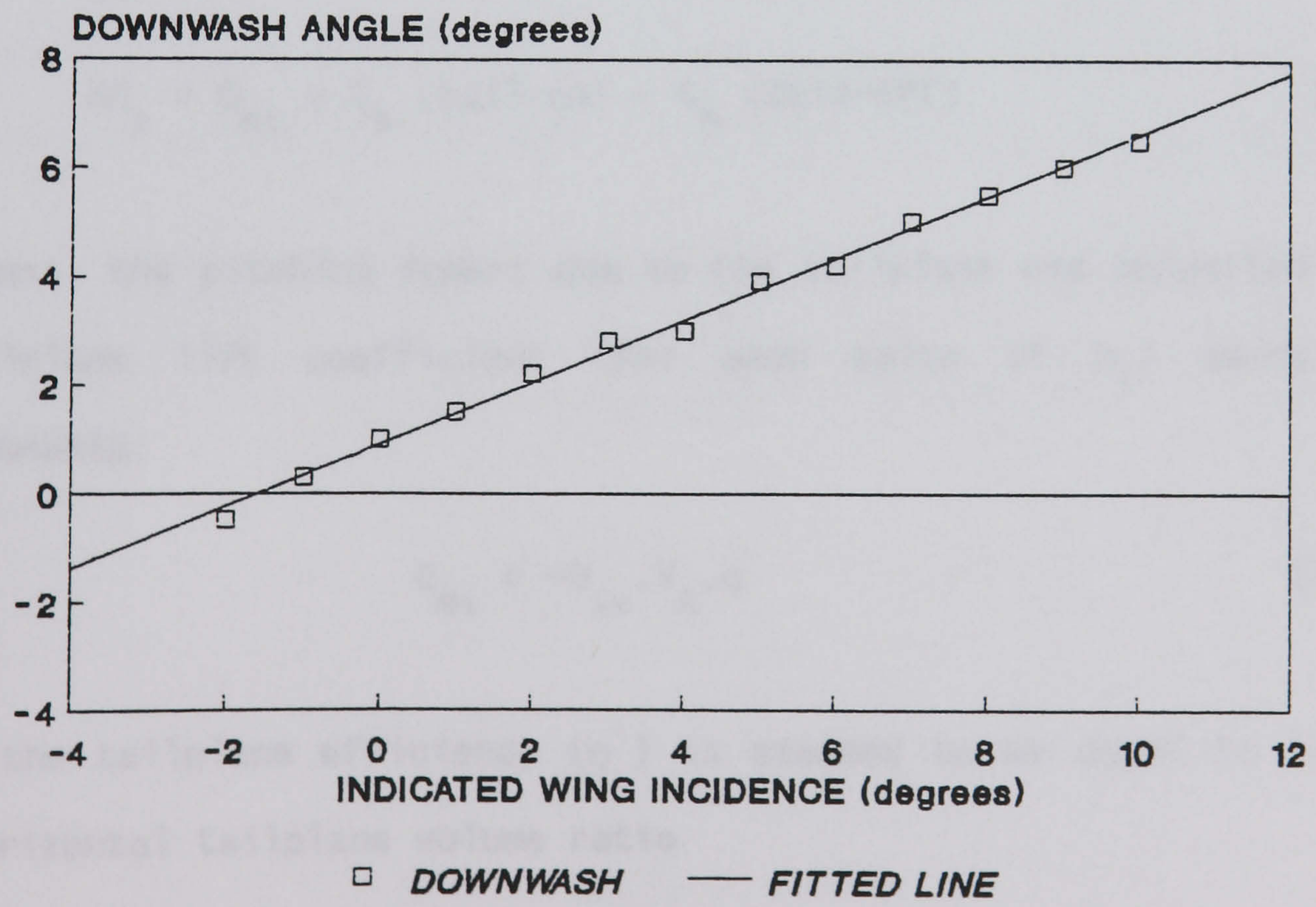

FIGURE 24: MEAN DOWNWASH ANGLE vs ANGLE OF INCIDENCE

7.4.3 Tailplane lift curve slope.

The tailplane lift curve slope is usually evaluated from the C_M vs α data at a specified incidence. The difference in pitching moment (δC_M) between the tail-off and tail-on aircraft configurations, at the given incidence (α) and tailplane angle (η_t), corresponds to the moment due to the tailplane lift C_{Lt} about the balance pivot point. It is therefore possible to convert values of δC_M to C_{Lt} knowing the tailplane moment arm (l_t), the tailplane area (S_t), the wing area (S) and the geometric mean chord ($\bar{c}$); the values of these parameters are given in Appendix C.

It was decided to use an incidence angle of $\alpha = 4^\circ$, this being at the middle of the aircraft trim range. Values of C_M (tail-on) and C_M (tail-off) were tabulated for each tailplane angle (η_t). The pitching moment, (C_{Mt}), due to the tailplane was calculated using:

$$\delta C_M = C_{Mt} = C_M \text{ (tail-on)} - C_M \text{ (tail-off)} \qquad [7.10]$$

Next, the pitching moment due to the tailplane was converted into a tailplane lift coefficient (for each value of η_t) using the relationship:

$$C_{Mt} = -C_{Lt}.V_H.\eta' \qquad [7.11]$$

where the tailplane efficiency (η') is assumed to be equal to 1, and the horizontal tailplane volume ratio

$$V_H = \frac{l_t\ S_t}{S\ \bar{c}} = 0.61 \qquad [7.12]$$

The downwash angle for $\alpha_w = 4$ was estimated from Figure 24 and found to be equal to 3.2°. Thus the tailplane incidence angle α_t was corrected using equation [7.7] as follows:

$$\alpha_t = \alpha_w + \eta - \varepsilon$$

$$\Rightarrow \quad \alpha_t = 4 + \eta - 3.2 \qquad [7.13]$$

A plot of α_t vs C_{Lt} was then made, Figure 25, and from this the tailplane lift curve slope (a_1) was estimated from a linear portion of the slope:

$$a_1 = dC_{Lt}/d\alpha_t = 0.04 \text{ deg}^{-1} \text{ or } 2.29 \text{ rad}^{-1} \qquad [7.14]$$

The lift curve graphs for the whole aircraft (tail and wing) were also plotted, Figure 26 and these were found to have an average slope of:

$$a = dC_L/d\alpha = 0.065 \text{ deg}^{-1} \text{ or } 3.72 \text{ rad}^{-1} \qquad [7.15]$$

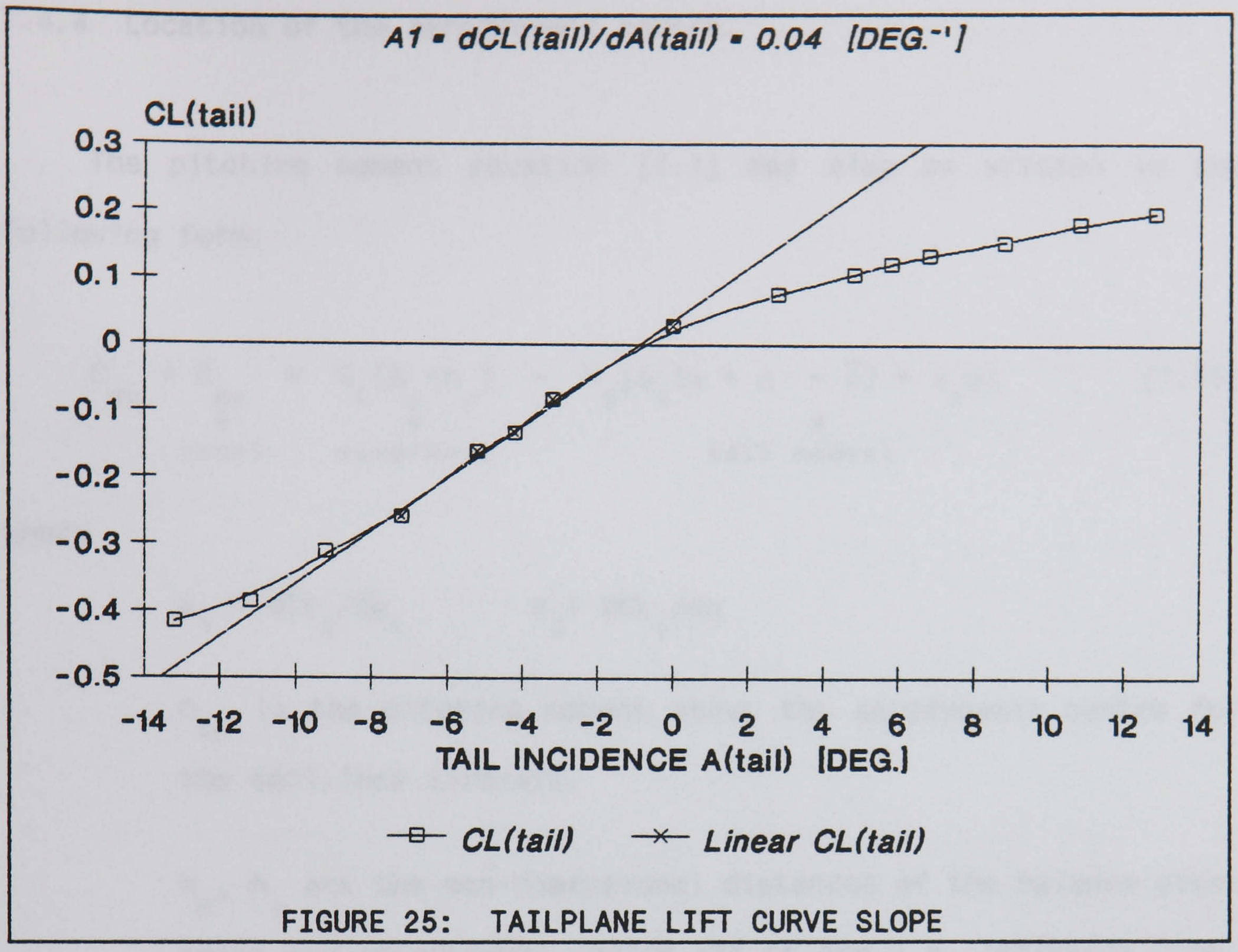

FIGURE 25: TAILPLANE LIFT CURVE SLOPE

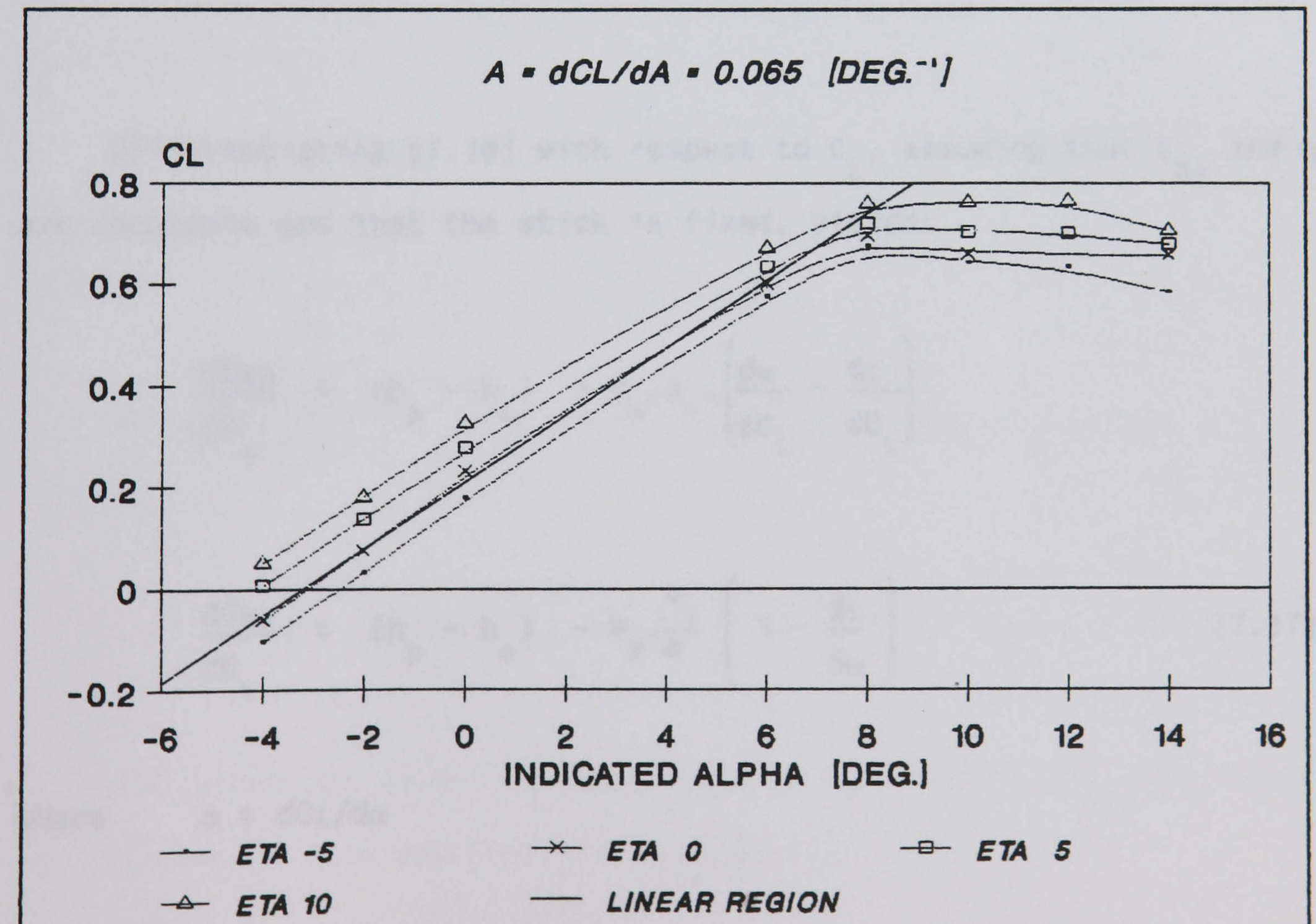

FIGURE 26: AIRCRAFT LIFT CURVE SLOPE

7.4.4 Location of the aerodynamic centre.

The pitching moment equation [7.1] may also be written in the following form:

$$C_{Mp} = C_{Mo} + C_L(h_p - h_o) - V_H[a_1(\alpha + \eta - \bar{\varepsilon}) + a_2\eta] \qquad [7.16]$$

↑ const. ↑ wing/body ↑ tail moment

where

$a_1 = dC_{L_t}/d\alpha_t \qquad a_2 = dC_{L_t}/d\eta$

C_{Mo} is the pitching moment about the aerodynamic centre for the tail-less aircraft.

h_p, h_o are the non-dimensional distances of the balance pivot point and aerodynamic centre aft of the l.e. reference line.

Differentiating [7.16] with respect to C_L, assuming that C_{Mo} and η are constants and that the stick is fixed, yields:

$$\frac{dC_{Mp}}{dC_L} = (h_p - h_o) - V_H.a_1.\left(\frac{d\alpha}{dC_L} - \frac{d\varepsilon}{dC_L}\right)$$

$$\frac{dC_{Mp}}{dC_L} = (h_p - h_o) - V_H.\frac{a_1}{a}\left(1 - \frac{d\varepsilon}{d\alpha}\right) \qquad [7.17]$$

where $a = dC_L/d\alpha$

For the tail-less aircraft, $a_1 = 0$ and the above equation becomes:

$$\left(\frac{dC_{Mp}}{dC_L}\right)_{\text{tail-off}} = (h_p - h_o) \qquad [7.18]$$

A graph of C_{Mp} vs C_L for the tail-off configuration was plotted, as shown in Figure 27. The gradient of the linear region of the graph was found to be 0.254, i.e.

$$\left(\frac{dC_{Mp}}{dC_L}\right)_{\text{tail-off}} = 0.254 = (h_p - h_o) \qquad [6.19]$$

For the Hawk model $h_p = 0.797\bar{\bar{c}}_{ref} = 118mm$. Thus the location of the aerodynamic centre (h_o) for the body and wing was calculated from [7.9] and found to be equal to $0.543\bar{\bar{c}}_{ref}$, i.e. 80.4mm aft of the l.e. reference line.

7.4.5 The static margin, stick fixed.

If the stick is fixed, the pitching moment equation may be written as:

$$\left(-\frac{dC_{Mcg}}{dC_L}\right)_{\substack{\text{stick}\\\text{fixed}}} = -(h - h_o) + V_H \cdot \frac{a_1}{a}\left(1 - \frac{d\varepsilon}{d\alpha}\right) \qquad [7.20]$$

The signs are usually changed in this way, since (dC_{Mcg}/dC_L) must be negative to give positive static stability.

All the quantities in this equation are fixed by the aircraft configuration except h, the position of the c.g. By varying h the stability can be made positive, negative or zero. Rearward movement of the c.g. increases $(h-h_o)$ and is therefore destabilising. The position of the c.g. which gives neutral stability, is designated h_n and is called the *stick fixed neutral point.* At this point equation [7.20] is equal to zero, giving:

$$V_H \cdot \frac{a_1}{a} \left(1 - \frac{d\varepsilon}{d\alpha} \right) = (h_n - h_o) \qquad [7.21]$$

Substituting [7.21] back into the original equation [7.20] yields the following expression for the stability of the aircraft for any position of the c.g.:

$$\left(- \frac{dC_{Mcg}}{dC_L} \right)_{\substack{stick \\ fixed}} = -(h - h_o) + (h_n - h_o) = (h_n - h) \qquad [7.22]$$

The distance of the c.g. from the stick fixed neutral point is called the *static centre of gravity margin, stick fixed* (H_n).

However, all of the experimental data was measured with respect to the TEM balance pivot point as opposed to the c.g. and therefore [7.22] may be written as

$$\left(\frac{dC_{Mp}}{dC_L} \right)_{\substack{stick \\ fixed}} = (h_p - h_n) \qquad [7.23]$$

Graphs of $\frac{dC_{Mp}}{dC_L}$ for the tail-on configuration were plotted for each tailplane setting angle η. The linear regions of the graphs, as shown in Figure 28, were found to have a gradient of:

$$\left(\frac{dC_{Mp}}{dC_L}\right)_{\substack{stick\\fixed}} = (h_p - h_n) = 0.081$$

As $h_p = 0.797\bar{\bar{c}}_{ref}$, the position of the neutral point could then estimated as $h_n = 0.716\bar{\bar{c}}_{ref}$ i.e. 106mm aft of the reference line.

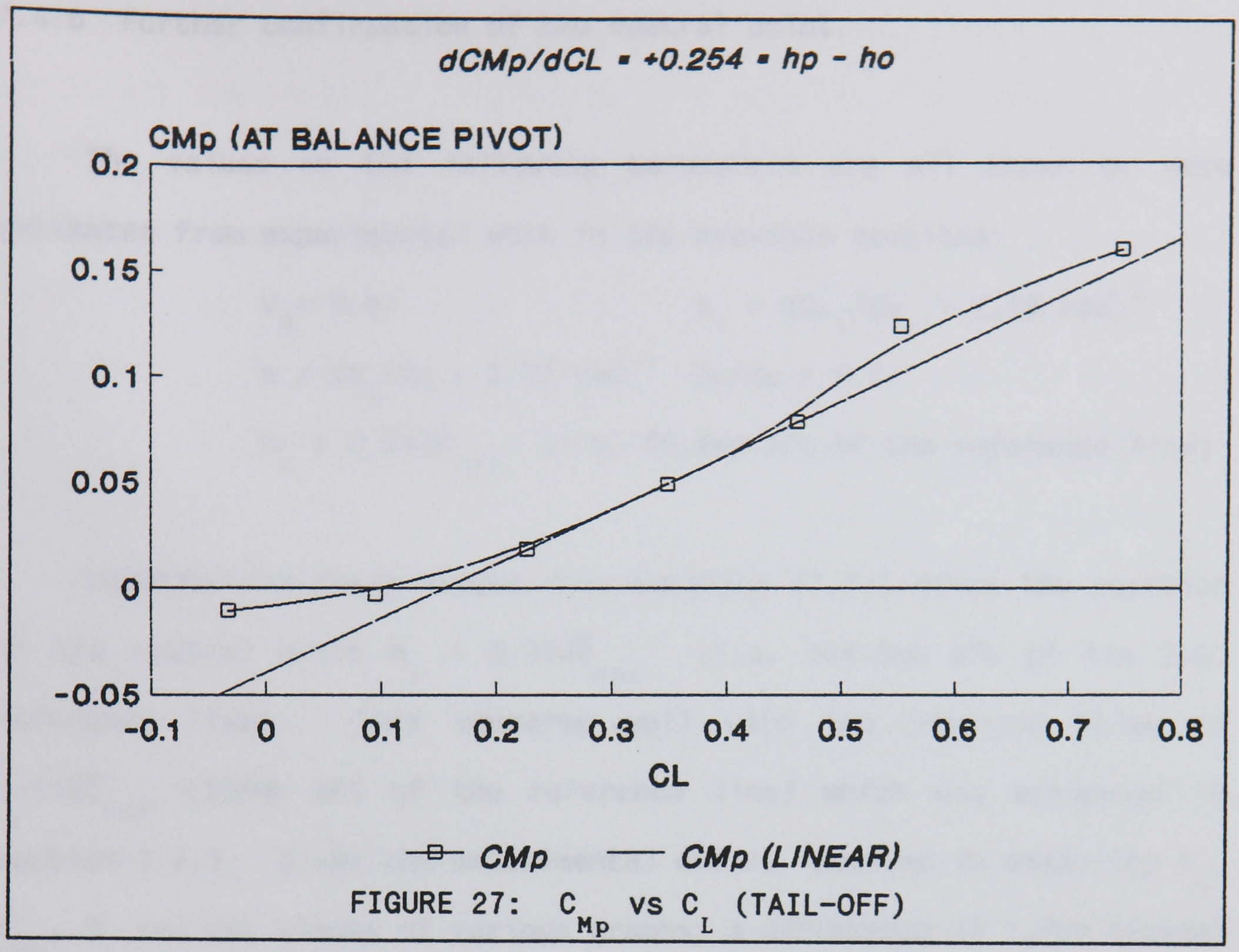

FIGURE 27: C_{Mp} vs C_L (TAIL-OFF)

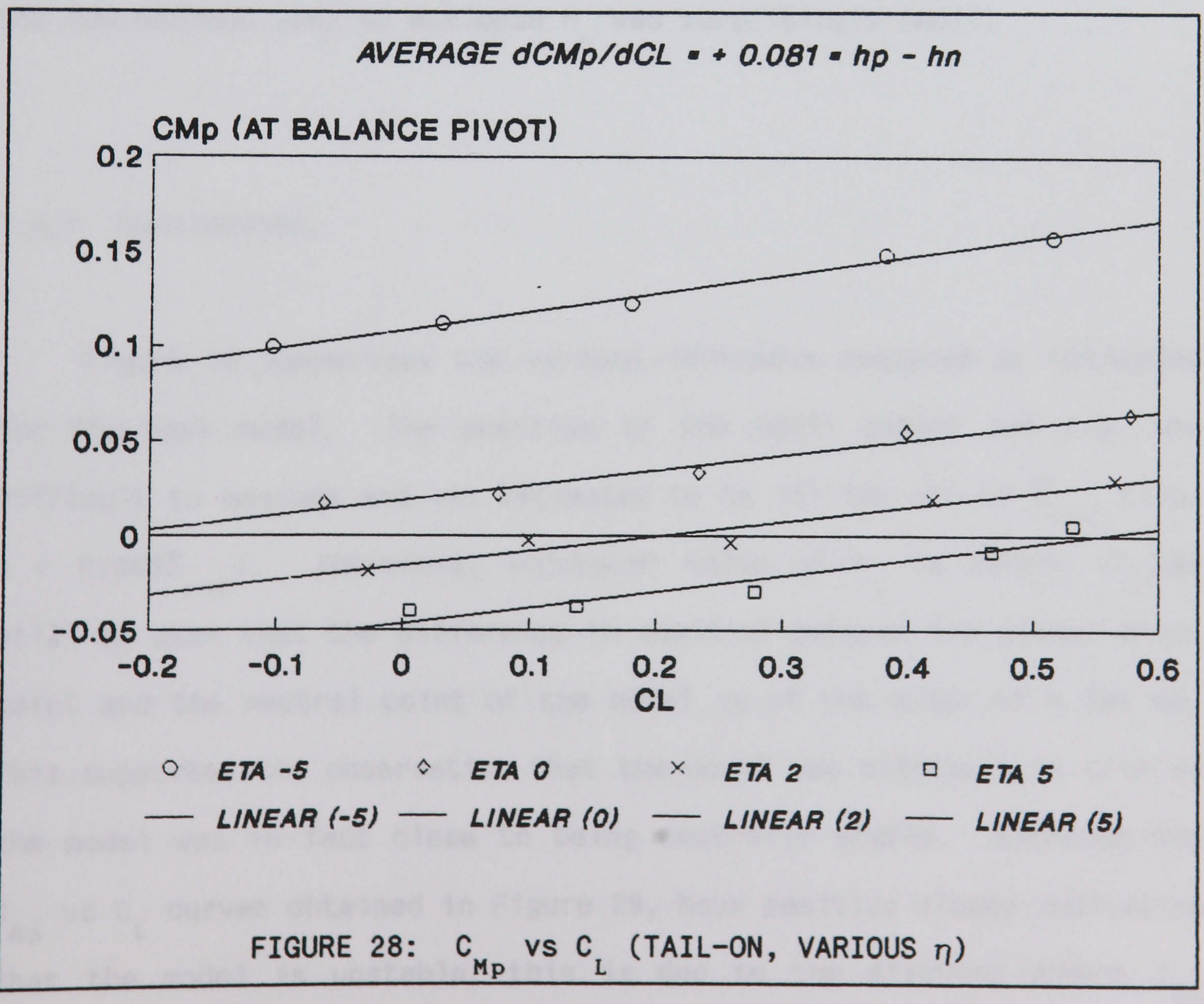

FIGURE 28: C_{Mp} vs C_L (TAIL-ON, VARIOUS η)

7.4.6 Further confirmation of the neutral point.

The values of the following parameters are all known or were estimated from experimental work in the previous sections:

$V_H = 0.61$ $\quad a_1 = dC_{L_t}/d\alpha_t = 2.29\ rad^{-1}$

$a = dC_L/d\alpha = 3.72\ rad^{-1}$ $\quad d\epsilon/d\alpha = 0.57$

$h_o = 0.543\bar{\bar{c}}_{ref}$ (i.e. 80.4mm aft of the reference line)

Substituting these values into equation [7.21] gives the position of the neutral point $h_n = 0.704\bar{\bar{c}}_{ref}$ (i.e. 104.3mm aft of the l.e. reference line). This compares well with the previous value of $0.716\bar{\bar{c}}_{ref}$ (106mm aft of the reference line) which was estimated in section 7.4.5. Given the experimental errors involved in measuring h_p, C_{Mp}, C_L and the slopes of various graphs, a difference of 1.7mm between the two methods used to estimate h_n was surprisingly small.

7.4.7 Conclusions.

Figure 18 summarises the various reference measured or estimated for the Hawk model. The position of the model gimbal and c.g. was difficult to measure and was estimated to be 101.5mm aft of $\bar{\bar{c}}_{ref}$ (i.e. $h = 0.686\bar{\bar{c}}_{ref}$). Therefore, whichever value of h_n is taken, it can still be seen that the difference in position between the gimbal pivot point and the neutral point of the model is of the order of a few mm. This supported the observation that the model was difficult to trim as the model was in fact close to being neutrally stable. Although the C_{Mp} vs C_L curves obtained in Figure 28, have positive slopes indicating that the model is unstable, this is due to the pitching moment C_{Mp}

being measured at the balance pivot which is 12-14mm aft of the neutral point of the model. Therefore, to confirm that the model is approximately neutrally stable values of the pitching moments and coefficients were calculated at the gimbal/c.g. point on the model (i.e. 16.5 mm in front of the TEM balance pivot point.) This was done by modifying the BASIC program used to produce the original values of C_L, C_D and C_{Mp} from experimental data measured by the balance. Pitching moment coefficients were also calculated at 10mm and 15mm in front of the gimbal/c.g.position and denoted C_{M10} and C_{M15}.

For various tailplane angles, graphs of C_M vs C_L were then plotted for various points aft of the l.e. reference line to show how static stability changes with the reference point (Ref 8). Graphs of C_M vs C_L for various reference positions at a tailplane angle of zero are presented in Figure 29. Hence it may be seen that at the model neutral point the graph is almost horizontal with a slope of -0.001, i.e. ≈ 0 as expected. At the model gimbal/c.g. the distance to the neutral point from the centre of the gimbal is only 4.4mm and the slope is slightly negative with $dC_M/dC_L = -0.03$. At distances of 10mm and 15mm in front of the gimbal position the stability of the model is increased, as seen by the more negative slopes of Figure 29.

On the basis of this analysis, it was decided to move the gimbal forward by 10mm only as the distance that the gimbal could be moved was restricted by the construction of the model. The movement of the gimbal also required a small enlargement of the central open access hole of the model to ensure an adequate clearance of the vertical support rod which passes through the centre of the model and gimbal. Note that it is the original position of the gimbal which is shown in

Figure 18. Following movement of the gimbal, the c.g. position was adjusted using the small brass weights in the aircraft. The Hawk model seemed slightly easier to trim following these changes.

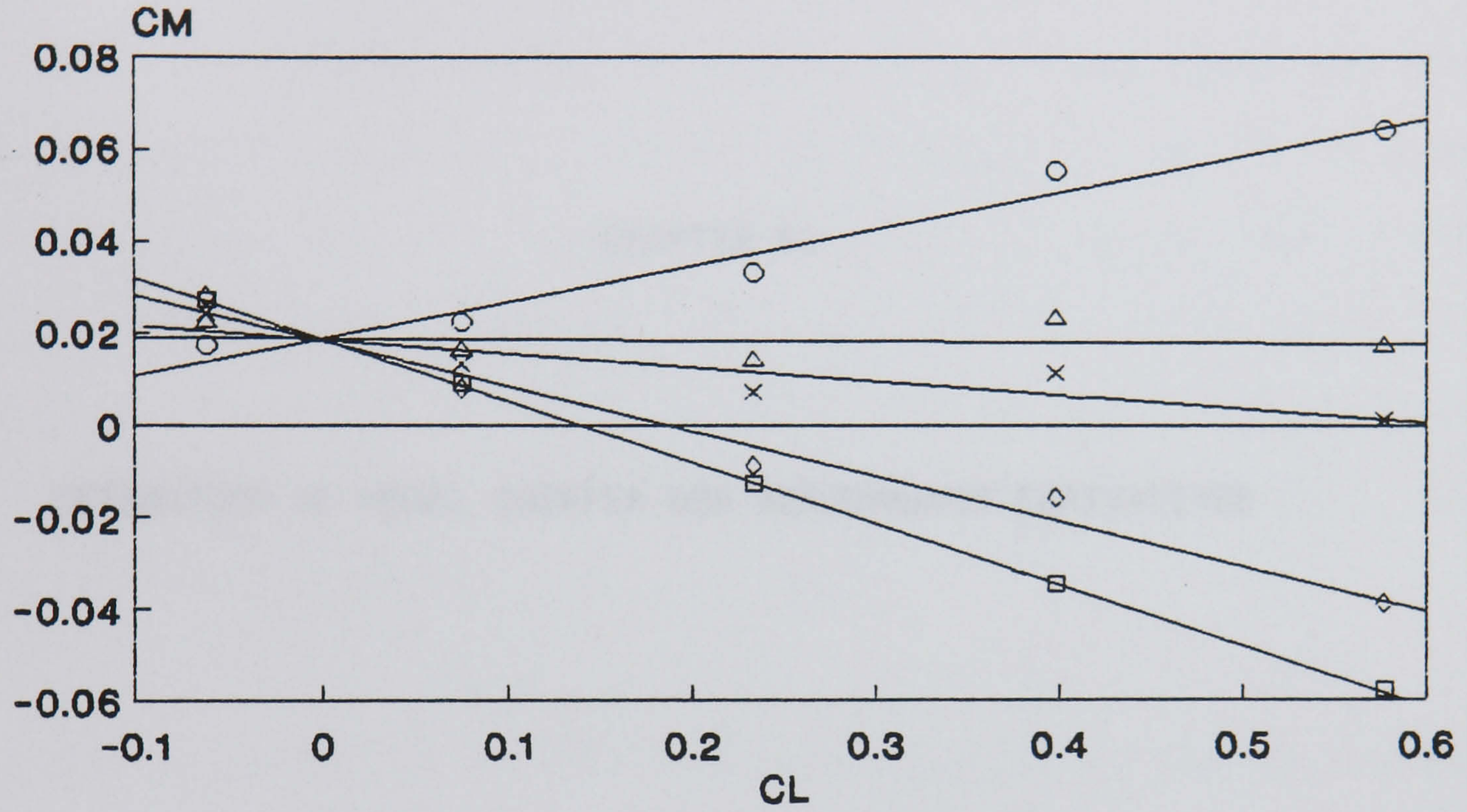

FIGURE 29: C_M vs C_L (η = 0, VARIOUS POSITIONS)

CHAPTER 8:

ESTIMATION OF MODEL INERTIA AND AERODYNAMIC DERIVATIVES

8.0 ESTIMATION OF MODEL INERTIA AND AERODYNAMIC DERIVATIVES.

The moments of inertia of the Hawk model were estimated using a free oscillation method, Ref 27. To use this method, the model was mounted within the Dexion framework of the dynamic rig with the vertical rod, passing through the model gimbal. The model was then suitably restrained by wires and springs attached to the Dexion frame and to a wing (for roll inertia experiments) or to the rear of the aircraft model (for pitch and yaw experiments). The model and framework were placed in the wind tunnel and the model was deflected from the zero displacement equilibrium condition. Upon release, the model performed a damped oscillatory motion.

With the wind on, the amplitude and frequency of the oscillatory motion was dependent on the relevant aerodynamic stability derivatives, (for example N_v & N_r), as well as the restraining spring characteristics and the friction in the mounting. With the wind off, the aerodynamic derivatives are assumed to be approximately zero and the motion is only dependent on the restraining spring characteristics and mechanical friction.

The wind-off damped oscillations were recorded and analysed to yield estimates of the moments of inertia and the mechanical friction of the model gimbal. These wind-off experiments were performed twice during the course of the PhD programme as the first set of experiments had highlighted a problem with the way in which the yaw attitude potentiometer was mounted in the rig. The second set of experiments were carried out for both wind-off and wind-on conditions and took place after the model gimbal had been moved forward by 10mm.

8.1 Derivation of free oscillatory equations of motion.

The derivation of the equations of motion and theoretical basis for the estimation of inertias using the free oscillation method is best explained by the following example, in which the Hawk model is set up to perform a lateral oscillatory motion in yaw. The equations of motion for the pitch and roll oscillations are derived in a similar manner. Figure 30 shows a plan view of the Hawk model set up in the wind tunnel with two springs and wires attached horizontally to the tail, at a distance l from the vertical rod on which the model was held.

Choosing the directional reference axis to coincide with the wind direction in the tunnel, i.e. $\alpha = 0$ in Figure 31, it may be seen that:

$$\psi = -\beta \qquad [8.1]$$

The relationship between the side slip velocity v and yaw angle ψ may also be derived. From Figure 31 it may be seen that:

$$v = V.\sin(-\beta) \qquad [8.2]$$

and

$$U_\infty = -V.\cos(-\beta) \qquad [8.3]$$

where

V is the resultant velocity vector of the aircraft

U_∞ is the wind tunnel speed

Dividing equation [8.2] by [8.3], noting that $\sin(-\beta) = -\sin(\beta)$ and $\cos(-\beta) = \cos(\beta)$, gives:

$$\frac{v}{U_\infty} = \frac{-V.\sin(\beta)}{-V.\cos(\beta)} = \tan(\beta) \cong \beta$$

and hence

$$v \cong U_\infty.\beta = -U_\infty.\psi \qquad [8.4]$$

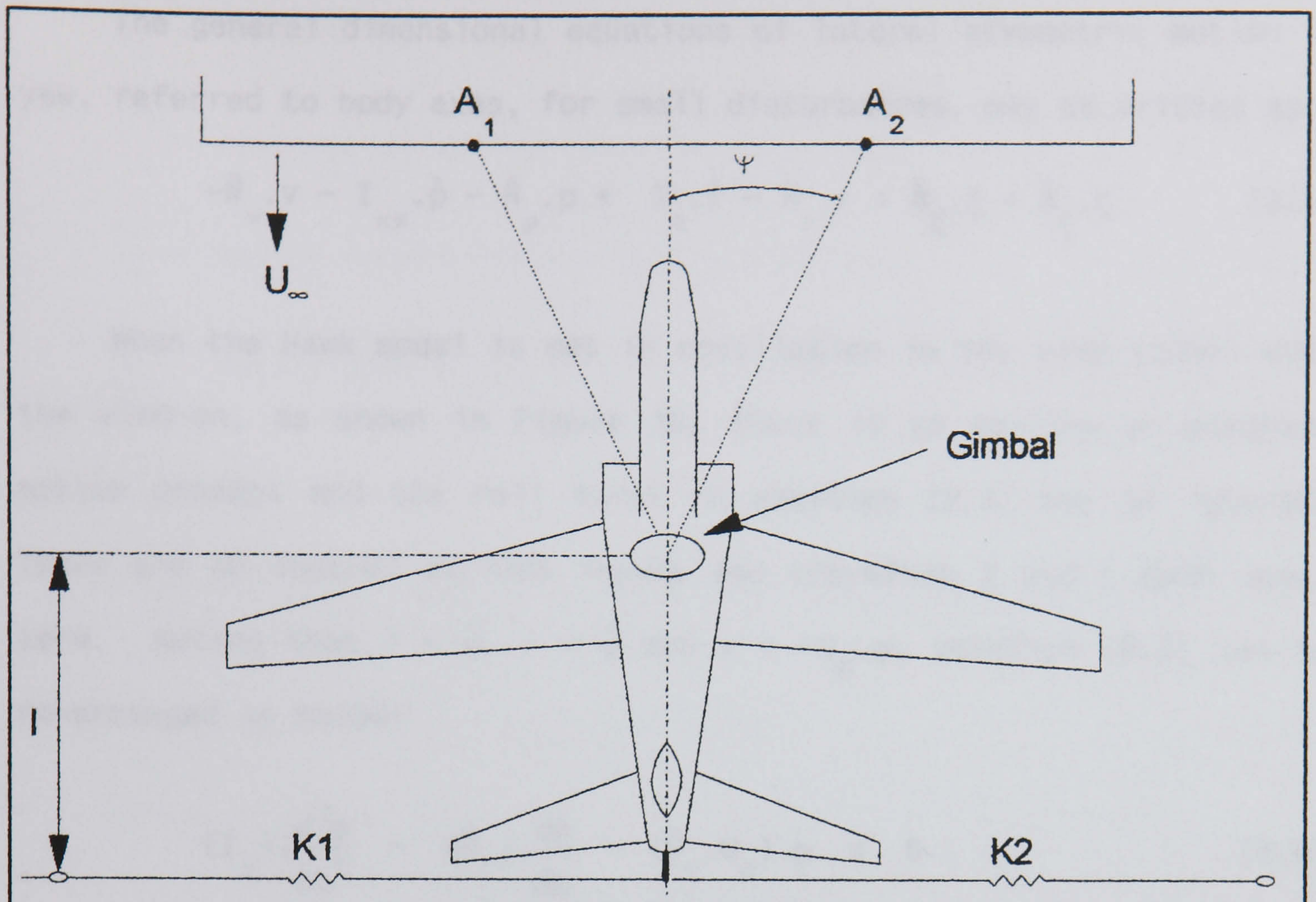

FIGURE 30: HAWK MODEL IN THE WIND TUNNEL, RESTRAINED IN YAW

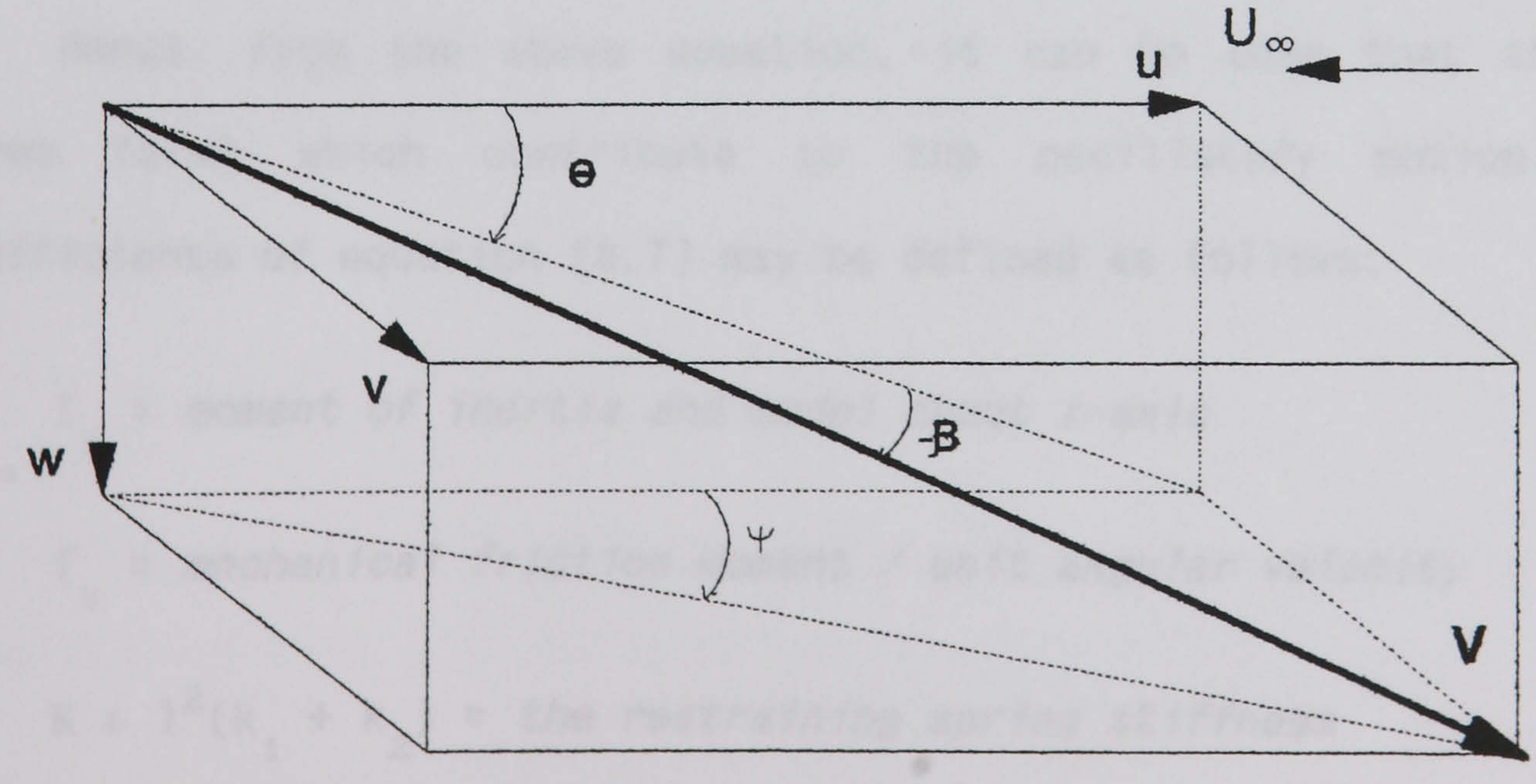

FIGURE 31: ORIENTATION OF RELATIVE WIND AND BODY FIXED AXES

The general dimensional equations of lateral asymmetric motion in yaw, referred to body axes, for small disturbances, may be written as:

$$-\mathring{N}_v.v - I_{xz}.\dot{p} - \mathring{N}_p.p + I_z.\dot{r} - \mathring{N}_r.r = \mathring{N}_\xi.\xi + \mathring{N}_\zeta.\zeta \qquad [8.5]$$

When the Hawk model is set in oscillation in the wind tunnel with the wind-on, as shown in Figure 30, there is no rolling or pitching motion present and the roll terms in equation [8.5] may be ignored. There are no control surface inputs and therefore ξ and ζ both equal zero. Noting that $\dot{r} = \ddot{\psi}$, $r = \dot{\psi}$ and $v = -U_\infty.\psi$, equation [8.5] can be re-arranged as below:

$$(I_z).\frac{d^2\psi}{dt^2} - (\mathring{N}_r).\frac{d\psi}{dt} + (\mathring{N}_v.U_\infty).\psi = 0 \qquad [8.6]$$

The mechanical friction damping term ($f_z\dot{\psi}$) and restoring force ($K\psi$) also contribute to the yawing motion and may be included to give

$$(I_z).\frac{d^2\psi}{dt^2} - (\mathring{N}_r + f_z).\frac{d\psi}{dt} + (\mathring{N}_v.U_\infty + K).\psi = 0 \qquad [8.7]$$

Hence, from the above equation, it can be seen that there are three terms which contribute to the oscillatory motion. The coefficients of equation [8.7] may be defined as follows:

I_z = *moment of inertia and model about z-axis*

f_z = *mechanical friction moment / unit angular velocity*

$K = l^2(k_1 + k_2)$ = *the restraining spring stiffness*

l = *distance along the model axis from the pivot point to the point on the model that is connected to the restraining springs*

k_1 = *restraining spring constant (port side)*

k_2 = *restraining spring constant (starboard side)*

$\mathring{N}_r$ = *yawing moment due to rate of yaw* $\delta N/\delta r$

$\mathring{N}_v$ = *yawing moment due to rate of side slip* $\delta N/\delta v$

Alternatively, equation [8.7] can be expressed in the form:

$$\frac{d^2\psi}{dt^2} + 2\zeta\omega_o.\frac{d\psi}{dt} + \omega_o^2.\psi = 0 \qquad [8.8]$$

where:

ζ = system damping ratio.

ω_o = system undamped natural frequency.

A general solution to equation [8.8] is given by

$$\psi = A_o.e^{-\mu t}.\cos(\omega_d t + \delta) \qquad [8.9]$$

where:

$$\mu = -\zeta\,\omega_o \qquad [8.10]$$

δ is some initial yaw angle on the recorded oscillations

ω_d is the system damped frequency given by:

$$\omega_d = \frac{2\pi}{T} = \omega_o.(1-\zeta^2)^{1/2} \qquad [8.11]$$

T = period of oscillatory motion.

From [8.10], it may be seen that $\zeta^2 = (\mu)^2/(\omega_o)^2$ and substituting this into the square of equation [8.11] gives:

$$\omega_d^2 = \frac{4\pi^2}{T^2} = \omega_o^2.\left[\,1 - \frac{\mu^2}{\omega_o^2}\,\right]$$

or

$$\omega_d^2 = \frac{4\pi^2}{T^2} = \omega_o^2 - \mu^2 \qquad [8.12]$$

Upon comparing equation [8.7] with [8.8], for the wind-on case, it may be seen that:

$$2\zeta\omega_o = -(\mathring{N}_r + f_z)/I_z \qquad [8.13]$$

and

$$\omega_o^2 = (U_\infty \mathring{N}_v + K)/I_z \qquad [8.14]$$

If the model is set into oscillation with the wind off, the aerodynamic terms of equation [8.7] may be neglected since $\mathring{N}_v \cong 0$ and $\mathring{N}_r \cong 0$. Further, U_∞ will also be zero and the following terms can be defined for the wind-off case:

$$\mu = -\zeta\omega_o = f_z/2.I_z \qquad [8.15]$$

$$\omega_o^2 = [l^2(k_1 + k_2)]/I_z \qquad [8.16]$$

8.2 Graphical analysis of the recorded oscillations.

The voltage output from the model's attitude potentiometers enabled the damped oscillations of the model to be recorded using a graph plotter. In yaw for example, the oscillations are of the form given by equation [8.9]. It may be shown that the maximum and minimum peaks of the recorded oscillations correspond to times when the term $\cos(\omega_d t + \delta) = 1$. Thus taking any two maximum peaks, A_1 and A_2 at times t_1 and t_2, μ may be found equation [8.17] below:

$$\ln\left(\frac{A_1}{A_2}\right) = \mu.(t_2 - t_1) \qquad [8.17]$$

There are two other methods which could be used to estimate μ. Firstly, by finding the change in time (Δt) from the peak to half amplitude, μ may be found as $\mu = \Delta t/0.693$. Alternatively, a graph of $\ln(A_n/A_{n+1})$ vs t will yield a straight line of gradient μ. Using experimental data, all three methods produced values for μ which were in close agreement, Ref 8.

The damped period T of the motion can also be easily estimated from the record of the oscillatory motion. Substituting the values of T and μ into [8.12] will then yield the natural frequency of oscillation ω_o. Finally, by re-arranging equations [8.16] and [8.15] respectively, I_z and f_z may be found:

$$I_z = [l^2(k_1 + k_2)]/(\omega_o^2) \qquad [8.18]$$

$$f_z = 2.I_z.\mu \qquad [8.19]$$

8.3 Pitch experiments.

To measure the pitch inertia two springs were attached vertically between the tail of the model and the dexion framework using very stiff wire, similar to piano wire. The distance from the centre of the vertical rod (which passes through the model gimbal) to the tail attachment point was measured. Various springs were attached to the model to see which gave the best vertical oscillations in pitch when the model was disturbed from its zero rest position. The two springs

finally chosen had their spring constants estimated in experiments whereby the spring length or extension was measured for various masses which were hung from the spring. The spring constant, k, could then be calculated from the slope of the straight line graph of weight vs extension, assuming a simple law of (force = k $_x$ extension), as detailed in Ref 8.

The Hawk model was set in oscillation and the decay curve recorded on a graph plotter. This was done by taking the voltage signal giving the variation in pitching angle θ directly from the dynamic rig electronic control unit to the graph plotter. It was not necessary to convert the measurements into degrees or radians because only the period and damping of the motion are required and the amplitude could therefore be recorded in arbitrary units.

When the model inertias were measured for a second time, after having moved the model gimbal position forward by 10mm, the way in which the oscillations were recorded was changed. The graph plotter was replaced by a CED1401, the analogue to digital conversion equipment utilised in the data acquisition system which was developed for the model. The damped oscillations were recorded in data files on an IBM PC. The data files were filtered to remove high frequency noise and centered around 0 volts using CED software. A CED software package called Waterfall was then utilised to display the recorded oscillations and to estimate the average damped period of the motion. The magnitudes of the peaks and troughs of the motion were also found.

8.3.1 Derivation of the pitching moment equations.

As explained in Appendix B, the reduced model equation of motion may be expressed as follows:

$$-\mathring{M}_w.w - \mathring{M}_{\dot{w}}.\dot{w} - \mathring{M}_q.q + I_y.\dot{q} = \mathring{M}_\eta.\eta \qquad [B.14]$$

Noting that $\eta = 0$, $\dot{q} = \ddot{\theta}$, $q = \dot{\theta}$, $w = U_\infty.\theta$, $\dot{w} = U_\infty.\dot{\theta}$, and also adding in the frictional term $-f_y.\dot{\theta}$ and spring stiffness term $K.\theta$, leads to the following equation:

$$I_y.\ddot{\theta} + (-\mathring{M}_q - \mathring{M}_{\dot{w}}.U_\infty - f_y).\dot{\theta} + (-\mathring{M}_w.U_\infty + K).\theta = 0 \qquad [8.20]$$

where

$$K = l^2.(k_1 + k_2)$$

Comparing equation [8.20] with the equivalent of equation [8.8] for pitch oscillatory motion, and further noting that a solution of equation [8.20] is given by $\theta = \theta_o e^{-\mu t}\cos(\omega_d t + \delta)$, leads to the following identities for the wind-on case:

$$2\zeta\omega_{o_{on}} = -2\mu_{on} = (-\mathring{M}_q - \mathring{M}_{\dot{w}}.U_\infty - f_y)/I_y \qquad [8.21]$$

$$\omega_{o_{on}}^2 = (-\mathring{M}_w.U_\infty + K)/I_y \qquad [8.22]$$

8.3.2 Estimation of pitch inertia and mechanical friction.

If the model is tested with the wind off, the aerodynamic term $\mathring{M}_q$ of [8.21] is assumed to be negligible. The value of U_∞ is zero and the following terms may therefore be defined for the wind-off case:

$$\omega_{o_{off}}^2 = K/I_y \qquad \Rightarrow I_y = [1]^2(k_1 + k_2)]/\omega_{o_{off}}^2 \qquad [8.23]$$

$$2\mu_{off} = f_y/I_y \qquad \Rightarrow f_y = 2.I_y.\mu_{off} \qquad [8.24]$$

8.3.2.1 Wind-off experiments - SET 1:

The model was displaced from the equilibrium position by hand, to set it into oscillatory motion and the pitch angle response was recorded. Values of the maximum peaks were found from the decay graph and plotted against time, Figure 32. Using functions within Harvard Graphics, an exponential curve of the form $x = A_o.e^{-\mu t}$ was fitted to the maximum points. Then choosing two points on the fitted curve, the value of μ was found using equation [8.17] as follows:

$$\mu = \ln\left(\frac{35.352}{29.231}\right) \div (9.735 - 5.625) = 0.046 \text{ (rad/sec)}$$

The average period of the oscillation, T_{off}, was measured from the response graph and found to be equal to 1.25sec. The values of T and μ were then substituted into equation [8.12], as shown below, to calculate the undamped natural frequency of the oscillations.

$$\omega_o^2 = (\omega_d^2 + \mu^2) = \frac{4\pi^2}{T^2} + \mu^2 = (5.0265)^2 + (0.046)^2 = 25.268 \text{ (rad/sec)}^2$$

Hence ω_o = 5.0267 rad/sec

It can be seen that the undamped frequency of oscillation is almost the same as the damped frequency as μ is very small.

In this set of experiments l = 0.4m and the sum of the spring constants $(k_1 + k_2)$ = 15.1 N/m. Thus using equations [8.18] and [8.19], the values of I_y and f_y were found, as follows:

(i) $I_y = [l^2(k_1 + k_2)]/(\omega_o^2) \Rightarrow I_y = 0.0956$ kgm^2 or 0.07 slug.ft^2

(ii) $f_y = 2.I_y.\mu \Rightarrow f_y = 0.0088$ kgm^2.rad/sec

(Note: f_y is the mechanical friction moment / unit angular velocity)

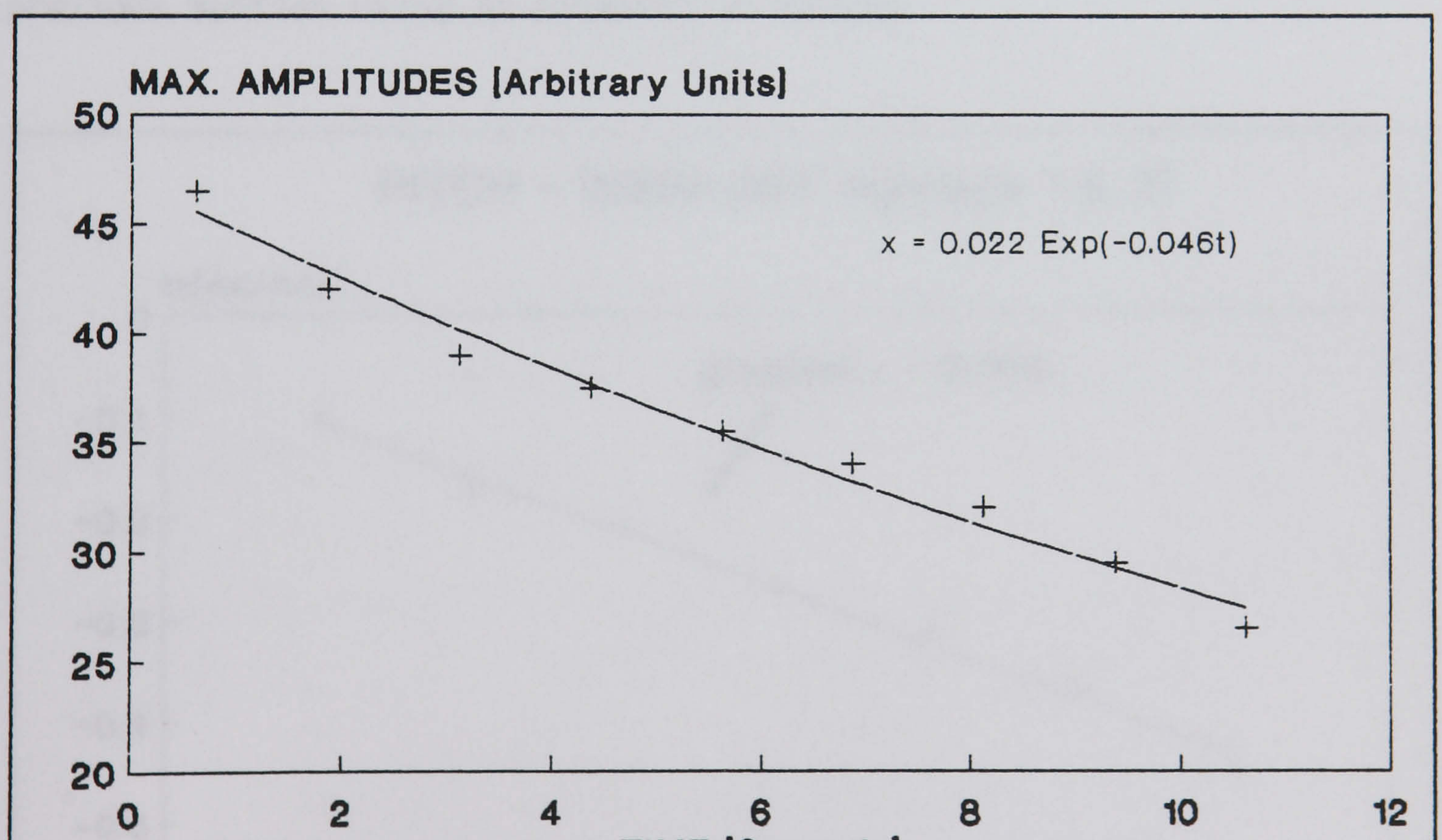

FIGURE 32: MAXIMUM AMPLITUDES OF PITCH OSCILLATIONS (WIND-OFF)

8.3.2.1.1 Alternative calculation of μ.

A general solution of the pitch oscillatory motion may be written in the form $A_n = A_o.e^{-\mu t}$. Considering successive maximum peaks where $t = nT$, n is the peak number and T is the period of the motion, the general solution of motion may also be written as $A_n = A_o.e^{-\mu nT}$. This equation may be re-arranged to give $\ln\left(\frac{A_n}{A_o}\right) = -(\mu T).n$

Hence a graph of $\ln(A_n/A_o)$ vs n will be a give a straight line of gradient $-\mu T$ as shown below. In this pitch example the gradient was found to be equal to -0.056. As stated earlier, the period of the motion was T = 1.25sec giving an estimate of μ = 0.044rad/sec. This compares well with the value of 0.046rad/sec which was estimated in the previous section using an alternative method.

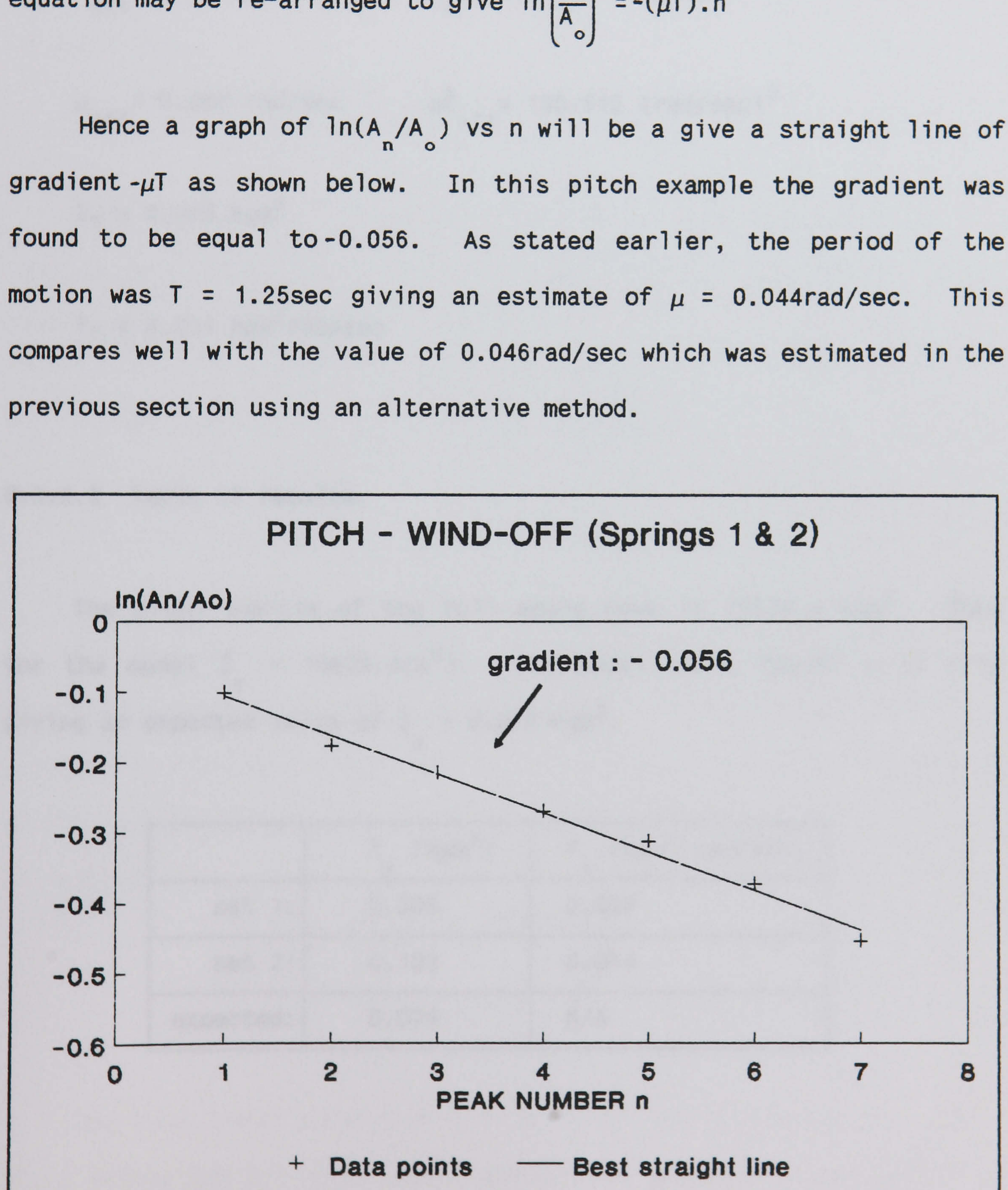

FIGURE 33: CALCULATION OF μ USING $\ln(A_n/A_o)$ vs PEAK NUMBER

8.3.2.2 Wind-off experiments - SET 2:

In this set of experiments l = 0.46m and the sum of spring constants ($k_1 + k_2$) = 63.5 N/m. The inertia and friction terms were as follows:

T_{off} = 0.55 sec ω_d^2 = 130.507 (rad/sec)^2

μ_{off} = 0.069 rad/sec $\omega_{o_{off}}^2$ = 130.512 (rad/sec)^2

I_y = 0.103 kgm^2

f_y = 0.014 kgm^{2}rad/sec

8.3.2.3 Table of results.

The pitch inertia of the full scale Hawk is 19534.4 kgm^2. Thus for the model I_y = 19534.4(λ^5). The model scale factor λ is 1/12 giving an expected value of I_y = 0.079 kgm^2.

	I_y (kgm^2)	f_y (kgm^2.rad/sec)
set 1:	0.096	0.009
set 2:	0.103	0.014
expected:	0.079	N/A

8.3.3 Estimation of pitching moment derivatives.

Substituting $f_y/I_y = 2\mu_{off}$ into the wind-on equation [8.21], it can be shown that:

$$-\mathring{M}_q - \mathring{M}_{\dot{w}}.U_\infty = 2.I_y.(\mu_{off} - \mu_{on}) \qquad [8.25]$$

Similarly, substituting $K/I_y = \omega_o^2{}_{off}$ into equation [8.22] it may be shown that:

$$\mathring{M}_w = -(I_y/U_\infty).(\omega_o^2{}_{on} - \omega_o^2{}_{off}) \qquad [8.26]$$

The second set of inertia experiments were performed for the wind-on case and analysis of the recorded responses gave the following data values:

$T_{on} = 0.49$ (sec) $\qquad \omega_d^2 = 164.425$ (rad/sec)^2

$\mu_{on} = 2.359$ (rad/sec) $\qquad \omega_o^2{}_{on} = 169.99$ (rad/sec)^2

The experimental data wind-on was recorded at a tunnel speed of 65.4 mm H_2O which corresponds to $U_\infty = 32.125$ m/s. Therefore substituting the appropriate wind-off and wind-on values into equations [8.25] and [8.26] leads to the following aerodynamic derivative estimates:

$$\mathring{M}_w = -0.126 \text{ kg.m/s}$$

$$-\mathring{M}_q - \mathring{M}_{\dot{w}}.U\infty = 0.471 \text{ kg.m}^2/\text{s}$$

The Hawk model parameter S = 0.115 m^2 and $\bar{\bar{c}}$ = 0.148 m. Using these values and ρ_o = 1.225 kg/m^3 enabled the non-dimensional values of the derivatives to be calculated, as shown below.

$$M_w = \mathring{M}_w \,/\, (0.5).\rho_o.U_\infty.S.\bar{\bar{c}} \qquad [8.27]$$

hence

$$M_w = -0.126 \,/\, 0.3349 = -0.376$$

$$-M_q - M_{\dot{w}} = (-\mathring{M}_q - \mathring{M}_{\dot{w}}.U_\infty) \,/\, (0.5).\rho_o.U_\infty.S.(\bar{\bar{c}})^2 \qquad [8.28]$$

hence

$$-M_q - M_{\dot{w}} = 0.471 \,/\, 0.0496 = 9.49$$

8.3.4 Pitching moment derivatives from static stability experiments.

The longitudinal static stability experiments provided a number of parameters which could be utilised in estimating values of various aerodynamic stability derivatives for the new gimbal/c.g. position at $0.618\bar{\bar{c}}_{ref}$. These estimates could then be compared with values obtained from the inertia experiments and those estimated by Malik in earlier experiments with the Hawk model, Ref 22. The formulae used to obtain the derivatives and a comparison of experimental values is given below.

(i) $$M_w = -(a).(K_n)\ ,\quad h \text{ at } 0.618\bar{\bar{c}}_{ref} \qquad [8.29]$$

$$M_w = -(3.72)(0.716 - 0.618) = -0.365$$

(ii) $$M_q = -(a_1).\frac{V_H\ l_t}{\bar{\bar{c}}_{ref}} \qquad [8.30]$$

$$M_q = \frac{-2.29 \times 0.61 \times 0.358}{0.148} = -3.382$$

(iii) $$M_{\dot{w}} = -(a_1).\frac{V_H\ l_t}{\bar{\bar{c}}_{ref}} \cdot \frac{d\varepsilon}{d\alpha} = M_q.\frac{d\varepsilon}{d\alpha} \qquad [8.31]$$

$$M_{\dot{w}} = -3.382 \times 0.57 = -1.928$$

(iv) $$(-M_q - M_{\dot{w}}) = (3.382 + 1.928) = 5.31$$

Derivative	From inertia experiments	From stability experiments	From Malik (Ref 22)
(i) M_w	-0.376	-0.365	-0.267
(ii) M_q	N/A	-3.382	-6.30
(iii) $M_{\dot{w}}$	N/A	-1.928	-2.73
(iv) $-M_q - M_{\dot{w}}$	9.51	5.31	9.03

Overall, the correlation between derivatives estimated from different sources is quite encouraging. Based on the correlation of $(-M_q - M_{\dot{w}})$ between Malik and the inertia experiments it could be assumed that Malik's estimates for M_q and $M_{\dot{w}}$ are better than the estimates obtained from the static stability experiments. Closer examination of the formulae used to calculate M_q and $M_{\dot{w}}$ then suggests that the longitudinal static stability experiments possibly under-estimated the value of a_1 = 2.29 rad/sec. Malik used a_1 = 4.2 rad/sec in his work.

8.4 Roll inertia experiments.

To measure the roll inertia the two springs were attached vertically to the port wing of the model, with one spring above and the

other spring below the wing. The spanwise distance along the wing from the vertical rod and gimbal was measured as l = 0.22m. The model was set in oscillation and the decay recorded using the electronic control unit and graph plotter.

8.4.1 Derivation of the rolling moment equations.

The reduced model equation of motion in roll may be expressed as follows (Ref 6):

$$\mathring{L}(t) = -\mathring{L}_v.v - \mathring{L}_p.p + I_x.\dot{p} - I_{xz}.\dot{r} - \mathring{L}_r.r \qquad [B.21]$$

If the oscillations are assumed to be purely a rolling action of the model the yawing term ($\mathring{L}_r$) and side slip term ($\mathring{L}_v$) may be ignored. Noting that $p = \dot{\phi}$; $\dot{p} = \ddot{\phi}$; and introducing the spring stiffness term ($K.\phi$) and frictional term ($f_z.\phi$) leads to:

$$I_x.\ddot{\phi} + (-\mathring{L}_p - f_x).\dot{\phi} + (K).\phi = 0 \qquad [8.32]$$

where $K = l^2.(k_1 + k_2)$

l = distance from c.g. to wire attachment point = 0.21m

k_1+k_2 = sum of spring constants = 63.5 N/m

Comparing equation [8.32] with the appropriate equation of the form of [8.8] (with ψ replaced by ϕ) leads to the identities:

$$2\zeta\omega_{o_{on}} = -2\mu_{on} = (-\mathring{L}_p - f_x)/I_x \qquad [8.33]$$

and

$$\omega_{o_{on}}^2 = (K)/I_x \qquad [8.34]$$

8.4.2 Estimation of roll inertia and mechanical friction.

As the model is tested with the wind off, the aerodynamic term $\mathring{L}_p$ of equation [8.33] is assumed negligible leading to the equations:

$$I_x = [l^2(k_1 + k_2)]/(\omega_{o_{off}}^2) \qquad [8.35]$$

$$f_x = 2.I_x.\mu_{off} \qquad [8.36]$$

8.4.2.1 Wind-off experiments - SET 1:

The model was displaced from the equilibrium position and the oscilliatory reponse recorded. From the decay graph the period of oscillation, T, was estimated to be equal to 1.05 sec. Next, the values of the maximum peaks were estimated from the decay graph and plotted against time. Values of μ and ω_o^2 were calculated as follows:

$$\mu = \ln\left(\frac{55.292}{18.684}\right) \div (5.425 - 1.225) = 0.258 \text{ (rad/sec)}$$

$$\omega_o^2 = (\omega_n^2 + \mu^2) = \frac{4\pi^2}{T^2} + \mu^2 = (5.984)^2 + (0.258)^2 = 35.875 \text{ (rad/sec)}^2$$

$\omega_o = 5.99$ rad/sec.

Finally, using equations equations [8.18] and [8.19] again, the values of I_x and f_x were found (see below).

(i) $I_x = []^2(k_1 + k_2)]/(\omega_o^2) \Rightarrow I_x = 0.0204$ kgm^2 or 0.015 slug.ft^2

(ii) $f_x = 2.I_x.\mu \Rightarrow f_x = 0.0105$ kgm^2.rad/sec

8.4.2.2 Wind-off experiments - SET 2:

$T_{off} = 0.65$ (sec) $\omega_n^2 = 93.440$ (rad/sec)^2

$\mu_{off} = 0.094$ (rad/sec) $\omega_{o\,off}^2 = 93.449$ (rad/sec)^2

Substituting these values into equations [8.35] and [8.36] gives:

$I_x = 0.030$ kgm^2 or 0.022 slug.ft^2

$f_x = 0.006$ kgm^2.rad/sec

Note: It was impossible to record any data for the wind-on case.

8.4.2.3 Table of results.

The roll inertia of the full scale Hawk is 5346.7 kgm^2. Thus for the model $I_x = 5346.7(\lambda^5)$. The model scale factor λ is 1/12 giving an expected value of $I_x = 0.022$ kgm^2.

	I_x (kgm^2)	f_x (kgm^2.rad/sec)
set 1:	0.020	0.011
set 2:	0.030	0.006
expected:	0.022	N/A

8.5 Yaw inertia experiments.

To measure the yawing moment of inertia two springs were attached horizontally to the aft of the model at l = 0.4m from the vertical rod. The model was set in lateral oscillation and the decay curve recorded. However, it was not possible to obtain a proper decay curve from the model for two main reasons. Firstly the yawing motion was subject to a fairly large mechanical friction because of the way that the vertical rod supporting the model needed to be restrained at the top of the dexion framework. Thus, the motion tended to damp out very quickly. The second problem was due to the way in which the yaw attitude potentiometer was attached to the rig. The spindle of the potentiometer slotted into the bottom of the vertical support rod with the main body of the potentiometer being fixed to a stationary horizontal disc on the rig using insulating tape. The potentiometer was difficult to secure in position and did not always remain stationary. Thus, it was necessary to fill the gap around the potentiometer with foam to ensure that the main body did not move.

8.5.1 Derivation of the yawing moment equations.

A description of the equations of motion for yaw has already been presented in section 8.1. The reduced model equation of motion may be expressed as follows (Ref 6):

$$\mathring{N}(t) = -\mathring{N}_v.v - \mathring{N}_p.p + I_z.\dot{r} - \mathring{N}_r.r - I_{xz}.\dot{p} \qquad [B.22]$$

As shown earlier in section 8.1, solution of the yawing moment equation for oscillatory motion leads to equations [8.13] and [8.14].

8.5.2 Estimation of yaw inertia and mechanical friction

If the model is tested with the wind off, the aerodynanamic terms of equations [8.13] and [8.14] may be neglected since $N_v \cong 0$ and $N_r \cong 0$. Moreover U_∞ will be zero, leading to equations [8.18] and [8.19], which are reproduced below for convenience.

$$I_z = [l^2(k_1 + k_2)]/(\omega_o{}^2_{off}) \qquad [8.18]$$

and

$$f_z = 2.I_z.\mu_{off} \qquad [8.19]$$

8.5.2.1 Wind-off experiments - SET 1:

Unfortunately accurate measurements could not be made for the first set of wind-off experiments due to practical problems with the mounting of the yaw potentiometer.

8.5.2.2 Wind-off experiments - SET 2:

$T_{off} = 0.61$ (sec) $\qquad \omega_n^2 = 106.096$ (rad/sec)^2

$\mu_{off} = 0.459$ (rad/sec) $\qquad \omega_o{}^2_{off} = 106.307$ (rad/sec)^2

Substituting the above values into equations [8.18] and [8.19] gives:

$$I_z = 0.126 \text{ kgm}^2 \quad \text{or} \quad 0.093 \text{ slug.ft}^2$$

$$f_z = 0.184 \text{ kgm}^2\text{.rad/sec}$$

8.5.2.3 Table of results.

The yaw inertia of the full scale Hawk is 23786.5 kgm^2. Thus for the model $I_z = 23786.5(\lambda^5)$. The model scale factor λ is 1/12 giving an expected value of $I_z = 0.022 \text{ kgm}^2$.

	I_z (kgm^2)	f_z (kgm^2.rad/sec)
set 1:	N/A	N/A
set 2:	0.126	0.184
expected:	0.096	N/A

8.5.3 Estimation of yawing moment derivatives.

As shown earlier, with the wind-on the following equations may be obtained:

$$2\zeta\omega_{o_{on}} = -2\mu_{on} = -(\mathring{N}_r + f_z)/I_z \qquad [8.13]$$

and

$$\mu_{off} = -\zeta\omega_o = f_z/2.I_z \qquad [8.15]$$

It may then be shown that:

$$\mathring{N}_r = 2.I_z.(\mu_{on} - \mu_{off}) \qquad [8.37]$$

Similarly, using equation [8.14], $\omega_{o}^{2}{}_{on} = (U_{\infty}\mathring{N}_{v}+K)/I_{z}$, and noting that $K/I_{z} = \omega_{o}^{2}{}_{off}$, it may be shown that:

$$\mathring{N}_{v} = (I_{z}/U_{\infty}).(\omega_{o}^{2}{}_{on} - \omega_{o}^{2}{}_{off}) \qquad [8.38]$$

From wind-on experiments the following values were estimated:

$T_{on} = 0.55$ (sec) $\qquad \omega_{n}^{2} = 130.507$ (rad/sec)^2

$\mu_{on} = 0.893$ (rad/sec) $\qquad \omega_{o}^{2}{}_{on} = 131.304$ (rad/sec)^2

Substituting the appropriate wind-off and wind-on values into equations [8.37] and [8.38] leads to

$\mathring{N}_{v} = 0.099$ kg.m/s

$\mathring{N}_{r} = -0.109$ kg.m^2/s

The experimental data wind-on was recorded at a tunnel speed of 63.8 mm H_2O which corresponds to $U_{\infty} = 32.73$ m/s.

The model parameters $S = 0.115$ m^2 and $b = 0.782$ m yield the following to non-dimensionalise the derivatives:

$$N_{v} = \mathring{N}_{v} / (0.5).\rho.U_{\infty}.S.b = \mathring{N}_{v} / 1.7478$$

$$N_{r} = \mathring{N}_{r} / (0.5).\rho.U_{\infty}.S.b^{2} = \mathring{N}_{r} / 1.3667$$

and thus

$$\Rightarrow N_{v} = 0.057 \quad \text{and} \quad \Rightarrow N_{r} = -0.08$$

A comparison can be made between values of the non-dimensional derivatives estimated above and those estimated by Malik (Ref 22); the results are summarised in the table below.

Derivative	Experimental	Estimated (Malik)
N_v	0.057	0.084
N_r	-0.080	-0.103

CHAPTER 9

COMPUTER SIMULATION OF AIRCRAFT

9.0 COMPUTER SIMULATION OF AIRCRAFT.

Computer simulations of various aircraft were developed and written in the Advanced Continuous Simulation Language (ACSL), Ref 28. The main purpose of the simulations was to model the small perturbation aircraft equations of motion so that the responses to inputs to the real aircraft, or to the wind tunnel model, could be reproduced. It was also intended that the simulations be used as a tool to aid development of the MSR in the form of F77 software and to re-create wind tunnel motion using S&C derivatives estimated using MSR.

For the Hawk model in the wind tunnel only three or four degrees of freedom of motion are available rendering some terms and aerodynamic force equations redundant. Since small perturbation equations are always assumed, it was not thought necessary to consider coupled aircraft responses and thus separate simulation programs were produced to model the longitudinal and lateral motion.

The ACSL simulation programs were initially developed using the full aircraft equations of motion, with changes introduced later to obtain reduced freedom wind tunnel aircraft simulations. Mathematical models for the aircraft equations of motion are discussed in Chapter 4. It was necessary to obtain a complete set of stability and control derivatives for the full scale Hawk aircraft, as detailed in Appendix D. The derivatives were used in the ACSL simulation programs.

Chapter 14 details the further simulations produced, with and without noise, for an alternative aircraft mathematical model structure in which the Hawk is fully restrained in the wind tunnel.

9.1 Development and testing of the simulation programs.

The way in which the ACSL aircraft simulation programs were developed has been described in various reports which were written during the course of the research programme, Refs 4 to 7. The structure of a typical ACSL program, *"*.csl"*, is shown below. The simulation language structure is such that FORTRAN 77 statements may also be inserted, for example to specify the file and data format to be output. The compiled program can be run interactively using a command file, *"*.cmd"*, and data output to the screen and/or default files.

```
PROGRAM TITLE
     small perturbation longitudinal aircraft simulation

INITIAL REGION

     specify constants (e.g. to convert radians to degrees)
     specify the flight condition
     define values of stability and control derivatives

END OF INITIAL


DYNAMIC REGION

     specify the time for the simulation to run
     specify the intervals at which data is to be saved


     DERIVATIVE REGION

          specify the integration algorithm to use
          specify the time step
          define table: magnitude & duration of control surface input
          define equations of motion
          integrate states
          perform any angular conversions necessary
          output to data file (if required)

     END OF DERIVATIVE


END OF DYNAMIC


END OF PROGRAM
```

Once the programs were written any aircraft could be used to test the program as simulating a particular aircraft simply required the numerical values of the stability and control derivatives in the program to be reset and the appropriate flight conditions to be defined. It was therefore decided to initially use Phantom (F4) data to test the simulation program since a design package on the BBC microcomputers had previously been used to produce graphs of step and impulse responses for the aircraft. The response graphs obtained from this work could therefore be compared directly with the responses output by the ACSL simulation. Details on the Phantom and full scale Hawk simulations are presented later in this Chapter. Before this, a brief description of the way in which control surface inputs to the aircraft are modelled is given.

9.2 Modelling of control surface inputs.

In ACSL a TABLE function can be used to define a dependent variable which has up to three independent parameters. The control surface angle inputs to the aircraft model can thus be defined using the TABLE function with only one independent parameter, that of time. For example, the rudder doublet (shown below) may be defined using the following ACSL statement:

```
TABLE ZTDEG,  1, 7
     / 0.0, 0.99, 1.0, 1.01, 1.99, 2.0, 500.0
     / 1.0, 1.00, 0.0, -1.0, -1.0, 0.0,   0.0
```

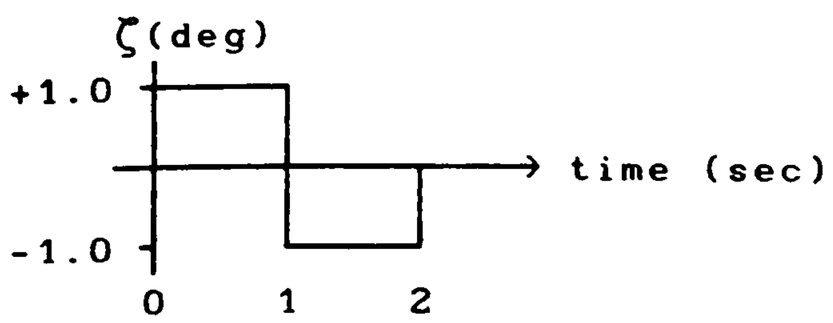

The first line of the ACSL table statement shows that there is one independent x variable (in this case time) and that there are seven values of the dependent y variable of ZTDEG, defined at seven points in time. When the simulation is run ACSL interpolates between the values defined in the table to calculate the value of ZTDEG at each time step in the integration procedure. At times t = 0.99 sec, t = 0.0 sec and t = 1.01 sec, ZTDEG is defined as changing from +1.0 to 0.0 to -1.0. This is to ensure that a "smooth" change in ZTDEG is seen by the simulation equations rather than a sudden jump from +1.0 to -1.0 in a single time step.

It is also possible to define the TABLE function in a separate ACSL procedure which can be read from the main ACSL program, in the same way that a FORTRAN program accesses a subroutine. This facility could be utilised when recorded control surface inputs from the dynamic rig are modelled in order to test the integrity of any derivatives estimated using the MSR procedure.

9.3 Phantom longitudinal motion simulation.

The small perturbation longitudinal equations of motion may be written in a state variable form (i.e. $\dot{\underset{\sim}{x}} = A.\underset{\sim}{x} + B.\underset{\sim}{u}$) as follows:

$$\begin{pmatrix} \dot{u} \\ \dot{w} \\ \dot{q} \\ \dot{\theta} \\ \dot{h} \end{pmatrix} = \begin{pmatrix} X_u & X_w & (X_q - W_e) & -g & 0 \\ Z_u & Z_w & (U_e + Z_q) & 0 & 0 \\ m_u & m_w & m_q & 0 & 0 \\ 0 & 0 & 1 & 0 & 0 \\ 0 & -1 & 0 & U & 0 \end{pmatrix} \begin{pmatrix} u \\ w \\ q \\ \theta \\ h \end{pmatrix} + \begin{pmatrix} X_\eta \\ Z_\eta \\ m_\eta \\ 0 \\ 0 \end{pmatrix} \begin{pmatrix} \eta \end{pmatrix} \qquad [9.1]$$

Numerical values for the terms in the A and B state matrices were obtained from Ref 26 for the following flight conditions:

Aircraft mass	m	=	17671 kg
Sea level height	H	=	0 m
Mach no.	M	=	1.10
Speed	U	=	377 m/sec
Inertias	I_x	=	34447 kgm^2
	I_y	=	168351 kgm^2
	I_z	=	192534 kgm^2
	I_{xz}	=	3000 kgm^2

$$A = \begin{pmatrix} -0.068 & 0.011 & 0.0 & -9.8 \\ 0.023 & -2.1 & 375 & 0.0 \\ 0.011 & -0.16 & -2.2 & 0.0 \\ 0.0 & 0.0 & 1.0 & 0.0 \\ 0.0 & -1.0 & 0.0 & 377 \end{pmatrix} \qquad B = \begin{pmatrix} -0.4 & 1 \\ -77. & 0 \\ -61. & 0 \\ 0. & 0 \\ 0. & 0 \end{pmatrix}$$

The simulation was built up as shown by the following example: The first line of equation [9.1], i.e.

$$\dot{u} = x_u.u + x_w.w + (x_q - W_e).q - g.\theta + x_\eta.\eta$$

appears in the ACSL program, as

```
UDOT = XU*U + XW*W + (XQ-WE)*Q - G*THETA + XETA*ETA
```

where the derivatives XU, XW, XQ are defined as constants at the beginning of the program and where θ and η are in radians.

A similar notation is adopted to model the other equations of [9.1]. However, because of a constraint which only allows variable names with a maximum of six characters, $\dot{\theta}$ (THETADOT) is called THETAD.

To model a step input in the program, ETA is set to 0.01745 rad (i.e. 1°) at the beginning of the program for an arbitrary period of time, for example TIMEON = 100 sec. TIMEON was chosen to be far longer than the time needed to produce the short period step response of the aircraft. A comparison of the step responses for θ and q using the BBC package and the ACSL program was performed and a very good correspondence between the two sources was found, Figures 34 and 35.

For the impulse input ETA is set to 1.0 at the start of the program and then reset to zero after a fraction of a second, typically about 0.01 sec. The shortest time that ETA can be set to 1.0 is with TIMEON equal to 10^{-10}sec. This figure corresponds to the smallest integration time step possible in ACSL. However, in practice, a variation in TIMEON between 10^{-10}sec and 0.01sec was found to make no discernible difference to the quality of the results.

9.4 Phantom lateral motion simulation.

The lateral equations of motion used in the simulation are of the form:

$$\begin{pmatrix} \dot{v} \\ \dot{p} \\ \dot{r} \\ \dot{\phi} \\ \dot{\psi} \end{pmatrix} = \begin{pmatrix} y_v & y_p & (y_r - U_e) & g & 0 \\ l_v & l_p & l_r & 0 & 0 \\ n_v & n_p & n_r & 0 & 0 \\ 0 & 1 & 0 & 0 & 0 \\ 0 & 0 & 1 & 0 & 0 \end{pmatrix} \begin{pmatrix} v \\ p \\ r \\ \phi \\ \psi \end{pmatrix} + \begin{pmatrix} y_\xi & y_\zeta \\ l_\xi & l_\zeta \\ n_\xi & n_\zeta \\ 0 & 0 \\ 0 & 0 \end{pmatrix} \begin{pmatrix} \xi \\ \zeta \end{pmatrix} \qquad [9.2]$$

where the state matrices A and B, for the flight conditions given in section 9.2 were defined as follows, Ref 26:

$$A = \begin{pmatrix} -0.49 & 0.0 & -377 & -9.8 \\ -0.13 & -3.1 & 0.80 & 0.0 \\ 0.10 & 0.018 & -1.2 & 0.0 \\ 0.0 & 1.0 & 0.0 & 0.0 \\ 0.0 & 0.0 & 1.0 & 0.0 \end{pmatrix} \qquad B = \begin{pmatrix} 3.9 & 11.6 \\ -15.0 & 9.3 \\ -2.5 & -8.8 \\ 0.0 & 0.0 \\ 0.0 & 0.0 \end{pmatrix}$$

For convenience, it was decided to produce two lateral simulation programs, LATROL.CSL and LATYAW.CSL to model the roll response and yaw responses separately. These programs are identical in every respect apart from one having constants called XI and TIMEXI for modelling aileron inputs and the other constants called ZETA and TIMEZT for the rudder inputs. The lateral equations of motion were specified in a similar way to the longitudinal equations of motion.

For example, taking the first line of [9.2], that is

$$\dot{v} = y_v.v + y_p.p + (y_r - U_e).r + g.\phi + y_\xi.\xi + y_\zeta.\zeta$$

this appears in both the lateral simulation program as:

```
VDOT = YV*V + YP*P + (YR-UE)*R + G*PHI + YXI*XI + YZETA*ZETA
```

where the derivatives YV, YP, YR are defined at the beginning of the program and all angles are in radians.

A comparison of the step responses for ϕ, p, ψ and r using the BBC package and the LATROL.CSL program was made. Again a very good correspondence in the step responses from the two sources was obtained. For example, Figures 36 and 37 show the comparison of the lateral roll responses produced for ϕ and p.

BBC

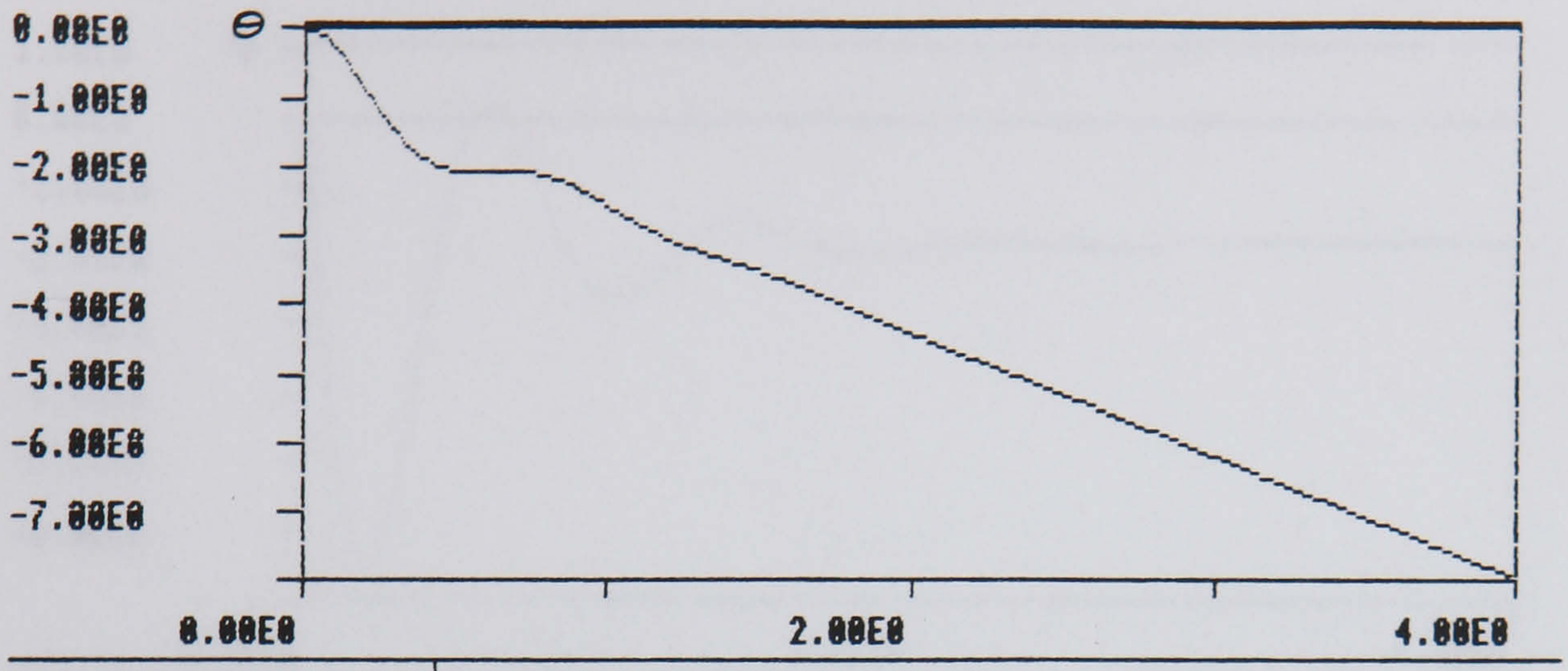

Step of 1.00E0 | Time : 3.98E0 Output : -7.86E0

-41.4
+0.945*Exp(-2.15*T)*Sin(7.75*T+1.06)
-41.5*Exp(-3.51E-2*T)*Sin(4.14E-2*T-1.36)

ACSL

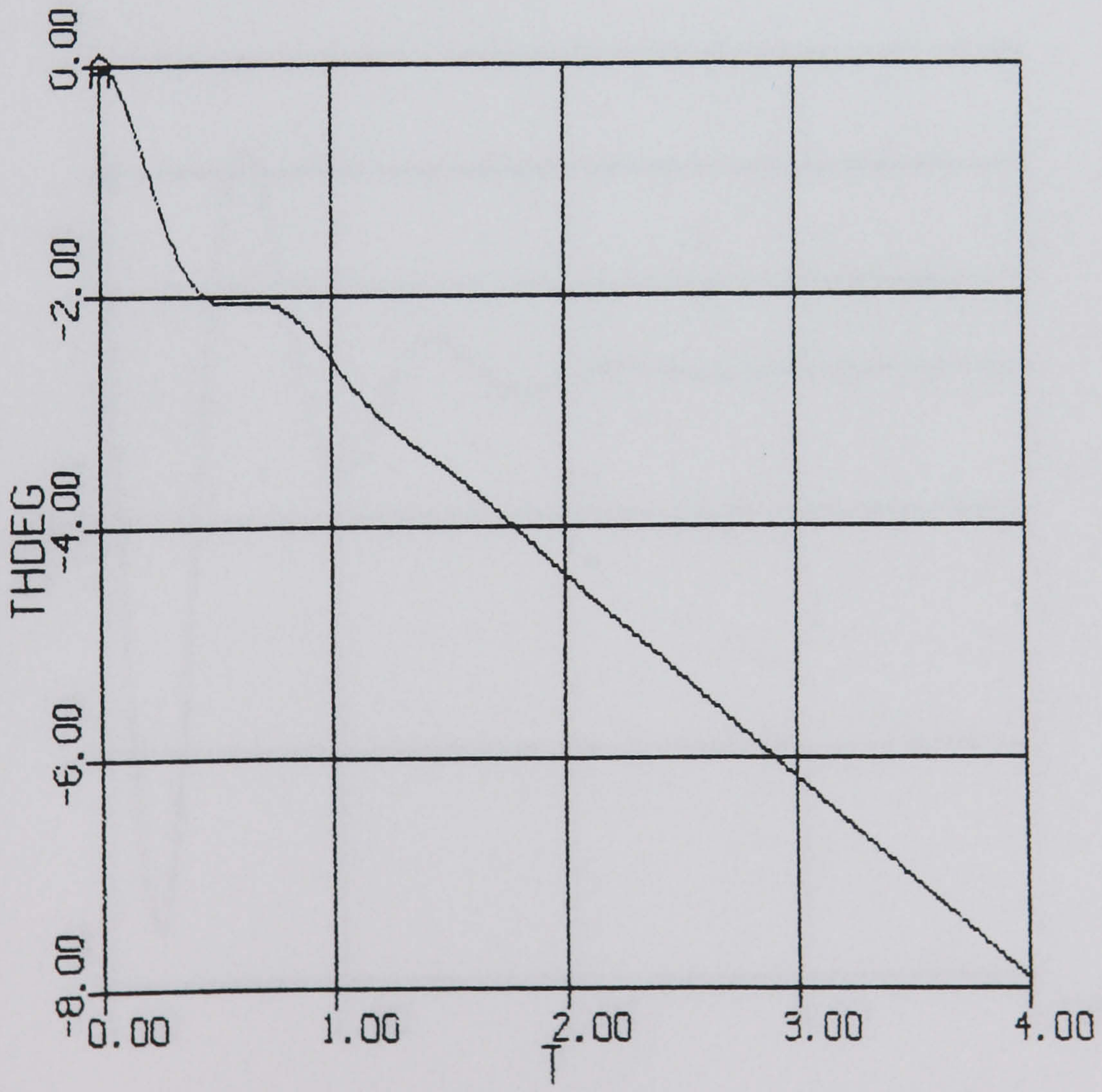

FIGURE 34: PITCH RESPONSE (1° STEP INPUT TO η)

BBC

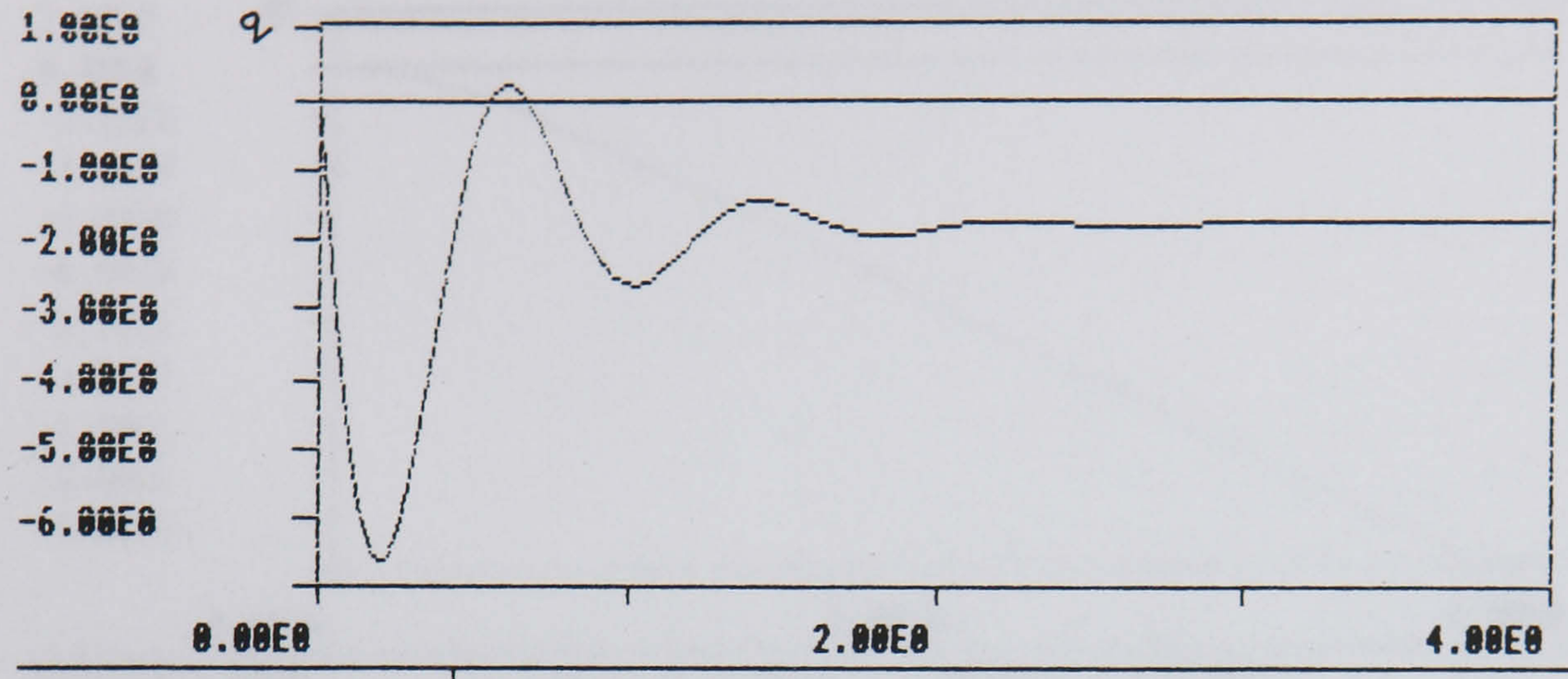

Step of 1.00E0 | Time : 3.98E0 Output : -1.73E0

-3.48E-6
-7.59*Exp(-2.15*T)*Sin(7.75*T-0.238)
-2.26*Exp(-3.51E-2*T)*Sin(4.14E-2*T+0.917)

ACSL

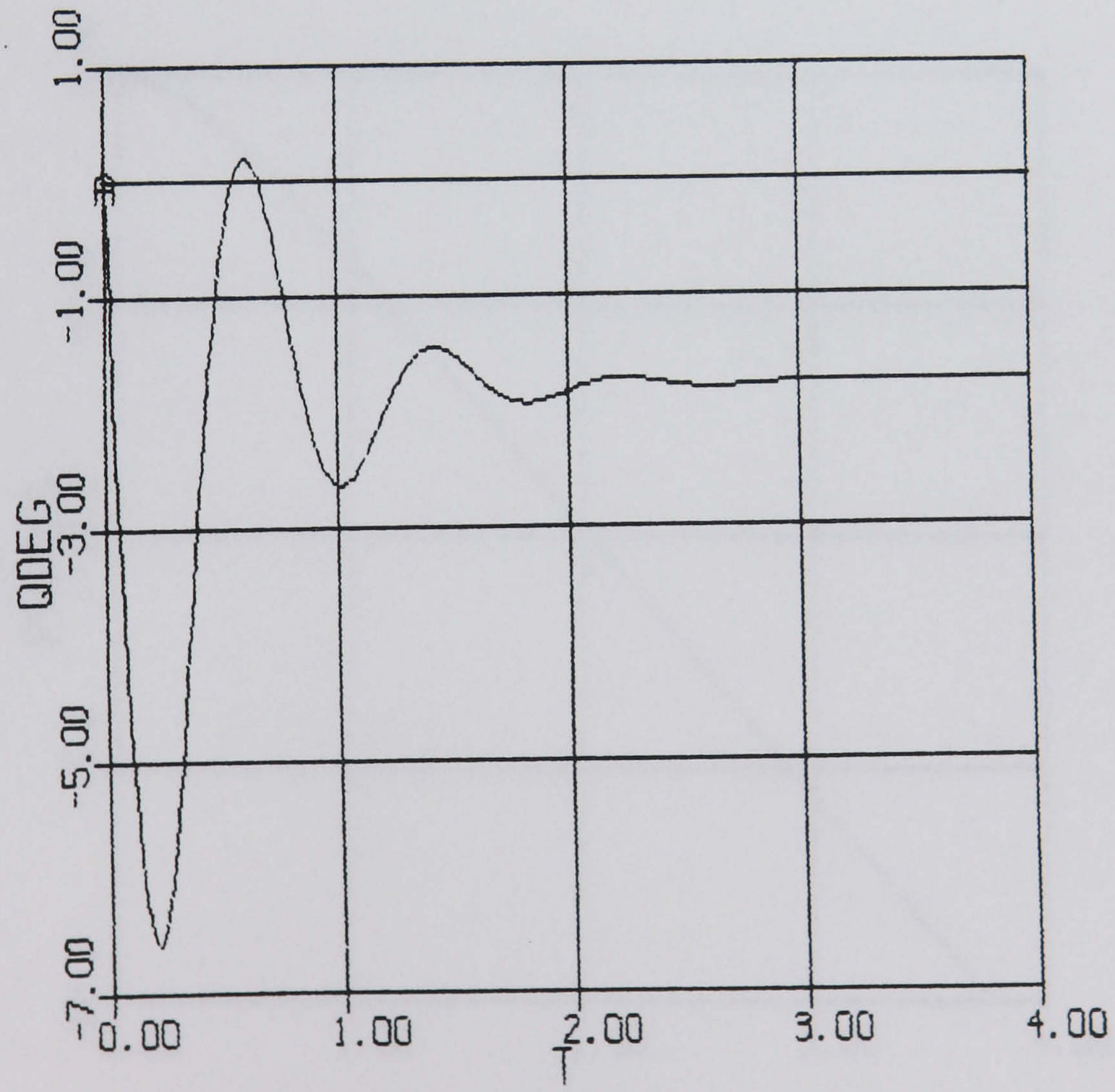

FIGURE 35: PITCH RATE RESPONSE (1° STEP INPUT TO η)

BBC

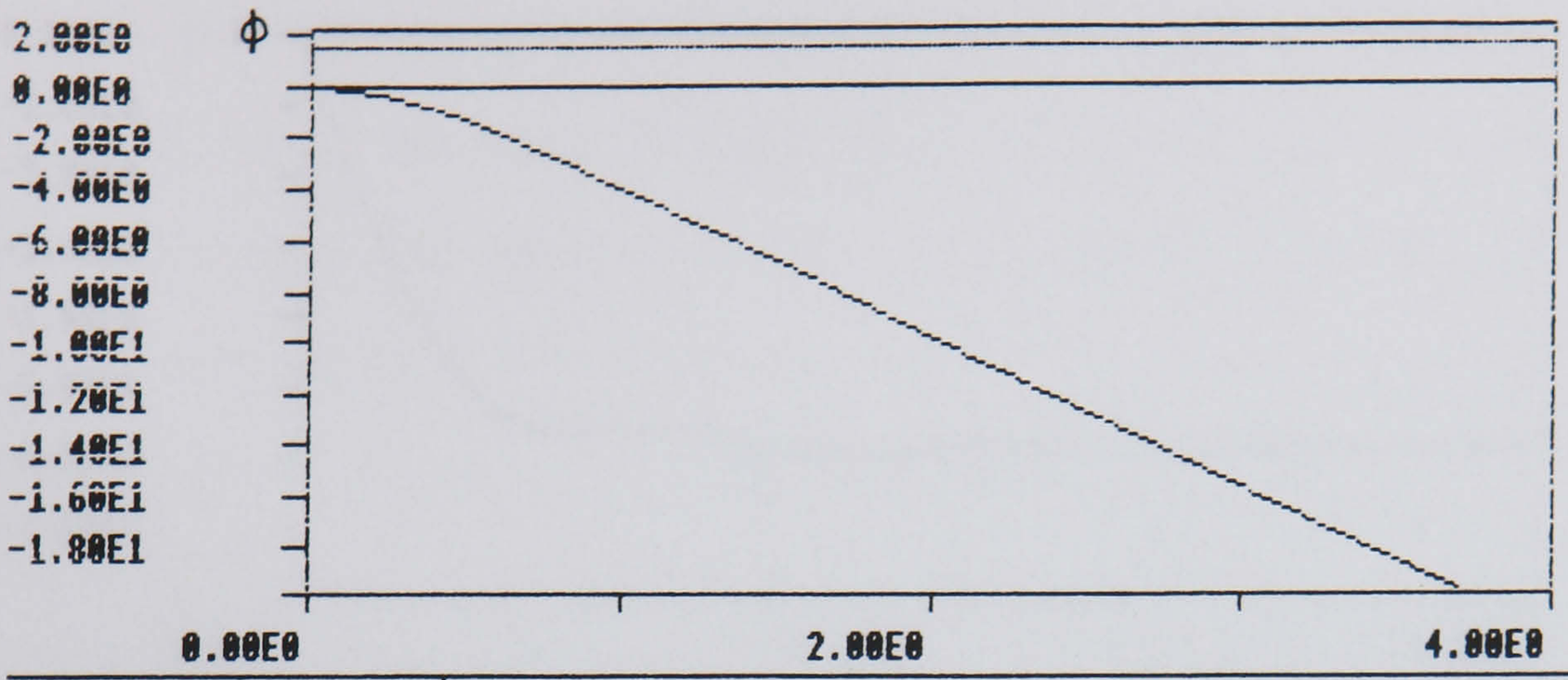

Step of 1.00E0 | Time : 3.98E0 Output : -2.13E1

```
+1.53
-938*Exp(6.22E-7*T)
+938*Exp(-6.28E-3*T)
-1.84*Exp(-3.1*T)
+8.02E-2*Exp(-0.84*T)*Sin(6.13*T-1.35)
```

ACSL

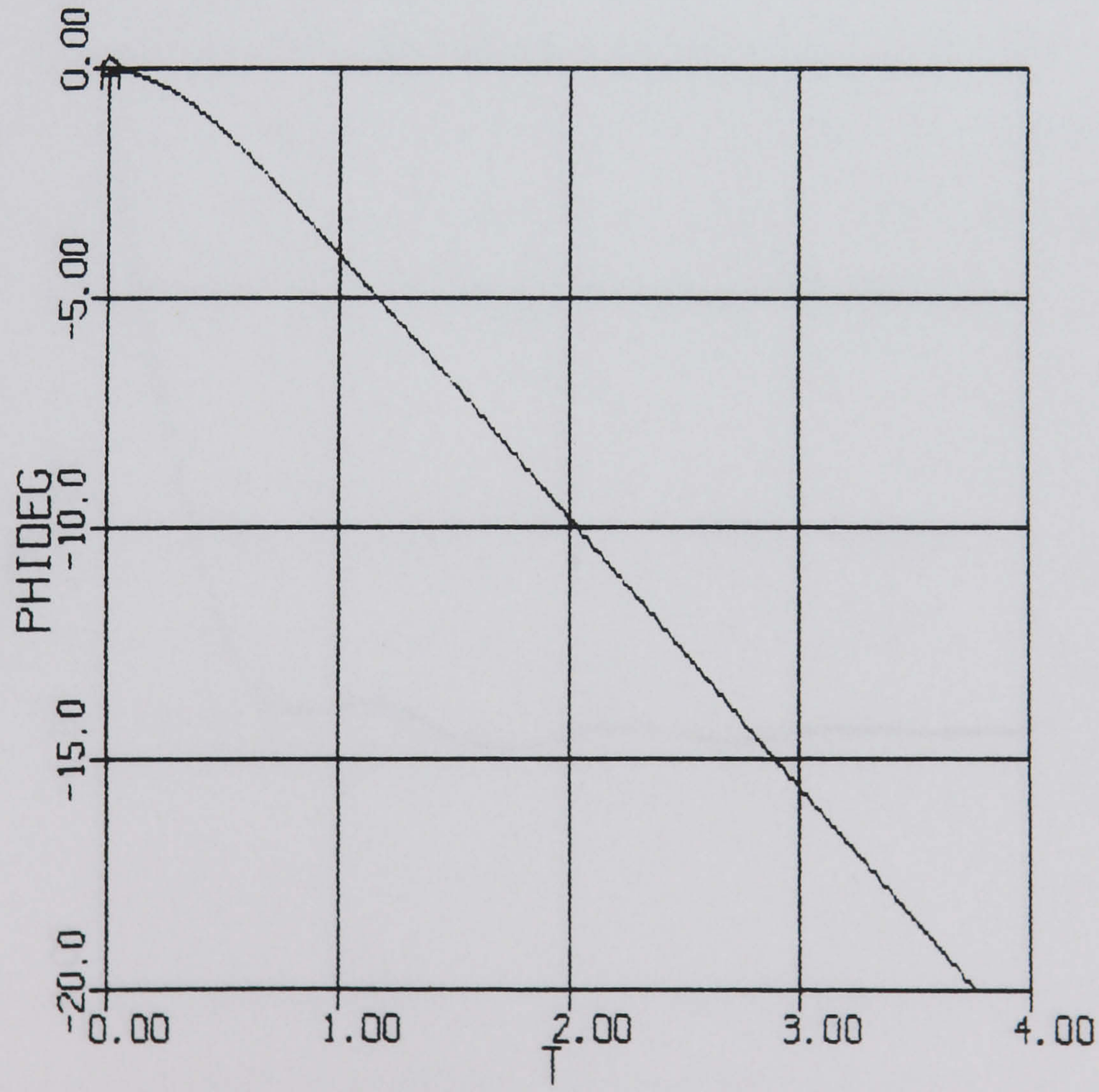

FIGURE 36: ROLL RESPONSE (1° STEP INPUT TO ξ)

BBC

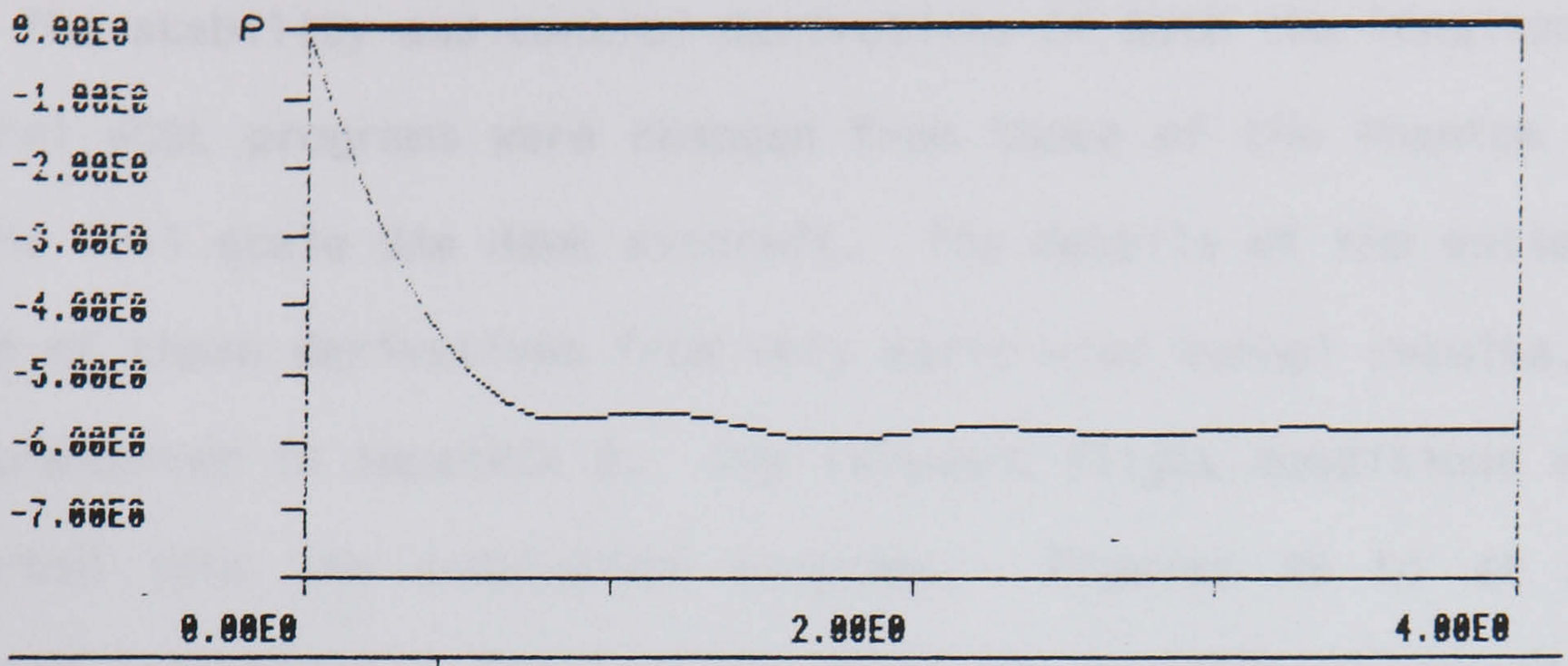

Step of 1.00E0 | Time : 3.98E0 Output : -5.75E0

```
-10.7
+10.7*Exp(6.22E-7*T)
-5.89*Exp(-6.28E-3*T)
+5.72*Exp(-3.1*T)
+0.496*Exp(-0.84*T)*Sin(6.13*T+0.352)
```

ACSL

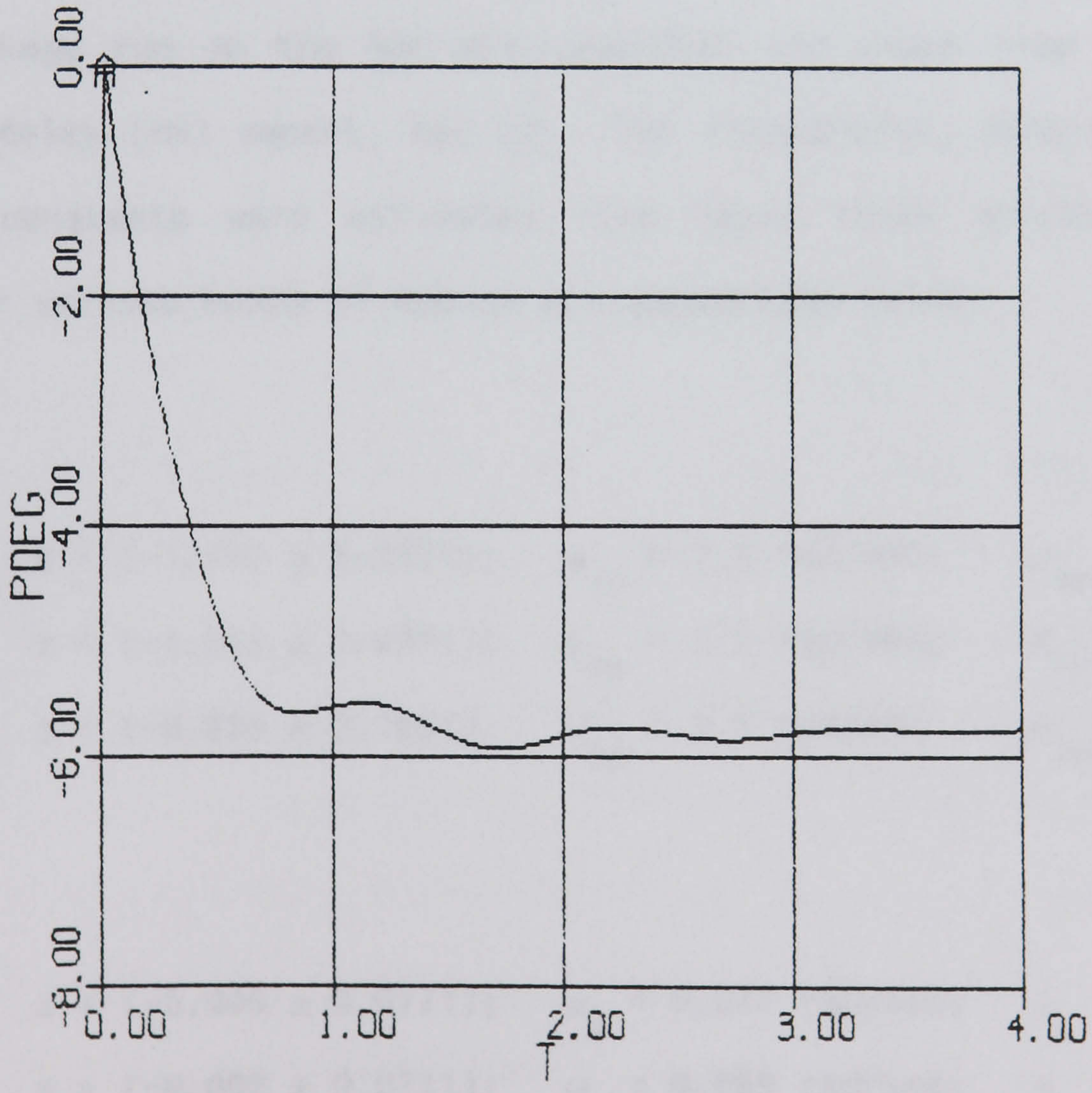

FIGURE 37: ROLL RATE RESPONSE (1° STEP INPUT TO ξ)

9.5 Full scale Hawk simulations.

The stability and control derivatives of both the longitudinal and lateral ACSL programs were changed from those of the Phantom to those of the full scale BAe Hawk aircraft. The details of the estimation of a set of these derivatives from very early wind tunnel results, Ref 29, are presented in Appendix D. The relevant flight conditions were also inserted into the simulation programs. Figures 38 to 42 show the various longitudinal and lateral modes of aircraft motion which were produced by the ACSL simulation of the full scale Hawk.

The longitudinal and lateral ACSL programs were run to compare the aircraft responses obtained with those obtained using a control system design package run on the BBC microcomputer and those from an early Hawker Siddeley (HS) report, Ref 29. The frequencies, damping ratios and time constants were estimated from these three sources. The results for various modes of motion are summarised below:

<u>SPPO:</u>

HS	$s = (-1.512 \pm 2.357i)$;	$\omega_{sp} = 2.8$ rad/sec;	$\rho_{sp} = 0.54$
BBC	$s = (-1.512 \pm 2.231i)$;	$\omega_{sp} = 2.7$ rad/sec;	$\rho_{sp} = 0.56$
ACSL GRAPH	$s = (-0.805 \pm 2.155i)$	$\omega_{sp} = 2.3$ rad/sec	$\rho_{sp} = 0.68$

<u>PHUGOID:</u>

HS	$s = (-0.005 \pm 0.077i)$;	$\omega_{p} = 0.077$ rad/sec;	$\rho_{p} = 0.065$
BBC	$s = (-0.002 \pm 0.071i)$;	$\omega_{p} = 0.069$ rad/sec;	$\rho_{p} = 0.073$
ACSL GRAPH	$s = (-0.001 \pm 0.071i)$;	$\omega_{p} = 0.071$ rad/sec;	$\rho_{p} = 0.070$

ROLL SUBSIDENCE:

HS	$s = (-3.0\ sec^{-1})$;	$T_R = 0.33sec$
BBC	$s = (-3.8\ sec^{-1})$;	$T_R = 0.26sec$
ACSL GRAPH	$s = (-2.3\ sec^{-1})$;	$T_R = 0.43sec$

SPIRAL MODE:

HS	$s = (-0.0109\ sec^{-1})$;	$T_s = 91.73sec$
BBC	$s = (-0.0005\ sec^{-1})$;	$T_s = 2000sec$
ACSL GRAPH	$s = (-0.0321\ sec^{-1})$;	$T_s = 31.11sec$

DUTCH ROLL:

HS	$s = (-0.356 \pm 1.968i)$;	$\omega_{dr} = 2.0$ rad/sec;	$\rho_{dr} = 0.178$
BBC	$s = (-0.320 \pm 2.090i)$;	$\omega_{dr} = 2.1$ rad/sec;	$\rho_{dr} = 0.153$
ACSL GRAPH	$s = (-0.152 \pm 2.044i)$	$\omega_{dr} = 2.05$ rad/sec;	$\rho_{dr} = 0.148$

9.6 Discussion of initial simulation results.

Using an estimated set of the full scale Hawk stability and control derivatives in the ACSL simulation programs led to aircraft responses which were very close to those expected. The damping ratios and frequencies of the longitudinal SPPO and phugoid oscillation were in good agreement, as were the lateral dutch roll and roll subsidence modes. The spiral mode was the only mode not clearly defined. The spiral time constant T_s is a difficult root to obtain accurately as it is relatively small and close to zero. It was concluded that the ACSL simulation programs provided a satisfactory representation of the full scale Hawk aircraft. Furthermore, data produced by the simulations could be used as input data to test the MSR computer program.

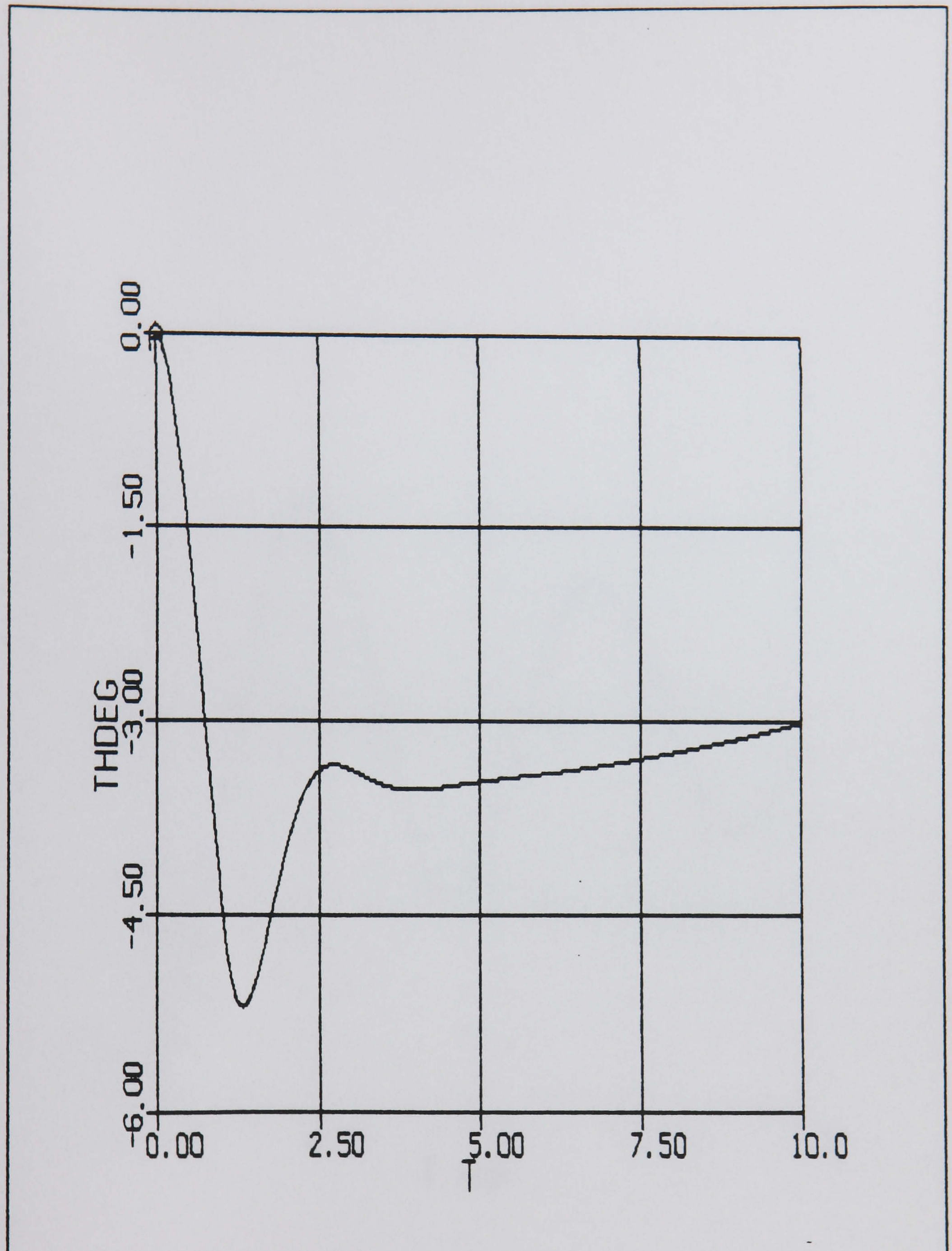

FIGURE 38: LONGITUDINAL SPPO (IMPULSE TO η)

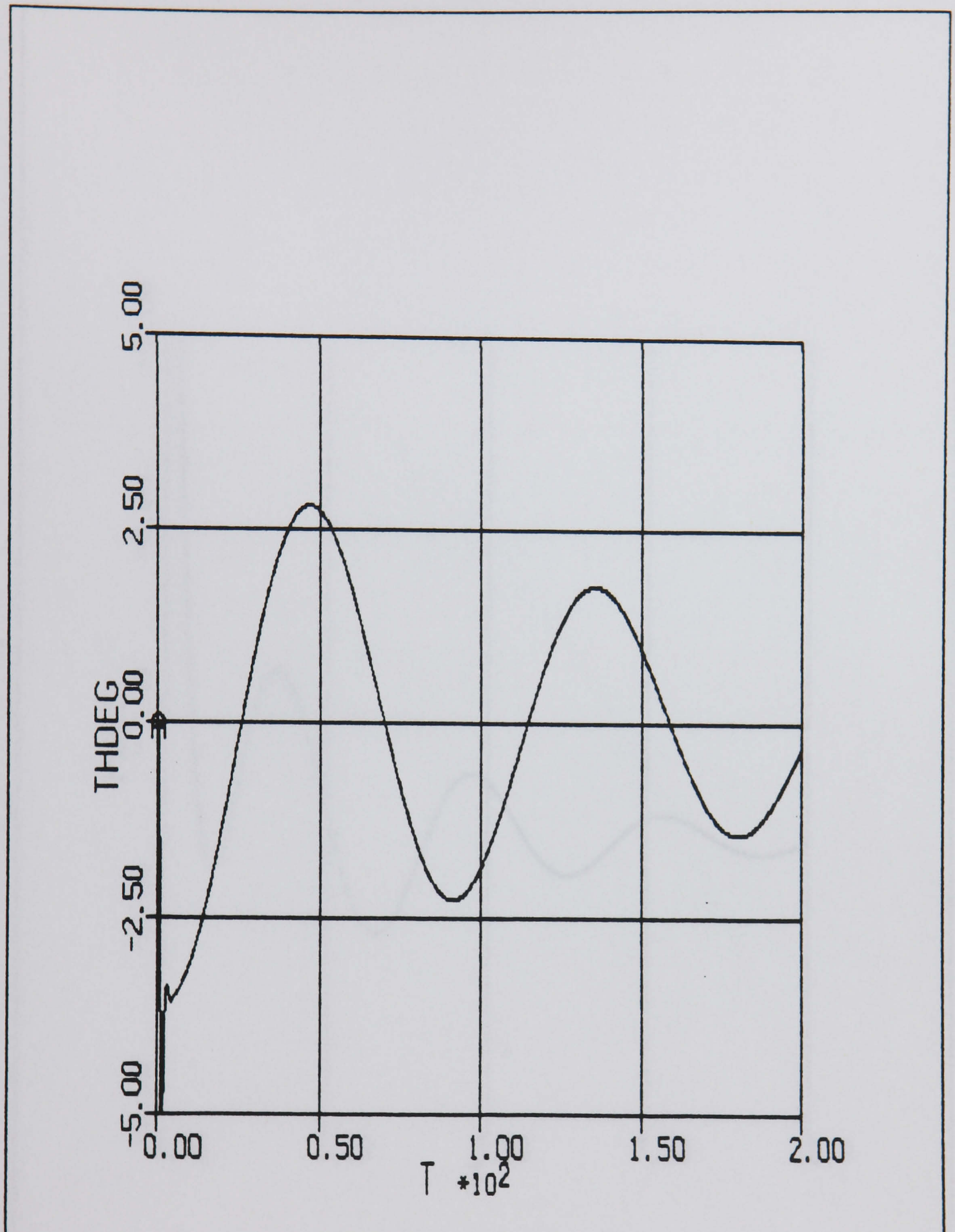

FIGURE 39: LONGITUDINAL PHUGOID OSCILLATION (IMPULSE TO η)

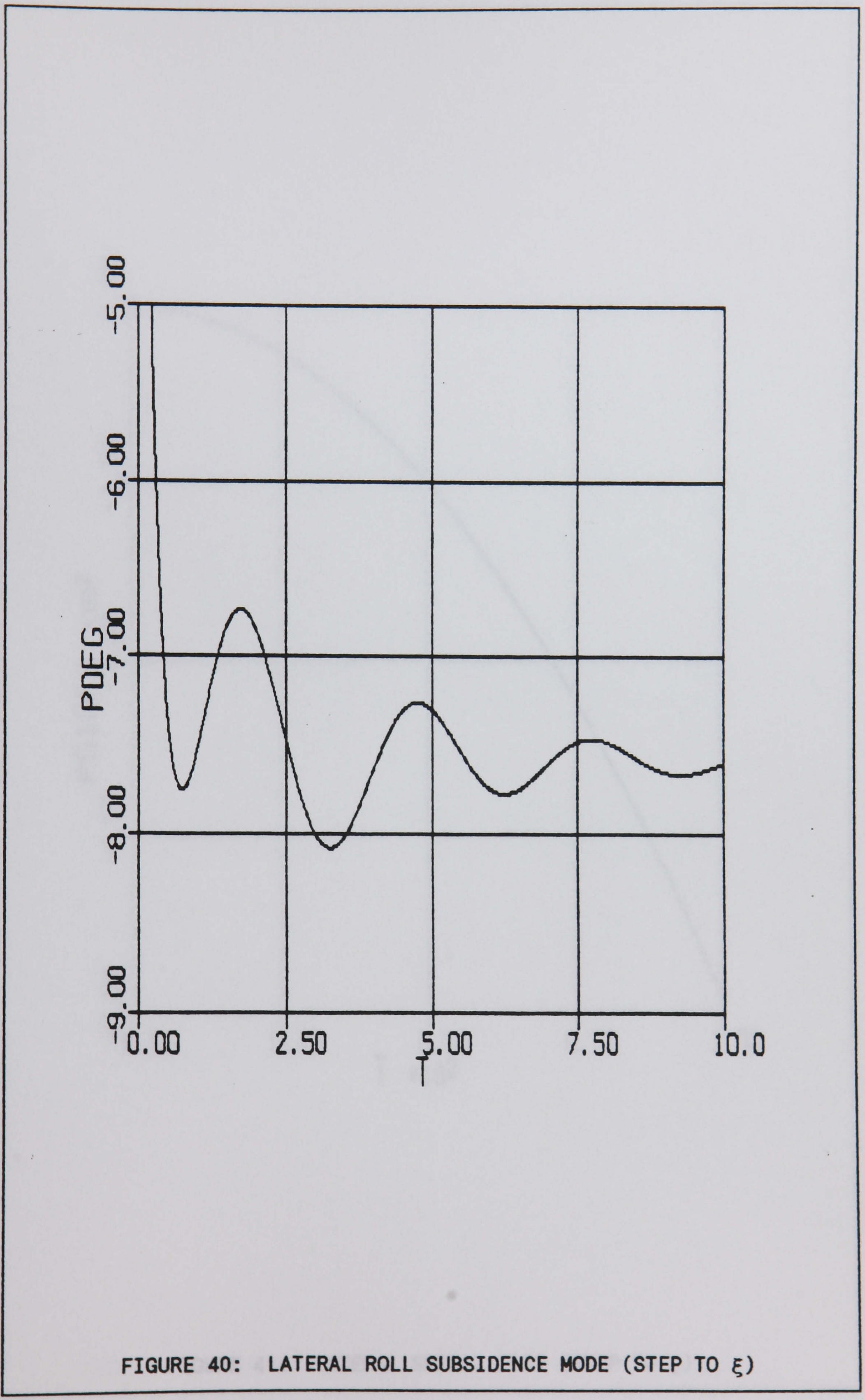

FIGURE 40: LATERAL ROLL SUBSIDENCE MODE (STEP TO ξ)

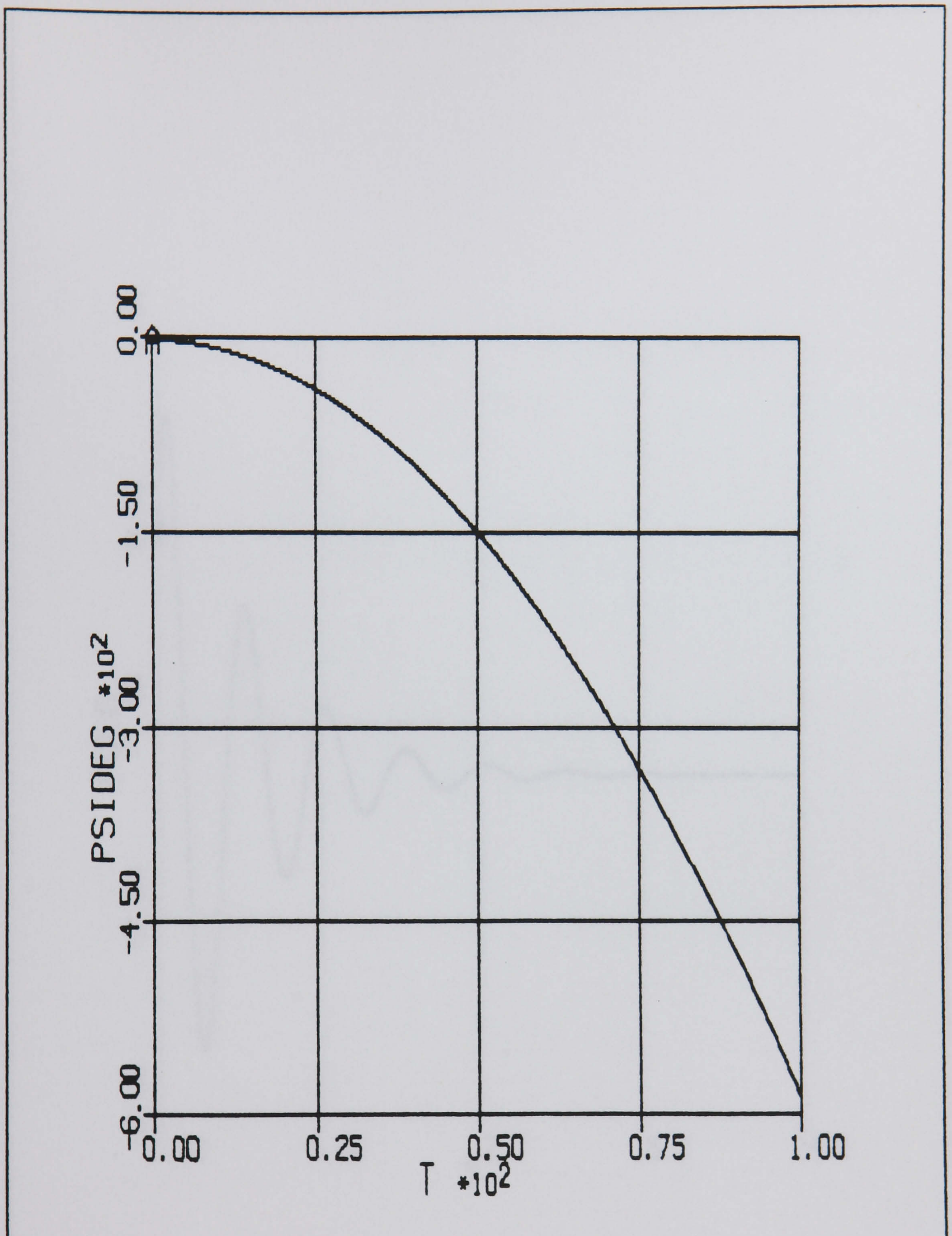

FIGURE 41: LATERAL SPIRAL MODE (STEP TO ζ)

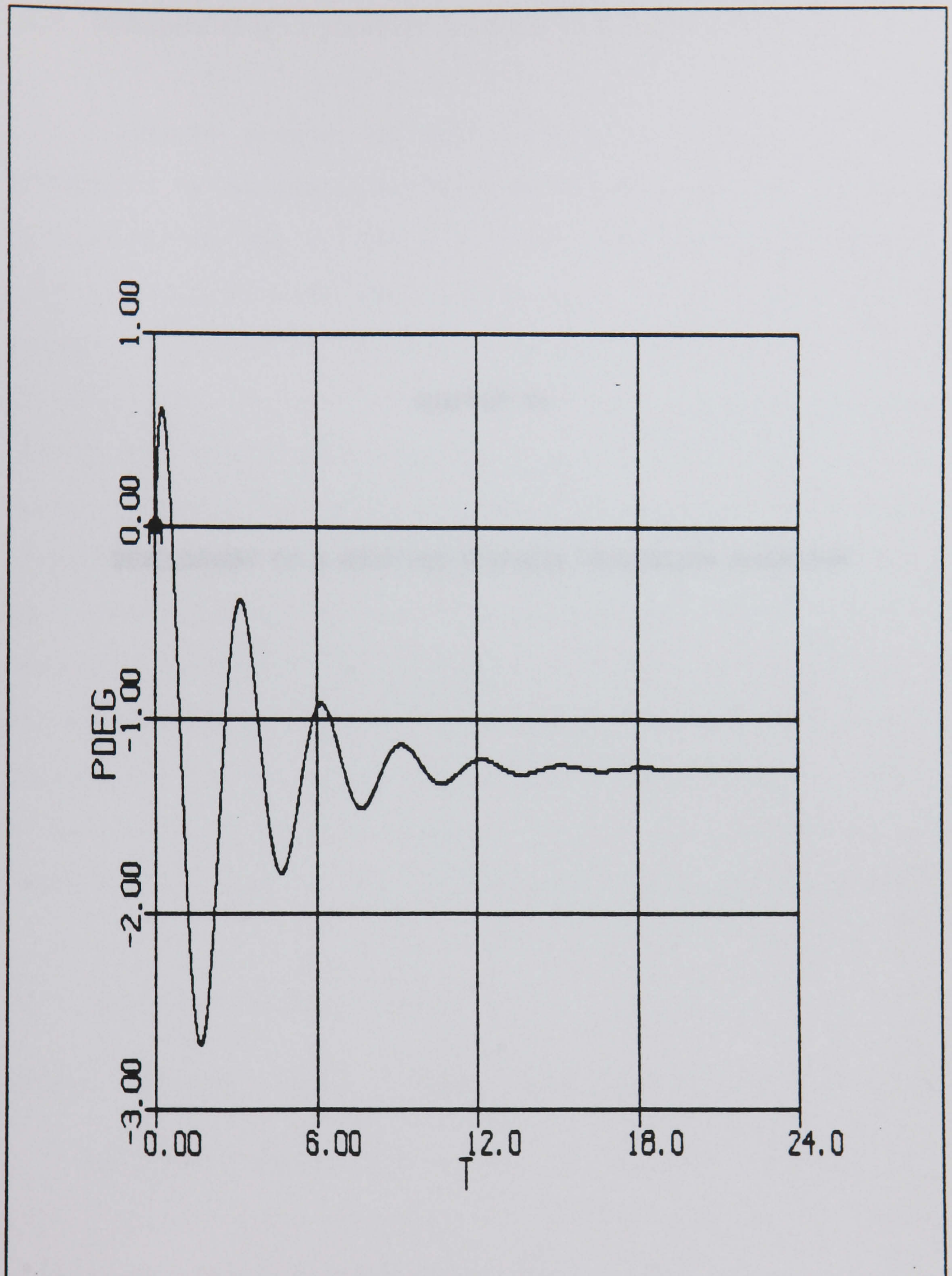

FIGURE 42: LATERAL DUTCH ROLL OSCILLATION (IMPULSE TO ζ)

CHAPTER 10

DEVELOPMENT OF A MODIFIED STEPWISE REGRESSION ALGORITHM

10.0 DEVELOPMENT OF A MODIFIED STEPWISE REGRESSION ALGORITHM.

A computer program has been designed and written in standard FORTRAN 77 to implement the modified stepwise regression procedure computationally, Ref 7. The program was tested using data generated with the ACSL aircraft simulation programs. The program was also tested using a data set referred to as "HALD" data, obtained from Ref 16 which used the HALD data to demonstrate a stepwise regression method. Ref 16 also gave values for parameters and various statistical terms expected at each iterative stage of the method. A flow diagram which summarises the steps of the the MSR process is shown in Figure 43. The final output is a "best" estimate of the coefficients in the regression equations from which the aerodynamic stability derivatives 'β' may be deduced. A comprehensive statistical theory describing the implementation of the MSR procedure may be found in Refs 7, 15 and 16. A description of the main steps in the MSR procedure follows with comments on how the procedure was implemented in the computer program.

10.1 MSR computational procedure.

STEP 1: Read data, initialise variables and evaluate constant matrices.

Referring to equation [10.1] below, a sequence of N readings of x_i ($i = 1$ to $n-1$) and y are taken over a short time interval and the measured data are used to construct matrices $\underline{X}$ and $\underline{Y}$.

$$\begin{pmatrix} y_{(1)} \\ y_{(2)} \\ \vdots \\ y_{(N)} \end{pmatrix} = \begin{pmatrix} 1 & x_{1(1)} & x_{2(1)} & \cdots & x_{n-1(1)} \\ 1 & x_{1(2)} & x_{2(2)} & \cdots & x_{n-1(2)} \\ \vdots & \vdots & \vdots & & \vdots \\ 1 & x_{1(N)} & x_{2(N)} & \cdots & x_{n-1(N)} \end{pmatrix} \begin{pmatrix} \beta_0 \\ \beta_1 \\ \vdots \\ \beta_{n-1} \end{pmatrix} + \begin{pmatrix} \varepsilon_{(1)} \\ \varepsilon_{(2)} \\ \vdots \\ \varepsilon_{(N)} \end{pmatrix} \qquad [10.1]$$

$$\underline{Y} = \underline{X} \cdot \underline{\beta} + \underline{\varepsilon}$$

The values of the statistical variables are set to appropriate acceptance levels and various variables and arrays are initialised to zero.

From the output data Y(N,1) the matrices YT = Y^T and YTY = Y^T* Y are evaluated and the value of the mean of Y, YAV was calculated using the formula $\bar{y} = \frac{1}{N} \sum y(i)$. These parameters, which all involve Y, need only be calculated once during the first iteration as their values will not change in subsequent iterations.

STEP 2: Formulate and output the current mathematical model.

The mathematical model is formulated using the output (y) and the appropriate dependent (x) variables for the current iteration of the MSR procedure. (Note that the first iteration model is formulated by including all linear x variables).

The current iteration number and the regression model corresponding to that iteration is formulated and output as:

ITERATION NUMBER: 1
Y = BO + B1 X1 + B2 X2 + B3 X3.

STEP 3: Estimate derivatives.

The number of unknown parameters in the regression equation is denoted by n and for N » n, the first estimate of the derivatives, β, can be made using the method of least squares:

$$\beta = \left(X^T X\right)^{-1} X^T Y \qquad [10.2]$$

The estimates of the coefficients, β, are then output.

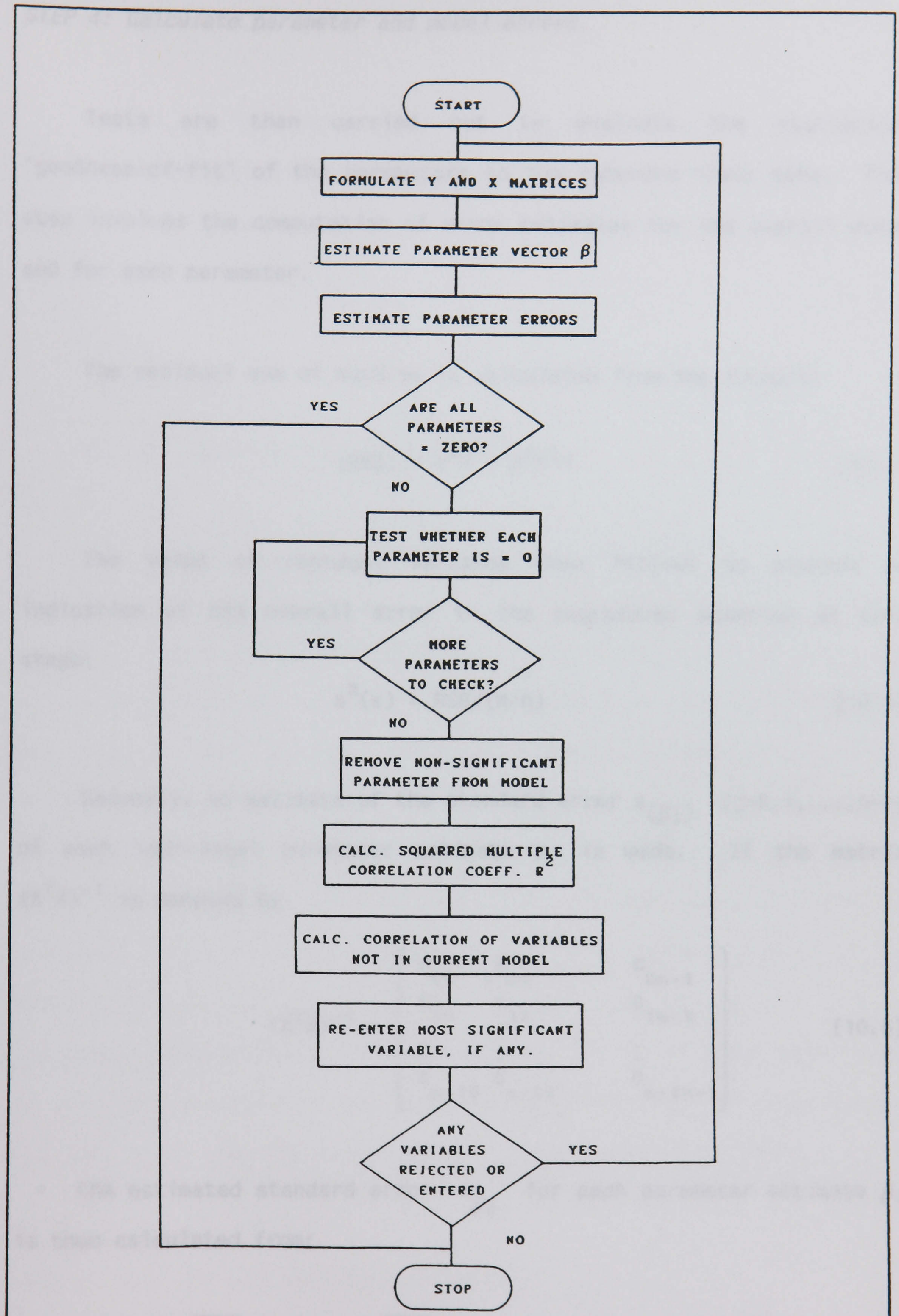

FIGURE 43: MSR FLOWCHART

STEP 4: Calculate parameter and model errors.

Tests are then carried out to evaluate the statistical "goodness-of-fit" of the parameters to the recorded input data. This step involves the computation of error estimates for the overall model and for each parameter.

The residual sum of squares is calculated from the formula:

$$(RSS) = Y^T Y - \beta^T X^T Y \qquad [10.3]$$

The value of residual variance then follows to provide an indication of the overall error in the regression equation at this stage:

$$s^2(\varepsilon) = RSS/(N-n) \qquad [10.4]$$

Secondly, an estimate of the standard error $s_{(\beta_j)}$ $(j=0,1,\ldots,n-1)$ of each individual parameter estimate β_j is made. If the matrix $(X^T X)^{-1}$ is denoted by

$$(X^T X)^{-1} = \begin{pmatrix} c_{00} & c_{01} & \cdots & c_{0n-1} \\ c_{10} & c_{11} & & c_{1n-1} \\ \vdots & \vdots & & \vdots \\ c_{n-10} & c_{n-11} & \cdots & c_{n-1n-1} \end{pmatrix} \qquad [10.5]$$

the estimated standard error s_{β_j} for each parameter estimate β_j is then calculated from:

$$s_{\beta o} = s\sqrt{c_{00}}\ ;\quad s_{\beta 1} = s\sqrt{c_{11}}\ ;\quad \ldots\ ;\quad s_{\beta n-1} = s\sqrt{c_{n-1}}; \qquad [10.6]$$

where $s = \sqrt{s^2(\varepsilon)}$ and is obtained from equation [10.4].

STEP 5: Test whether all parameters are zero.

The overall regression model is examined for the possibility that all of the parameter estimates β_j are equal to zero. The following hypotheses are therefore tested:

$$H_o: \beta_1 = \beta_2 = \ldots = \beta_{n-1} = 0$$

$$H_1: \text{not all } \beta_j = 0$$

The null hypothesis H_o is rejected if $F > F(\upsilon_1, \upsilon_2, \alpha_p)$ where:

$$F = \frac{\beta^T X^T Y - N \bar{y}^2}{(n-1)\, s^2(\varepsilon)} ; \qquad \bar{y} = \frac{1}{N} \sum y(i) \qquad [10.7]$$

F is a random variable having an F-distribution with $\upsilon_1 = n-1$ and $\upsilon_2 = N-n$ degrees of freedom. Tabulated values of the F-distribution, $F(\upsilon_1, \upsilon_2, \alpha_p)$ for various confidence levels α_p may be found in statistical reference tables. If at least 100 sets of observations have been recorded the effect of n (the number of unknown parameters) on the tabulated values of F is small and a critical value of F = 12 is selected. Thus if the calculated value of F is greater than 12 it is possible to say that not all of the derivatives β_0, β_1, β_2, ... , β_{n-1} are zero, although one or two may be zero. If it is found that there is a strong possibility that all the parameters are in-significant, i.e. all zero, then the computation is terminated at this point.

STEP 6: Test for any variables to reject.

The significance of individual terms in the regression is examined next using a partial F-test. The hypotheses used are:

$$H_0: \beta_j = 0$$

$$H_1: \beta_j \text{ is not } = 0$$

For each independent variable the partial F test criterion used is

$$F_p = \frac{[\beta_j]^2}{s^2_{\beta j}} \qquad [10.8]$$

where $s^2_{\beta j}$ is the variance estimate of β which was obtained in step 4.

The null hypothesis is rejected if $F_p > F(\upsilon_1, \upsilon_2, \alpha_p)$, where $\upsilon_1 = 1$ and $\upsilon_2 = N-n$, as it may be assumed that the parameter being tested is significant, ie. not equal to zero and should therefore be retained in the regression equation. If $F_p < F(\upsilon_1, \upsilon_2, \alpha_p)$ there is a chance that $\beta_j = 0$ and that variable should be removed from the model. If one or more parameters are found to be in-significant, i.e. could equal zero because $F_p <$ FPMIN where FPMIN is chosen to be equal to 12, then the x variable corresponding to the parameter with the lowest value of F_p is rejected from the regression equation.

STEP 7: Goodness of fit calculation.

The squared multiple correlation coefficient R^2 is calculated as it gives an indication of the goodness of fit of the regression equation to the recorded data. The nearer the value of R^2 to 1, the better the estimated model. R^2 is given by the expression:

$$R^2 = \frac{\beta^T X^T Y - N(\bar{y})^2}{Y^T Y - N(\bar{y})^2} = \frac{F}{(N-n)/(n-1) + F} \qquad [10.9]$$

STEP 8: Select the next variable to enter the model.

The variables which are not included in the current iteration of the mathematical model are examined to see how well they correlate with the recorded values of y(i), given the variables which are already in the regression equation. Any variables which show an improved correlation with y when they are re-entered into the model are identified. The variable which gives the best improvement in correlation is selected to be the next variable to include in the model.

For example, consider the case where the current iteration of the regression equation contains only the two variables x_2 and x_3, say, and the other variables $x_1, x_4, x_5, \ldots, x_{n-1}$ are not yet included in the equation. The mathematical model used to fit the experimental measured data would be:

$$y = b_0 + b_2.x_2 + b_3.x_3 + \epsilon \qquad [10.10]$$

A new independent variable z_1 is then constructed as shown below by finding the residuals of x_1 after regressing it on both x_2 and x_3.

$$z_1 = x_1 - (\beta_0 + \beta_2.x_2 + \beta_3.x_3) \qquad [10.11]$$

Similarly, the variables $z_4, z_5, \ldots, z_{n-1}$ are formed by regressing the variable z_4 on (x_2,x_3), z_5 on (x_2,x_3), etc. A new dependent variable y^* is represented by the residuals of y regressed on (x_2,x_3) using the model given by equation [10.10]. This yields

$$y^* = y - \beta_0 - \beta_2.x_2 - \beta_3.x_3 \qquad [10.12]$$

A new set of correlations which involve the variables y^*, z_1, z_4, z_5, ..., z_{n-1} is formulated. These partial correlations can be written as $r_{jy.23}$ meaning that the correlations of z_j and y^* are related to the model containing the variables x_2 and x_3. The expressions for the set of partial correlation coefficients $r_{jy.23}$ is given below in equations [10.13] - [10.16], where y is replaced by y^* and x_j replaced by z_j.

The correlation coefficient is given by the expression;

$$r_{jy} = \frac{s_{jy}}{(s_{jj}\, s_{yy})^{1/2}} \qquad [10.13]$$

where:

$$s_{jy} = \sum_{N} [\, x_j(i) - \bar{x}_j \,][\, y(i) - \bar{y} \,] \qquad [10.14]$$

$$s_{jj} = \sum_{N} [\, x_j(i) - \bar{x}_j \,]^2 \qquad [10.15]$$

$$s_{yy} = \sum_{N} [\, y(i) - \bar{y} \,]^2 \qquad [10.16]$$

$$\bar{x}_j = \frac{1}{N} \sum_{N} x_j(i); \qquad \bar{y} = \frac{1}{N} \sum_{N} y(i) \qquad [10.17]$$

The next variable selected for inclusion in the regression equation is the one whose partial correlation coefficient is the greatest. A new set of parameters are then estimated and the whole process of steps 2 to 8 is repeated iteratively. However, if none of the variables are significant, i.e. have F_p > FPMIN, then no new variable is selected for inclusion the mathematical model at the end of that particular iteration.

STEP 9: Termination.

When no more variables are available for rejection or inclusion in the regression model then, during that particular iteration, the procedure will stop and output the final form of the mathematical model and the value of the parameter estimates.

10.2 Selection of the best mathematical model.

It should be noted that the final mathematical model obtained using MSR will be the one which has the maximum F-value and gives the best fit to the simulated or experimental data. However, it cannot be guaranteed that MSR alone will select the best model to act as a predictor. It is also possible that iterations of the MSR will have two or more models with very close "maximum F-values", making it hard to decide on a final model. To ensure that the final model chosen will be a good predictor in addition to being a good fit to data, a rule known as the "Principle of Parsimony" can be applied, Ref 1. The principle states that "Given two models fitted to the same data with residual variances or "maximum" F-values which are close to each other, chose the model which involves the smaller number of parameters". To apply the Principle of Parsimony, it is possible to utilise a Prediction Sum of Squares (PRESS) criterion where the PRESS term is may be defined by the following equation, as described in Appendix E:

$$PRESS = \sum_{i=1}^{N} \{y(i) - \hat{y}[i|x(1),...,x(i-1),x(i+1),...,x(N)]\}^2 \quad [10.18]$$

where y(i) is the original measured data and $\hat{y}$ the predicted value of y(i) given $\underline{x}$, i.e. those terms in the final "best model structure".

The predictor $\hat{y}$ chosen by the MSR procedure can be considered to be an optimal predictor if it is also the model which has the minimum value of the PRESS term. Draper and Smith, Ref 16, state that the PRESS provides much detailed information about the stability of various fitted models over the data space and can help to focus attention on influential data points. However, there is a disadvantage in the enormous amount of computation required and there are no precise rules for choosing the best model. Despite this, Klein and Batterson, Ref 1, plotted graphs of F and PRESS values against iteration number and used the PRESS criterion as an additional source of information which can be used to help choose between "best-fit" models with similar F values.

10.3 Analysis of the MSR Procedure.

When any of the small perturbation equations of motion are manipulated into the mathematical format required for analysis using the MSR procedure, there is more than one arrangement of the equation which can be used. For example, an equation may have all terms positioned on the right hand side giving $\underline{B}.\underline{X} = \underline{Y} = \underline{0}$; OR terms involving all state variables which have been re-constructed around a particular measured variable can be grouped together resulting in combined derivative estimates from the final MSR model structure.

To aid analysis of the wind tunnel experimental results and make it easier to relate trends and observations to particular steps or matrix manipulations in the MSR process, it was decided to conduct some preliminary analysis of MSR using a simple set of data. The HALD data (Ref 16) was chosen for this as the final "best-fit" model structure

and the numerical values of the coefficients were known. Furthermore, with n = 4 independent X variables and N = 13 sets of observations, manipulation of the data file HALD.DAT was easy to perform.

10.3.1 Dependant Y variable set equal to zero.

$\underline{B}.\underline{X} = \underline{Y} = \underline{0}$. To obtain this structure an extra column of zeros was inserted in HALD.DAT. It was found that whatever the initial model structure used, (e.g. Y = B1.X1 + B2.X2 or Y = B1.X1 + B2.X2 + B3.X3), the MSR program always gave a) all parameter estimates as β=0; b) model residual sum of squares RSS = 0; c) all parameter errors s_{β_j}=0; and d) a program crash due to a "divide by zero" run-time computational error.

Analysis:

a) In the calculation of $\beta = \left(X^T X\right)^{-1} X^T Y$, the vector of observations, Y, is equal to zero resulting in all parameter estimates $\beta(j)$ being calculated as zero. A further view of this is that whenever $\underline{B}.\underline{X} = \underline{0}$, the MSR procedure will identify the trivial solution $\underline{B} = \underline{0}$.

b) and c) Again the vector Y=0 is used in the computation of the residual sum of squares RSS and then, indirectly, in subsequent calculation of the residual variance SSQR = RSS/(N-n) and the standard error s_{β_j} of each parameter. Hence, Y=0 results in a value of zero for all of these terms (see MSR STEP 4, Eqns [10.3], [10.4] and [10.6]).

d) the F77 software always crashed during the calculation of the F statistic. From Eqn [10.7] it can be seen that SSQR, i.e. $s^2(\varepsilon)$, is used in the denominator which will result in a"divide by zero" error whenever SSQR = 0, as is the case here.

10.3.2 Y set equal to one of the independent X variables.

To create a data file in which Y is equal to one of the independent x variables for all of the observations, an extra state variable X5 was inserted by copying the Y column. The initial start models of the MSR runs were varied but during any iterations in which X5 was included in the model structure, the correlation between Y and X5 was found to dominate the MSR parameter estimates with $\beta(5) = 1.0$ and $\beta(j \neq 5)$ all having small numerical values of the order of $\sim 10^{-12}$.

It was also noted that, with X5 included, RSS and SSQR have small negative values. This makes no numerical sense because RSS and SSQR are both squared statistical terms. The negative values simply fall out as a consequence of the equations used in the calculations in MSR STEP 4. This is probably due to having one highly correlated variable and several numerically small parameters which have "relatively high" errors associated with them. MSR uses the square root of SSQR in the calculation of the individual parameter errors (see Eqn [10.6]). The software always crashed at this point in the procedure with a run-time error caused by trying to take the square root of a negative number.

10.3.3 Two independent X variables set equal to each other.

It was decided to set X2 = X3 and the original HALD.DAT file was edited accordingly. When the MSR program was run it always crashed in iterations in which both X2 and X3 were included in the model structure. The error message produced pointed to an invalid operation occurring in the sub-routine used to find the inverse matrix of $\left(X^T X\right)$.

Although the exact reason for the failure could not be identified the inversion process may become unstable when there are two identical matrix rows present.

10.3.4 Model structure containing only one $\underline{X}$ variable.

MSR runs were performed to investigate the effect of only having one X variable in the model structure. Initial iterations containing only Y = B0, Y = B1.X1 and Y = B2.X2 were tested. In each case, the program crashed in MSR step 5 due to an attempt to divide by zero in the calculation of the F statistic. Eqn [10.7] is used to calculate F and it is noted that the term (n-1) occurs in the denominator. With only one independent variable in the model structure, (n-1) is equal to zero and will always give rise to the computational error observed.

10.3.5 Effect of increasing the number of observations.

The 13 sets of observations contained in HALD.DAT were copied a number of times to produce files containing 26, 52 and 65 sets of data. MSR was then run with different initial model structures. In each case identical final model structures and parameter estimates were obtained. However, as the number of sets of observations were increased the correlation coefficient (R^2) decreased and the residual sum of squares (RSS) increased. Both trends can be expected as they indicate firstly, a decreasing goodness of fit of data to the final model structure chosen and secondly, an increasing overall error as the number of observations increase.

CHAPTER 11

DEVELOPMENT OF A DATA ACQUISITION SYSTEM

11.0 DEVELOPMENT OF A DATA ACQUISITION SYSTEM.

The electronic control unit (ECU) for the dynamic wind tunnel test rig has a control panel with various accessible bus bar networks, see Figure 44. It is possible to record any combination of aircraft control surface inputs, outputs and attitude angles from the ECU. In earlier work involving the use of the Hawk model, up to six parameters could be linked by free wires to a pen recorder. All data analysis at that time, Ref 22, was therefore based on the use of analogue time histories recorded onto a strip chart via the six-channel pen recorder.

Subsequent development of the facility for use with the forward swept wing aircraft model necessitated the addition of a digital data-acquisition system (DAS) and thus the development of a computer based DAS started. The basic facility consisted of a signal processor to convert or digitize analogue data into the form needed for a digital computer link up.

A digital computer data-acquisition system was employed once again for present work with the Hawk model and Figure 45 gives a schematic representation of the system employed. At the heart of the system was a CED 1401 analogue-digital interface linked to an IBM PC-AT microcomputer. The CED 1401 is an intelligent peripheral which can be used to generate and, more importantly, receive waveform, digital and timing signals. Using its own processors, clocks and memory the 1401 can be programmed through a host computer in a variety of languages.

In this application, the host IBM PC was set up to use PASCAL programs to communicate with the 1401 interface. There was already

some software available for this purpose in the form of a library of routines provided with the CED1401, Ref 30. Additionally, using these software libraries a PASCAL program had been written by Gomes (Ref 27) to control the CED1401. It was found possible to adapt this software in order to establish the interface required between the host computer and the experimental rig's ECU.

To record the aircraft data required for the MSR procedure, the appropriate parameter outputs on the ECU were linked by a free wire to one of eight ports, shown in the lower left hand side of Figure 44. These ports were then connected to a shielded eight channel data cable to the CED1401. The CED1401 then automatically performed the necessary analogue to digital conversion of data and recorded the data on hard disk via a special card in the host computer. It was possible to simultaneously record up to eight channels in separate data files on the host computer. Using some further CED 1401 software, called Waterfall, it was also possible to immediately examine the recorded data to assess noise levels and to see whether the short period aircraft response had been suitably captured on computer.

During development, testing of the DAS was carried out using a signal generator to simulate some inputs. Several sets of data files were recorded and subsequently examined using the Waterfall software. This enabled a check to be made on what had been recorded and confirmed that the program was working as expected. Voltages recorded by the CED1401 are stored in data files in a hexadecimal format and using Waterfall also overcame the difficulty of easily examining this data. To facilitate signal conditioning of data for the MSR process further computer programs had to be written; these are described in Chapter 13.

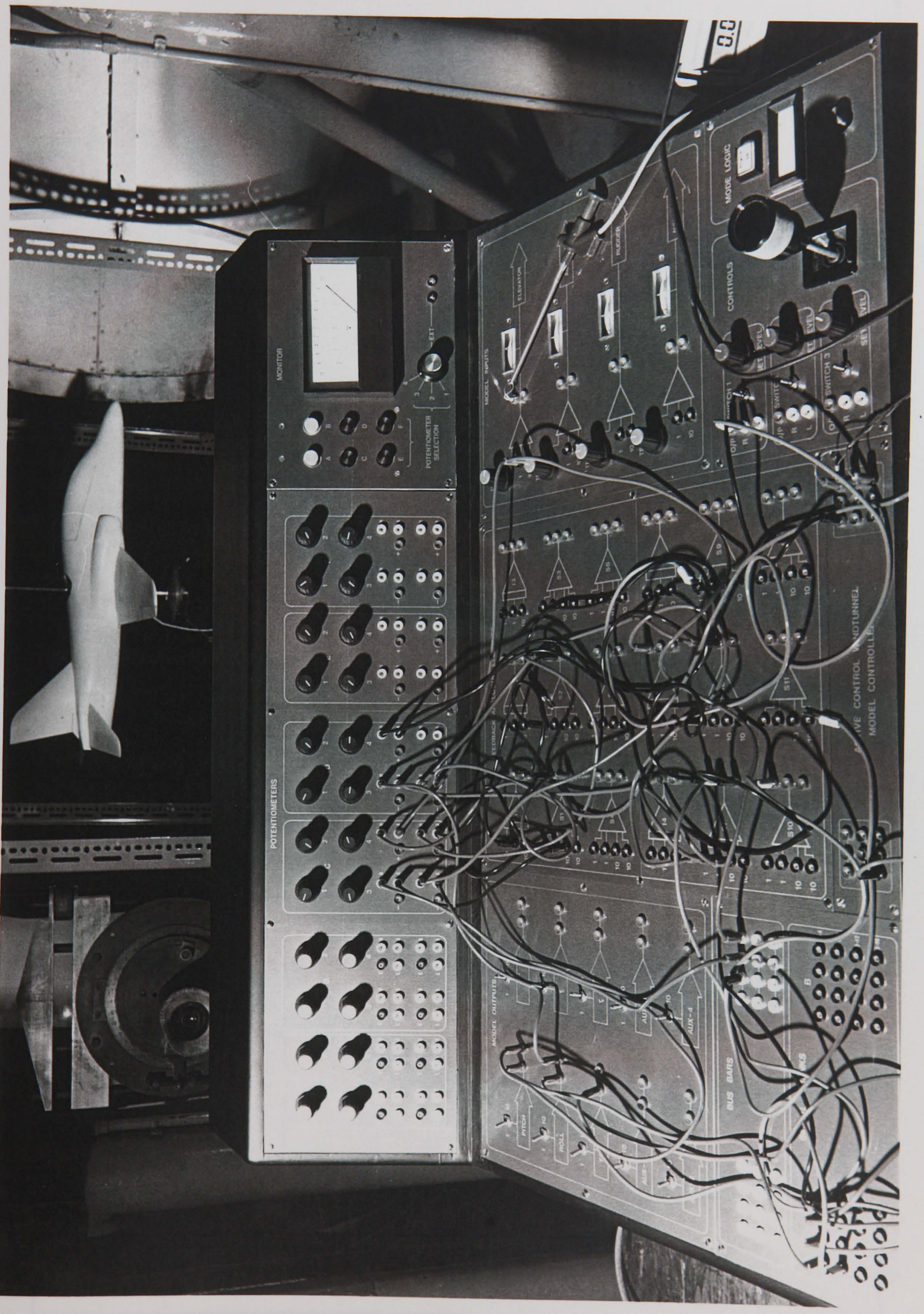

FIGURE 44: ECU WITH PATCHED WIRES

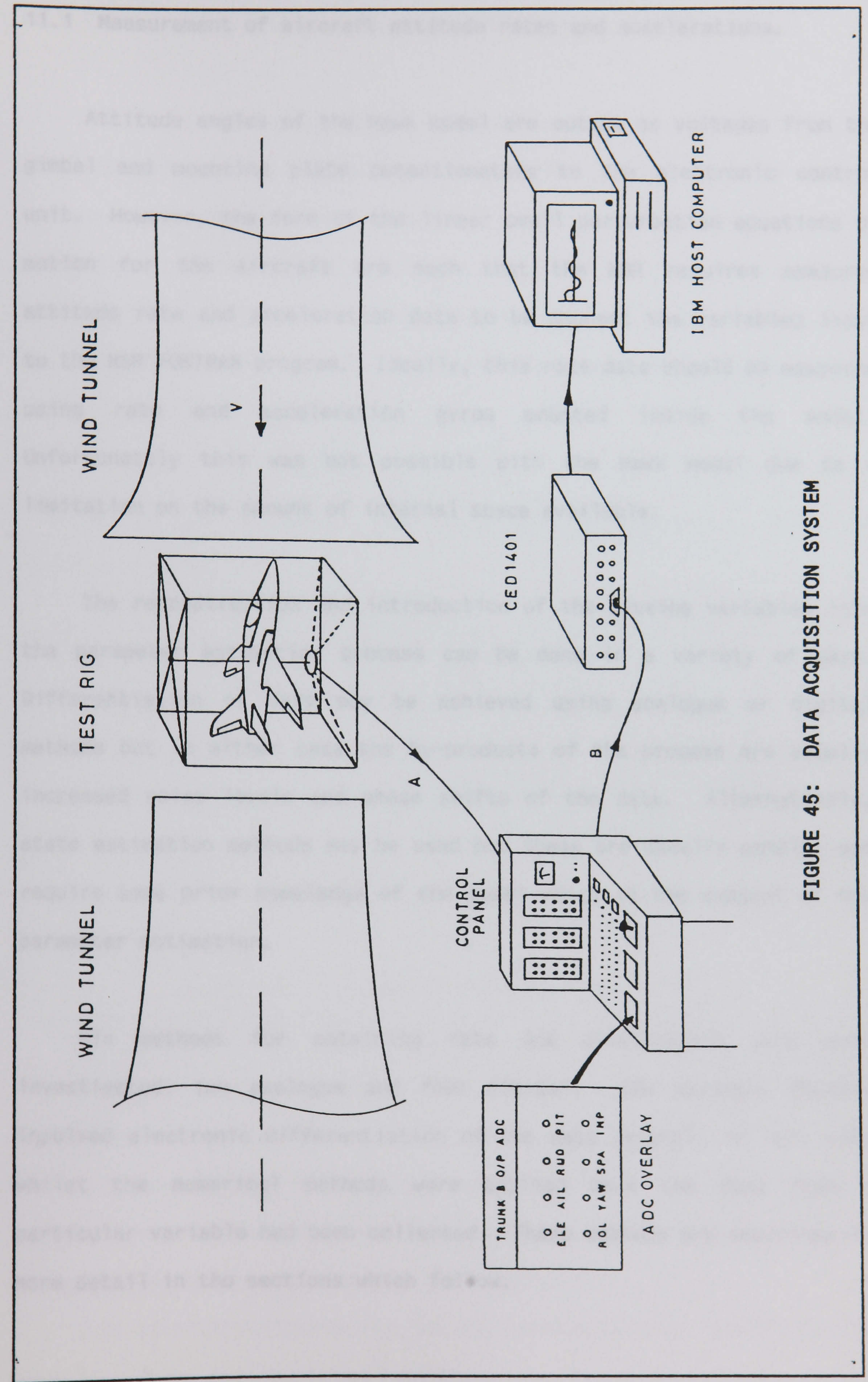

FIGURE 45: DATA ACQUISITION SYSTEM

11.1 Measurement of aircraft attitude rates and accelerations.

Attitude angles of the Hawk model are output as voltages from the gimbal and mounting plate potentiometers to the electronic control unit. However, the form of the linear small perturbation equations of motion for the aircraft are such that the MSR requires measured attitude rate and acceleration data to be amongst the variables input to the MSR FORTRAN program. Ideally, this rate data should be measured using rate and acceleration gyros mounted inside the model. Unfortunately this was not possible with the Hawk model due to a limitation on the amount of internal space available.

The reconstruction and introduction of the missing variables into the parameter estimation process can be done in a variety of ways. Differentiation of data may be achieved using analogue or digital methods but in either case the by-products of the process are usually increased noise levels and phase shifts of the data. Alternatively, state estimation methods may be used but these are usually complex and require some prior knowledge of the model which is the subject of the parameter estimation.

Six methods for obtaining rate and acceleration data were investigated, two analogue and four digital. The analogue methods involved electronic differentiation of the data (signal) in real time whilst the numerical methods were applied once the data from a particular variable had been collected. These methods are described in more detail in the sections which follow.

11.1.1 Analogue differentiation using the ECU.

The first analogue method employed to obtain angular rate and acceleration response data was to use analogue circuitry in the ECU to generate rate data, Ref 31. Figure 46 shows a circuit, based on three operational amplifiers (op-amps), which can be used to obtain an approximate differentiation of the input signal x. Ref 32 describes the properties of the circuit which is based upon the solution of the implicit differential equation:

$$(1-a).\frac{dx}{dt} + z = \frac{dx}{dt} \qquad [11.1]$$

As 'a' is increased towards unity, z approaches the time derivative dx/dt.

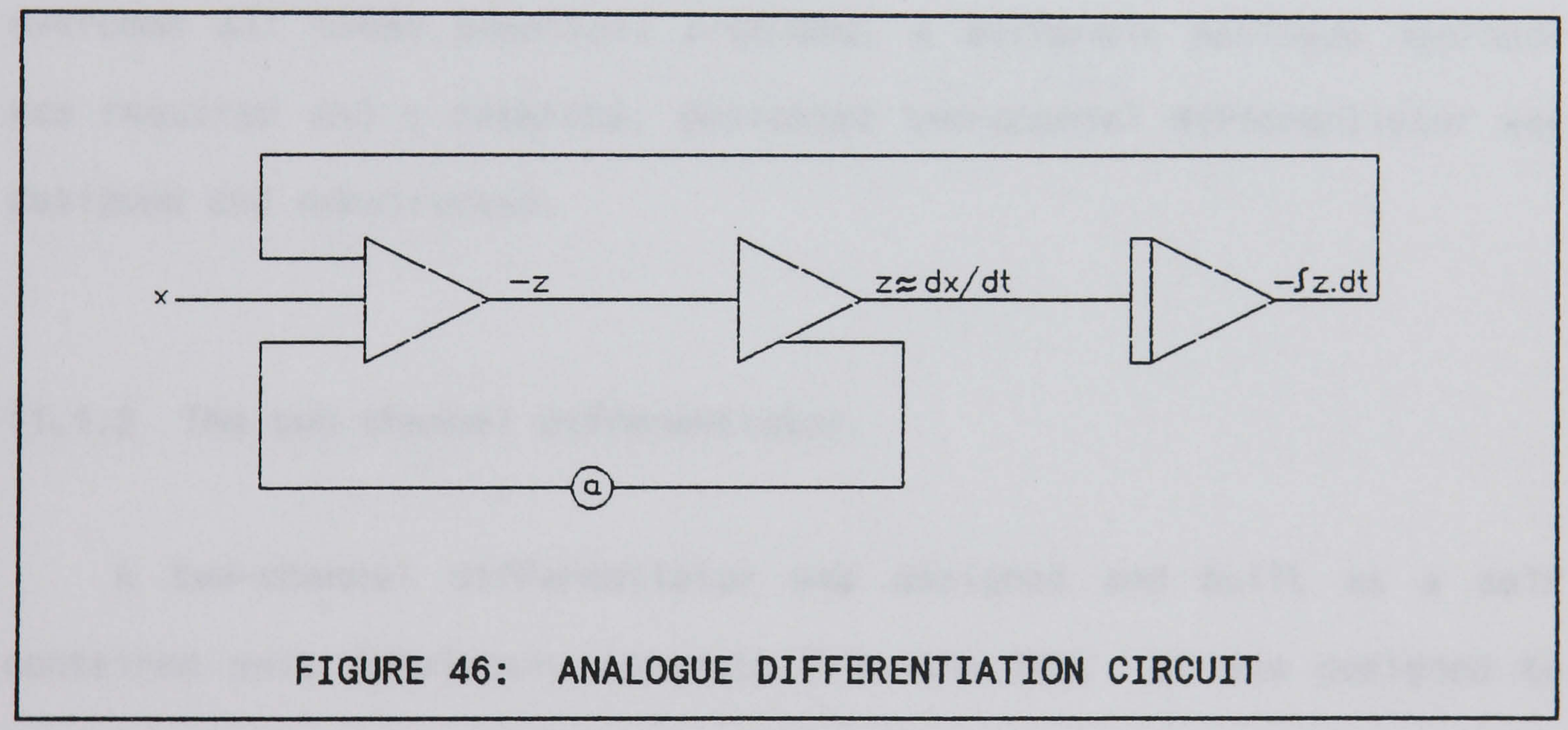

FIGURE 46: ANALOGUE DIFFERENTIATION CIRCUIT

The use of such an analogue differentiator has the following main drawbacks:

i) It decreases the signal to noise ratio in the circuit.

ii) An operational amplifier used as a differentiator may frequently be driven to saturation and overload.

iii) Stability problems may be encountered as some amplifiers are quite sensitive to capacitive loading.

In practice, it was found that the differentiator gave a satisfactory response at very low frequencies for use in the roll feedback loops which were used to improve control of the Hawk model in the wind tunnel. Unfortunately, because of the fixed analogue summer and integrator amplifiers on the ECU, the time constant τ of the differentiation circuit was fixed at 1 second. This introduced a large lag into the circuit, meaning that it was not practical to use rate data produced in this way as input to the MSR procedure, although the data continued to be used successfully in the control feedback loops.

Furthermore, the output voltage, $V_{out} = \tau.(dV_{in}/dt)$, could become too large to be used as beyond ±5V, the signal could not be used for accurate analogue-to-digital (A-to-D) conversion by the CED1401. To overcome all these practical problems, a different analogue approach was required and a separate, dedicated two-channel differentiator was designed and constructed.

11.1.2 The two channel differentiator.

A two-channel differentiator was designed and built as a self contained unit completely separate from the ECU. It was designed to calculate the first and second differentials of an input signal as indicated in Figure 47 (where R and C are the resistor and capacitor values for each stage contributing to the differentiator time constant, RC). The circuit used for each channel was a standard op-amp differentiator with accurate output attenuation to allow the maximum range of the A-to-D converter to be used, Ref 33. An instrumentation-quality integrated circuit was employed and means were provided for adjusting the small dc offset.

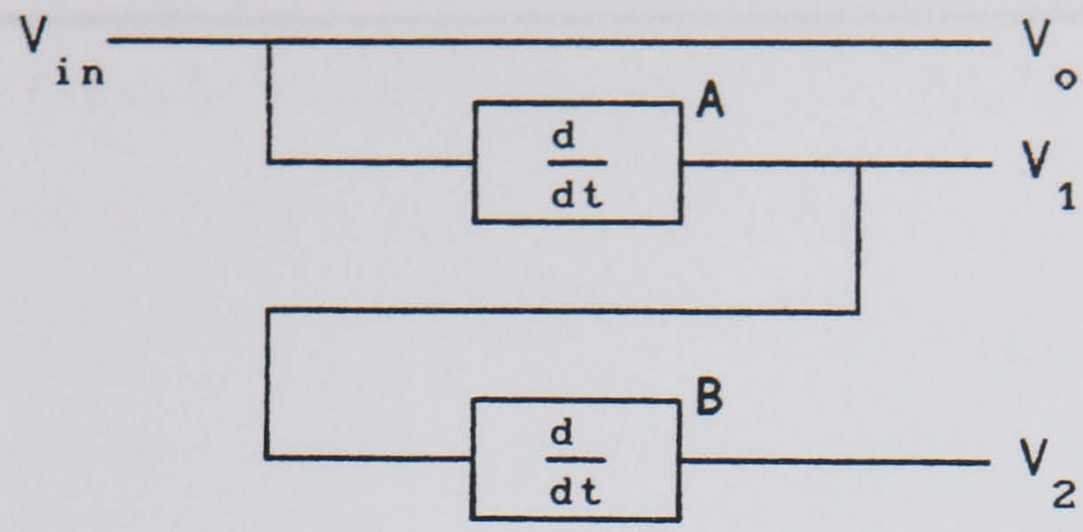

$$V_o = k\,\theta$$

$$V_1 = -(RC)_A \frac{dV_o}{dt} = -(RC)_A\, k \frac{d\theta}{dt}$$

$$V_2 = -(RC)_B \frac{dV_1}{dt} = (RC)_B\,(RC)_A\, k \frac{d^2\theta}{dt^2}$$

FIGURE 47: USE OF THE TWO CHANNEL DIFFERENTIATOR

A full circuit diagram is given in Figure 48. The inverting input is a virtual earth, i.e. at ground potential and hence, the changing input signal produces a current

$$i = C \frac{dV_{in}}{dt}$$

and an output voltage

$$V_{out} = -RC \frac{dV_{in}}{dt}$$

Unfortunately these circuits are prone to noise and instability, particularly because of the op-amp's large gain and internal phase shifts. This was best suppressed by means of capacitors and resistors which act to roll off the response and ensure that the circuit operates as an integrator at high frequencies, see full circuit diagram. The exact choice of these components was dictated by the individual op-amp and the noise present on the input signal. The switches were labelled by their order of magnitude contribution to the time constant (RC) i.e. -6 is $\simeq 10^{-6}$, -7 is $\simeq 10^{-7}$, etc.

FIGURE 48: TWO CHANNEL DIFFERENTIATOR - CIRCUIT DIAGRAM

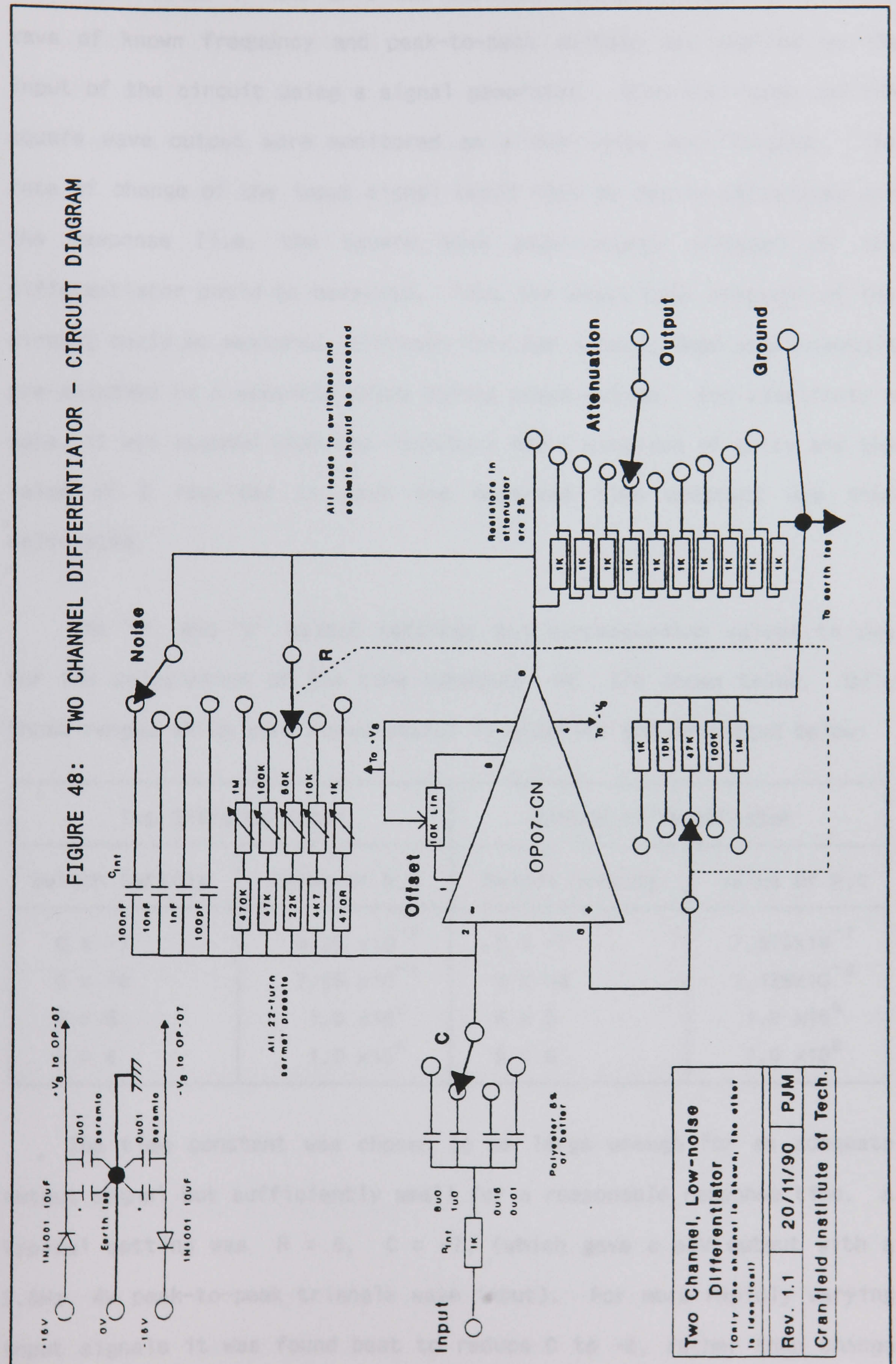

Two Channel, Low-noise Differentiator (only one channel is shown, the other is identical)		
Rev. 1.1	20/11/90	PJM
Cranfield Institute of Tech.		

Calibration of the unit was carried out as follows: A triangle wave of known frequency and peak-to-peak voltage was applied to the input of the circuit using a signal generator. Both the input and the square wave output were monitored an a dual beam oscilloscope. The rate of change of the input signal could then be easily calculated and the response (i.e. the square wave peak-to-peak voltage) of the differentiator could be measured. Thus the exact time constant of the circuit could be measured, although this had already been approximately pre-adjusted to a sensible value during construction. For simplicity's sake, it was assumed that the resistors had a mantissa of unity and the value of C required to give the observed time constant was then calculated.

The "R" and "C" switch settings and corresponding values to use for the calculation of the time constant RC are shown below. Only those ranges which were found useful in practice are tabulated below:

Top Differentiator		Bottom Differentiator	
Switch Setting	Value of R,C	Switch Setting	Value of R,C
C = -7	5.25×10^{-7}	C = -7	7.875×10^{-7}
C = -8	7.25×10^{-8}	C = -8	1.125×10^{-8}
R = 5	1.0×10^{5}	R = 5	1.0×10^{5}
R = 6	1.0×10^{6}	R = 6	1.0×10^{6}

The time constant was chosen to be large enough for an adequate output signal but sufficiently small for a reasonable response time. A typical setting was R = 6, C = -7, (which gave a ±5V output with a 2.5Hz, 4V peak-to-peak triangle wave input). For more rapidly varying input signals it was found best to reduce C to -8, rather than change R, since this was better for suppressing any latent instability.

The "Noise" switch was labelled "-7", "-6", "-5", "-4" corresponding to time constants of 10^{-7} to 10^{-4} seconds. The "-5" setting was found to be adequate for most purposes although some 10mV of noise and slight instability was present with C = -7. The "-4" noise switch setting reduced excess noise from the wind tunnel but put an upper limit on the maximum input signal frequency of $\simeq$ 2.5Hz for the top differentiator and $\simeq$ 1.8Hz for the bottom differentiator. At frequencies above roll-off the output signal still had the correct form but did not have time to slew to the correct extreme values.

11.2 Digital differentiation strategies.

As an alternative to analogue differentiation various techniques for digitally differentiating data were investigated. The numerical methods all involved fitting a curve to the collected data and then differentiating the fitted curve to calculate the gradient at the data point of interest. Three of the numerical methods investigated involved fitting a curve to just a few data points near the point of interest and are described in the sections which follow. The fourth method investigated, but not applied practically, involved fitting the "whole" measured data set with a series of Tschebyschev polynomials, Ref 10 gives further details on this particular method.

11.2.1 Taylor-series expansions.

The first method applied to recorded data was a formula based on a simple Taylor Series expansion for a function y = f(x). The method works by obtaining the expansion series at points either side of x_i,

that is at points (x_i - "h") and (x_i + "h"); it is then possible to subtract the two series to yield central-difference expressions for various derivatives of y = f(x). A number of formulae can be obtained depending on the number of terms considered in the Taylor series expansions, Ref 34. The derivative equations produced will also have corresponding levels of error associated with them dependent upon the number of terms taken and the magnitude of "h". For example, the central-difference equation [11.2] has an error of order h^4.

$$y'_i = \frac{- y_{i+2} + 8y_{i+1} - 8y_{i-1} + y_{i-2}}{12h} \qquad [11.2]$$

This is an example of a "five-point" central difference formula which gives an estimate for the first derivative of function y. A number of Taylor expansion formulae were presented in a previous report, Ref 5. To use this method practically, the formula was applied many times over the whole range of recorded data points, with the exception of four data points at each end of the data set being differentiated. Figure 49 shows the result of using a five point formula to obtain pitch rate data q from recorded pitch angle data θ.

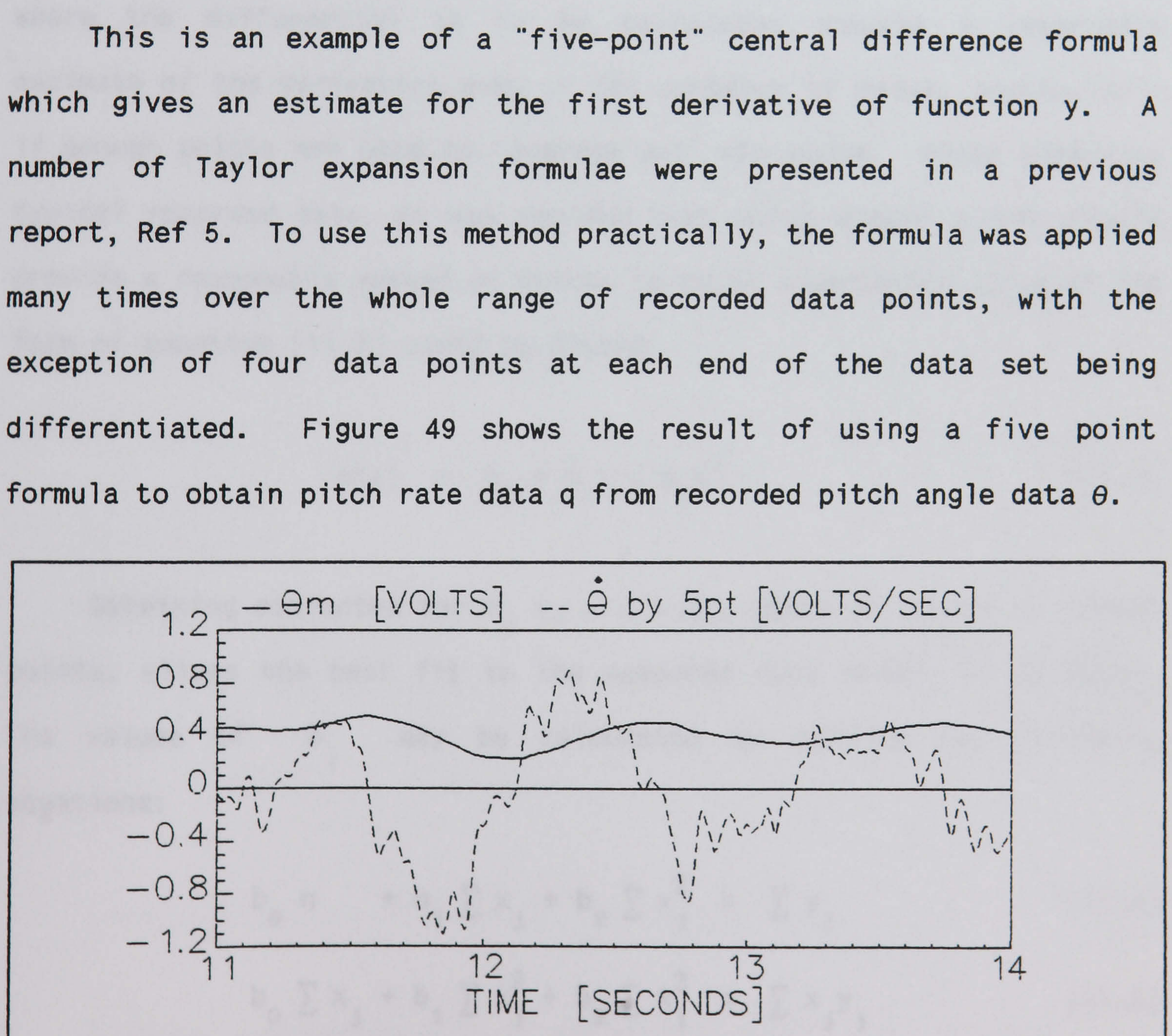

FIGURE 49: TYPICAL DATA DIFFERENTIATED BY A 5 POINT FORMULA.

In general, tabulated data is not usually used directly in numerical differentiation because any scatter (i.e. noise) in the data set can cause serious accuracy problems and whenever possible, it is preferable to obtain an analytical expression for a smooth curve which will fit the data and then differentiate the curve. This type of method is described next.

11.2.2 Parabolic curve fit.

Fitting a parabolic curve to a set of data points in the region where the differential is to be calculated ensures a reasonable estimate of the derivative even in the presence of noise, particularly if enough points are used to "average out" the noise. After examining typical recorded data, it was decided that using eleven points should provide a reasonable spread of points to which a parabolic curve of the form of equation [11.3] could be fitted.

$$p(x) = b_0 + b_1 x + b_2 x^2 \qquad [11.3]$$

Obtaining estimates for b_j $(j = 0,1,2)$, based on groups of eleven points, allows the best fit to the measured data points to be found. The values of b_j may be calculated by solving the following equations:

$$b_0 n + b_1 \sum x_j + b_2 \sum x_j^2 = \sum y_j \qquad [11.4]$$

$$b_0 \sum x_j + b_1 \sum x_j^2 + b_2 \sum x_j^3 = \sum x_j y_j \qquad [11.5]$$

$$b_0 \sum x_j^2 + b_1 \sum x_j^3 + b_2 \sum x_j^4 = \sum x_j^2 y_j \qquad [11.6]$$

Solutions to equations [11.4], [11.5] and [11.6] are given by

$$b_0 = \frac{D_0}{D} \qquad b_1 = \frac{D_1}{D} \qquad b_2 = \frac{D_2}{D} \qquad [11.7]$$

where

$$D = \begin{vmatrix} a & a & a \\ a_{11} & a_{12} & a_{13} \\ a_{21} & a_{22} & a_{23} \\ a_{13} & a_{32} & a_{33} \end{vmatrix} \qquad D_0 = \begin{vmatrix} c & a & a \\ c_1 & a_{12} & a_{13} \\ c_2 & a_{22} & a_{23} \\ c_1 & a_{32} & a_{33} \end{vmatrix}$$

$$D_1 = \begin{vmatrix} a & c & a \\ a_{11} & c_1 & a_{13} \\ a_{21} & c_2 & a_{23} \\ a_{13} & c_3 & a_{33} \end{vmatrix} \qquad D_2 = \begin{vmatrix} a & a & c \\ a_{11} & a_{12} & c_1 \\ a_{21} & a_{22} & c_2 \\ a_{13} & a_{32} & c_3 \end{vmatrix}$$

and further,

$$a_{11} = n; \quad a_{12} = \sum x; \quad a_{13} = \sum x^2; \quad a_{23} = \sum x^3; \quad a_{33} = \sum x^4$$

$$c_1 = \sum y; \quad c_2 = \sum xy \quad c_3 = \sum x^2 y$$

Thus considering eleven data points points (0,h,2h,...,10h) of equal separation, h, the following values are obtained:

$$a_{11} = 11; \quad a_{12} = 55h; \quad a_{13} = 385h^2; \quad a_{23} = 3025h^3; \quad a_{33} = 25333h^4$$

and $D = 1038180$

$$D_0 = (602580c_1 - 228690c_2 + 18150c_3)h^6$$

$$D_1 = (-228690c_1 + 130438c_2 - 12100c_3)h^5$$

$$D_2 = (18150c_1 - 12100c_2 + 1210c_3)h^4$$

Differentiating [11.3] gives $p'(x) = b_1 + 2b_2x$ [11.8]

Further, evaluating p(x) at the central point $x = 5h$ gives

$$p'(5h) = \frac{1}{D}\left(D_2 + 10h\, D_3\right) \qquad [11.9]$$

Substituting the values of D, D_2 and D_3, calculated for eleven data points, into [11.9] yields:

$$p'(5h) = \frac{1}{110h}\left(-5b_1 + b_2\right) \qquad [11.10]$$

OR

$$p'(x_i) = \frac{1}{110h}\left(-5y_{i-5} - 4y_{i-4} - 3y_{i-3} - y_{i-2} - y_{i-1} + y_{i+1} + 2y_{i+2} + 3y_{i+3} + 4y_{i+4} + 5y_{i+5}\right) \qquad [11.11]$$

Similarly, differentiating equation [11.8] gives $p''(x) = 2b_2$ and substituting in the appropriate terms again from [11.7] yields:

$$p''(x_i) = \frac{1}{429h^2}\left(15y_{i-5} + 6y_{i-4} - y_{i-3} - 6y_{i-2} - 9y_{i-1} - 10y_i - 9y_{i+1} - 6y_{i+2} - y_{i+3} + 6y_{i+4} + 15y_{i+5}\right) \qquad [11.12]$$

In practice this method was found to provide acceptable results for the first differential but the second differential still appeared rather noisy, because of the inherent way differentiation tends to amplify noise.

11.2.3 Legendre polynomials.

In this method, the differential at a point in the data set is calculated by fitting a Legendre polynomial of order n to the points on either side of the point of interest. Rather than evaluating the coefficients in the polynomial and then calculating the differential for each point of interest, the differential is calculated for a general set of y-values, $(y_1, y_2, \ldots, y_i)$ at equally spaced intervals. This results in a formula which can be utilised to

calculate the differential directly, with a considerable saving in the processing required and in time.

Here it is appropriate to make a point about "exact fit" polynomials. If a polynomial of order x^{n-1} is used to fit n points, there are enough variable parameters to enable it to be an exact fit at each measured y-value. Thus, unless the data is free from noise, the calculated differentials are guaranteed to be wrong although the error may be acceptably small.

Two possible ways out of this dilemma suggest themselves. The first is the "Legendre Method" which is to fit a curve which is known to be theoretically of the right form to a large number of data points. Alternatively, it is possible to fit a curve a curve of constant curvature, locally to a smaller number of data points. An example of this latter method was discussed in the previous sub-section on fitting a parabolic curve to groups of eleven data points.

The basic principle of the Legendre method is simple. First a Legendre polynomial of degree $n-1$ is constructed to pass through all n points, $\{y_1,x_1\}$ ... $\{y_n,x_n\}$ of interest; for a central- difference formula, the n points will lie either side of the point at which the differential is required:

$$p_{n-1} = y_1 l_1(x) + y_2 l_2(x) + y_3 l_3(x) + \ldots + y_n l_n(x) \qquad [11.13]$$

where

$$l_j(x) = \frac{(x-x_1)(x-x_2)\cdots(x-x_{j-1})(x-x_{j+1})\cdots(x-x_n)}{(x_j-x_1)(x_j-x_2)\cdots(x_j-x_{j-1})(x_j-x_{j+1})\cdots(x_j-x_n)}$$

for $j = 1,2,\ldots,n.$

The expression for $p_{n-1}(x)$ is then differentiated using the product rule to give $p'_n(x)$ and $p''_n(x)$ if required. It is worth noting that the difference h, between adjacent x values is always the same (eg. $h = x_2 - x_1$; $h = x_3 - x_2$), Ref 35.

11.3 Comparison of analogue and numerical differentiation.

Figures 50 and 51 which follow, both show part of a filtered output voltage trace θ_m which was recorded directly from the ECU onto the host computer's hard disk. Figure 50 additionally shows the measured analogue rate data $\dot{\theta}_m$ which was obtained by feeding θ_m into the first channel of the two channel differentiator. The rate data was "simultaneously" recorded onto the host computer. Figure 51 additionally shows the numerical differentiation data $\dot{\theta}_{11pt}$ obtained when an 11 point Legendre formula was applied to the recorded data θ_m.

Examination of Figure 50 shows that the analogue two channel differentiator introduces a small phase lag into the rate data recorded. Although it is theoretically possible to shift the rate data slightly forward in time, it is very difficult to estimate the magnitude of the lag/shift in practice.

The rate data obtained when the numerical method was applied to the recorded data can be seen to contain some noise, Figure 51. The amount of noise was substantially reduced to the level shown in Figure 51 by utilising some CED1401 software libraries to filter the pitch angle data to remove some of the noise and hence obtain much better rate data.

If the rate data trace in Figure 51 ($\dot{\theta}_{11pt}$) is compared to the rate data trace in Figure 49 ($\dot{\theta}_{5pt}$), it can be seen that there is less noise in the data obtained using an 11 point formula. This is because using more data points at any particular point in time acts to smooth the data.

Various strategies, other than utilising CED1401 software, were also implemented for noise reduction and these are discussed in the next section which describes the experimental data gathering carried out for the MSR procedure.

In general, differentiation is inherently susceptible to noise since although the absolute magnitude of the noise might only be small, its rate of change and hence the output signal from the differentiator might be relatively much larger. This drawback will apply as much to analogue differentiation as it does to numerical. However, because analogue electronic circuitry tends to exhibit some roll-off at higher frequencies, in practice, analogue circuits tend to suffer less from this noise problem when differentiating.

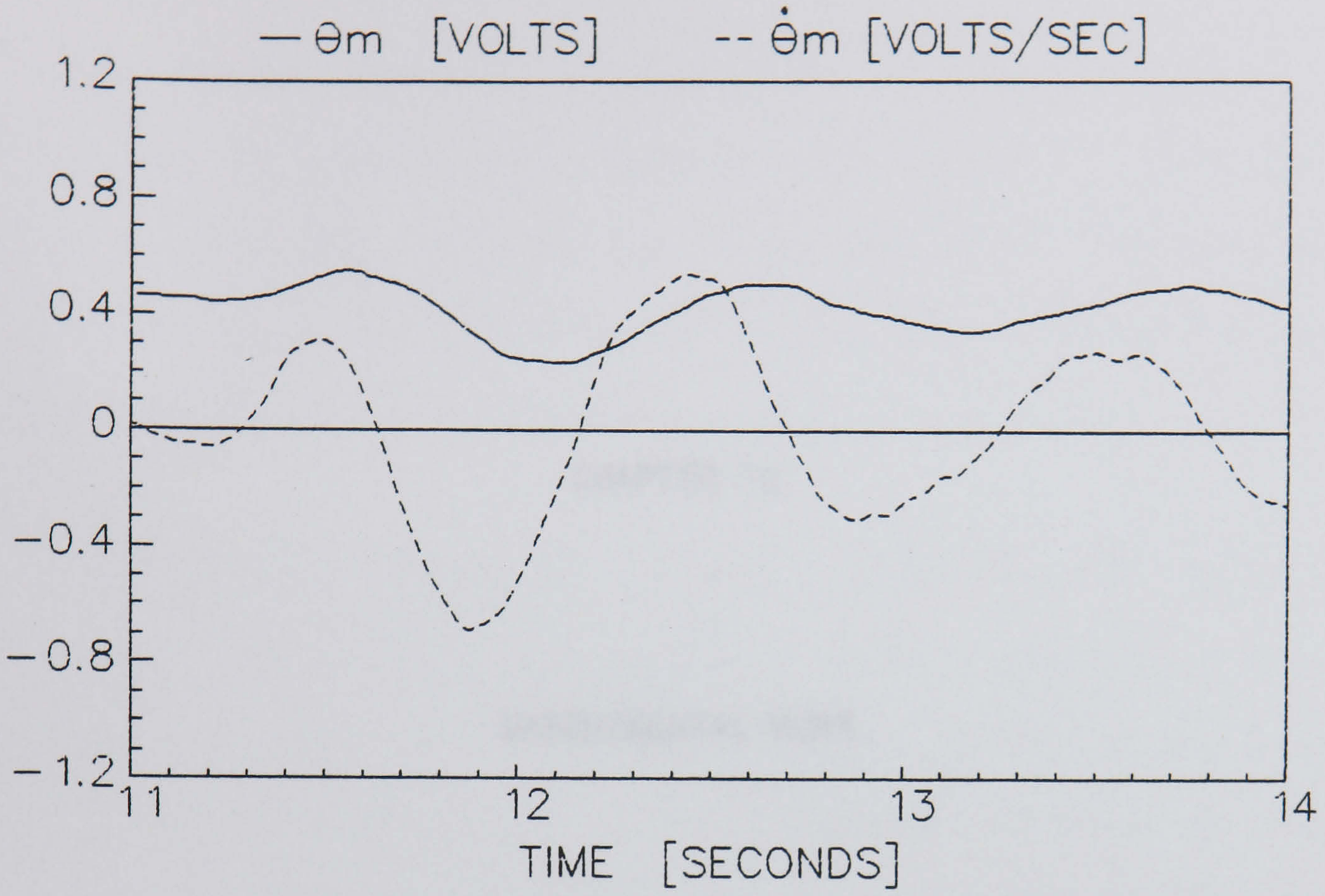

FIGURE 50: TYPICAL MEASURED ATTITUDE AND RATE DATA

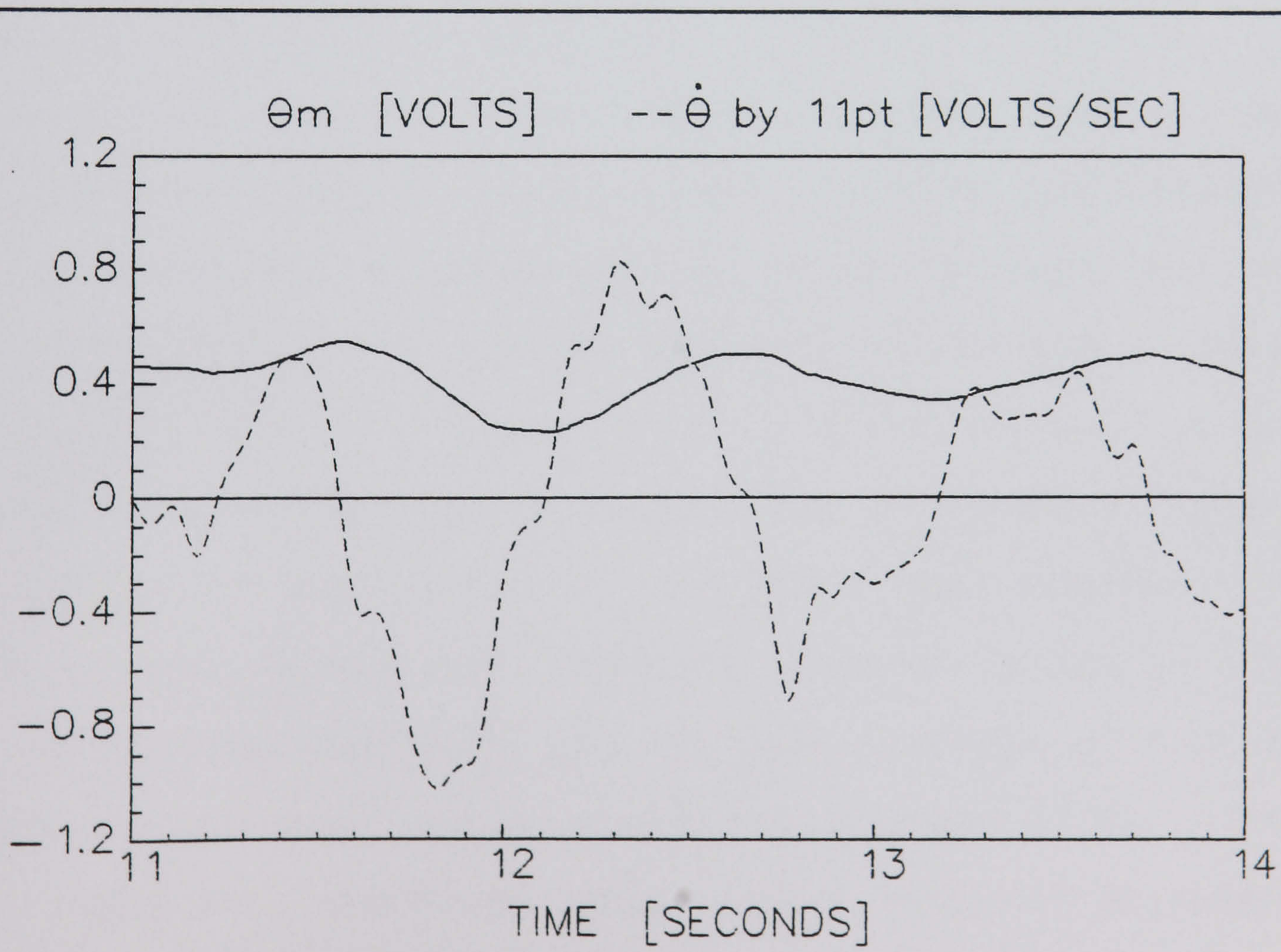

FIGURE 51: TYPICAL DATA DIFFERENTIATED BY AN 11 POINT FORMULA

CHAPTER 12

EXPERIMENTAL WORK

12.0 EXPERIMENTAL WORK.

This Chapter contains a description of the experimental work carried out to record the responses for analysis using the MSR software. The way in which the model was flown and the various observations and gradual changes made to the rig to improve the quality of data recorded are also described.

After gaining familiarisation with the dynamic rig, through the preliminary experimental programmes, various impulses and short doublets were input to the control surfaces to excite short period modes of motion of the model. As many response variables as possible were recorded via free wires patched on the ECU to connect variables to the signal trunk, which acted as the interface to the CED1401 and other DAS equipment. A typical arrangement employed in the signal recovery from dynamic longitudinal experiments is shown in Figure 52. The schematic patch diagrams for the experimental series described below are presented in Appendix F. Many practical problems were encountered during the course of the experiments and various strategies were tried in order to obtain better aircraft model responses and data recordings. For example, when it proved difficult to control the model in roll, autostabilisation loops were implemented, with corresponding changes to the mathematical model structure. Furthermore, some experiments were performed with the Hawk model completely restrained vertically, Figure 53, whilst other experiments gave the model a freedom of 2 or more inches with the model set up in different positions on the vertical rod, Figure 54. Significant noise problems were also encountered, mainly due to the power supply in the ECU. This resulted in a variety of tactics to eliminate the noise at source when recording data.

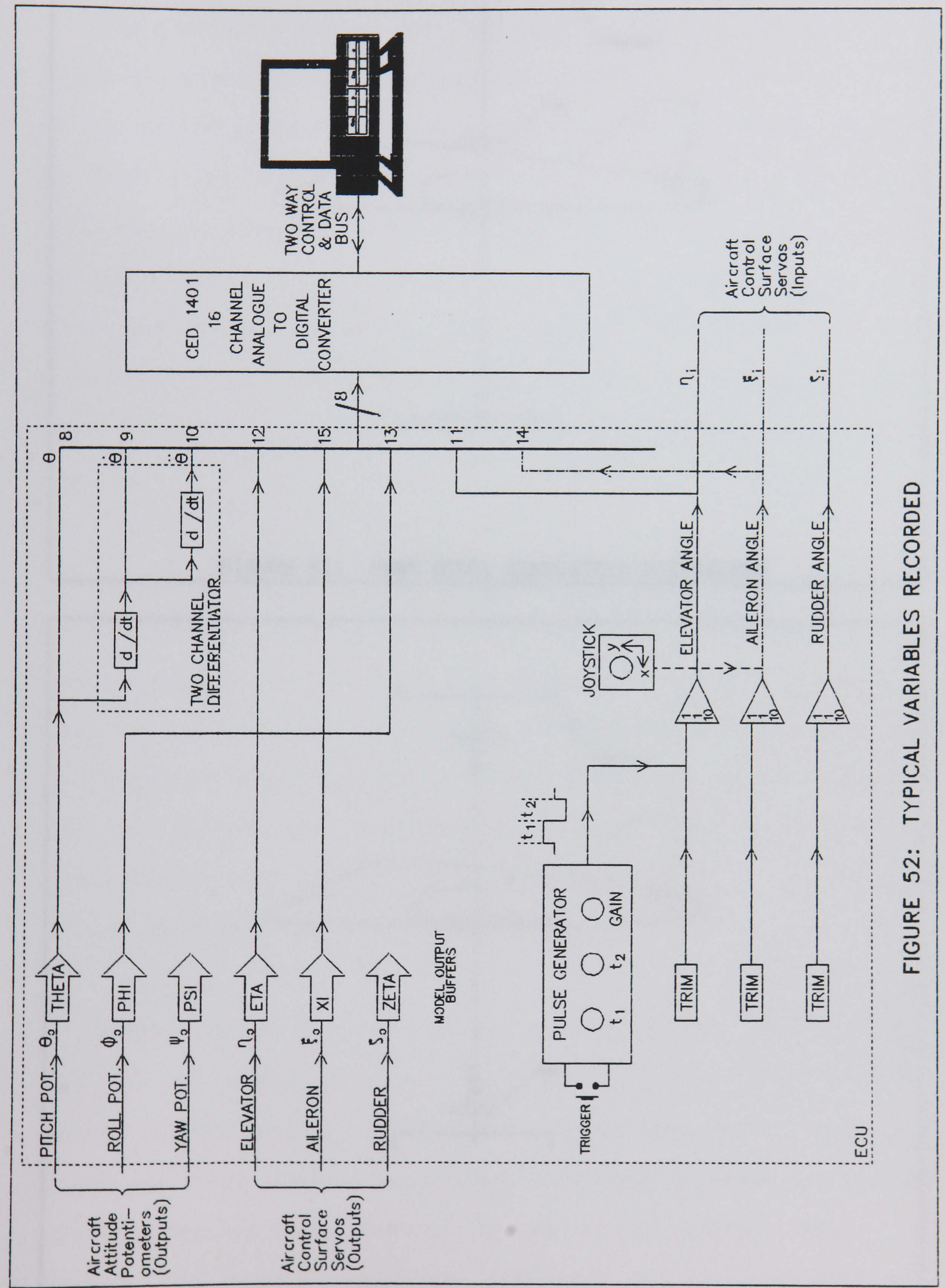

FIGURE 52: TYPICAL VARIABLES RECORDED

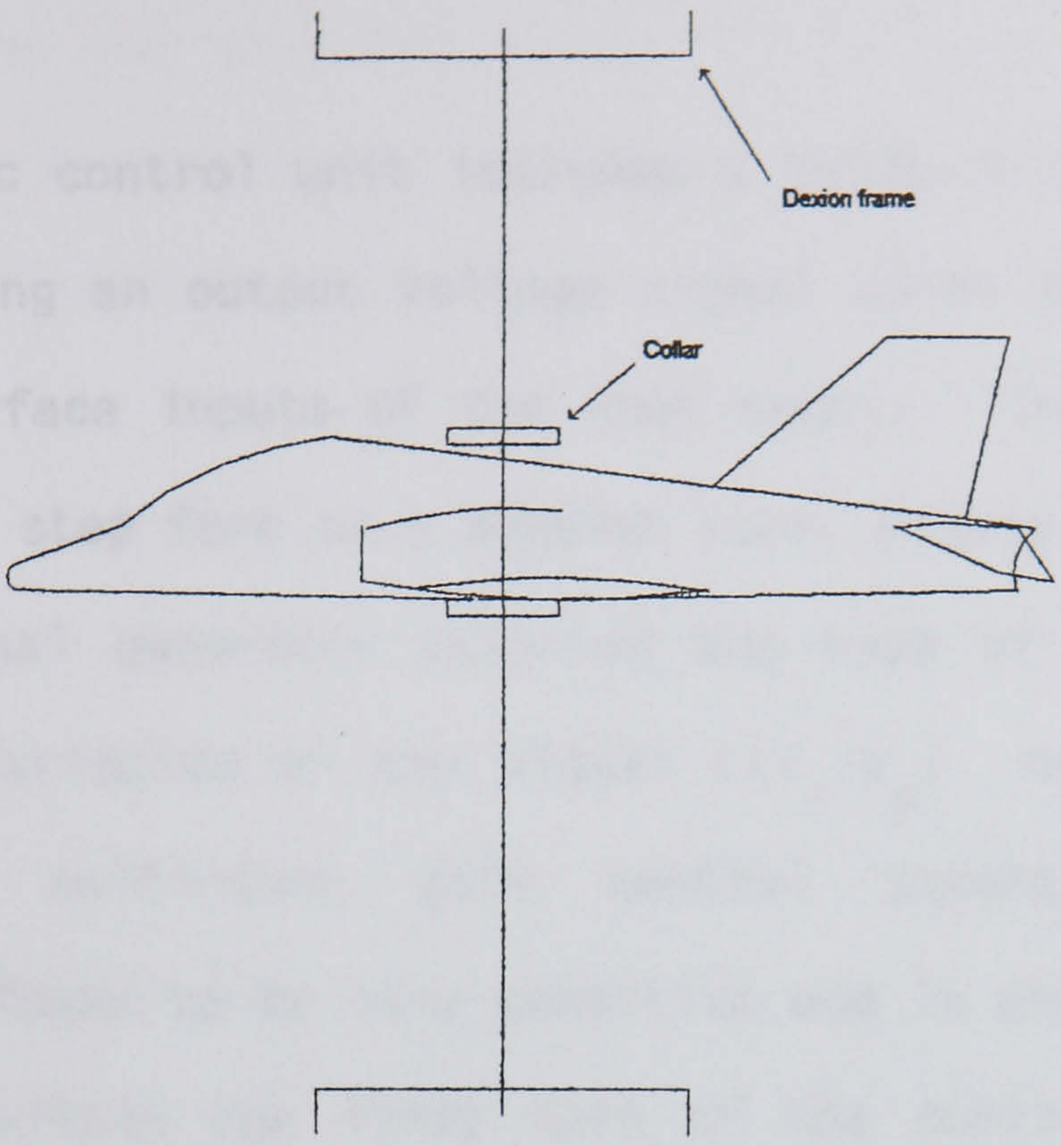

FIGURE 53: HAWK MODEL COMPLETELY RESTRAINED

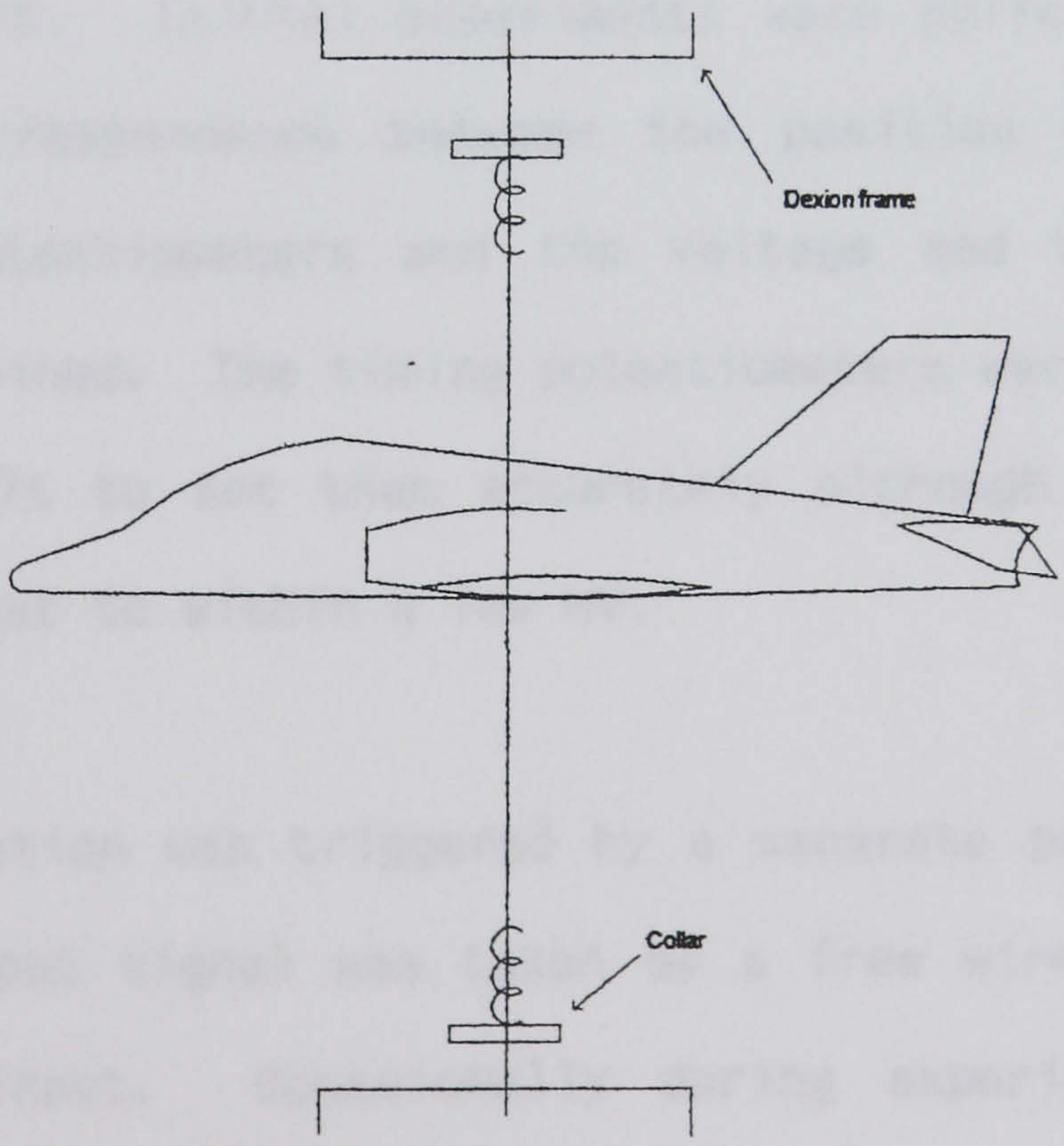

FIGURE 54: HAWK MODEL WITH VERTICAL FREEDOM

12.1 Generation of control surface inputs.

The electronic control unit includes a built-in signal generator, Figure 55, providing an output voltage signal which may be fed to any of the control surface inputs of the Hawk model. The signal produced can be of either a step form or a doublet form, Figure 56. The "pulse" switch on the signal generator selected the type of signal required. The peak-to-peak variation of the signal ($|V_1-V_0|$ or $|V_1-V_2|$) was controlled by a multi-turn gain control potentiometer. This potentiometer was found to be very sensitive and in practice only small gains lying well within the first turn of the controlling dial were required.

The timing of the output signal was controlled by two timers, one for the positive-going part of the duty cycle, the other for the negative-going part. Initial experiments were performed in order to establish the correspondence between the position of the gain and timing control potentiometers and the voltage and timing variations that might be obtained. The timing potentiometers were very sensitive, making it difficult to set them accurately although the peak-to-peak voltage could be set to within a few mV.

Signal generation was triggered by a separate push-button on the panel and the output signal was taken by a free wire directly to the control surface input. Occasionally during experimental work, the signal was first inverted by passing it through a summer on the ECU before continuing the connection to the control surface input. In practice, the doublet signal was used most frequently as after the initial disturbance the aircraft model tended to return to the original

trimmed condition. When a step input was used, the aircraft could rapidly depart from the original trimmed state and only the initial part of the response could be considered as a small perturbation response and be analysed as such.

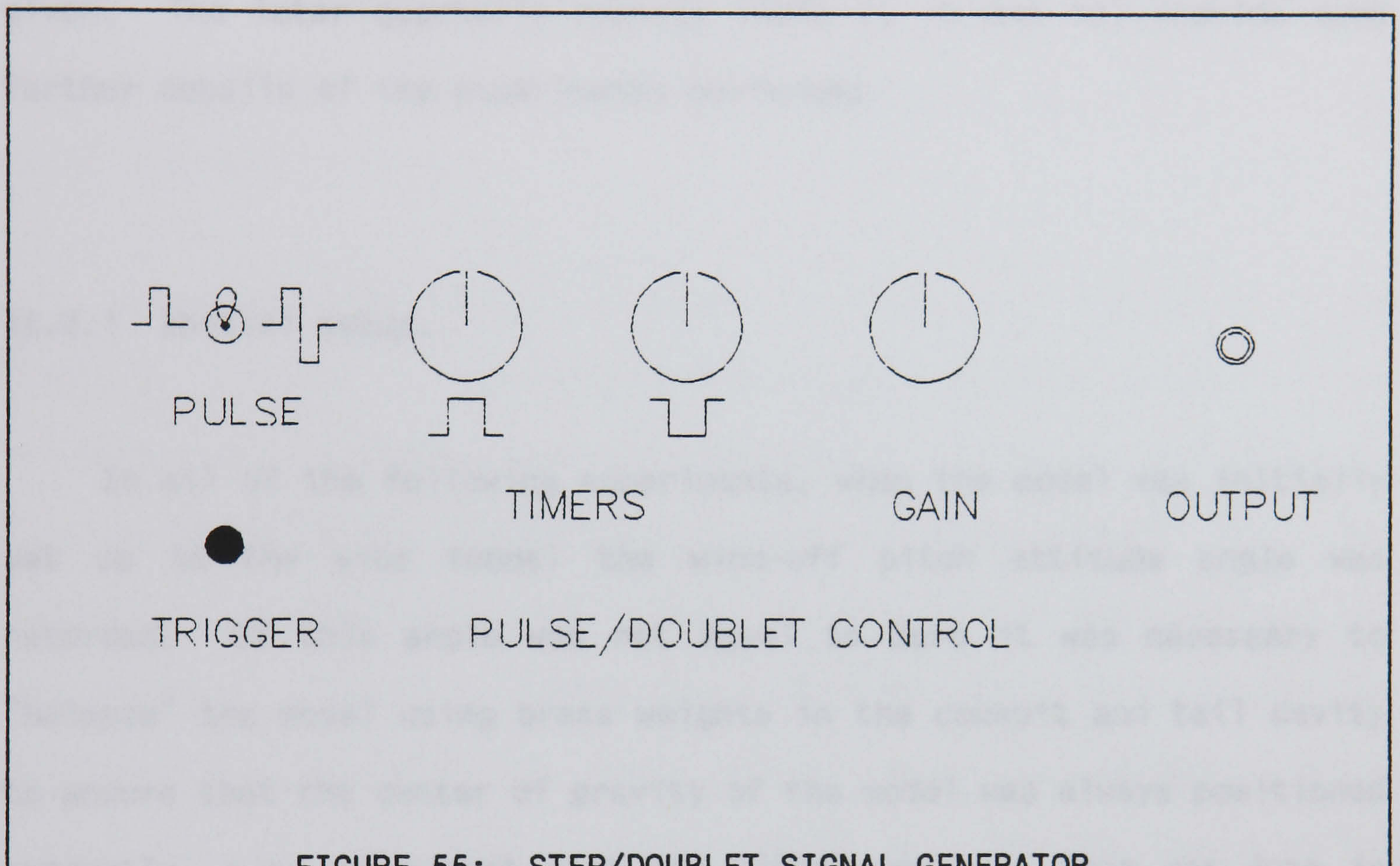

FIGURE 55: STEP/DOUBLET SIGNAL GENERATOR.

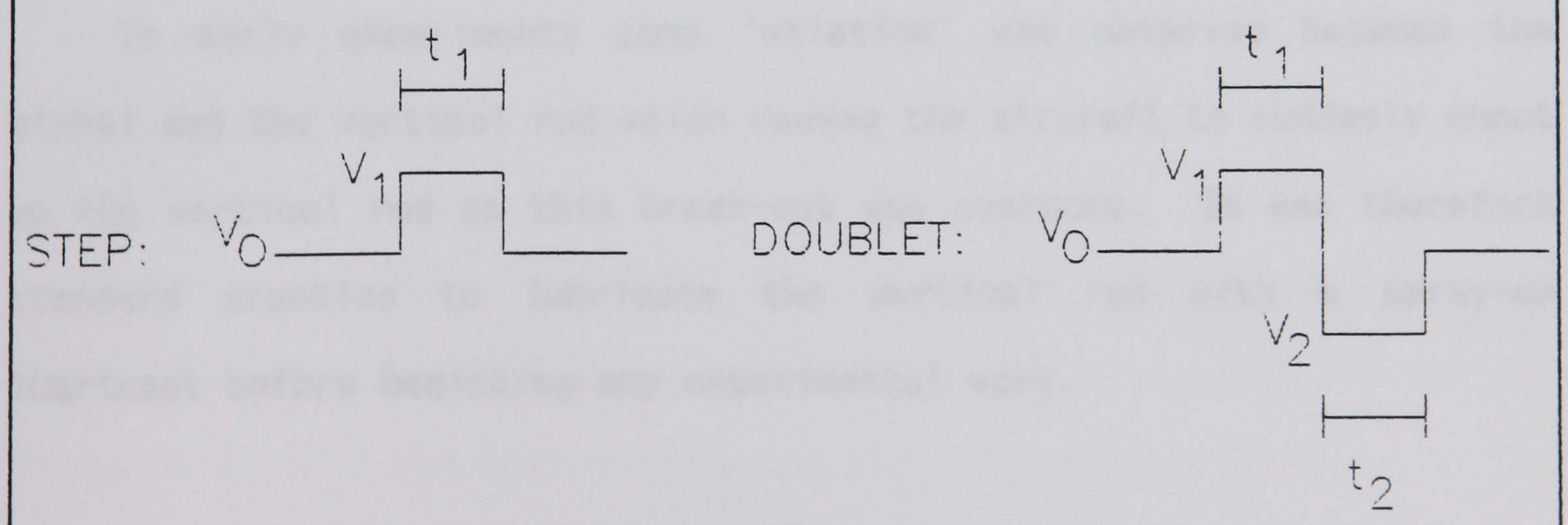

FIGURE 56: TYPES OF ECU PULSES

12.2 Explanation of experiments.

The main sets of experiments which were performed are presented below as a series in chronological order. Comments on the problems encountered and the solutions tried to overcome these problems are given. The later quarterly reports (Refs 9, 10 and 11) provide some further details of the experiments performed.

12.2.1 Initial setup.

In all of the following experiments, when the model was initially set up in the wind tunnel the wind-off pitch attitude angle was recorded. If this angle was not equal to zero it was necessary to "balance" the model using brass weights in the cockpit and tail cavity to ensure that the center of gravity of the model was always positioned correctly, i.e. coincident with the gimbal centre. This was done in order to simplify the later mathematical representation of the model.

In early experiments some "stiction" was observed between the gimbal and the vertical rod which caused the aircraft to suddenly shoot up the vertical rod as this break-out was overcome. It was therefore standard practice to lubricate the vertical rod with a spray-on lubricant before beginning any experimental work.

The cable between the ECU and CED1401 was checked to confirm that it was properly shielded. The common ground between the ECU and CED1401 was also checked as, in preliminary inertia experiments for example, the lack of this connection had given rise to a noise problem.

12.3 Longitudinal pitch experiments.

When the model was first flown with a roll autostabiliser control loop implemented in the electronic control unit (ECU) a dutch roll was induced. Without the roll control loop the dutch roll was not present so it was decided that the model was best flown without feedback control initially until more experience of flying and controlling the model had been obtained.

In early experiments, in which the Hawk model had very little vertical freedom, it was observed that when a doublet movement of the elevator control surface was input the nose up motion was suppressed by the shock absorbing spring resting above the model gimbal, Figure 54. Therefore the model was given a vertical freedom of about one inch and was setup to fly in a trimmed attitude with the spring above the gimbal almost touching the upper restraining collar on the vertical rod. The doublet inputs were arranged so that the model would initially pitch down, then up and then finally return to its original position.

12.3.1 Longitudinal series 1.

In this set of longitudinal experiments no feedback control loops were employed. The ECU was patched, as shown in Appendix F, so that channels 8-15 of the CED1401 recorded the following variables:

Variable	θ_m	$\dot{\theta}_m$	$\ddot{\theta}_m$	η_i	η_o	ϕ_m	ξ_i	ξ_o
Channel	8	9	10	11	12	13	14	15
Data file extension	.c8	.c9	.c10	.c11	.c12	.c13	.c14	.c15

The notation "$_i$" and "$_o$" is used to refer to the input and output voltage signals of the elevator. "$_m$" is used to indicate an attitude angle measured from the ECU. The two channel differentiator was used to produce $\dot{\theta}_m$ (via channel B) and $\ddot{\theta}_m$ (via channel A). "$_m$" is also used to indicate that the measured rate and acceleration data was obtained by an analogue method rather than digital numerical differentiation. The two channel differentiator is described in Chapter 11 and in this particular set of experiments the time constant (RC) and noise potentiometers settings were R_A=6, C_B=-7 (τ_A=0.525secs), N_A=-4 (noise damping $\tau_{NA}=10^{-4}$secs) for channel A and R_B=6, C_B=-7 (τ_B=0.788secs), N_B=-4 (noise damping $\tau_{NB}=10^{-4}$secs) for channel B.

Responses to various doublet inputs were recorded at sampling frequencies of 100Hz and 200Hz using the two pascal programmes REC100.PAS and REC200.PAS. The wind tunnel speed was measured via a Betz manometer in mm of water and converted to m/s as described in Appendix C. In a series of experiments the speed was varied over a small range, from 31.03m/s to 31.78m/s (61.0-64.0mmH_2O on the Betz manometer). The following example shows the data which needed to be recorded for one typical experimental run.

EXAMPLE 1:

FILENAME	f(Hz)	V(mmH_2O)	V(m/s)	Bursts	INPUT
P15DB_C	200	61.4	31.13	4	DOUBLET

During this run 8 data files were recorded on the host computer with the file names P15DB_C.C8, P15DB_C.C9, etc. containing the corresponding variables θ_m, $\dot{\theta}_m$, etc. One burst of data contains 512 data points and therefore recording 4 bursts, at a frequency of 200Hz, resulted in 8 data files containing 2049 data points recorded over a

10.24 second period. Figure 57 shows the variables recorded using channels 8-13 of the CED. Only part of the data is shown, from 1.5 sec to 5.5 sec, as this is the period of interest where the model response is captured. For example, channel 8 shows that the model was initially set up in a trimmed attitude of approximately 6.5° and then performed a short period pitch oscillation (SPPO) in response to the elevator doublet input at $\simeq$ 2.3 secs. Channel 13 shows that there was slight roll coupling present with this particular experimental set-up although this might also be attributable to the SPPO disturbing the tunnel airflow.

In the longitudinal series 1 experiments various signal amplitudes were tried. With doublet inputs of very small amplitude no aircraft response could be observed. With larger amplitude inputs it was found that the model responded by oscillating vertically up and down the vertical rod. Examination of the data files using the Waterfall software showed that there was a substantial level of noise on channel 12 (η_o) except when there was a positive input to the elevator, which was the first part of the doublet cycle causing the initial pitch down of the model. Further investigation of the recorded outputs showed a high level of noise on the output of all three of the control surface servos. Adding a 16μF electrolytic capacitor between each servo output and ground on the ECU was tried as it was thought that together with the output resistance of the servos this would effectively form a low-pass filter and thus reduce the noise level. The roll-off frequency of this filter was expected to be sufficiently high to have a negligible effect on the phase response of these outputs. With these capacitors in place a new set of control surface voltage calibrations were performed before the next experimental series was started.

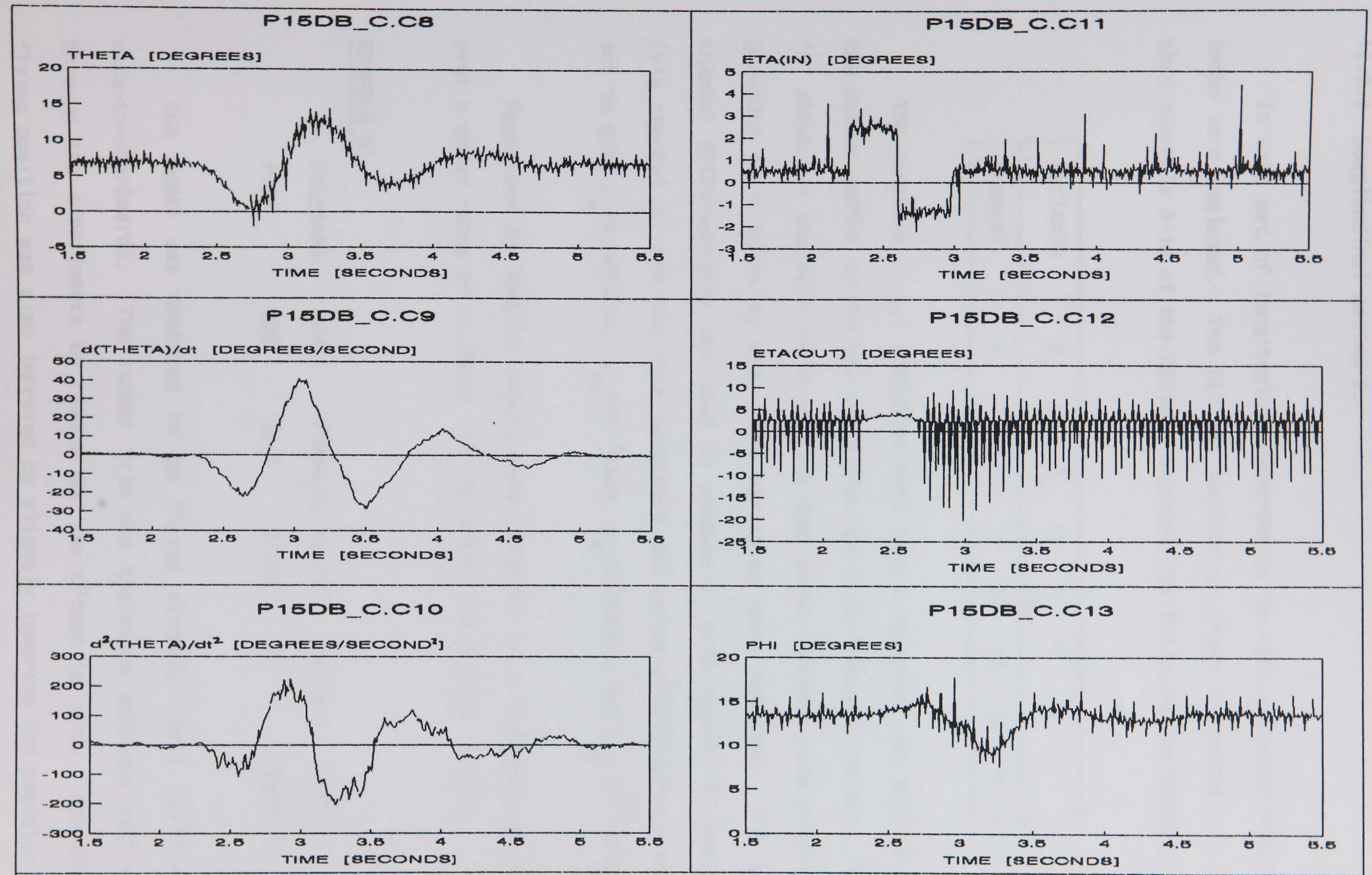

FIGURE 57: TYPICAL LONGITUDINAL SPPO (EXAMPLE 1)

12.3.2 Longitudinal series 2.

In this set of longitudinal experiments no roll autostabilisation loops were employed. The ECU was patched as shown in Appendix F, so that channels 8-15 of the CED1401 recorded the following variables:

Variable	θ_m	$\dot{\theta}_m$	$\ddot{\theta}_m$	η_i	η_{o+cap}	0	0	0
Channel	8	9	10	11	12	13	14	15

The notation "$_{+cap}$" indicates that that a capacitor was applied to the output buffer on the ECU (to filter out high-frequency noise). The "0" shown for channels 13-15 implies that those channels were actually grounded to 0 Volts as only five variables were required. The two channel differentiator was used to produce $\dot{\theta}_m$ (via channel B) and $\ddot{\theta}_m$ (via channel A) and the time constants and noise potentiometers were set to give τ_A=0.525secs, $\tau_{NA}=10^{-4}$secs, τ_B=0.788secs and $\tau_{NB}=10^{-4}$secs.

Responses to doublet inputs were recorded at a frequency of 200Hz, over a speed range of 31.28m/s to 32.47m/s (62.0-66.8 mmH_2O).

EXAMPLE 2:

FILENAME	f(Hz)	V(mmH_2O)	V(m/s)	Bursts	INPUT
P18A	200	62.0	31.28	6	DOUBLET

The model was observed to be flying slightly yawed (with the nose-to-starboard). The rudder trim was therefore adjusted part-way through the experiments to reduce the yaw offset to zero. The model flying position was also improved by slightly lowering its position in

the working section of the wind tunnel. This was done by adjusting the fixed positions of both the top and bottom collars. It was very difficult to keep the aircraft flying in a trimmed position due to small fluctuations in the wind tunnel speed and disturbances to the wind flow when the model moved. The flow at the wing-tips of the model seemed particularly turbulent and the model tended to roll a lot.

12.3.3 Longitudinal series 3.

It was next decided to try to employ a roll autostabilistaion loop in which the roll-rate signal was fed back to the aileron input, this being generated on the ECU as shown in Figure 58. The circuit used a gain of k_1= 0.896, obtained by setting pot number F4 on the ECU to 0.0896volts and feeding the signal to the input of the summer for the aileron control surface. The summer input used was that which multiplied the signal by a factor of 10. Because the ECU has only one type of summer and one type of integrator the time constant of the rate circuit was fixed at 1 second, resulting in an unacceptable lag in the attitude rate information making the recorded data unusable in the MSR. However, the attitude rate feedback produced was sufficient to achieve a significantly better flying position.

Roll-rate ($\dot{\phi}$) feedback damps out the roll by giving the aircraft a more sluggish response to disturbances. The feedback must be sufficient to damp out wing oscillations in the model but should ideally be kept to a minimum. (Note: It is more usual to employ roll-attitude feedback to help maintain roll attitude at zero. Roll-rate feedback is normally used to improve damping in roll.)

The ECU was patched to record the variables shown below. The relevant circuit diagram is presented in Appendix F.

Variable	θ_m	$\dot{\theta}_m$	$\ddot{\theta}_m$	η_i	$\eta_{o_{+cap}}$	$\dot{\phi}_{ECU}$	ξ_i	$\xi_{o_{+cap}}$
Channel	8	9	10	11	12	13	14	15

The subscript "ECU" implies the rate information was generated using an analogue circuit patched on the ECU. The two channel differentiator was used to produce $\dot{\theta}_m$ and $\ddot{\theta}_m$ (via channels B and A respectively) with τ_A=0.525secs, $\tau_{NA}=10^{-4}$secs, τ_B=0.788secs and $\tau_{NB}=10^{-4}$secs.

In this experimental series, a few responses to doublet inputs were recorded at a frequency of 200Hz, over a speed range of 32.25m/s to 32.52m/s (65.9-67.0 mmH_2O).

EXAMPLE 3:

FILENAME	f(Hz)	V(mmH_2O)	V(m/s)	Bursts	INPUT
P20B1	200	67.0	32.52	12	DOUBLET

12.3.4 Longitudinal series 4.

It was next decided that it would be better to apply a more standard autostabilisation loop which used both roll attitude feedback and roll-rate feedback to aileron. Figure 59 shows the circuit diagram which was patched on the ECU. The following variables were recorded; the circuit diagram is given in Appendix F:

Variable	θ_m	$\dot{\theta}_m$	$\ddot{\theta}_m$	η_i	$\eta_{o_{+cap}}$	ϕ_m	$\dot{\phi}_{ECU}$	$\xi_{o_{+cap}}$
Channel	8	9	10	11	12	13	14	15

The two channel differentiator was used to produce $\dot{\theta}_m$ (via channel B) and $\ddot{\theta}_m$ (via channel A) with τ_A=0.525secs, τ_{NA}=10^{-4}secs, τ_B=0.788secs and τ_{NB}=10^{-4}secs. Model responses to both step and doublet inputs were recorded at 200Hz, over a speed range of 31.18m/s to 32.12m/s (61.6-65.4 mmH_2O).

EXAMPLE 4:

FILENAME	f(Hz)	V(mmH_2O)	V(m/s)	Bursts	INPUT
P20C1	200	64.6	31.93	8	DOUBLET
P20C5	200	65.0	32.03	12	STEP

In experimental series 4 the model was flown mainly in the second quartile from the bottom of the wind tunnel, with about two inches of vertical freedom. The observed response was mainly a vertical height translation. To obtain noticeable pitch responses it was found that more vertical freedom was required by the model and that it was best to use step and doublet inputs with the aircraft flying in a trimmed position such that it was just above the bottom collar. These experiments are described next.

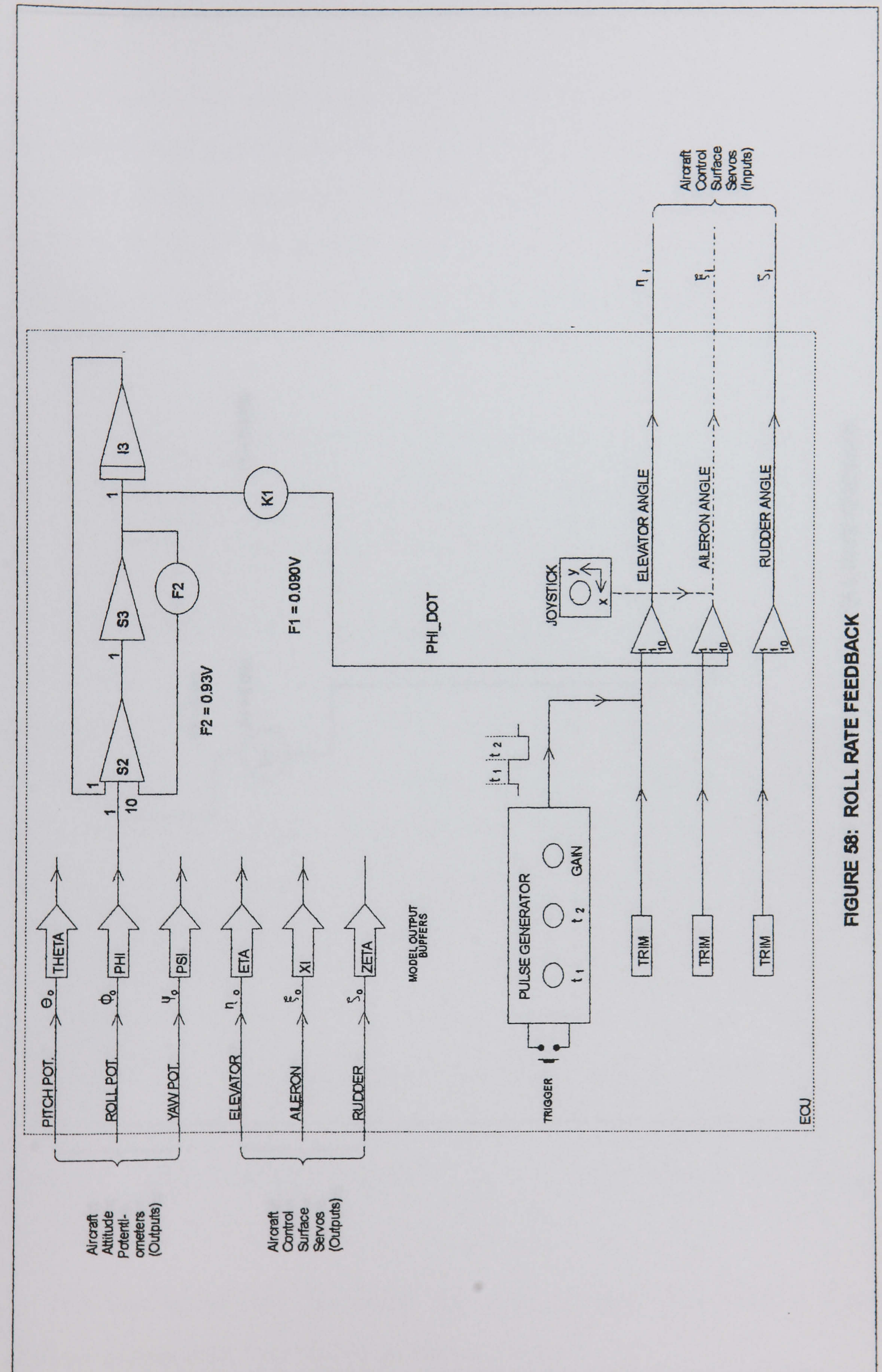

FIGURE 58: ROLL RATE F

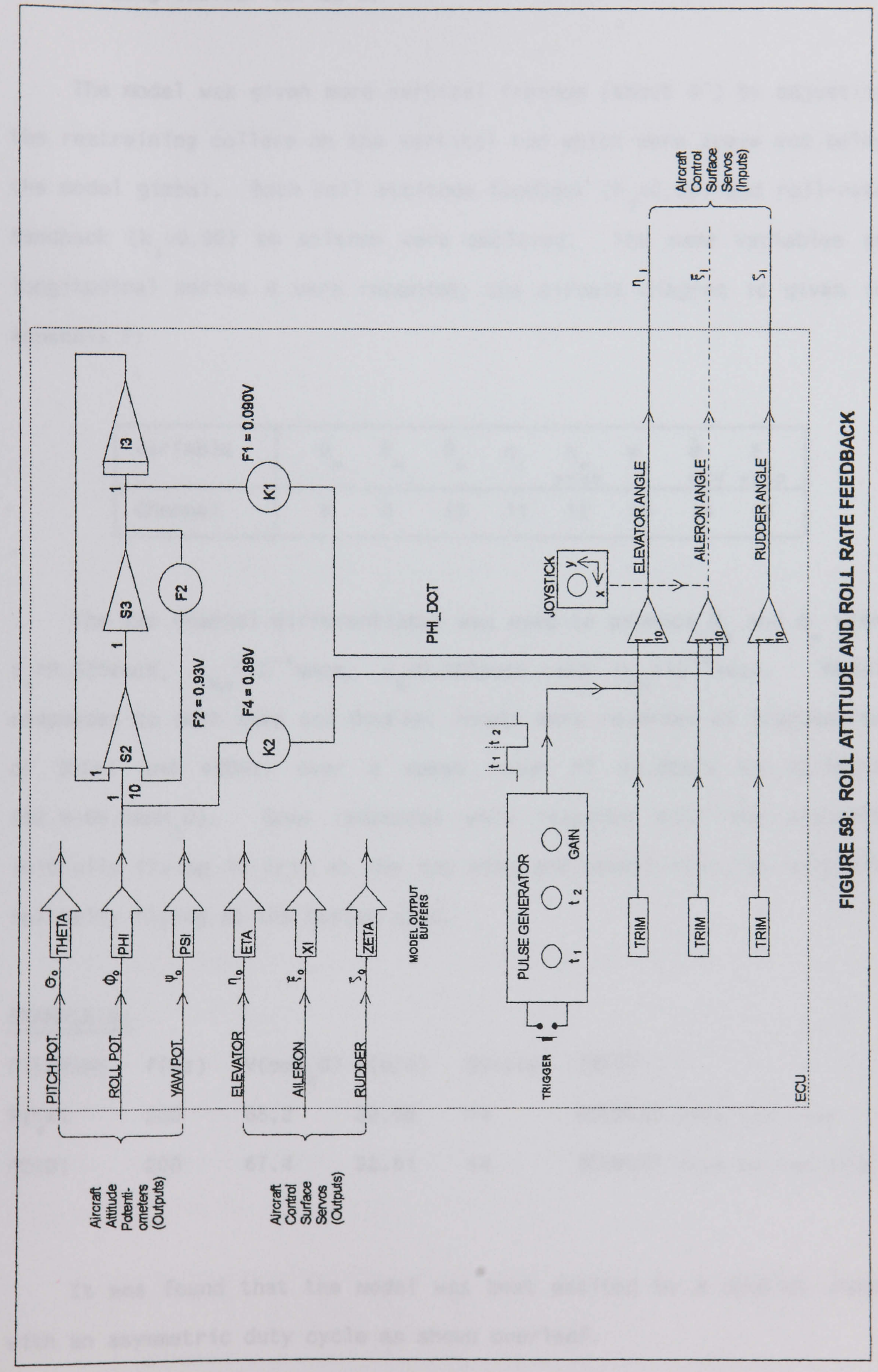

FIGURE 59: ROLL ATTITUDE AND ROLL RATE FEEDBACK

12.3.5 Longitudinal series 5.

The model was given more vertical freedom (about 4") by adjusting the restraining collars on the vertical rod which were above and below the model gimbal. Both roll attitude feedback (k_2=0.89) and roll-rate feedback (k_1=0.90) to aileron were employed. The same variables as longitudinal series 4 were recorded; the circuit diagram is given in Appendix F:

Variable	θ_m	$\dot{\theta}_m$	$\ddot{\theta}_m$	η_i	$\eta_{o_{+cap}}$	ϕ_m	$\dot{\phi}_{ECU}$	$\xi_{o_{+cap}}$
Channel	8	9	10	11	12	13	14	15

The two channel differentiator was used to produce $\dot{\theta}_m$ and $\ddot{\theta}_m$ with τ_A=0.525secs, τ_{NA}=10^{-4}secs, τ_B=0.788secs and τ_{NB}=10^{-4}secs. Model responses to both step and doublet inputs were recorded at frequencies of 200Hz and 400Hz, over a speed range of 31.48m/s to 32.76m/s (62.8-68.0mmH_2O). Some responses were recorded with the aircraft initially flying in trim at the top stop and others with the aircraft initially flying at the bottom stop.

EXAMPLE 5:

FILENAME	f(Hz)	V(mmH_2O)	V(m/s)	Bursts	INPUT
P21A1	200	65.2	32.08	14	DOUBLET from top stop
P21B1	200	67.4	32.61	14	DOUBLET from bottom stop

It was found that the model was best excited by a doublet input with an asymmetric duty cycle as shown overleaf.

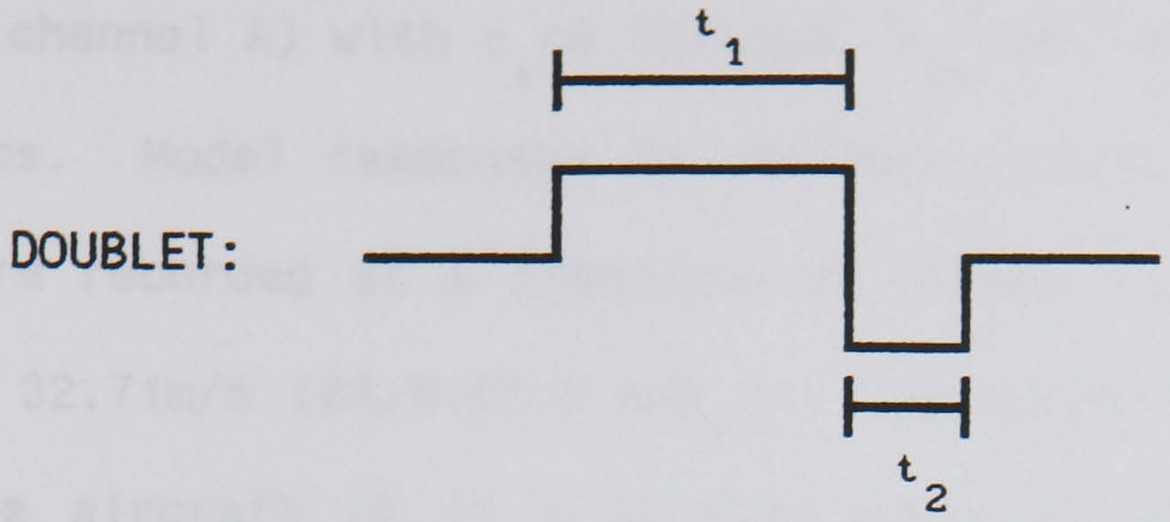

FIGURE 60: ASYMMETRIC DUTY CYCLE.

12.4 Lateral roll experiments.

Only a few lateral roll experiments were performed at this stage as it had been decided to concentrate initially on obtaining results from the MSR procedure using longitudinal data. Two examples of lateral roll experiments are presented below.

12.4.1 Lateral series 1.

The model was set up with the bottom restraining collar half way down the vertical rod. A gap of approximately 4" of vertical freedom was allowed above the model gimbal. Both roll attitude (with k_2=0.89) and roll-rate feedbacks (with k_1=0.90) to aileron were employed. The ECU was patched to record the variables shown overleaf; the circuit diagram is given in Appendix F.

Variable	ϕ_m	$\dot{\phi}_m$	$\ddot{\phi}_m$	ξ_i	$\xi_{o_{+cap}}$	$\dot{\phi}_{ECU}$	θ_m	ψ_m
Channel	8	9	10	11	12	13	14	15

The two channel differentiator was used to produce $\dot{\phi}_m$ (via channel B) and $\ddot{\phi}_m$ (via channel A) with τ_A=0.525secs, τ_{NA}=10^{-4}secs, τ_B=0.788secs and τ_{NB}=10^{-4}secs. Model responses to various aileron control surface step inputs were recorded at a frequency of 400Hz, over a speed range of 31.73m/s to 32.71m/s (63.8-67.8 mmH_2O). In practice, it was found best to set the aircraft up in a trimmed position and apply to step inputs by hand using the joystick rather than using the signal generator.

EXAMPLE 6:

FILENAME	f(Hz)	V(mmH_2O)	V(m/s)	Bursts	INPUT
R21A1	400	67.0	32.52	4	STEP by joystick

The model was initially flown in trim at the bottom stop in the second quartile from the top of the wind tunnel. Because of the roll rate feedback loops employed the response motion damped out very quickly.

Figure 61 shows the roll response recorded in channel 8 and compares two methods of producing rate data, namely the two-channel differentiator and an analogue circuit patched on the ECU.

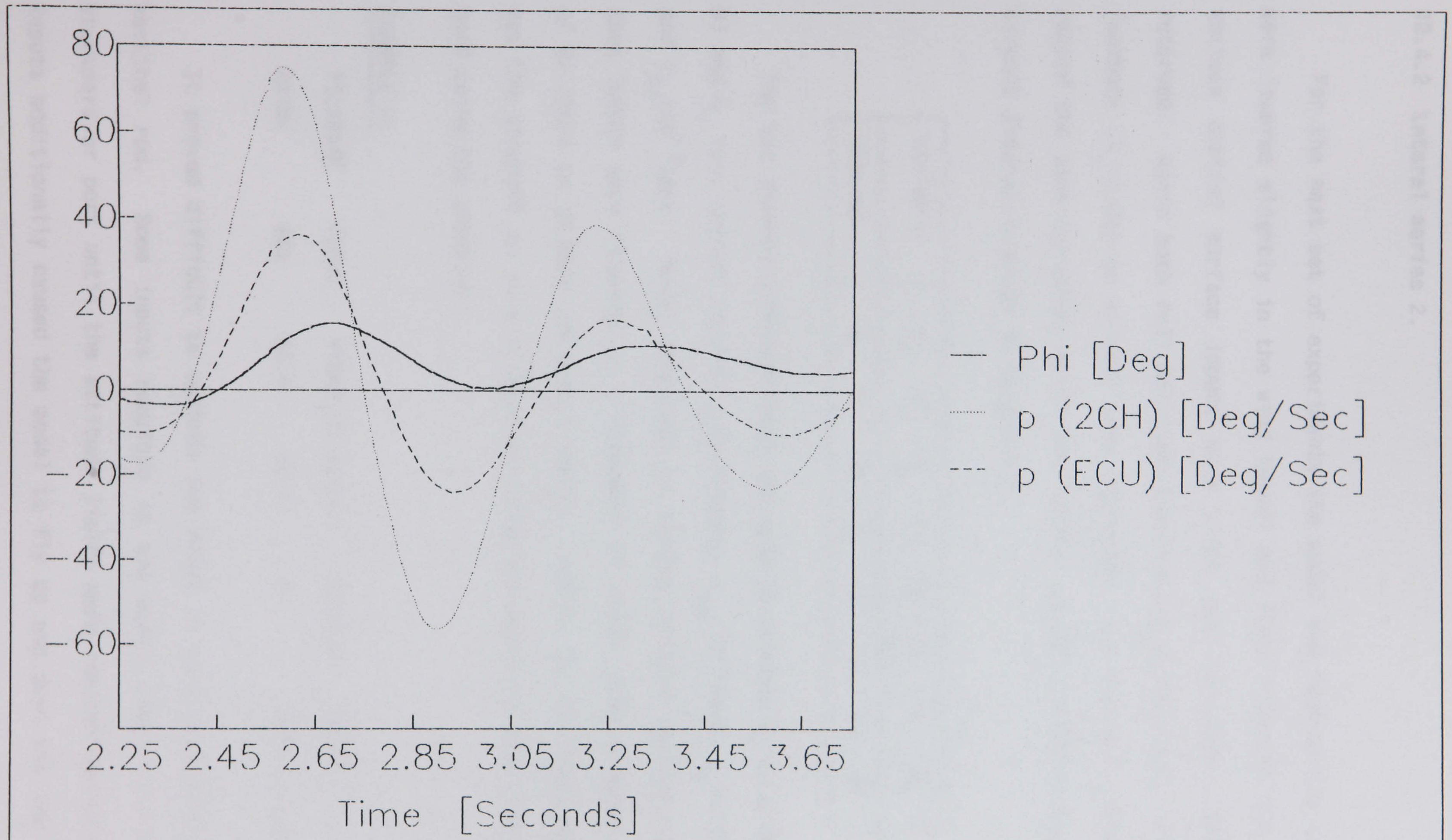

FIGURE 61: LATERAL EXPERIMENT RESPONSES ROLL ATTITUDE AND RATE DATA

12.4.2 Lateral series 2.

For the next set of experiments the model and restraining collars were lowered slightly in the wind tunnel and flown from the top stop; various control surface inputs were tried and the model responses recorded. Again both roll attitude feedback (k_2=0.089) and roll-rate feedback (k_1=0.09) to aileron were employed. The ECU was patched to record the same variables as in the lateral series 1 experiments; the circuit diagram is given in Appendix F:

Variable	ϕ_m	$\dot{\phi}_m$	$\ddot{\phi}_m$	ξ_i	ξ_o	$\dot{\phi}_{ECU}$	θ_m	ψ_m
Channel	8	9	10	11	12	13	14	15

The two channel differentiator was used to produce $\dot{\phi}_m$ (via channel B) and $\ddot{\phi}_m$ (via channel A) with τ_A=0.525secs, τ_{NA}=10^{-4}secs, τ_B=0.788secs and τ_{NB}=10^{-4}secs. Model responses to various aileron control surface step inputs were recorded at a frequency of 400Hz, over a speed range of 32.12m/s to 33.0m/s (65.4-69.0 mmH_2O). Again, it was found best to set the aircraft up in a trimmed position and apply to step inputs by hand using the joystick.

EXAMPLE 7:

FILENAME	f(Hz)	V(mmH_2O)	V(m/s)	Bursts	INPUT
R21B1	400	66.0	32.27	8	STEP by joystick

It proved difficult to control the model in this position on the vertical rod. Some inputs resulted in the model simply rolling to starboard or port until the attitude limits were reached whilst other inputs additionally caused the model to fly up and down the rod in an uncontrolled manner.

12.5 Noise problems.

Typical longitudinal series short period responses are shown in Figure 57. Analysis of the responses using the Waterfall software revealed that a high level of noise was present in all the channels. After a number of possible sources had been investigated this noise was eventually linked to a problem with a switched mode power supply unit (PSU) in the ECU. Discussion with the manufacturers revealed an undocumented mode of behaviour which resulted in the PSU producing high frequency noise if insufficiently loaded. This explained the unusual behaviour which had been noted, namely that the noise appeared to be reduced when the control surfaces were actually in motion ie. when the PSU loading was transiently increased.

The problem was eventually dealt with by replacing the ECU power supplies by external power supplies of a different design (two Farnell Instruments Limited L30-2 Stabilised Power Supplies). These new PSUs were found to dramatically reduce the level of noise and experimental work then continued. Figure 62 compares typical elevator servo outputs with the old and new power supplies.

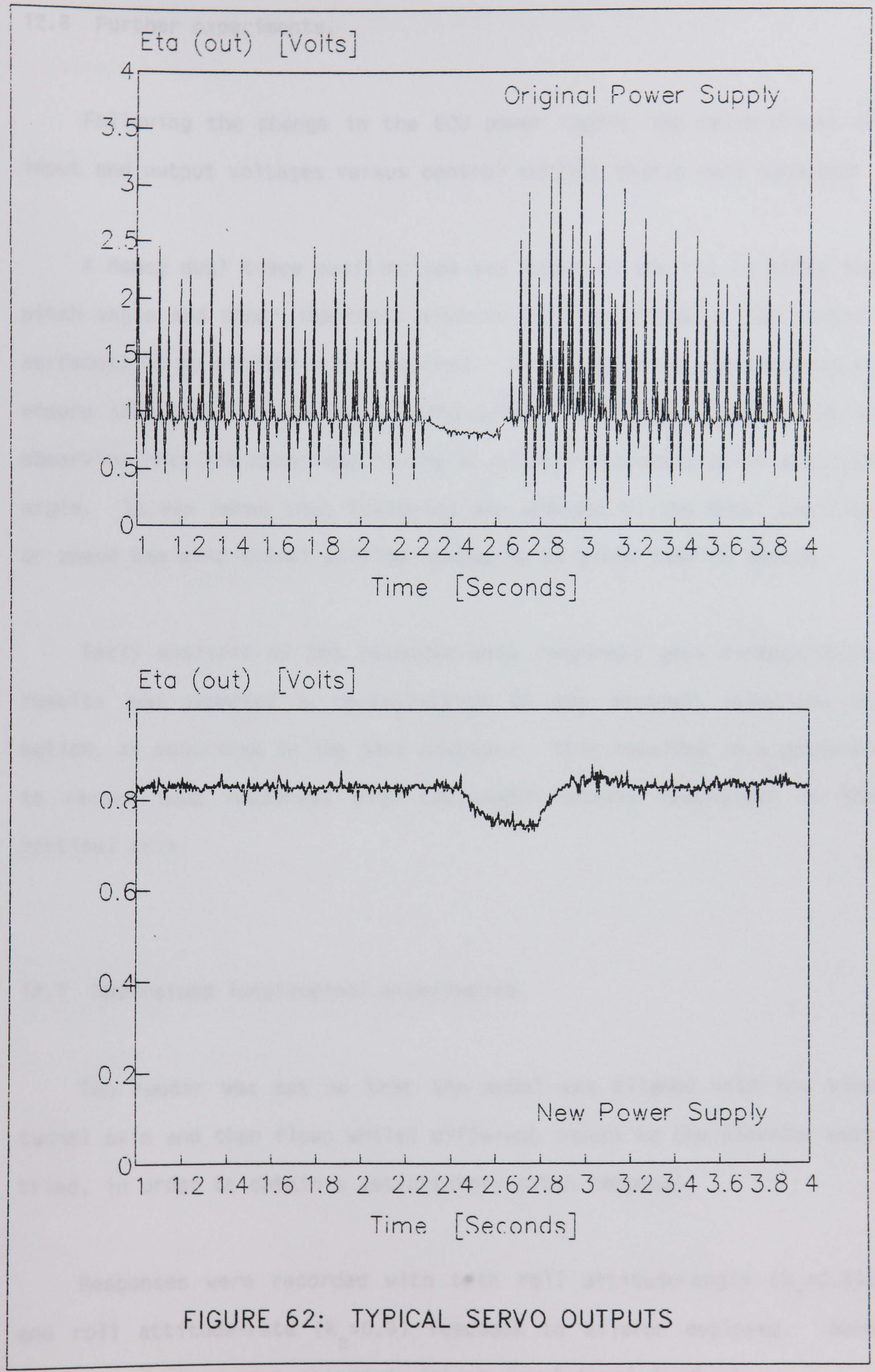

FIGURE 62: TYPICAL SERVO OUTPUTS

12.6 Further experiments.

Following the change in the ECU power supply new calibrations of input and output voltages versus control surface angles were obtained.

A Hameg dual trace oscilloscope was added to the rig to allow the pitch angle and other important signals (such as those to the control surfaces) to be monitored as required. This simplified the checking to ensure that the aircraft was flying properly in trim, carried out by observing that the model was flying at a fairly constant pitch attitude angle. It was noted that following any changes to the model position or speed the wind tunnel airflow needed to be given time to settle.

Early analysis of the recorded data responses gave disappointing results and prompted a re-evaluation of the aircraft equations of motion, as described in the next chapter. This resulted in a decision to record some responses with the model totally restrained in the vertical axis.

12.7 Restrained longitudinal experiments.

The rudder was set so that the model was aligned with the wind tunnel axis and then flown whilst different inputs to the elevator were tried, in order to obtain a satisfactory pitch response.

Responses were recorded with both roll attitude-angle (k_1=0.89) and roll attitude-rate (k_2=0.9) feedback to aileron employed. Some further responses were recorded without any lateral feedback.

The ECU was patched to record the variables shown below via channels 8 to 15.

Variable	θ_m	$\dot{\theta}_m$	$\ddot{\theta}_m$	η_i	$\eta_{o_{+cap}}$	ϕ_m	$\dot{\phi}_{ECU}$	$\xi_{o_{+cap}}$
Channel	8	9	10	11	12	13	14	15

with feedback to aileron

or

Variable	θ_m	$\dot{\theta}_m$	$\ddot{\theta}_m$	η_i	$\eta_{o_{+cap}}$	ϕ_m	0	0
Channel	8	9	10	11	12	13	14	15

without feedback to aileron

The two channel differentiator was used to produce $\dot{\theta}_m$ and $\ddot{\theta}_m$ with τ_A=0.525secs, $\tau_{NA}=10^{-4}$secs, τ_B=0.788secs and $\tau_{NB}=10^{-4}$secs.

Many experiments were performed using this basic model and equipment configuration (i.e. with the external power supplies and oscilloscope monitoring). Model responses to a number of aileron control surface inputs were recorded at a sampling frequency of 400Hz, over a speed range of 32.27m/s to 33.31m/s (66.0-70.3 mmH_2O). Various amplitudes and durations were used in the generation of the control surface inputs on the ECU panel; some inputs were also generated by hand using the joystick.

EXAMPLE 8: (without feedback)

FILENAME	f(Hz)	V(mmH_2O)	V(m/s)	Bursts	INPUT
APR4A	400	67.5	32.64	8	DOUBLET

12.8 Restrained lateral roll experiments.

Many experiments were performed both with and without lateral feedback to aileron.recorded, i.e. roll attitude feedback (k_2=0.089) and roll-rate feedback (k_1=0.09) to aileron were employed. The ECU was patched to record the variables shown below.

Variable	ϕ_m	$\dot{\phi}_m$	$\ddot{\phi}_m$	ξ_i	ξ_{o+cap}	ψ_m	ζ_m	$\dot{\phi}_m$
Channel	8	9	10	11	12	13	14	15

with feedback to aileron

or

Variable	ϕ_m	$\dot{\phi}_m$	$\ddot{\phi}_m$	ξ_i	ξ_{o+cap}	ψ_m	ζ_m	θ_m
Channel	8	9	10	11	12	13	14	15

without feedback to aileron

The two channel differentiator was used to produce $\dot{\phi}_m$ (via channel B) and $\ddot{\phi}_m$ (via channel A) with τ_A=0.525secs, τ_{NA}=10^{-4}secs, τ_B=0.788secs and τ_{NB}=10^{-4}secs. Model responses to a number of aileron control surface inputs were recorded at a sampling frequency of 400Hz, over a speed range of 32.76m/s to 33.24m/s (68.0-70.0mmH_2O). Various different gains and durations were used to generate the control surface inputs on the ECU panel; some inputs were also generated by hand using the joystick.

EXAMPLE 9:

FILENAME	f(Hz)	V(mmH_2O)	V(m/s)	Bursts	INPUT
R28B1	400	69.5	33.12	16	DOUBLET by joystick

12.9 Restrained lateral yaw experiments.

A number of experiments were performed with and without lateral autostabilisation loops employed. The ECU was patched to record the variables shown below.

Variable	ψ_m	$\dot{\psi}_m$	$\ddot{\psi}_m$	ζ_i	ζ_o	ϕ_m	$-10\dot{\phi}$ ECU	$\dot{\xi}_o$
Channel	8	9	10	11	12	13	14	15

with feedback to aileron

or

Variable	ψ_m	$\dot{\psi}_m$	$\ddot{\psi}_m$	θ_m	ζ_o	ϕ_m	$-10\dot{\phi}$ ECU	$\dot{\xi}_o$
Channel	8	9	10	11	12	13	14	15

without feedback to aileron

In practice, $\dot{\phi}_m$ was found to be such a small value that the signal was amplified by 10 using a summer on the ECU before being recorded. The two channel differentiator was used to produce $\dot{\psi}_m$ and $\ddot{\psi}_m$.

EXAMPLE 10:

FILENAME	f(Hz)	V(mmH_2O)	V(m/s)	Bursts	INPUT
DRA1	400	70.0	33.24	18	DOUBLET

Model responses to a number of aileron control surface inputs were recorded at a sampling frequency of 400Hz, over a speed range of 32.76m/s to 33.42m/s (68.0-70.8 mmH_2O). Various different gains and time durations were used to generate the control surface inputs from the ECU panel. Further inputs were also generated by hand using the joystick.

12.10 Experimental observations.

It was possible to demonstrate the following modes of motion of the Hawk model on the experimental rig:

1. SPPO - excited by applying a short disturbance in pitch to the aircraft, for example, by a short doublet applied to the elevator.

2. Spiral mode - produced by a small step to the rudder causing the aircraft to side-slip and roll.

3. Roll subsidence mode - produced by a small step to aileron ξ causing the model to return to the datum/initial trim after a few seconds. This mode was clearly visible.

4. Dutch roll - produced by an impulse or short doublet to the rudder causing the aircraft to roll and yaw from side to side, the wing-tips performing a figure-of-eight.

12.10.1 Trimming the aircraft.

With feedback employed the following method was found to be the best way to trim the aircraft model: First the rudder was adjusted using the rudder trim pot to give a zero yaw angle so that the model was flying straight in the wind tunnel. Next the pitch of the aircraft was trimmed using the elevator trim pot. Finally the aileron trim pot was used to adjust the roll angle and get the model flying with its wings as close to horizontal as possible.

Fluctuations in the wind tunnel flow mainly affect the roll trim and hence it was sometimes necessary to employ lateral autostabilisation in the form of roll rate and roll angle feedback to aileron to damp out roll perturbations as far as possible.

It was not readily possible to significantly reduce perturbations to pitch caused by fluctuations in the wind tunnel flow. It was found best to allow time for the flow to settle down between the recording of the various responses.

Another problem observed was the slight backlash present in the control surface to servo linkages which it was not possible to eliminate. There was also considerable backlash in the measurement of yaw angle.

12.10.2 Residual low-frequency noise.

Following the experimental work, close examination of the recorded data revealed a low level signal at 25Hz superimposed on the aircraft response, Figure 63. The frequency was strongly suggestive of an origin derived from the UK 50Hz domestic mains supply. Care had been taken to eliminate possible sources of interference such as the accidental formation of earth loops, however a low residual level of mains-related interference is not unusual in electronic data gathering equipment. Despite the fact that the interference was only at a low level, it was found to have an important effect on the signal differentiation. For example, at a sampling rate of 400Hz there are 16 data points per 25Hz cycle. Thus if a 5-point formula is used for

differentiation at this sampling frequency it will readily "see" the ripples, ie. changes in slope, present on the aircraft response. Since differentiation tends to amplify noise the results are out of proportion to the original cause, Figure 64.

For the data analysis, several possible solutions to this problem were identified. The options were:

1. Use data from the analogue differentiator, the frequency response of which does not extend up to 25Hz.
2. Use data recorded with, say, a 100Hz sampling frequency together with an 11-point formula for digital differentiation.
3. Form a moving average over data points covering one or more 25Hz cycles before differentiation.
4. Retain only those data points which occur at equivalent points of a 25Hz cycle (for example, every 16^{th} data point when sampling at 400Hz).
5. Use a 16-point formula or greater at the higher sampling frequencies.
6. Pre-process the data using a 25Hz digital notch or low-pass filter.
7. Use a differentiation strategy based on fitting a smooth curve to the data whose parameters are constrained so as not to follow the 25Hz oscillations (for example, fit a set of Tschebyschev polynomials).

Of these, option (2) was easiest to apply and most successful. It had the additional advantage that because of the lower sampling frequency, data covering a longer time interval could be analysed.

Option (3) was tried using a 16-point moving average and proved successful at removing the 25Hz signal. However, a phase shift was introduced and though small (<5%) it was decided not to use this method because of the known sensitivity of the MSR procedure to phase errors. Option (4) was judged impractical as aside from the reduction of the quantity of data the 25Hz signal was not expected to remain exactly in phase with the sampling clock. Options (5) to (7), whilst potentially effective, would have necessitated considerable extra effort writing new software.

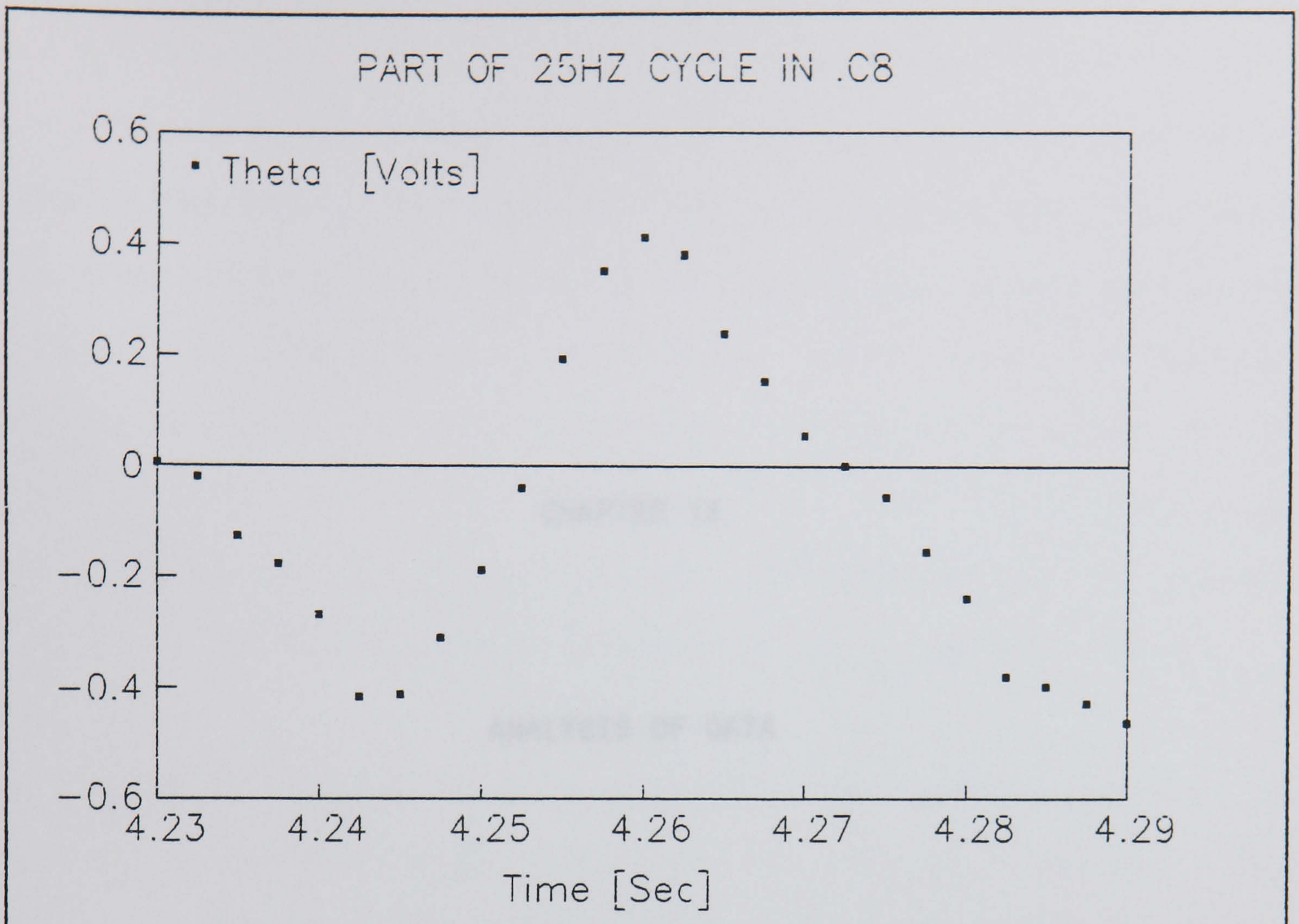

FIGURE 63: MAGNIFIED 400Hz AIRCRAFT RESPONSE DATA

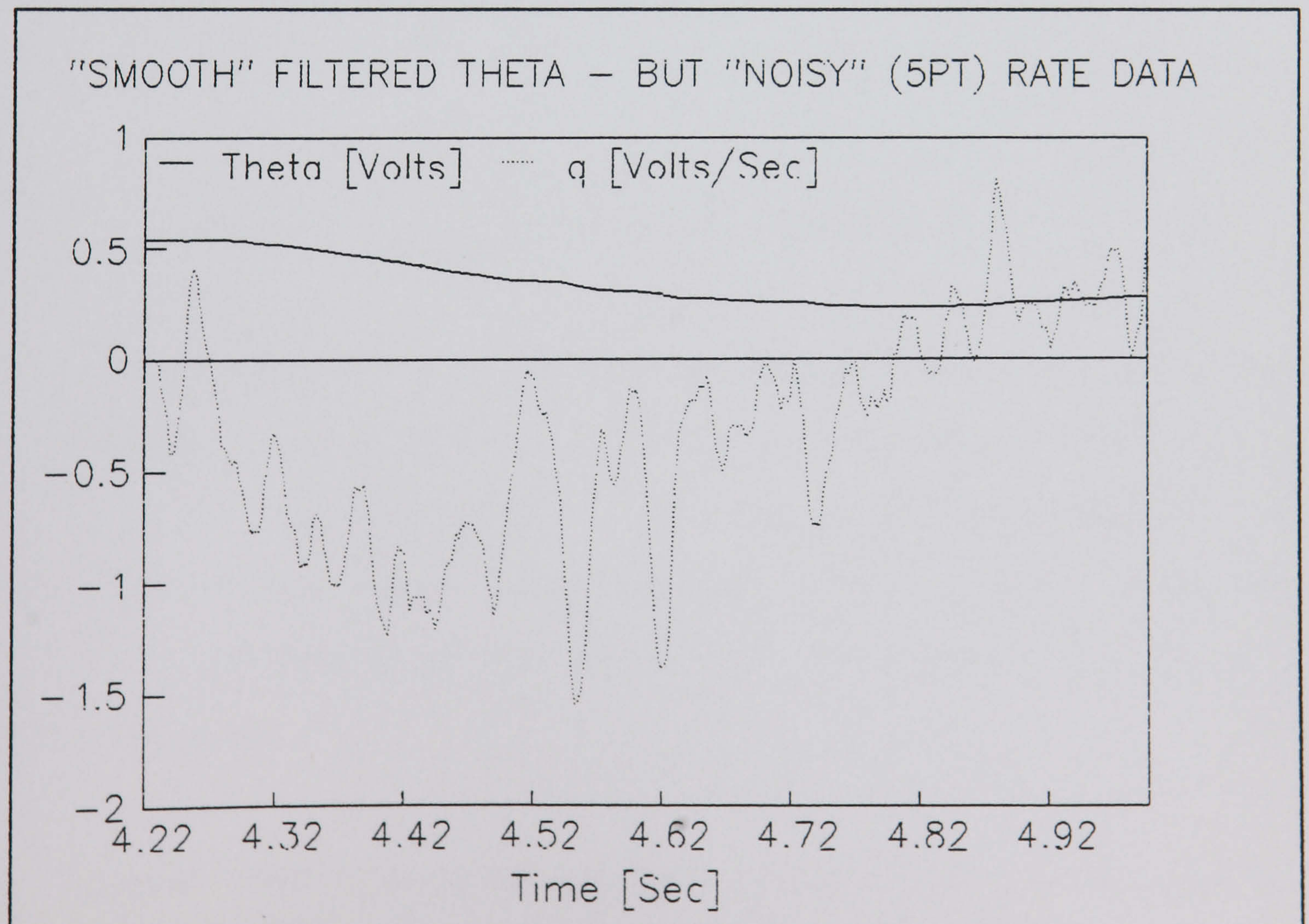

FIGURE 64: 400Hz AIRCRAFT RESPONSE DATA

CHAPTER 13

ANALYSIS OF DATA

13.0 ANALYSIS OF DATA.

There are many stages involved in the conversion of experimental data to the format required by the MSR. For example, attitude signals recorded in volts need to be converted into the appropriate engineering units, i.e. into degrees. This signal conditioning also includes derivation of the attitude rates and accelerations required for the initial linear MSR mathematical model. The experimental setup must also be analysed and allowances made, where appropriate, for factors such as mechanical friction or backlash in control surface linkages.

Starting with the raw data recorded in the eight data files on the IBM PC for each particular wind tunnel run, the steps outlined below are performed to produce a data file suitable for input to the MSR FORTRAN 77 program. The processing of the experimental data is best demonstrated by using the following typical run.

13.1 Experimental setup for wind tunnel run P18A1.C*

In the P18A1.C* experimental run the Hawk model was positioned mid-way down the vertical rod. The restraining collars were fixed so as to allow the model about 4" of vertical or heave freedom. No autostabilisation loops were employed to artificially alter the stability and controllability of the Hawk model when it was flown in the wind tunnel.

Aside: Ref 11 contains details of experimental runs in which the Hawk model is fully restrained with no vertical movement allowed.

The ECU was set up to record the following variables:

P18A1.C8 = θ_m the pitch potentiometer reading.

P18A1.C9 = $\dot{\theta}_m$ analogue differentiation of C8 using the bottom section of the two channel differentiator box with C,R,N equal to -7, 6 and 4.

P18A1.C10 = $\ddot{\theta}_m$ analogue differentiation of C8 using the top section of the differentiator box with C,R,N = -7, 6 and 4.

P18A1.C11 = η_i the voltage input to the control servo.

P18A1.C12 = η_o the voltage output from the control servo which indicates the actual elevator angle achieved.

Channels 13 - 15 were not required and were therefore grounded to earth. "P18A1" contained 8 bursts of 512 data points and was recorded at a frequency of 100Hz; thus giving a total recorded run of 40.96 sec.

The Betz manometer reading was 66.8mm H_2O, indicating that the wind tunnel speed was 32.47 m/sec.

13.2 Signal Conditioning Steps.

STEP 1: Initial examination of recorded data.

Wind tunnel data for experimental run P18A1 was recorded on hard disk, via the CED1401, in eight IBM PC data files. The aircraft inputs and responses were automatically recorded in a HEX format which meant

that, in this raw form, the data could only be examined using the WATERFAL software package. WATERFAL provides a graphical display of the voltage data against time and was initially used to check that "good" short period traces had been obtained and to confirm that the aircraft model had been set up in a stable trimmed condition before the control surface was input.

Examination of the variables of channels 8 to 12 of P18A1 showed that a good pitch response had been captured on all channels. For parameter estimation purposes, 1.5sec of data covering the experimental time period 11.0sec to 12.5sec was used. This particular period was chosen as it contained all of the elevator input and approximately 1.5 cycles of the subsequent pitch response.

During the analysis of C8 using WATERFAL, the trimmed angle of incidence α_e = 0.457 Volts had also been noted. Using the calibration equation θ_m = (-19.1*V) + 9.52, it was possible to calculate that the model was flying at a trimmed incidence angle of 0.47 degrees before the elevator doublet was input at 11.07sec.

STEP 2: Filtering of noise from the data files.

It is desirable to have experimental data with as little noise as possible because some of the data requires numerical differentiation which magnifies any noise present. Therefore a Turbo-Pascal program called FILT.PAS was employed next to reduce noise in the 'raw' CED1401 data. The program applies a Butterworth filter in both a forward and a backward direction through the data in order to cancel out any phase shifts introduced in the data by the use of a digital filter.

The P18A1 data files for channels *.C8 to *.C12 were all filtered using FILT.PAS and the new files stored as FP18A1.C8 to FP18A1.C12. For comparison purposes, Figure 65 shows the original unfiltered pitch response as well as various filtered aircraft responses. If required, it is possible to run the data through FILT.PAS more than once to obtain even smoother data; however this was not found necessary as good results were normally obtained after one pass of the program.

STEP 3: Conversion to ASCII and numerical differentiation of files.

This step utilizes a TURBO-BASIC program called COND11.BAS, which was written to convert the various CED data channels from raw HEX voltage data to ASCII numbers, also in volts. COND11.BAS combines any number of channels into a single file with time as the first column of data. It can also numerically differentiate data once or twice with respect to time using the eleven point formula described in Chapter 11.

If a channel is to be differentiated once ',1' is appended to the channel number. To obtain both the first and second differentials ',1,1' is appended. (Note: Various programs were written to investigate other differentiation strategies).

For this P18A1 example, only channels C8 (θ_m) and C12 (η_o) were required because numerical rate data was used instead of the "out of phase" measured rate and acceleration data of channels 9 and 10. Thus C8 was differentiated twice to produce $\dot{\theta}_{11} \simeq q$ and $\ddot{\theta}_{11} \simeq \dot{q}$. Figure 66 shows the filtered pitch response data and numerically derived data. (Aside: Ref 11 contains an example run which uses measured rate and acceleration data). When COND11.BAS was run the generic filename was specified and the channels were input as '8,1,1' and '12'.

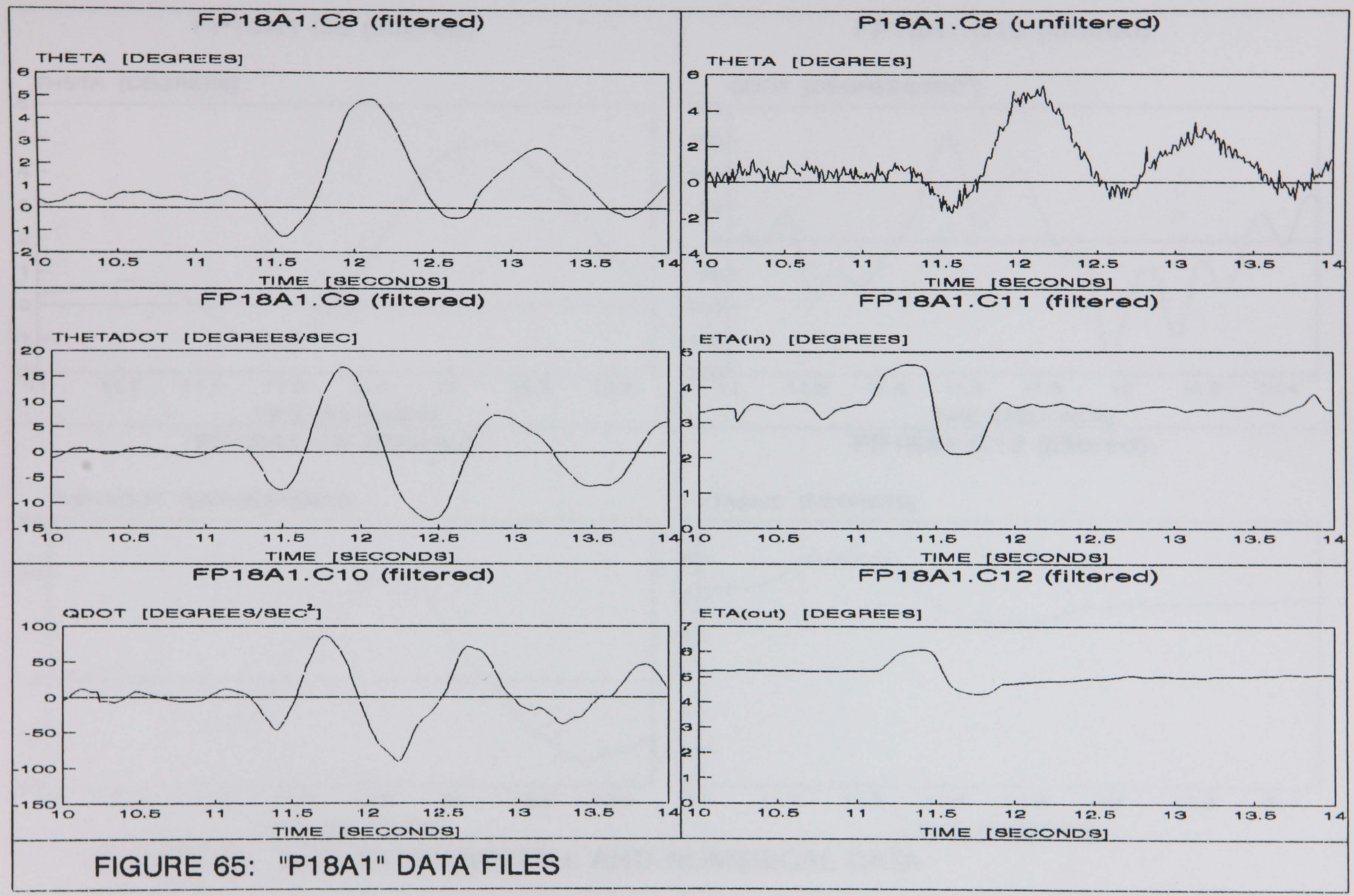

FIGURE 65: "P18A1" DATA FILES

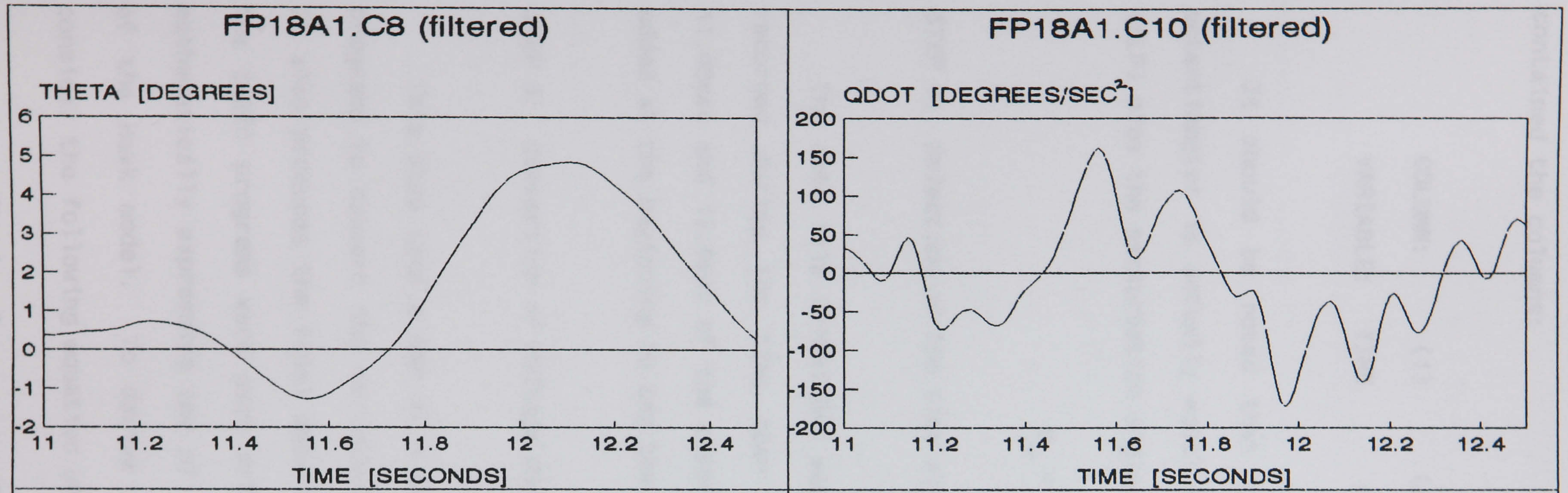

FIGURE 66: MSR EXPERIMENTAL AND NUMERICAL DATA

The output file obtained from COND11.BAS was called FP18A1.DAT and contained the columns:

COLUMN:	(1)	(2)	(3)	(4)	(5)
VARIABLE:	TIME	θ_m	$\dot{\theta}_{11}$	$\ddot{\theta}_{11}$	η_o

It should be noted that the angle θ_m measured by the model potentiometer is actually equal to the trimmed angle of incidence α_e (ALP) plus the perturbation angle θ, i.e.:

$$\theta_m = \alpha_e + \theta \qquad [13.1]$$

STEP 4: Selection of the time slice to analyse using MSR.

The data file FP18A1.DAT was then edited to leave only the data recorded during the time span of interest, in this case between 11.00sec and 12.5sec of the experimental run. A line of comments was added at the beginning to tag the data for the users benefit.

STEP 5: Conversion of voltage data to engineering units.

This step uses a one of a number of almost identical TURBO-BASIC programs to convert the variables in FP18A1.DAT to engineering units. It also produces the final data file for input into the MSR program. The BASIC programs were each written to reflect a particular way of mathematically expressing one of the longitudinal equations of motion of the Hawk model. To derive the EQN1_1.BAS program for example, consider the following equation of longitudinal motion:

$$(m-\mathring{Z}_{\dot{w}}).\dot{w} = \mathring{Z}_w.w + (mU_e+\mathring{Z}_q).q + \mathring{Z}_\eta.\eta + m.g.\sin\theta_e.\theta \qquad [13.2]$$

Assuming that the flight path angle γ is equal to zero, that $\mathring{Z}_{\dot{w}}$ is zero and finally dividing through by m, it is possible to show that:

$$\dot{w} = \mathring{Z}_w.w + (U_e + \mathring{Z}_q).q + \mathring{Z}_\eta.\eta + g.\sin\alpha_e.\theta \qquad [13.3]$$

Next consider the following aerodynamic relationships, Ref 10 and Appendix B.5, where V_t is wind tunnel speed and α_e trimmed incidence angle:

$$w = V_t.\theta.\cos\alpha_e \qquad U_e = V_t.\cos\alpha_e$$

$$\dot{w} = V_t.\dot{\theta}.\cos\alpha_e \qquad q = \dot{\theta} \qquad [13.4]$$

These relationships represent wind velocity and angular perturbation terms and does not explicitly consider the inertial heave freedom of the Hawk in the experimental setup being analysed. An alternative expression for small perturbation motion in the wind tunnel is presented in Chapter 14.

Substituting these relationships into [13.3] and inserting an additional term $\mathring{Z}_0$ to allow for the trimmed initial condition yields:

$$V_t\dot{\theta}\cos\alpha_e = \mathring{Z}_0.1 + g\sin\alpha_e.\theta + \mathring{Z}_w.V_t\theta\cos\alpha_e + (V_t\cos\alpha_e + \mathring{Z}_q).\dot{\theta} + \mathring{Z}_\eta.\eta \qquad [13.5]$$

$$\uparrow \quad \uparrow\uparrow \quad \uparrow \quad \uparrow\uparrow \quad \uparrow \quad \uparrow \quad \uparrow \quad \uparrow\uparrow$$

$$Y = B0.1 + B1.X1 + B2.X2 + B3.X3 + B4.X4$$

From the wind tunnel experiments V_t and α_e are known, θ and η are measured and $\dot{\theta}$ may also be measured or derived. Thus all of the "X" variables in equation [13.5] are known. The data file obtained from Step 4, FP18A1.DAT in this example, contains the following columns:

COLUMN:	(1)	(2)	(3)	(4)	(5)
VARIABLE:	TIME	θ_m	$\dot{\theta}_{11}$	$\ddot{\theta}_{11}$	η_o

EQN1_1.BAS uses FP18A1.DAT as the input file and the equations shown below/overleaf are used to calculate the output "Y" and the state variables "X1", ..., "X4", all in SI units. The calibration equations used for converting data from volts to degrees were those measured in the preliminary experiments (see Chapter 6).

During the SPPO of the aircraft the pitch potentiometer measures θ_m which is actually equal to $\theta + \alpha_e$. Therefore α_e (ALP) needs to be subtracted, as shown in the equations below, to obtain just the perturbed pitch response. The final output data is expressed in radians using the multiplier TORAD (equal to $\pi/180$).

```
 THETA = { [COL(2)-ALP] * MPI + CPI } * TORAD      ' to obtain θ^c

THEDOT = { COL(3) * MPI + CPI } * TORAD            ' to obtain θ̇^c

  VCA = V*COS(ALP)                                 ' to obtain V_t cosα_e

X(1) = THETA

X(2) = VCA * THETA                                 ' to obtain X2 = w

X(3) = THEDOT

X(4) = { COL(5) * MEL + CEL } * TORAD              ' to obtain η_o^c

   Y = VCA * THEDOT                                ' to obtain Y = ẇ
```

Using the current example, the data file output at the end of this step is called EQN1_1.DAT and it contains the required columns of data in the "MSR format", as shown below. EQN1_1.DAT can therefore be used as the input file for running the MSR FORTRAN program.

COLUMN:	X(1)	X(2)	X(3)	X(4)	Y
VARIABLE:	θ	w	$\dot{\theta}$	η_o	$\dot{w}$

13.2.1 Modelling of the elevator angle.

Calibrations of the control surfaces had given the equations below for obtaining the "actual" elevator control surface angle achieved η_o, in degrees, from the voltage recorded from the elevator control servo output V_{out}, in volts. Two equations were obtained as the calibration depends upon the direction of travel of the elevator. This arises because there is some backlash present in the control servo linkages.

From +ve V to -ve V: $$\eta_o = \{ -9.09 * V_{out} \} + 10.1 \qquad [13.6]$$

From -ve V to +ve V: $$\eta_o = \{ -9.00 * V_{out} \} + 11.0 \qquad [13.7]$$

The modelling of the elevator control surface was tested using the signal generation facility on the ECU. A doublet, of similar magnitude and duration to those used in the main wind tunnel experiments, was input to the elevator η to excite the Hawk model. The CED1401 was used to record the control surface input and output voltages, V_{in} and V_{out}. Examination of this data showed that initially V_{out} was at 0.808V, it then moved to 0.708V, then 0.867V and finally back to 0.808V:

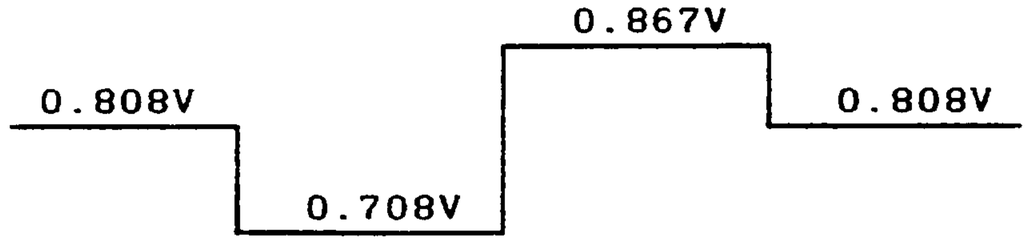

The appropriate calibration equations were then used to calculate the angle achieved by the elevator control surface. These values were found to be 2.76°, 3.66° and 3.2° respectively as depicted overleaf.

The dashed line shows what could ideally be expected without any backlash in the system.

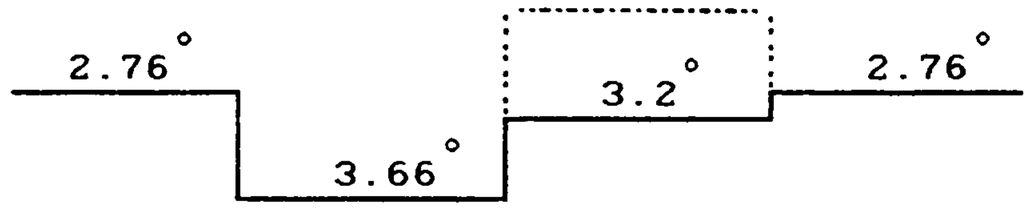

Obviously there is some error in setting the position of the elevator control surface angle. Unfortunately, with a small magnitude doublet input the control surface is not moved sufficiently to overcome backlash in the servo/rod system. Practical constraints enforce a fairly small magnitude of doublet because with a larger input the model oscillation was often violent and uncontrollable. Given the level of noise in the recorded data and the amount of backlash in the system, it was deemed reasonable to use a calibration equation for the MSR model which was based on the mean gradient and intercept of equations [13.6] and [13.7].

$$\eta_o = \{ -9.05 * V_{out} \} + 10.55 \qquad [13.8]$$

Based on the mean equation, [13.8], the elevator movement would be modelled as follows:

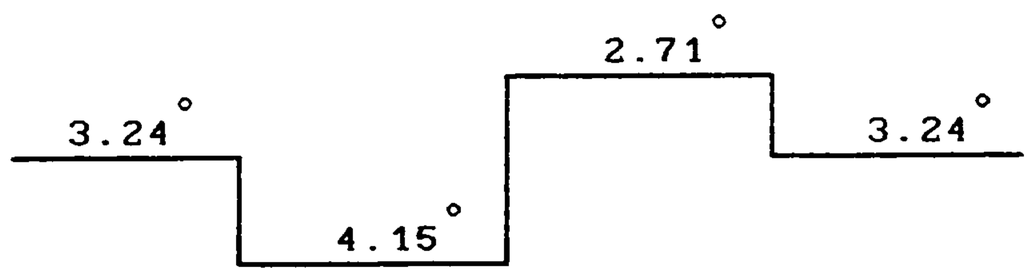

13.3 Equations of motion analysed.

When the Hawk model is flown in the wind tunnel the following two longitudinal equations of motion can be assumed to apply:

EQN 1: $$\dot{w} = \mathring{z}_w.w + (U_e + \mathring{z}_q).q + \mathring{z}_\eta.\eta + g.\sin\alpha_e.\theta \qquad [13.3]$$

EQN 2: $$\dot{q} = \mathring{m}_w.w + \mathring{m}_{\dot{w}}.\dot{w} + \mathring{m}_q.q + \mathring{m}_\eta.\eta \qquad [13.9]$$

For the remainder of this chapter, equations [13.3] and [13.9] will simply be referred to as EQN 1 and EQN 2. Various ways of describing these two equations were developed by substituting into them expressions containing parameters measured in the wind tunnel such as tunnel speed V_t - for example, $V_t.\cos\alpha_e.\theta$ was used to replace w. Where it was found that terms were being repeated in a particular equation, these terms were regrouped.

The main reason behind the manipulation of the equations of motion was to enable an analysis to be conducted into which form of mathematical model structure works best with the MSR. The advantages and disadvantages of having particular variables or derivatives as the "Y" variable or the effect of grouping some derivatives together could also be explored.

Four variations of EQN 1 and three variations of EQN 2 were derived, each with the format "Y = B0.1 + B1.X1 + ...", as shown below. Starting with EQN 1, substituting in the appropriate aerodynamic relationships gives:

EQN1_1: $$(V_t\cos\alpha_e\dot{\theta}) = (g\sin\alpha_e)(\theta) + (\mathring{z}_w)(V_t\cos\alpha_e\theta) + (V_t\cos\alpha_e + \mathring{z}_q)(\dot{\theta}) + (\mathring{z}_\eta)(\eta)$$

$$Y = B1.X1 + B2.X2 + B3.X3 + B4.X4$$

Dividing EQN1_1 through by the term ($V_t \cos\alpha_e$) gives:

EQN1_2: $(\dot{\theta}) = ([g/V_t]\tan\alpha_e)(\theta) + (\mathring{z}_w)(\theta) + (1+\mathring{z}_q/V_t\cos\alpha_e)(\dot{\theta}) + (\mathring{z}_\eta/V_t\cos\alpha_e)(\eta)$

$Y = B1.X1 + B2.X2 + B3.X3 + B4.X4$

Grouping terms together which involve θ in EQN1_2 gives:

EQN1_3: $(\dot{\theta}) = ([g/V_t]\tan\alpha_e + \mathring{z}_w)(\theta) + (1+\mathring{z}_q/V_t\cos\alpha_e)(\dot{\theta}) + (\mathring{z}_\eta/V_t\cos\alpha_e)(\eta)$

$Y = B1.X1 + B2.X2 + B3.X3$

Subtracting the term ($V_t \cos\alpha_e \dot{\theta}$) from each side of EQN1_1 gives:

EQN1_4: $(0) = (g\sin\alpha_e)(\theta) + (\mathring{z}_w)(V_t\cos\alpha_e\theta) + (V_t\cos\alpha_e + \mathring{z}_q)(\dot{\theta}) + (\mathring{z}_\eta)(\eta)$

$Y = B1.X1 + B2.X2 + B3.X3 + B4.X4$

Running the MSR program with initial variables X1, X3 and X4 only, with data produced using EQN1_4.BAS, effectively yields another variation of EQN1_4 as these initial variables could be considered to group the two terms involving θ together.

Starting with EQN 2 this time, i.e. [13.9], and substituting in the appropriate aerodynamic relationships, it can be shown that:

EQN2_1: $(\ddot{\theta}) = (\mathring{m}_w)(V_t\cos\alpha_e\theta) + (\mathring{m}_{\dot{w}})(V_t\cos\alpha_e\dot{\theta}) + (\mathring{m}_q)(\dot{\theta}) + (\mathring{m}_\eta)(\eta)$

$Y = B1.X1 + B2.X2 + B3.X3 + B4.X4$

Using the measured variable $\dot{\theta}$ alone as the X variable gives:

EQN2_2: $(\ddot{\theta}) = (\mathring{m}_w V_t\cos\alpha_e)(\theta) + (\mathring{m}_{\dot{w}} V_t\cos\alpha_e)(\dot{\theta}) + (\mathring{m}_q)(\dot{\theta}) + (\mathring{m}_\eta)(\eta)$

$Y = B1.X1 + B2.X2 + B3.X3 + B4.X4$

Grouping like terms involving $\dot{\theta}$ in EQN2_2 gives:

EQN2_3: $(\ddot{\theta})=(\mathring{m}_w V_t \cos\alpha_e)(\theta)+(\mathring{m}_{\dot{w}} V_t \cos\alpha_e+\mathring{m}_q)(\dot{\theta})+(\mathring{m}_\eta)(\eta)$

$$Y = B1.X1 + B2.X2 + B3.X3$$

Several Turbo-Basic programs were written to reflect the different mathematical forms of EQNS 1 and 2. The programs were used in *Step 5* of the experimental data preparation, which is the last step required in the production of data files for the MSR program.

13.4 Running the MSR program.

Parameter estimates are finally obtained using an easily run FORTRAN program called MSR.EXE. The first item of information needed is the name of the input data file to be used. The subscript of the X variables to be used in the initial mathematical model are required next and these are input as numbers on separate lines. Just prior to this point, the MSR program reads the data file and informs the user of the number of valid range of variables with which the program can operate by printing to screen, for example, the message: "You must not enter any number less than 0 (constant term) or greater than 4". An input of "99" is used to signal that the user has reached the end of the "initial model" variable list.

The MSR then starts to run through one or more iterations, adding or rejecting model variables as appropriate. When perfect noise free data from the ACSL simulation was used the MSR program always terminated normally. However, with experimental wind tunnel data the

program would often crash after only a few iterations, typically because of floating point errors such as divide by zero or trying to calculate the square root of a negative number. One reason for these abrupt endings of the computer program could be the noise levels present in the data. Results from an MSR run are saved in a *.RES file with the same generic name as the input file, for example, EQN2_1.RES.

The following listing shows a typical output from an MSR run.

```
 DATA FILE USED: EQN2_1.DAT

 FFP18A1; EQN2_1
 TZERO =  +11.0000  TMAX =  +12.5000  n =  1   POINTS =  151
 NO. OF X AND NO. OF DATA SETS =           4         151


 ITERATION NUMBER   0

 MODEL BEING USED THIS ITERATION IS:
 Y = B1 X1  + B2 X2  + B3 X3  + B4 X4

  YAV =   5.398203973509938E-002

 THE COEFFS OF B ARE:
 B( 1) =-.447742D+00
 B( 2) = .487567D+02
 B( 3) =-.158152D+04
 B( 4) = .307853D+02

 RSS= .170001D+03  SSQR= .115647D+01

 SBETA( 1) IS :  .609632D-01
 SBETA( 2) IS :  .505214D+02
 SBETA( 3) IS :  .164020D+04
 SBETA( 4) IS :  .445499D+01

 R SQUARED IS .274685D+00
 F IS .185569D+02

 FOR VARIABLE 1, THE Fp TO REMOVE =  .539412D+02
 FOR VARIABLE 2, THE Fp TO REMOVE =  .931358D+00
 FOR VARIABLE 3, THE Fp TO REMOVE =  .929736D+00
 FOR VARIABLE 4, THE Fp TO REMOVE =  .477523D+02

 VAR TO REJECT IS  3
 FOR VARIABLE  0, THE PARTIAL CORRELATION COEFF. (RJY) IS = .828757D+00
 VARIABLE ADDED  0

 AT THE END OF ITERATION  0 :
 THE VARIABLE TO BE REJECTED IS X3.
 AND THE VARIABLE TO BE ADDED IS X0.
```

```
ITERATION NUMBER   1

MODEL BEING USED THIS ITERATION IS:
Y = B0 + B1 X1  + B2 X2  + B4 X4

THE COEFFS OF B ARE:
B( 0) = .132564D+02
B( 1) =-.108808D+01
B( 2) =-.532977D-01
B( 4) =-.810838D+02

RSS= .543344D+02  SSQR= .369622D+00

SBETA( 1) IS :  .497882D-01
SBETA( 2) IS :  .992742D-02
SBETA( 4) IS :  .678675D+01

R SQUARED IS .768180D+00
F IS .162371D+03

FOR VARIABLE 0, THE Fp TO REMOVE =  .315840D+03
FOR VARIABLE 1, THE Fp TO REMOVE =  .477605D+03
FOR VARIABLE 2, THE Fp TO REMOVE =  .288233D+02
FOR VARIABLE 4, THE Fp TO REMOVE =  .142739D+03

NO VARIABLE TO REJECT
FOR VARIABLE  3, THE PARTIAL CORRELATION COEFF. (RJY) IS = -.152143D+00
VARIABLE ADDED  3

AT THE END OF ITERATION  1 :
THE VARIABLE TO BE REJECTED IS X**
AND THE VARIABLE TO BE ADDED IS X3.



ITERATION NUMBER   2

MODEL BEING USED THIS ITERATION IS:
Y = B0 + B1 X1  + B2 X2  + B3 X3  + B4 X4

THE COEFFS OF B ARE:
B( 0) = .132672D+02
B( 1) =-.108690D+01
B( 2) = .526345D+02
B( 3) =-.171053D+04
B( 4) =-.813273D+02

RSS= .530767D+02  SSQR= .363539D+00

SBETA( 0) IS :  .739781D+00
SBETA( 1) IS :  .493809D-01
SBETA( 2) IS :  .283268D+02
SBETA( 3) IS :  .919640D+03
SBETA( 4) IS :  .673195D+01

R SQUARED IS .775953D+00
F IS .124681D+03
```

```
FOR VARIABLE 0, THE Fp TO REMOVE =   .321627D+03
FOR VARIABLE 1, THE Fp TO REMOVE =   .484464D+03
FOR VARIABLE 2, THE Fp TO REMOVE =   .345260D+01
FOR VARIABLE 3, THE Fp TO REMOVE =   .345959D+01
FOR VARIABLE 4, THE Fp TO REMOVE =   .145946D+03

VAR TO REJECT IS  2



ITERATION NUMBER    3

MODEL BEING USED THIS ITERATION IS:
Y = B0 + B1 X1  + B2 X2  + B4 X4

THE COEFFS OF B ARE:
B( 0) = .132564D+02
B( 1) =-.108808D+01
B( 2) =-.532977D-01
B( 4) =-.810838D+02

RSS= .543344D+02  SSQR= .369622D+00

SBETA( 0) IS :   .745922D+00
SBETA( 1) IS :   .497882D-01
SBETA( 2) IS :   .992742D-02
SBETA( 4) IS :   .678675D+01

R SQUARED IS .768180D+00
F IS .162371D+03

FOR VARIABLE 0, THE Fp TO REMOVE =   .315840D+03
FOR VARIABLE 1, THE Fp TO REMOVE =   .477605D+03
FOR VARIABLE 2, THE Fp TO REMOVE =   .288233D+02
FOR VARIABLE 4, THE Fp TO REMOVE =   .142739D+03

NO VARIABLE TO REJECT

NO MORE VARIABLES TO ADD IN
NO MORE VARIABLES TO REJECT
THE FINAL MODEL IS THAT SHOWN ABOVE
```

The results of the above MSR run are more readily seen when they are summarised in the same format as Table 13.A over leaf. In this example the first variable rejected from the model was X3 as it had the lowest partial correlation coefficient (F_p). X0 was added next as it was the only "new" variable available. After four iterations the final model chosen was the one which was most highly correlated to the experimental data, as indicated by the maximum values of R^2 and F.

TABLE 13.A: RESULTS OF MSR RUN E2_1.RS1

E2_1.RS1

INITIAL MODEL VARIABLES: X1, X2, X3, X4

ITERATION 0

	PARAMETER:	STD. ERROR:	Fp TO REMOVE:	PARTIAL CORR.:
B0				0.8288
B1	= - 0.4477	± 0.06096	53.94	
B2	= 48.76	± 50.52	0.9314	
B3	= - 1582	± 1640	0.9297	
B4	= 30.79	± 4.455	47.75	

RSS=170.0; S^2=1.157; F=18.56; R^2=0.2747; Reject X3; Add X0

ITERATION 1

	PARAMETER:	STD. ERROR:	Fp TO REMOVE:	PARTIAL CORR.:
B0	= 13.26	± 0.7459	315.8	
B1	= - 1.088	± 0.04979	477.6	
B2	= - 0.05330	± 0.009927	28.82	
B3				- 0.1521
B4	= - 81.08	± 6.787	142.7	

RSS=54.33; S^2=0.3696; F=162.4; R^2=0.7682; Reject - ; Add X3

ITERATION 2

	PARAMETER:	STD. ERROR:	Fp TO REMOVE:	PARTIAL CORR.:
B0	= 13.27	± 0.7398	321.6	
B1	= - 1.087	± 0.04938	484.5	
B2	= 52.63	± 28.33	3.453	
B3	= - 1711	± 919.6	3.460	
B4	= - 81.33	± 6.732	145.9	

RSS=53.08; S^2=0.3635; F=124.7; R^2=0.7760; Reject X3; Add -

ITERATION 3 (NORMAL END)

	PARAMETER:	STD. ERROR:	Fp TO REMOVE:	PARTIAL CORR.:
B0	= 13.26	± 0.7459	315.8	
B1	= - 1.088	± 0.04979	477.6	
B2	= - 0.05330	± 0.009927	28.82	
B3				
B4	= - 81.08	± 6.787	142.7	

RSS=54.33; S^2=0.3696; F=162.4; R^2=0.7682; Reject - ; Add -

13.5 Tables of results.

The MSR program was run many times for each equation starting with various sets of initial variables. A subset of these runs are summarized in Table 13.B below. In this table, for example, "1234" in the "start model" column denotes a model starting with variables X1, X2, X3, X4. Also shown are the number of iterations, ITNS, of the program (each corresponding to an intermediate model/final model and the variables in final model (e.g. "3" denoting "Y = B3.X3").

TABLE 13.B: SUMMARY OF MSR RUNS

EQN	RUN	START MODEL	NO OF ITNS	FINAL MODEL	COMMENTS
1_1	RS1	1234	0-4	3	crashed due to ÷0 error in calc. of F
	RS2	01234	0-5	3	1st ITN rejects X0 then same pattern as RS1
	RS3	123	0-3	3	crashed due to ÷0 error in calc. of F
	RS4	0 3	0-2	3	crashed due to ÷0 error in calc. of F
	RS5	12 4	0	-	normal ending; all B(j)=0; F & R^2 negative!!
	RS6	3	0	-	crashed due to ÷0 error in calc. of F
1_2	RS1	1234	0	-	floating point error; X1=X3=θ
	RS2	01234	0	-	floating point error; X1=X3=θ
	RS3	01 4	0-1	-	crashed due to taking sq.root of -ve number
	RS4	1 34	0	-	floating point error
1_3	RS1	123	0	-	crashed due to ÷0 error in calc. of F
	RS2	01 3	0-1	0123	crashed due to ÷0 error in calc. of F
1_4	RS1	1234	0	-	crash due to ÷0; Y=0; all errors s^2= 0
	RS2	1 34	0	-	crash due to ÷0; Y=0; all errors s^2 = 0
2_1	RS1	1234	0-3	012 4	normal ending
	RS2	01234	0-3	01 34	normal ending
	RS3	23	0	-	all B(j) = 0
	RS4	1 34	0-3	01 34	normal ending
	RS5	12 4	0-3	012 4	normal ending
2_2	RS1	1234	0	-	crashed in MINV, i.e. when inverting matrix
	RS2	01234	0	-	crashed in MINV, i.e. when inverting matrix
	RS3	12 4	0-2	01234	crashed in MINV, i.e. when inverting matrix
	RS4	1 34	0-2	01234	crashed when X2 and X3 in model as both = q
	RS5	1 4	0-3	01234	crashed when X2 and X3 in model as both = q
2_3	RS1	123	0-1	0123	normal ending
	RS2	0123	0-2	0123	normal ending
	RS3	12	0-3	0123	normal ending
	RS4	1	0	-	crashed due to ÷0 error in calc. of F

13.6 Analysis of the MSR parameter estimates.

The following analysis of parameter estimates from the MSR procedure is based on the runs presented in Appendix G and summarized in table 13.B. The runs used wind tunnel data conditioned for use in the model structures presented in section 13.4, i.e. EQNS "1_1, 1_2, 1_3, 1_4, 2_1, 2_2, 2_3". The results obtained are discussed below and the observations closely matched those obtained from analysis of the MSR procedure using the Hald data (see section 10.3).

13.6.1 EQN1_1

$$(V_t \cos\alpha_e \dot{\theta}) = (g \sin\alpha_e)(\theta) + (\mathring{Z}_w)(V_t \cos\alpha_e \theta) + (V_t \cos\alpha_e + \mathring{Z}_q)(\dot{\theta}) + (\mathring{Z}_\eta)(\eta)$$

MSR RUN EQN1_1.RS1:

No matter what the initial model, the majority of runs with EQN1_1 end up with Y = B3. X3 as the model in the final iteration of the MSR program. Unfortunately, with only one variable included in the model the MSR would always crash with a "divide by zero error" in the calculation of F.

With a final iteration model containing only Y = B3.X3, the MSR estimated that parameter B3 is equal to 32.47 with a very small standard error of ±0.5783E-3. In intermediate iterations B3 was also estimated as 32.47, although the standard error was slightly higher due to other "insignificant" terms were being included in the model. The high correlation of B3 with experimental data can be seen by the value of the partial F coefficient (F_p = 0.17E10) which was consistently several orders of magnitude of 10 larger than any other parameters' Fp.

It is not surprising that B3 is the most significant term found by the MSR method as B3 = ($V_t.\cos\alpha_e + \mathring{z}_q$), X3 = ($\dot{\theta}$) and Y = ($V_t.\cos\alpha_e.\dot{\theta}$). In the P18A1 wind tunnel run V_t = 32.47m/sec and α_e = 0.47°, giving ($V_t.\cos\alpha_e$) = 32.47. As $\mathring{z}_q$ has a relatively small value, $V_t\cos\alpha_e$ will be the dominate term in "B3" and hence be more highly correlated with Y. The MSR therefore correctly identifies the value of B3 = 32.47, albeit at the expense of other parameters which should have been included in the final model. It may be a feature of the MSR procedure that if parameters do not have similar levels of significance the most highly correlated dominant term(s) will always be chosen at the expense of others.

In EQN 1_1 the coefficient of X1 (i.e. θ) is B1 = $g\sin\alpha_e$ = 0.0808, however, none of the iterations of the MSR produced a parameter estimate close to this. The nearest approximation was -2.2360 in iteration 1 of EQN 1_1.RS1.

MSR RUN EQN1_1.RS5:

To try to identify other parameters in EQN1_1 beside B3, an initial model which excluded the variable X3 was tested. With only X1, X2 and X4 present, the first iteration of the MSR run gave parameter estimates for B1, B2 and B3 which were all non-zero. However, the MSR concluded that these three parameters were all zero as they had high standard errors and were all insignificant terms with Fp < Fp min (the level set to reject terms from the model).

The statistical equations employed in the FORTRAN program algorithms do not appear to be very robust as negative values of F and

R^2 were calculated. It is thought that the negative values were caused by noisy experimental data and it is possible that alternative formulae for calculating F and R^2 could constrain these terms to positive values.

13.6.2 EQN1_2

$$(\dot{\theta})=([g/V_t]\tan\alpha_e)(\theta)+(\mathring{z}_w)(\theta)+(1+\mathring{z}_q/V_t\cos\alpha_e)(\dot{\theta})+(\mathring{z}_\eta/V_t\cos\alpha_e)(\eta)$$

MSR RUN EQN1_2.RS1:

The MSR program crashed in the first iteration when calculating the inverse of the matrix $[X^TX]$ where the first row of X is $(\theta\ \theta\ \dot{\theta}\ \eta)$. The "pivot" method employed in calculating the inverse matrix is susceptible to divide by zero errors which caused the program to crash. This error occurred whenever two identical state variables were included in the iteration model being processed, as can be seen in this particular example where X1 = X2 = θ.

MSR RUN EQN1_2.RS3:

A MSR run with only X1 in the initial model was performed next. After one iteration very small parameter estimates were obtained of the order of E-15. The MSR program crashed when calculating the standard error in the first parameter estimate due to trying to calculate the square root of a negative number. The MSR FORTRAN program was altered to set the errors to zero at this point and recompiled. Unfortunately this did not improve the situation because the program crashed a few steps later with a divide by zero error in the calculation of F.

13.6.3 EQN1_3

$$(\dot{\theta})=([g/V_t]\tan\alpha_e+\mathring{z}_w)(\theta)+(1+\mathring{z}_q/V_t\cos\alpha_e)(\dot{\theta})+(\mathring{z}_\eta/V_t\cos\alpha_e)(\eta)$$

MSR RUN EQN1_3.RS1:

To avoid having two identical state variables in the same regression model, terms B1.X1 and B2.X2 of EQN1_2 were combined into the single term B1.X1 of EQN1_3. The first run performed with EQN1_3 used all of the available variables, i.e. X1, X2 and X3, in the initial iteration model. Small parameter estimates for B1 and B3 were obtained and B2 was estimated as 1.0. In EQN1_3 X2 and Y are actually the same measured variable $\dot{\theta}$ and a high degree of correlation between B2 and Y is only to be expected. The MSR appears to ignore the relatively small part of B2 (i.e. $\mathring{Z}_q/V_t COS\alpha_e$) by assigning it to the overall equation error and thus produces a "correct" value of the B2 parameter estimate. The overall equation error and individual parameter errors are not available for this run as the program unfortunately crashed during their calculation, possibly because B1 and B3 were both so small (at approximetely 1E-15). Altering the FORTRAN to set the parameter errors to zero simply caused a divide by zero program crash to occur a few steps later during the calculation of F.

MSR RUN EQN1_3.RS2:

Because of the high correlation between Y and B2.X2, a run was performed without X2 in the initial model to try to obtain parameter estimates for B1 and B3. At the end of the first iteration no variables were rejected and X2 was chosen to enter. In the second iteration the program crashed, as observed in run EQN1_3:RS1.

13.6.4 EQN1_4

$$(0)=(g\sin\alpha_e)(\theta)+(\mathring{z}_w)(V_t\cos\alpha_e\theta)+(V_t\cos\alpha_e+\mathring{z}_q)(\dot{\theta})+(\mathring{z}_\eta)(\eta)$$

MSR RUN EQN1_4.RS1:

EQN1_4 had been manipulated to obtain the output Y, on the left hand side, as equal to zero and thus all of the data points were set to zero in the appropriate column of the MSR input file. A number of runs were performed with different combinations of initial variables. In every regression model processed by the MSR procedure, parameter estimates of 0.0 were obtained, quickly followed by the program crashing as it tried to calculate the individual parameter errors. The matrix Y is used extensively throughout the equations and algorithims of the MSR procedure. Therefore parameter estimates of 0.0 are not too surprising because Y is effectively a "null" vector in this particular format of the longitudinal equation of motion under consideration.

13.6.5 EQN2_1

$$(\ddot{\theta})=(\mathring{m}_w)(V_t\cos\alpha_e\theta)+(\mathring{m}_{\dot{w}})(V_t\cos\alpha_e\dot{\theta})+(\mathring{m}_q)(\dot{\theta})+(\mathring{m}_\eta)(\eta)$$

MSR RUN EQN2_1.RS1:

MSR runs using EQN2_1 were always found to terminate normally. This implies that the MSR may not be as sensitive to bad or noisy data, as had been suggested earlier. The major difference between the mathematical models derived from EQN1 and EQN2 is that an extra state variable appears in EQN2, in the form of $\ddot{\theta}$, which provides an extra degree of statistical freedom available for use in the MSR procedure.

It was noted that in MSR runs using EQN2_1, two different final models were being obtained depending on what starting model was used. With an initial model containing variables X1,X2,X3,X4, the final model obtained included X0,X1,X3 and X4 (see EQN2_1.RS1). However, if X0 was added to the list of initial variables the final model included the variable X2 instead of X3 (see EQN2_1.RS2).

Upon examination of EQN2_1, it can be seen that the state variable X2 represents $V_t \cos\alpha_e . \dot{\theta}$ and X3 represents $\dot{\theta}$; the corresponding physical coefficients B2 and B3, are $\mathring{m}_w$ and $\mathring{m}_q$ respectively. The parameter coefficients are therefore very different although the corresponding state variables X2 and X3 are both related or equal to $\dot{\theta}$. In the initial and intermediate iterations of EQN2_1.RS1, B2 and B3 were found to have very similar values of Fp and hence a similar levels of significance and correlation to Y, making it impossible to choose between them.

MSR RUN EQN2_1.RS2:

To establish whether X2 or X3 was more highly correlated with Y, a run was performed with only X2 and X3 in the initial model. This resulted in a normal run in which the error in each parameter estimate is almost exactly the same value as the parameter estimate itself. Furthermore, B2 and B3 had similar values of the partial correlation coefficient, these being 0.9923 and 0.9920 respectively. The correlation coefficient R^2 also had a very low value of 0.0084. These factors led to the MSR accepting the hypothesis that both X1 and X2 were insignificant variables with the parameter estimates for B2 and B3 both equal to zero.

13.6.6 EQN2_2

$$(\ddot{\theta})=(\mathring{m}_w V_t \cos\alpha_e)(\theta)+(\mathring{m}_{\dot{w}} V_t \cos\alpha_e)(\dot{\theta})+(\mathring{m}_q)(\dot{\theta})+(\mathring{m}_\eta)(\eta)$$

MSR RUN EQN2_2.RS1:

Using the EQN2_2 form of the equation of motion, variables X2 and X3 are both represented by $\dot{\theta}$. It was observed that if both X1 and X2 were included in the initial model the MSR program crashed when trying to invert the matrix $[X^T X]$.

MSR RUN EQN2_2.RS3:

To prove that the MSR does not work properly with two identical state variables included in the same regression model, a run was performed so that X3 was excluded from the variables in the initial regression model. The MSR cycled through two iterations before crashing in the third iteration due to both X2 and X3 appearing in the regression model being processed. Analysis of the initial and intermediate iterations, which were recorded in the MSR results file enabled both the expected decrease in the overall equation error (S^2) and the increase in the correlation coefficient (R^2) to be observed as the MSR progressed.

13.6.7 EQN2_3

$$(\ddot{\theta})=(\mathring{m}_w V_t \cos\alpha_e)(\theta)+(\mathring{m}_{\dot{w}} V_t \cos\alpha_e+\mathring{m}_q)(\dot{\theta})+(\mathring{m}_\eta)(\eta)$$

MSR RUN EQN2_3.RS1:

All runs performed with this form of the pitching moment equation

ended normally. Furthermore, all of the runs predicted the same final model which corresponded exactly to equation being modelled, i.e. the same state variables appeared in the final MSR model. The constant term B0 was selected for the final regression model. Examination of consecutive iterations found the expected increases in F and R^2 and the corresponding decrease in S^2.

CHAPTER 14

ALTERNATIVE REPRESENTATION OF AIRCRAFT EQUATIONS OF MOTION

14.0 ALTERNATIVE REPRESENTATION OF AIRCRAFT EQUATIONS OF MOTION.

In the mathematical representation of the Hawk model in the wind tunnel there are two important aspects to consider, namely variable re-construction and the representation, and subsequent manipulation or reduction, of the small perturbation equations of motion.

In variable re-construction there is more than one way to model the physical situation in the wind tunnel. It is possible to consider different axes systems and to resolve the aircraft responses as appropriate to obtain expressions for the state variables in terms of parameters which can be experimentally measured using the dynamic facility. For example, the aircraft's small perturbation motion may be modelled in terms of components of both the model's inertial response (e.g. heave motion up and down the vertical suspension rod) as well as changes in the pitch, roll and yaw attitude angles.

The concept of an inertial-angular representation was initially examined as presented in Chapter 13 and Appendix B of this thesis. In that work the "X" and "Z" equations of motion were removed for the case where the model is fully restrained and cannot undergo either longitudinal or vertical translations. The inertial u and w perturbation terms are therefore both equal to zero.

However, the concept of separating out the inertial response of the model can also be extended to the case where the model is only partially restrained and is free to move in heave up and down the vertical rod with a velocity $\dot{h}$. Firstly, as in the fully restrained case, it is possible to resolve the velocity of the wind tunnel air

into components along the 0_x and 0_z body axes thus giving expressions for the fluid velocity relative to the model. Secondly, constraint equations can be derived which express the inertial components of the u and w small perturbations in terms of the vertical heave velocity $\dot{h}$. It was realised that in the initial treatment of the models inertial components the potential to utilise $\dot{h}$ was not fully exploited. It was thus decided to re-examine the wind tunnel mathematical modelling.

This review has also been aided by the work published by Thomasson (Ref 36) in which a new formulation of the equations of motion of a rigid body in an unsteady non uniform heavy fluid is given. The work had been prompted by difficulties in applying a Langrangian formulation of the equations of motion of a body immersed in an unsteady heavy fluid. Although in principle the Langrangian equations should be equally as applicable to underwater vehicles as aircraft, it was found that the equations did not reduce to the small perturbation equations that are normally used for aircraft in gusts.

In his paper Thomasson identifies the source of the problems encountered and develops a new general set of motion equations in several stages using a semi-empirical approach. First the equations of motion of a rigid body in a moving perfect fluid are derived for the case in which the undisturbed moving velocities do not change significantly over distances comparable to the dimensions of the vehicle. Then the viscous forces and moments are added and combined with the perfect fluid terms that are a function of the relative velocity (between the body and fluid) alone. Finally gust penetration effects are introduced to represent the variation of the undisturbed moving fluid velocities over the vehicle.

This approach results in a new formulation of the equations of motion in which the inertias, the added masses and relative (i.e. fluid to body) velocity effects are clearly separated out. Additionally, the new formulation provides common derivation of the equations of motion for underwater vehicles, airships, parafoils and aircraft. It is also found that for small perturbations the equations revert to those that are normally used for both buoyant and lifting vehicles.

14.1 General equations for a rigid body in a fluid.

The general equations of motion of a rigid body in an unsteady non uniform heavy fluid given in Ref 36 may be written as:

$$M\dot{x}_i = -(P + W).(M_i - \bar{M}_i).x_i + (M_r - \bar{M}_i).\dot{x}_f + A.x_r + F \qquad [14.1]$$

where

M = the 6x6 mass matrix including added masses and inertias;

M_i = inertia mass matrix;

M_r = relative mass matrix between the fluid and vehicle;

$\bar{M}_i$ = buoyancy mass matrix representing fluid displaced by the vehicle;

$x_i = [u_i \; v_i \; w_i \; p_i \; q_i \; r_i]^T$ the inertial body axis "velocities";

$\dot{x} = [\dot{u}_i \; \dot{v}_i \; \dot{w}_i \; \dot{p}_i \; \dot{q}_i \; \dot{r}_i]^T$ the inertial body axis "accelerations";

$x_f = [u_f \; v_f \; w_f \; p_f \; q_f \; r_f]^T$ the fluid velocities along the body axes;

$\dot{x}_f = [\dot{u}_f \; \dot{v}_f \; \dot{w}_f \; \dot{p}_f \; \dot{q}_f \; \dot{r}_f]^T$ the fluid acceleration terms;

$x_r = x_i - x_f = = [u_i - u_f \; v_i - v_f \; w_i - w_f \; p_i - p_f \; q_i - q_f \; r_i - r_f]^T$

= relative velocities between the vehicle and fluid;

P and W are the angular and linear velocity matrices given by:

$$P = \begin{bmatrix} 0 & -r & q & 0 & 0 & 0 \\ r & 0 & -p & 0 & 0 & 0 \\ -q & p & 0 & 0 & 0 & 0 \\ 0 & 0 & 0 & 0 & -r & q \\ 0 & 0 & 0 & r & 0 & -p \\ 0 & 0 & 0 & -q & p & 0 \end{bmatrix}; \qquad W = \begin{bmatrix} 0 & 0 & 0 & 0 & 0 & 0 \\ 0 & 0 & 0 & 0 & 0 & 0 \\ 0 & 0 & 0 & 0 & 0 & 0 \\ 0 & -w & v & 0 & 0 & 0 \\ w & 0 & -u & 0 & 0 & 0 \\ -v & u & 0 & 0 & 0 & 0 \end{bmatrix};$$

A = the matrix representing terms due to the fluid dynamic forces and moments due to relative velocity;

F = the vector of other external forces and moments.

It is considered acceptable to apply the rigid body equations given in Eqn [14.1] to a vehicle such as a partially restrained wind tunnel model. The main justification for doing so is that it would be expected that the forces and moments due to the model's inertia would depend on its inertial acceleration whilst the forces and moments due to the fluid acceleration, the added mass and inertia terms would depend upon the relative acceleration between the fluid and the model.

14.2 Small Perturbation Equations.

When small perturbations about a steady flight condition are considered the general rigid body equations of motion given in Eqn [14.1] reduce to the normal small perturbation aircraft equations for flight in gusts (Ref 36). In this process it is assumed that the displaced fluid mass terms ($\bar{m}$) and added mass terms are negligible for conventional aircraft and can be ignored. Thus making the usual assumptions about the stability derivatives, the small perturbation equations of motion can be derived (Ref 36). The longitudinal and lateral equations can separated out and are given below:

Longitudinal Equations:

$$\left\{\begin{bmatrix} 0 & 0 & 0 \\ 0 & \mathring{Z}_{\dot{w}} & 0 \\ 0 & \mathring{M}_{\dot{w}} & 0 \end{bmatrix} + \begin{bmatrix} m & 0 & a_z m \\ 0 & m & -a_x m \\ a_z m & -a_x m & I_{yy} \end{bmatrix}\right\}\begin{bmatrix} \dot{u}_i \\ \dot{w}_i \\ \dot{q}_i \end{bmatrix} = \begin{bmatrix} X \\ Z \\ M \end{bmatrix} + \begin{bmatrix} 0 & 0 & 0 \\ 0 & \mathring{Z}_{\dot{w}} & 0 \\ 0 & \mathring{M}_{\dot{w}} & 0 \end{bmatrix}\begin{bmatrix} \dot{u}_f \\ \dot{w}_f \\ \dot{q}_f \end{bmatrix}$$

$$+ \begin{bmatrix} mU_o \end{bmatrix} q + \begin{bmatrix} \mathring{X}_u & \mathring{X}_w & \mathring{X}_q \\ \mathring{Z}_u & \mathring{Z}_w & \mathring{Z}_q \\ \mathring{M}_u & \mathring{M}_w & \mathring{M}_q \end{bmatrix}\begin{bmatrix} u_i - u_f \\ w_i - w_f \\ q_i - q_f \end{bmatrix} - \begin{bmatrix} mg \\ 0 \\ a_z m \end{bmatrix}\theta \qquad [14.2]$$

Lateral Equations:

$$\begin{bmatrix} m & -a_z m & a_x m \\ -a_z m & I_{xx} & -I_{zx} \\ a_x m & -I_{zx} & I_{zz} \end{bmatrix}\begin{bmatrix} \dot{v}_i \\ \dot{p}_i \\ \dot{r}_i \end{bmatrix} = \begin{bmatrix} Y \\ L \\ N \end{bmatrix} - \begin{bmatrix} mU_o \\ -ma_z U_o \\ 0 \end{bmatrix} r$$

$$+ \begin{bmatrix} \mathring{Y}_v & \mathring{Y}_p & \mathring{Y}_r \\ \mathring{L}_v & \mathring{L}_p & \mathring{L}_r \\ \mathring{N}_v & \mathring{N}_p & \mathring{N}_r \end{bmatrix}\begin{bmatrix} v_i - v_f \\ p_i - p_f \\ r_i - r_f \end{bmatrix} + \begin{bmatrix} mg \\ -a_z m \\ a_x m \end{bmatrix}\phi \qquad [14.3]$$

where

a_x, a_y and a_z offset (in m) between the aircraft body's centre of gravity and origin of the body axes.

m = vehicle mass

U_o = inertial reference velocity of the aircraft (along stability axes) when flying straight and level.

14.3 Variable reconstruction.

In considering the physical configuration of the model aircraft on the rig in the wind tunnel the following sets of axes systems may be

defined, (see Figs 5 and 67):

Earth or Local Fixed axes: (Ox_l, Oy_l, Oz_l); The origin may be at any arbitrary point along the vertical axis of the rod. Ox_l is parallel to the ground and aligned with the horizontal wind tunnel velocity vector; Oy_l is also parallel to the ground but at 90° to wind tunnel velocity vector; Oz_l points vertically downward along the gravity vector and is co-incident with the vertical suspension rod of the dynamic rig.

Body Axes: (Ox_b, Oy_b, Oz_b); The origin may be considered as being at the centre of the model gimbal at a point on the vertical rod. In the steady state, with the model flying straight and wings level in the tunnel, the Ox_b body axis is along the main fuselage of the model at a flight path angle of α_e to the horizontal Ox_l earth axis; Oy_b is along the wing at at 90° to Ox_b; Oz_b points "downwards" to complete the set.

The horizontal wind tunnel velocity vector V_t is always constant and is not affected by changes in the flight path angle of the aircraft. V_t may be considered as a free stream velocity of the fluid relative to the model which itself does not actually move along Ox_l or Ox_b in the tunnel. For convenience, V_t is defined to act in the same direction as the "imaginary" flight path of the aircraft.

In the steady state, with the model at α_e, the velocities of the model U_e and W_e along the Ox_b and Oz_b body axes respectively are given by:

$$U_e = u_{fo} + u_{io} \qquad [14.4]$$

and

$$W_e = w_{fo} + w_{io} \qquad [14.5]$$

u_{fo} and w_{fo} are defined as the components of the fluid velocity when the tunnel velocity V_t is resolved along the Ox_b and Oz_b body axes;

u_{io} (or U_o) and w_{io} are the inertial components which would arise if the model was free to fly or move along a flight path in the tunnel.

When suspended on the dynamic rig the model is unable to move along Ox_b. Furthermore, in the steady state, it is initially at rest giving $u_{io} = w_{io} = 0$. Thus, as shown in Fig 67, the steady state fluid velocities may be defined as:

$$U_e = u_{fo} = V_t.\cos(\alpha_e) \qquad [14.6]$$

and

$$W_e = w_{fo} = V_t.\sin(\alpha_e) \qquad [14.7]$$

If the model undergoes a small perturbation in pitch only where ϕ and ψ are zero and the pitch attitude of the aircraft increases by $\delta\theta$ say, then the perturbed velocities of the model U and W, along Ox_b and Oz_b, are given by:

$$U = U_e + u_f + u_i \qquad [14.8]$$

and

$$W = W_e + w_f + w_i \qquad [14.9]$$

To obtain expressions for the small perturbation fluid velocities alone the inertial velocity terms in [14.7] and [14.8] may be set to zero. Then, as shown in Fig 68, the fluid velocities are given by:

$$u_f = -V_t.\sin(\alpha_e).\delta\theta \qquad [14.10]$$

and

$$w_f = V_t.\cos(\alpha_e).\delta\theta \qquad [14.11]$$

To complete the set of reconstructed variables to be inserted into the rigid body equations of motion, the final expressions to be defined are for the small perturbation inertial velocities and accelerations. However, there are two separate inertial cases which must be examined for the motion of the model on the dynamic rig. The first being where the model is free to move in heave up and down the rod (along Oz_l) with a vertical velocity of $\dot{h}$. In the second case the model has no freedom in heave because it is fully restrained by collars immediately above and below the gimbal. Both of these situations are examined below and the corresponding equations of motion are derived.

14.4 Hawk model with freedom in heave.

Consider the situation where the model is initially at rest in a steady state and a small perturbing force then causes the aircraft to move vertically up (or down) the rod with a velocity $\dot{h}$. This velocity is along the local/earth axis Oz_l and, as shown in Fig 69, the following vertical constraint equation is obtained for the inertial motion:

$$\dot{h} = -u_i.\sin(\alpha_e) + w_i.\cos(\alpha_e) \qquad [14.12]$$

In addition, on the rig the model is not free to move along the local Ox_l axis and thus the horizontal components of inertial motion must balance each other. Therefore, as shown in Fig 69, the horizontal constraint equation is given by:

$$0 = u_i.\cos(\alpha_e) + w_i.\sin(\alpha_e) \qquad [14.13]$$

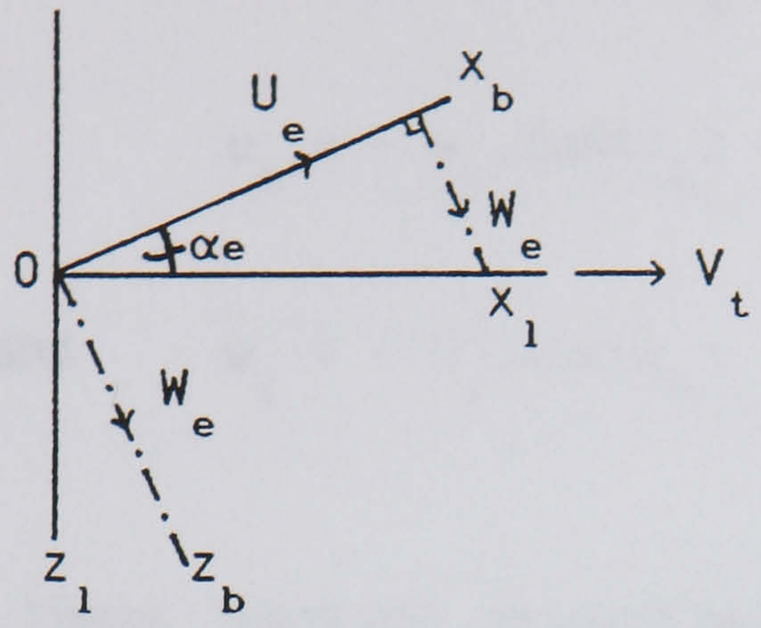

$$U_e = u_{fo} + u_{io} = u_{fo}$$

$$\Rightarrow u_{fo} = V_t.\cos(\alpha_e)$$

$$W_e = w_{fo} + w_{io} = w_{fo}$$

$$\Rightarrow w_{fo} = V_t.\sin(\alpha_e)$$

FIGURE 67: WIND TUNNEL STEADY STATE CONDITIONS.

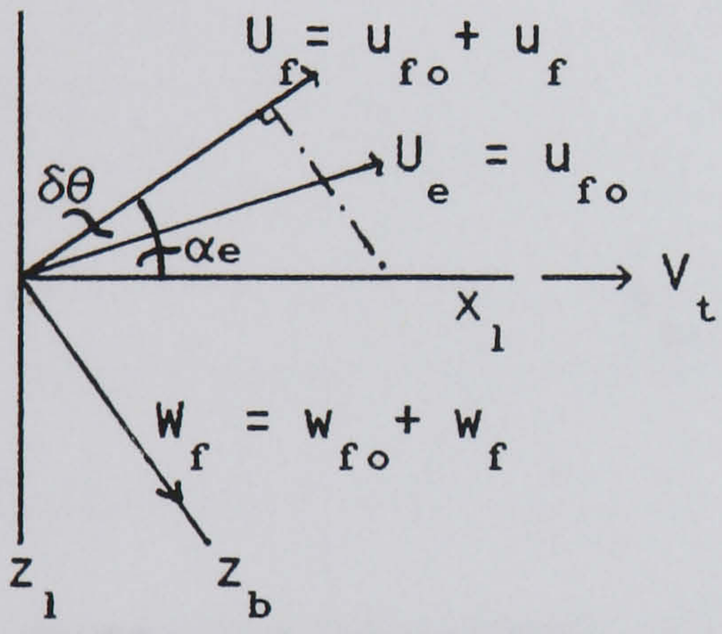

$$V_t\cos(\alpha_e+\delta\theta) = u_{fo} + u_f$$

$$V_t\{\cos(\alpha_e)-\sin(\alpha_e)\delta\theta\} = V_t\cos(\alpha_e)+u_f$$

$$\Rightarrow u_f = -V_t\sin(\alpha_e)\delta\theta$$

$$V_t\sin(\alpha_e+\delta\theta) = w_{fo} + w_f$$

$$V_t\{\sin(\alpha_e)+\cos(\alpha_e)\delta\theta\} = V_t\sin(\alpha_e)+w_f$$

$$\Rightarrow w_f = V_t\cos(\alpha_e)\delta\theta$$

FIGURE 68: SMALL PERTURBATION FLUID VELOCITIES.

Assume $\delta\theta\approx 0$ to obtain expressions for inertial constraint equations.

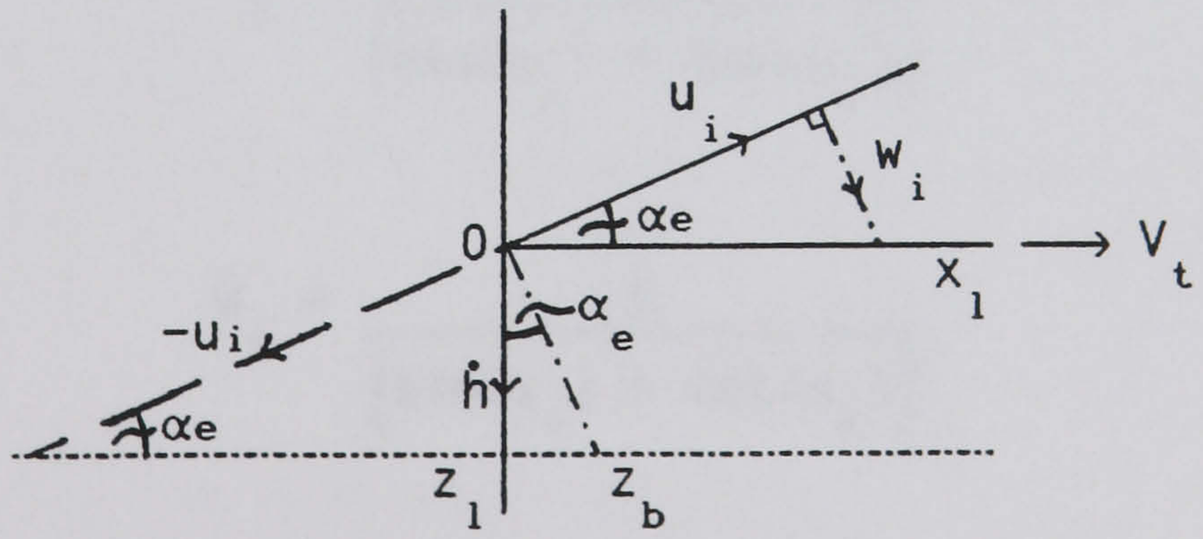

Resultant vertical velocity

$$\dot{h} = ver\{u_i\} + ver\{w_i\}$$

$$\dot{h} = -u_i\sin(\alpha_e) + w_i\cos(\alpha_e)$$

Resultant horizontal velocity

$$0 = hor\{u_i\} + hor\{w_i\}$$

$$0 = u_i\cos(\alpha_e) + w_i\sin(\alpha_e)$$

FIGURE 69: SMALL PERTURBATION INERTIAL VELOCITIES.

Eqn [14.13] may be rearranged to provide expressions for the inertial perturbation velocities along $0x_b$ and $0z_b$:

$$u_i = - w_i.\tan(\alpha_e) \qquad [14.14]$$

and

$$w_i = - u_i.\cot(\alpha_e) \qquad [14.15]$$

Substituting these inertial velocities in turn into the vertical constraint Eqn [14.12], and rearranging as appropriate, yields the following alternative relationships:

$$u_i = \frac{-\dot{h}}{\left(\cos(\alpha_e) + \tan(\alpha_e)\right)} \qquad [14.16]$$

$$w_i = \frac{\dot{h}}{\left(\sin(\alpha_e) + \cot(\alpha_e)\right)} \qquad [14.17]$$

Differentiating the inertial velocity equations w.r.t. time yields expressions for the inertial accelerations of the model, where $\ddot{h}$ can be numerically derived from $\dot{h}$:

$$\dot{u}_i = \frac{-\ddot{h}}{\left(\cos(\alpha_e) + \tan(\alpha_e)\right)} \qquad [14.18]$$

$$\dot{w}_i = \frac{\ddot{h}}{\left(\sin(\alpha_e) + \cot(\alpha_e)\right)} \qquad [14.19]$$

Finally, as there is no freedom for lateral translation of the model on the dynamic rig, the lateral constraint equation is simply:

$$v_i = 0. \qquad [14.20]$$

ASIDE:

It is also possible to formally derive the constraint Equations [14.12], [14.13] and [14.20] starting from the full Direction Cosine Matrix (DCM_{la}) for the transformation of the aircraft velocities in body axes (U,V,W) to the aircraft velocities in earth axes (U_l,V_l,W_l). Firstly, noting that in the wind tunnel the reference inertial velocities $U_o = V_o = W_o = 0$ and that the model velocities in earth local axes are given by $U_l = 0$, $V_l = 0$ and $W_l = \dot{h}$ leads to:

$$\begin{bmatrix} U_l \\ V_l \\ W_l \end{bmatrix} = \begin{bmatrix} 0 \\ 0 \\ \dot{h} \end{bmatrix} = DCM_{la} \left\{ \begin{bmatrix} U_o \\ V_o \\ W_o \end{bmatrix} + \begin{bmatrix} u_i \\ v_i \\ w_i \end{bmatrix} \right\} = DCM_{la} \begin{bmatrix} u_i \\ v_i \\ w_i \end{bmatrix}$$

Next, ϕ and ψ are set to zero in the DCM. A small change in pitch attitude from α_e to $\theta = (\alpha_e + \delta\theta)$ is inserted into the Direction Cosine Matrix. Then assuming that $\cos\delta\theta \approx 1$ and $\sin\delta\theta \approx 0$, the DCM_{la} reduces to the following constraint transformation equations which are identical to those derived earlier:

$$\begin{bmatrix} U_l \\ V_l \\ W_l \end{bmatrix} = \begin{bmatrix} 0 \\ 0 \\ \dot{h} \end{bmatrix} = \begin{bmatrix} \cos\alpha_e & 0 & \sin\alpha_e \\ 0 & 1 & 0 \\ -\sin\alpha_e & 0 & \cos\alpha_e \end{bmatrix} \begin{bmatrix} u_i \\ v_i \\ w_i \end{bmatrix} \qquad [14.21]$$

14.4.1 Equations of motion with heave freedom.

This section summarizes the variable re-construction expressions and defines and discusses the final terms required for insertion into the longitudinal small perturbation equations given in Eqn [14.2].

$$\left\{\begin{bmatrix} 0 & 0 & 0 \\ 0 & \mathring{Z}_{\dot{w}} & 0 \\ 0 & \mathring{M}_{\dot{w}} & 0 \end{bmatrix} + \begin{bmatrix} m & 0 & a_z m \\ 0 & m & -a_x m \\ a_z m & -a_x m & I_{yy} \end{bmatrix}\right\}\begin{bmatrix} \dot{u}_i \\ \dot{w}_i \\ \dot{q}_i \end{bmatrix} = \begin{bmatrix} X \\ Z \\ M \end{bmatrix} + \begin{bmatrix} 0 & 0 & 0 \\ 0 & \mathring{Z}_{\dot{w}} & 0 \\ 0 & \mathring{M}_{\dot{w}} & 0 \end{bmatrix}\begin{bmatrix} \dot{u}_f \\ \dot{w}_f \\ \dot{q}_f \end{bmatrix}$$

$$+ \begin{bmatrix} mU_o \end{bmatrix} q + \begin{bmatrix} \mathring{X}_u & \mathring{X}_w & \mathring{X}_q \\ \mathring{Z}_u & \mathring{Z}_w & \mathring{Z}_q \\ \mathring{M}_u & \mathring{M}_w & \mathring{M}_q \end{bmatrix}\begin{bmatrix} u_i - u_f \\ w_i - w_f \\ q_i - q_f \end{bmatrix} - \begin{bmatrix} mg \\ 0 \\ a_z m \end{bmatrix}\theta \qquad [14.2]$$

In all of the practical experiments the Hawk was always set up in a horizontal wind-off condition on the rig to ensure that the centre of gravity of the model was co-incident with the centre of the gimbal. Thus, in the above equations the c.g. offset terms may both be set to zero; ($a_x = a_z = 0$).

The pitch potentiometer of the model measures pitch attitude where $\theta_m = \alpha_e + \theta$. Thus θ can be easily obtained and the numerical differentiation techniques, described earlier in this thesis, employed to calculate q (i.e. $\dot{\theta}$) and $\dot{q}$ (i.e. $\ddot{\theta}$).

The remaining inertial acceleration terms are defined by Eqns [14.18] and [14.19].

The external forces and moments vector given by $F = [X\ Z\ M]^T$ will mainly contain the forces due to the movement of control surfaces from trimmed positions and, if autostabilisation loops are employed, this will obviously incorporate any parameters fed back to the control inputs. F could include frictional components arising from stiction on the vertical rod, X_{fr} and Z_{fr} say, as well as angular friction terms arising in the mechical components of the gimbal potentiometers (e.g. F_y in the pitching moment equation).

Considering each type of external force in turn the following expressions can be defined for F.

For control surface inputs without feedback loops:

$$F_1 = \begin{bmatrix} \mathring{X}_\eta \\ \mathring{Z}_\eta \\ \mathring{M}_\eta \end{bmatrix} \cdot [\eta] \qquad [14.22]$$

For control surface inputs employing, for example, roll attitude and roll rate feedback loops with feedback gains k_1 and k_2 and pilot stick control inputs η_{ctl}:

$$F_2 = \begin{bmatrix} \mathring{X}_\eta \\ \mathring{Z}_\eta \\ \mathring{M}_\eta \end{bmatrix} \cdot [\eta] \quad \text{where} \quad \eta = \left(\eta_{ctl} + k_1\phi + k_2\dot{\phi} \right)$$

For the frictional forces:

$$F_3 = \begin{bmatrix} \mathring{X}_\eta \\ \mathring{Z}_\eta \\ \mathring{M}_\eta \end{bmatrix} \cdot [\eta] + \begin{bmatrix} 0 \\ 0 \\ -f_y \end{bmatrix} \cdot [\dot{\theta}] + \begin{bmatrix} X_{fr} \\ Z_{fr} \\ 0 \end{bmatrix}$$

It is worth noting that the mechanical friction moment per unit angular velocity (f_y) was estimated to be 0.0088 kgm^2.rad/sec during the moment of inertia experiments described in Chapter 8. The inertial frictional forces along the rod have not been estimated but it is possible to assume that the steps taken to lubricate the vertical rod during experiments will result in a negligible amount of friction. In addition these inertial friction terms will be zero whenever the model is inertially stationary or fully restrained.

The expression for $F = F_1$ given by Eqn [14.22] will be used in the current application.

The fluid acceleration terms can all be set to zero in the wind tunnel as the wind tunnel speed V_t is constant; ($\dot{u}_f = \dot{w}_f = \dot{q}_f = 0$).

The reference inertial velocity U_o for the model aircraft is zero in the wind tunnel.

The inertial perturbation velocities in the X and Z force equations are given by the expressions in Eqns [14.16] and [14.17].

The fluid velocity term in the pitching moment equation is analogous to swirl and may be set to zero as it is assumed that the air flow in the wind tunnel is laminar; ($q_f = 0$). The remaining fluid perturbation velocities in the X and Z force equations are given by the expressions in Eqns [14.10] and [14.11].

Derivation of the wind tunnel equations of motion with heave freedom may be performed in two stages. Firstly, all of the terms in Eqn [14.2] which can be set to zero are eliminated to obtain:

$$\left\{\begin{bmatrix}0 & 0 & 0\\ 0 & \mathring{Z}_{\dot{w}} & 0\\ 0 & \mathring{M}_{\dot{w}} & 0\end{bmatrix} + \begin{bmatrix}m & 0 & 0\\ 0 & m & 0\\ 0 & 0 & I_y\end{bmatrix}\right\}\cdot\begin{bmatrix}\dot{u}_i\\ \dot{w}_i\\ \dot{q}_i\end{bmatrix} = \begin{bmatrix}X\\ Z\\ M\end{bmatrix} + \begin{bmatrix}\mathring{X}_u & \mathring{X}_w & \mathring{X}_q\\ \mathring{Z}_u & \mathring{Z}_w & \mathring{Z}_q\\ \mathring{M}_u & \mathring{M}_w & \mathring{M}_q\end{bmatrix}\begin{bmatrix}u_i - u_f\\ w_i - w_f\\ q_i - 0\end{bmatrix} - \begin{bmatrix}mg\\ 0\\ 0\end{bmatrix}\theta$$

or, considering each force and moment equation separately, by:

$$m.\dot{u}_i = X + \mathring{X}_u.(u_i - u_f) + \mathring{X}_w.(w_i - w_f) + \mathring{X}_q.q_i + mg.\theta \qquad [14.23a]$$

$$\mathring{Z}_{\dot{w}}.\dot{w}_i + m.\dot{w}_i = Z + \mathring{Z}_u.(u_i - u_f) + \mathring{Z}_w.(w_i - w_f) + \mathring{Z}_q.q_i \qquad [14.23b]$$

$$\mathring{M}_{\dot{w}}.\dot{w}_i + I_y.\dot{q}_i = M + \mathring{M}_u.(u_i - u_f) + \mathring{M}_w.(w_i - w_f) + \mathring{M}_q.q_i \qquad [14.23c]$$

Next, substituting the inertial and fluid perturbation parameters with the appropriate re-constructed variables and defining F yields:

$$m.\left[\frac{-\ddot{h}}{\cos\alpha_e + \tan\alpha_e}\right] = \mathring{X}_\eta.\eta + \mathring{X}_u.\left\{\left[\frac{-\dot{h}}{\cos\alpha_e + \tan\alpha_e}\right] + V_t.\sin\alpha_e.\theta\right\}$$

$$+ \mathring{X}_w.\left\{\left[\frac{\dot{h}}{\sin\alpha_e + \cot\alpha_e}\right] - V_t.\cos\alpha_e.\theta\right\} + \mathring{X}_q.\dot{\theta} + mg.\theta \qquad [14.24a]$$

$$\left[\mathring{Z}_{\dot{w}} + m\right].\left[\frac{\ddot{h}}{\sin\alpha_e + \cot\alpha_e}\right] = \mathring{Z}_\eta.\eta + \mathring{Z}_u.\left\{\left[\frac{-\dot{h}}{\cos\alpha_e + \tan\alpha_e}\right] + V_t.\sin\alpha_e.\theta\right\}$$

$$+ \mathring{Z}_w.\left\{\left[\frac{\dot{h}}{\sin\alpha_e + \cot\alpha_e}\right] - V_t.\cos\alpha_e.\theta\right\} + \mathring{Z}_q.\dot{\theta} \qquad [14.24b]$$

$$\mathring{M}_{\dot{w}}.\left[\frac{\ddot{h}}{\sin\alpha_e + \cot\alpha_e}\right] + I_y.\ddot{\theta} = \mathring{M}_\eta.\eta + \mathring{M}_u.\left\{\left[\frac{-\dot{h}}{\cos\alpha_e + \tan\alpha_e}\right] + V_t.\sin\alpha_e.\theta\right\}$$

$$+ \mathring{M}_w.\left\{\left[\frac{\dot{h}}{\sin\alpha_e + \cot\alpha_e}\right] - V_t.\cos\alpha_e.\theta\right\} + \mathring{M}_q.\dot{\theta} \qquad [14.24c]$$

14.4.2 MSR equations for a model with heave freedom.

The format of the equations of motion required for parameter identification using the MSR procedure is y = B.x where y is the independent variable, B is the matrix of parameters to be identified and x is the vector of measured variables. Considering each equation above in turn the following points are noted:

1) The X force Eqn [14.24a] is already in the required MSR format.

2) The Z force Eqn [14.24b] can easily be manipulated into the required MSR format with the term { $m.\ddot{h}./(\sin\alpha_e + \cot\alpha_e)$ } being an obvious choice for y.

3) The M pitching moment Eqn [14.24c] can also be easily manipulated into the format required for the MSR procedure where the term for y is given by $I_y.\ddot{\theta}$

In all three forms of the MSR equations it is important to note that individual "B" terms occur for the aerodynamic stability and control derivatives and individual terms occur for the measured "x" and y. This is thought to bode well for a successful application of MSR procedure as it should be possible to obtain separate estimates for each derivative. For example, having unique terms should prevent the MSR program crashing due to problems being encountered during matrix manipulations. In all previous derivations of the equations of motion some of the derivatives had to be grouped together because unique expressions for the measured state variables had not been produced and there was often no clear candidate for the y variable term.

The independent y term and the x state variables can all be derived from the limited set consisting of $\dot{h}$, $\ddot{h}$, V_t, α_e, θ, $\dot{\theta}$ and $\ddot{\theta}$ and all of these terms can be easily measured (or numerically derived) using the experimental rig. Unfortunately, in the practical experiments carried out during this programme of research measurements of $\dot{h}$ and $\ddot{h}$ were not available at the time because development of the dynamic height hold facility had not been completed. Expansion of the dynamic facility to measure height position and velocity have been the subject of two separate MSc research programmes, (Refs 24 and 37). Thus it is currently not possible to run the MSR program to obtain derivative estimates using the alternative heave free equations of motion derived above but this could be the subject of a future research programme utilizing the dynamic rig facility.

14.5 Hawk model fully constrained in heave.

This is the simplest case to analyse as the aircraft is only free to respond by rotating in pitch and the inertial velocity and acceleration terms u_i, w_i, $\dot{u}_i$ and $\dot{w}_i$ may all be set to zero. The first two "X" and "Z" equations of Eqn [14.2] are therefore redundant leaving only the third pitching moment equation.

Eqns [14.10] and [14.11] for the fluid velocity parameters u_f and w_f were derived for use in the previous heave free equations of motion are equally valid for the fully restrained case. Furthermore, the assumptions made in the heave free analysis which resulted in a number of terms being set to zero are also valid in this case, e.g. $a_z = 0$ etc. The pitching moment external force may be simply represented by $M = \mathring{M}_{\eta}.\eta.$

14.5.1 Equations of motion with no heave freedom.

Considering only the pitching moment equation presented in Eqn [14.2] and setting parameters to zero as appropriate yields:

$$I_y.\dot{q}_i = M + \mathring{M}_u.(-u_f) + \mathring{M}_w.(-w_f) + \mathring{M}_q.q_i \qquad [14.25]$$

Substituting the state variables with the re-constructed variables and defining M gives:

$$I_y.\ddot{\theta} = \mathring{M}_{\eta}.\eta + \mathring{M}_u.(V_t.\sin\alpha_e.\theta) + \mathring{M}_w.(-V_t.\cos\alpha_e.\theta) + \mathring{M}_q.\dot{\theta} \qquad [14.26]$$

Finally, Eqn [14.26] may be slightly simplified by dividing through by I_y to yield:

$$\ddot{\theta} = \mathring{m}_{\eta}.\eta + \mathring{m}_{u}.(V_t.\sin\alpha_e.\theta) + \mathring{m}_{w}.(-V_t.\cos\alpha_e.\theta) + \mathring{m}_{q}.\dot{\theta} \qquad [14.27]$$

14.5.2 MSR equations for a model without heave freedom.

The following MSR equation structure can be used to model the pitching moment equation of motion for the fully restrained Hawk model in the wind tunnel:

$$y = b_0 + b_1.x_1 + b_2.x_2 + b_3.x_3 + b_4.x_4 \qquad [14.28]$$

$$\ddot{\theta} = \mathring{m}_{\eta}.\eta + \mathring{m}_{u}.(V_t.\sin\alpha_e.\theta) + \mathring{m}_{w}.(-V_t.\cos\alpha_e.\theta) + \mathring{m}_{q}.\dot{\theta} \qquad [14.27]$$

14.6 Estimation of S&C Derivatives using the MSR Program.

Data from experimental run MAR28G was chosen for analysis with the mathematical structure given by Eqn [14.27] for two reasons. Firstly, the data was recorded in work where the Hawk model was fully vertically restrained and secondly, the same data had been previously analysed using the initial work in which the inertial components of motion were separated out. It was hoped to compare the results obtained from this previous analysis with the current alternative equations application. In doing so it may be possible to identify which is the best mathematical representation of the Hawk in the wind tunnel to use with the MSR procedure.

The MAR28G data channels were filtered and processed, using the steps described in Chapter 13. The only difference being that, in the last stage of signal conditioning, a new BASIC program was written using to produce the reconstructed state variables of Eqn [14.27]. When the MSR program was run were obtained all of the parameter estimates were calculated as zero, even though in this case, $\underline{Y} \neq \underline{0}$. This result was somewhat disappointing and indicated that all of the state variables are apparently un-correlated with $\ddot{\theta}$. However, there is much confidence in the derivation of the model structure given in Eqn [14.27] and the failure of the MSR procedure is thus thought to be due to the quality of data which was recorded from the experimental rig.

14.7 Model Aircraft Simulations.

To investigate the effect of the quality of the data obtained from the dynamic rig on MSR, it was decided to produce an aircraft simulation in which band limited white noise was added to the elevator input and pitch response signals. To do this the OU algorithm ACSL was used and required the mean value (M), the standard deviation (S) and the break frequency (TAU, where τ = 1/(2.π.f)) of the noise to be defined. It was decided to define M=0.0 and TAU = 0.0159 (i.e. a cut-off frequency of ~10Hz). The RMS value of the noise was roughly estimated as S = 0.0159 using the WATERFAL software. (Many textbooks, e.g. Refs 38 and 39, detail the statistical theory and analysis of signal noise). Unfortunately, practical problems with the ACSL environment, and a lack of time to identify the cause, prevented the output from ACSL of some of the critical variables required for analysis with MSR. It is recommended that this type of simulation be pursued in future as much useful information on MSR could be obtained.

CHAPTER 15

DISCUSSION

15.0 DISCUSSION.

The main question posed at the start of this research programme was "How far can the MSR method be stretched to cope with incomplete model descriptions and a limited number of response variables measured directly". Previous applications of the MSR had utilized six degree of freedom free-flight models, in a non-linear high-α flight regime, which naturally required complex mathematical structures to give the best-fit to the flight test data. In the current application linear aircraft motion with limited degrees of freedom has been examined, with a limited amount of measured information available. Consequently, with relatively simple mathematical models being used, in a linear flight regime, some insight has been gained into both the MSR process and the difficulties associated with obtaining suitable data when conducting experiments using a small dynamic aircraft model and rig facility.

This Chapter details the main theoretical and practical observations made during the research programme. The advantages and disadvantages associated with the experimental facility are discussed as well as the steps taken to overcome some of the practical difficulties. The development of aircraft simulations, the data acquisition system, the process required to re-construct the state variables and the MSR observations are also discussed.

15.1 Dynamic rig facility.

There are many practical and theoretical aspects of the dynamic rig to be considered, including, for example, the best way in which to

mathematically model the facility to represent or re-create the motion of the model in the wind tunnel.

Despite the many practical problems encountered when using the dynamic rig, not all of which could be overcome, it is worth noting that the MSR method can not be investigated using a static facility because dynamic responses are required. Moreover, as has been demonstrated in previous experimental programmes which used the dynamic rig facility, short period motion can still yield much valuable information about the aircraft under investigation. The dynamic facility provides ± 30° of freedom in roll, pitch and yaw altitude and this was considered more than sufficient to emulate the small perturbation equations of aircraft motion.

15.1.1 Weybridge wind tunnel.

In the Weybridge wind tunnel, there were found to be several wind speeds which caused a large resonance in the tunnel. This problem decreased at higher wind speeds but there was considerable disruption of the flow as the speed was increased to the desired range. It was therefore necessary to allow some time for the tunnel flow to settle before starting to record any experimental data.

During the course of this work it was observed that when the model is actually flying significant transient tunnel blockage effects come into play as the model manoeuvres. There was a noticeable decrease in tunnel speed when the model was moved off the bottom end stop.

Another uncontrollable problem sometimes encountered was related to the power supply to the Weybridge tunnel from the electric grid in the College of Aeronautics. Frequent periods of heavy demand on the grid resulted in fluctuations in the voltage and consequently caused small changes in the wind tunnel speed. This was particularly annoying as considerable time and patience was required to set the model up in a trimmed flying condition.

15.1.2 Suspension system.

The experimental facility would benefit considerably from a major overhaul as, because of its age, there is much "wear and tear". For example, the vertical rod is noticeably bent and there are numerous pit marks where the restraining collar screws have been tightened. Both of these factors will increase "stiction" (or "breakout friction force") on the rod and influence the dynamics of the aircraft whilst it is trying to "take off" or increase height. As the aircraft elevator angle was changed the model would not appear to respond until, without warning, it suddenly overcame the stiction and took off. Small control inputs and extreme caution were therefore required, especially during early flying with the model. Even when considerable experience had been gained the model would often depart for no apparent reason.

Before each experimental run, measures were taken to try and minimize the stiction between the rod and gimbal sleeve. These included adjusting the four bracing wires attached to the mounting plate of the suspension system to get the rod as near vertical as possible. The rod was also sprayed with a lubricant.

Additional friction arises within the gimbal itself and preliminary experiments were undertaken in an attempt to quantify this. These experiments also enabled the models moments of inertia to be measured. Furthermore, a limited number of aerodynamic derivatives could be estimated, these included $\mathring{N}_v$ and $\mathring{N}_r$.

15.1.3 12th scale Hawk model.

The scaled Hawk model was found to be particularly hard to fly in a controlled manner in the wind tunnel. This was quite surprising, especially as the full scale Hawk is a stable aircraft. Analysis of the static stability of the Hawk model showed that the original gimbal position was partly to blame for this and moving the gimbal (and hence also the coincident c.g.) forward by 10mm improved the models' controllability. Unfortunately, due to the construction of the model, it was not possible to move the gimbal any further forward.

In some of the wind tunnel experiments, at the end of a run, the c.g position of the aircraft was found to have altered due to movement of the brass weights which were placed inside the model for ballast. This phenomena could be observed by the change in wind off attitude which was adopted by the model following a wind tunnel run. Subsequent examination of the brass weights in the model cockpit then revealed that one or more of the weights had become loose and had therefore changed the position of the c.g.

The actual scale of the Hawk model presented further practical problems. For example, because the aircraft wing span was only just

small enough to facilitate flying in the Weybridge wind tunnel, the aircraft tended to roll considerably as it was constantly subjected to turbulent flow at the edges of the open air stream. To counteract this problem, roll autostabilisation loops were implemented in some of the experiments using analogue circuits patched on the ECU.

Another factor influenced by the scale of the model is Reynolds number. However, in this programme it was not considered necessary to try and prematurely trip the boundary layer of the aircraft. The only practical measure undertaken was to ensure that the mounting points for the TEM balance were filled with plasticine and that this was made as smooth and as flush with the wing structure as possible.

Backlash problems were encountered within both the attitude potentiometers and the control surface linkages. Attempts were made to reduce the particularly large backlash experienced in yaw attitude by inserting foam packaging into the worn groove of the mounting plate, into which the pot wiper fitted. During this programme of research no attempts were made to overcome the backlash in the control surface linkages because this backlash was actually due to the design of these linkages, which were essentially wires with two hooked ends which fitted into holes in plastic arms attached to the control servos and control surfaces. The hole clearances necessary to reduce friction in the mechanism inevitably introduces some slackness and hence backlash. Moreover, the hooks and wires tend to distort with use.

During the course of the research programme calibrations of the attitude angles and control surfaces were repeated several times. Internal changes to the model necessitated this because, for example,

the elevator and rudder control servos had to be replaced and this affected the amount of backlash and also changed the calibration equations for the control surfaces. Although time consuming to perform, it was considered important to always use the most up-to-date and accurate set of calibrations possible.

The multi-strand cable between the model aircraft and the ECU tended to flap around freely in the wind tunnel. To minimize the influence of this umbilical connector on the air stream the cable was taped to the vertical rod. However, some caution was necessary to ensure that, in experiments in which the Hawk model was given a few inches of vertical freedom, sufficient slack was allowed to avoid the cables being damaged as the model changed height. When the wind tunnel was being run, it is probable that some degree of noise was picked up both inside the model and the umbilical cable and thus superimposed on the data being transmitted to the ECU.

15.2 Aircraft simulation.

A number of aircraft simulations were produced using the programming language ACSL and both the full scale Hawk and the model aircraft were simulated. It was considered acceptable to decouple the longitudinal and lateral equations of motion and two separate simulations were written to represent the longitudinal and lateral motion. The ACSL programs were very easy to run and both graphical and tabular outputs of the data could be obtained.

The primary purpose was to obtain response data in order to test

the MSR FORTRAN program. MSR was found to produce perfect derivative estimates in that exactly the same numerical parameter values were obtained as had been used in the aircraft simulation programs. It was however, possible to vary the number of data points produced by the ACSL programs in order to observe the effect this had in slightly reducing the MSR prediction accuracies.

The second purpose for the simulation programs was to attempt to accurately model the physical constraints of the Hawk in the tunnel. initially, two simulation programs were written to reflect the reduced wind tunnel equations which are discussed in Chapter 4. Further simulation programs were written to model the alternative equations of rigid body fluid motion derived in Chapter 14. These later simulations also included a model for signal noise which was added to the elevator inputs and pitch response.

It would be possible to pursue this idea by enhancing the reduced equations of motion to include other dynamic influences arising on the rig. For example, terms could be included for gimbal friction using the numerical values estimated for each gimbal axis in the preliminary experiments. Additionally, the backlash present in the control surfaces could be modelled.

The simulation programs were developed with a further purpose in mind. There had been a plan to insert stability and control derivatives estimated from wind tunnel experiments, by the MSR method, into the simulation program. The wind tunnel flight conditions and control surface inputs could then have been modelled with a view to running the simulation program(s) to obtain predicted responses which

would hopefully closely match the aircraft responses observed in the wind tunnel. Unfortunately, in practice it proved impossible to carry out this type of analysis because of a lack of parameter estimates.

15.3 Data acquisition.

The data acquisition system developed during this programme enabled up to eight channels of data to be recorded from the ECU during wind tunnel experiments and it was quite simple to change the frequency at which the data was recorded. There were a number of computer programs written to automate the signal processing of the experimental data. This was necessary to obtain a single data file, in the correct S.I. units, for input to the MSR computer program. Although the process was automated as far as possible, it was very time consuming to filter individual data channels and further process and edit the data because many separate stages were involved. Even before the start of the signal processing stages, it took a long time to load individual data channels into the WATERFAL software program to evaluate whether or not a good, (i.e. relatively noise free), short period aircraft response had been captured on all eight data channels.

The ECU power supply developed a fault part-way through the experimental programme which for some time went undetected. The result of the fault was to impose high frequency noise on the power lines (which coupled into the signal lines) when the supply was insufficiently loaded. This problem was compounded by a noisy mains supply to the building, probably partially a result of the simultaneous operation of various wind tunnel motors etc.

Although these early power supply noise problems were cured it became apparent, after data collection had been completed, that some residual noise pickup remained. This was only noticeable on close examination of the recorded data and was only discovered after the relatively narrow window of availability on the wind tunnel, which had necessitated rapid data collection, had expired. A small amplitude 25Hz oscillation was superimposed on the data read from the model transducers which was sufficient to cause considerable disruption to the numerical differentiation. Filtering and averaging produced only limited improvements although the effect was much less noticeable at lower sampling frequencies. The frequency suggests a mains related origin although there may also have been aliasing affects linked to the sampling frequency which changed the apparent frequency of the noise.

There were other general noise problems encountered, only some of which could be traced. For example, a marked improvement in the data noise level was obtained when it was discovered that the cable between the ECU and CED1401 was not grounded properly and a earth connection was introduced between them.

Unfortunately, small amplitude manoeuvres, required or the small perturbation equations to be valid in the form in which they were being used, implies inherently small output signals and hence a degraded signal-to-noise ratio. In this application small manoeuvres were also required to maintain control of the model. Larger manoeuvres tend to result in larger signal-to-noise ratios and thus better parameter estimates. As a general rule, the variance of the estimates is said to be inversely proportional to the amplitude of the manoeuvre.

15.3.1 Variable reconstruction.

In an ideal parameter estimation process it is necessary to have a measure of the control variables and all of the corresponding response variables. When, for practical reasons this is not possible alternative ways have to be found for synthesizing estimates of the missing variables. The way in which this may be done and the number of missing variables determines how well the estimation process will work. In the dynamic Hawk model the control variables of aileron, elevator and rudder angles are measured from signals derived from the servo-actuator feedback circuitry. Roll, pitch and yaw attitudes are also measured with precision potentiometers built into the suspension system. Although all of these are independent variables, this catalogue still falls somewhat short of the ideal as unfortunately it was not practicable to install either a small rate gyro or an accelerometer within the model.

The reconstruction and introduction of the missing variables into the parameter estimation process can be done in a variety of ways. However, most can be expected to introduce additional problems and an objective has been to try to find an acceptable method for reconstructing variables. In the present application the main problem was to derive rate and acceleration signals from attitude signals. This was achieved by differentiation using analogue or digital methods but in either case the by-product of the process was high noise levels. State estimation methods were also considered but these are complex and require some prior knowledge of the aircraft model which is the subject of the parameter estimation and this was not a practical option within the limited time scales available.

The level of kinematic compatibility between the measured variables is considered important. Unlike digital filtering of a data file, where information is available before and after each instant of time, electronic differentiation inevitably introduces a phase lag into the signal. Thus it was not practical to remove phase differences between measured θ , $\dot{\theta}$ and $\ddot{\theta}$, where θ was obtained from the model's pitch potentiometer, and $\dot{\theta}_m$ and $\ddot{\theta}_m$ from the analogue differentiator.

15.4 Mathematical models.

The motion of the Hawk model is limited to four degrees of freedom with heave motion and three degrees of freedom when fully restrained. It was considered acceptable to seek out more than one method to mathematically represent the equations of motion. Furthermore, approximate equivalent relationships between measured variables and the state variables in the equations of motion were sought. Thus during the course of this PhD many mathematical models of the Hawk model were introduced by configuring the equations of motion to a limited extent and performing appropriate wind tunnel experiments.

Refs 8, 9 and 10 contain further information on the development of some equations of motion which are based upon this idea of separating out the angular and inertial velocity perturbations. These references also give details of the results of MSR runs using experimental data in which the Hawk model had been completely retrained in vertical freedom by two collars immediately above and below the gimbal. This arrangement was used in an attempt to prevent any pitch attitude response from being turned into a vertical translation of the model.

A control problem which arises when the model is flown in the wind tunnel is that it is difficult to get the model into a trimmed condition. Very small variations in the airflow of the tunnel can affect the model and take it out of trim. One way to improve this situation was to use the analogue circuitry of the ECU panel to artificially augment the stability of the model, especially in roll. Where roll autostabilisation was employed in wind tunnel experiments, the MSR could easily be used with extended equations of motion to generate estimates for the additional parameters introduced.

Although difficult to substantiate, it is thought that the formats of the equations of motion which were analysed during this programme may not be in an appropriate form for when real dynamic data is used; as opposed to "perfect" simulated data from which the MSR produced "perfect" parameter estimates. For example, Klein (Ref 1) allowed the use of used state variables which included longitudinal, lateral and vertical accelerations, incidence and sideslip, and non-linear combinations of variables in his regression equations. Alternatively, the MSR may simply have failed to predict the correct mathematical model because non-linear terms had been excluded from the reduced wind tunnel equations and these may have a bigger influence on the dynamics of the model than previously recognized.

15.5 MSR method/computer program.

A FORTRAN 77 program was written to computationally implement the algorithms required to carry out parameter identification using the MSR method. This program was initially tested using the "Hald" set of

experimental data (Ref 16) and the MSR program was seen to exactly replicate the intermediate and final best fit regression models reported by Smith and Draper for the Hald data.

The FORTRAN program was next tested using response data obtained from the ACSL aircraft simulations. These tests included a reduced set of aircraft equations of motion to check that the MSR would be able to cope with a limited amount of information and produce correct parameter estimates. "Perfect" results were again obtained and this enabled confidence to be built up in the correct implementation of the MSR procedure in the computer program MSR.EXE.

Once wind tunnel experiments had taken place and the appropriate signal conditioning performed on the recorded data, it was possible to use the MSR program to predict the stability and control derivatives of the scaled Hawk aircraft model. Strictly speaking, MSR program runs with this data should have been constrained to start with a mathematical model of the aircraft which contained the linear terms of the equation of motion under consideration. However, to investigate the robustness of the MSR procedure this rule was often usefully ignored, as can be seen by the initial models presented in Table 13.B of section 13.4. For example, a run starting with X1 and X2 only in the initial regression model, were X1 = X2 = θ, showed that the MSR program would always crash whenever two identical state variables were included in the same regression model.

Analysis of experimental data confirmed that the MSR is sensitive to the number of independently measured variables which are available for inclusion in the iterative models which are produced as the MSR

tries to find the best model to fit the data. However, this is a well known disadvantage of using the experimental rig which was purposely exploited, because one of the main aims of this research programme was to investigate whether the MSR method is able to cope with only a limited amount of data available.

In future, it would be worth investigating ways of making use of any a priori information available for the mathematical equation under consideration. One method would be to insert into MSR input data file or FORTRAN program, the numerical values of one or more known parameters (e.g. $g\sin\alpha_e$) multiplied by the corresponding state variable (e.g. θ), effectively as a constant term, to see if this improves predictive capability of the MSR. This is expected to improve the quality of the parameter estimates obtained because fewer parameters will be sought from the set number of state variables. This will then increase the statistical degrees of freedom by one if only one known term is utilized in this manner.

The number of data points available to the MSR will affect the numerical value of the $F_{p\,min}$ statistic which sets the level for deciding whether or not a parameter is significant or should be rejected from the iteration model being processed. Due to computer processing power available the number of data points (or time span) analysed had to be limited and this may have had a considerable impact on the ability of the MSR to provide parameter estimates from the wind tunnel. With the level of noise in the wind tunnel data, it could be considered that the MSR requires a large number of data points before it is able to "spot" any trends or correlations in the data set under investigation.

The main observations obtained from the analysis of the all the the MSR runs carried out using experimental wind tunnel data are listed below.

15.5.1 Summary of MSR observations.

1. The MSR program always crashed if there was only one variable included in the regression model being processed by the MSR for a particular iteration.

2. If two identical state variables are included in the same regression model, even though their coefficients are completely different, the program will crash due to a divide by zero error during the inversion of a matrix.

3. The statistical equations and algorithms employed in the MSR FORTRAN program do not appear to be very robust as they are prone mathematical floating point errors which cause the program to crash.

4. A further sign of an unsuitable computational format of the statistical equations is that negative values of F and R^2 were sometimes obtained.

5. Manipulation of the aircraft equations of motion to obtain output Y as equal to zero proved impossible because of the extensive use and influence of the matrix Y in the MSR computational equations. When Y was set to zero all parameter estimates were given as 0.0 ± 0.0.

6. If the variable recorded as part of the state output term is multiplied by a constant term, e.g. $Y = \theta.V_t\cos\alpha_e$, and the same measured variable (e.g. X1 = θ) and constant term (B1 = $V_t\cos\alpha_e$) appear in the regression equation model, then there will be a high correlation of the state variable to Y. Furthermore, the numerical value of B1 will be correctly estimated and all other state variables may be excluded from the final best-fit model.

7. As the MSR procedure progresses through an increasing number of iterations it is possible to observe the value of the overall equation error decreasing as insignificant terms are gradually removed from the regression equation. The correlation coefficient and F statistic can also be seen to increase with the final model chosen, as the best fit to the experimental data, being the model with the highest value of F.

8. MSR runs which included measured or derived variables based on the set (θ, $\dot{\theta}$, $\ddot{\theta}$, η) were found to perform much better than runs with a lesser number measured variables available (e.g. θ, $\dot{\theta}$, η). This showed that the more statistical degrees of freedom available to the MSR the better it performs and the better quality of the parameter estimates.

CHAPTER 16

CONCLUSIONS AND RECOMMENDATIONS

16.0 CONCLUSIONS AND RECOMMENDATIONS.

In a new aircraft programme for example, flight test data is required as soon as possible to check wind tunnel and analytical predictions of aircraft stability and control derivatives. Good flight estimates are important in allowing for a safe expansion of the aircraft envelope during flight test phases. Therefore a number of parameter identification techniques will be employed to obtain as much information about the aircraft as possible, Modified Stepwise Regression being one such technique.

The MSR method has performed very well up to now, enabling large amounts of flight data to be processed. Experimental error and noise do not require modelling because they are implicitly taken account of when minimising the overall equation error, although there will naturally be some bias in the parameter estimates because of this approach. A further benefit is that the structure of the aerodynamic model does not need to be pre-defined and it is easy to include additional variables in order to model non-linear characteristics. The major disadvantage of the method however, is that the MSR is highly dependent on the kinematic compatibility and quality of the input data which it uses. This is demonstrated by the fact that the MSR will only include statistically significant terms in the final best-fit model structure.

Wind tunnel testing can yield reasonable derivative estimates but it is very difficult to precisely match real flight conditions. There are very few dynamic wind tunnel facilities available and even these fall somewhat short of reproducing a realistic flight environment.

Support system effects are always a problem when carrying out wind tunnel tests and further discrepancies with flight trial results will arise due to Reynolds number differences.

In this particular experimental programme there were many practical difficulties encountered and only a limited amount of information was available for use in the parameter identification exercise. These factors proved to be major influences which affected the quality of the MSR parameter estimates obtained. The list below summarises the lessons learned and conclusions which can be drawn following the research work described in this thesis.

16.1 Conclusions.

1. Many practical problems were encountered with the dynamic rig and not all of them could be overcome. Efforts were made to minimise noise, backlash, wind tunnel resonance and blockage effects. The development of careful operating procedures were shown to help somewhat, providing small perturbations about trim were adhered to.

2. When flown in the wind tunnel the Hawk model was very lively, sufficiently so as to make autostabilisation a prudent action. Simple feedback loops have been demonstrated to work well.

3. Preliminary experiments, performed to evaluate the static stability of the Hawk model and the moments of inertia, enabled a limited number of aerodynamic derivatives to be estimated.

4. The dynamics of the Hawk model on the rig were not fully understood and the vertical rod and stiction of the mounting system appeared to have a bigger influence on the model than was realised at the start of the programme. The mathematical equations used to represent the scaled model were too simplistic and involved linear terms only.

5. State and input variable reconstruction was necessary. Rate data and acceleration data had to be derived from measured attitude signals. Analogue and numerical methods were tested for this purpose, consequently introducing further noise and uncertainty into the experimental data.

6. Kinematic compatibility of experimental data needs to be ensured.

7. Data preparation for the MSR was time consuming as a number of stages were required, involving many different programs to run and data files to edit. However, once the input data file was available, the MSR only took a few minutes to run and provided very quick results.

8. With only four degree of freedom available on the dynamic rig, too many parameters were being estimated from the limited amount of data available. The MSR requires as many independent state variables as possible to be made available to get the method to method work with dynamic wind tunnel data.

9. When wind tunnel data was input to the MSR it was not possible to satisfactorily separate all of the parameters which appeared in the intermediate and final regression models.

10. The fitting of the best mathematical model to data generated by the ACSL simulations yielded the correct model structures and gave perfect parameter estimates.

16.2 Recommendations.

The list below contains suggestions for future work which could be carried out to improve the dynamic wind tunnel facility and the recording and analysis of data, with a view to enhancing the understanding and practical performance of the MSR method.

1. Ensure that the main suspension rod in the Dexion framework is rigidly fixed in a vertical position; This is to minimise stiction and prevent distortion of the Hawk model dynamics.

2. Minimise the amount of backlash within the potentiometers and control servos; Provide new potentiometers with tighter fitting wipers; Replace servo to control surface linkages by ball and joint connectors and rigid PTFE tubes.

3. Ensure the c.g is kept constant for a particular wind tunnel run. Improve the "fixing" of any ballast necessary inside the model.

4. Paint new reference lines on the Hawk model; Improve the attitude angle and control surface calibrations.

5. Increase the accuracy of the potentiometers and control servos through a manufacturers service or complete replacement of these units.

6. A high priority should be given to the inclusion of a small rate gyro and an accelerometer within the Hawk model.

7. Improve the aircraft and ECU electrical circuit designs paying particular attention to the likelihood of noise pickup. Consider using a radio control link to replace the long umbilical connector between the aircraft model and ECU.

8. Introduce mains filtering and replace old analogue integrators and summers in the ECU with newer components. This will improve signal-to-noise ratios and reduce the time constants of any differentiation circuits introduced for use in autostabilisation loops for example.

9. Develop an alternative data acquisition system to the CED1401 which includes some on-line analysis capability to check both the model trim and whether a suitable response, with a good signal-to-noise ratio has been recorded.

10. Modern software packages now available will be able to the improve the signal conditioning of experimental data - for example, by better filtering of noise and the removal of any phase differences between signals.

11. Try to reducing the number of stages and time required to process and combine data channels into a single file for use by the MSR.

12. Explore alternative methods for the reconstruction of state and input variables and for the production of rate and acceleration data.

13. Analyse MSR runs using the lateral response data recorded in case the rig particularly influences the longitudinal motion of the Hawk model.

14. Pursue alternative mathematical representations of the Hawk which try to incorporate the rig dynamics. Include non-linear terms or different state variables e.g. α, α^2, β, etc. Make use of any a priori information available on the aircraft model structure and insert numerical values of any known stability and control derivatives into the MSR program.

15. MSR input files containing larger amounts of data could be used by combining wind tunnel runs which have the same initial conditions. Alternatively, data could be partitioned into data sets (i.e. bins) covering one or two degrees of pitch attitude. This technique does not require the bins of data to be continuous in time, however, it will be limited by the ability to replicate trimmed initial conditions in the wind tunnel.

16. Make greater use of ACSL aircraft simulations to investigate MSR performance when, for example, noise and phase shifts are injected into the simulation response data.

17. In the MSR computer program, implement alternative statistical formulae for calculating F and R^2.

18. The performance of the MSR technique could be evaluated using real aircraft flight data, possibly that obtained using the facilities provided by the College of Aeronautics Jetstream aircraft.

REFERENCES

1. KLEIN, V.; BATTERSON, J.G.; MURPHY, P.C. — Determination of Airplane Model Structure from Flight Data by Using Modified Stepwise Regression. NASA TP-1916, October 1981.

2. COOK, M.V. — A Proposal For a Programme of Research Into the Use of a Stepwise Regression Method for the Estimation of Aircraft Stability and Control Derivatives. College of Aeronautics, Cranfield Institute of Technology, August 1988.

3. COOK, M.V. and HINDS, H.A. — Initial Review of Research Into the Application of Modified Stepwise Regression for the Estimation of Aircraft Stability and Control Parameters. College of Aeronautics Report No. 8903, Cranfield Institute of Technology, January 1989.

4. HINDS, H.A. and COOK, M.V. — Second Quaterly Report on the Application of Modified Stepwise Regression for the Estimation of Aircraft Stability and Control Parameters. College of Aeronautics Report No. 8905, Cranfield Institute of Technology, April 1989.

5. HINDS, H.A. and COOK, M.V. — Third Quarterly Report on the Application of Modified Stepwise Regression for the Estimation of Aircraft Stability and Control Parameters. Unpublished College of Aeronautics Report, Cranfield Institute of Technology, April 1989.

6. HINDS, H.A. and COOK, M.V. — Preliminary Studies for Aircraft Parameter Estimation using Modified Stepwise Regression. College of Aeronautics Report No. P8911, Cranfield Institute of Technology, Nov. 1989.

7. HINDS, H.A. and COOK, M.V. — Evaluation of a Modified Stepwise Regression FORTRAN Program to Predict Aircraft Stability and Control Derivatives. College of Aeronautics Report No. NFP9002, Cranfield Institute of Technology, February 1990.

8. HINDS, H.A. and COOK, M.V. — Measurement of the Longitudinal Static Stablity and the Moments of Inertia of a 1/12th Scale Model of a B.Ae. Hawk. College of Aeronautics Report No. P9009, Cranfield Institute Of Technology, May 1990.

9. HINDS, H.A. and COOK, M.V. — Review of Initial Experiments Using the Hawk Model, Dynamic Rig Facility and the CED1401 Digital Data Acquisition Equipment. College of Aeronautics Report No. P9017, Cranfield Institute of Technology, July 1990.

10. HINDS, H.A. and COOK, M.V. — The Acquisition and Signal Conditioning of Experimental Wind Tunnel Data For Use With a Modified Stepwise Regression Method to Estimate Aircraft Stability and Control Parameters. College of Aeronautics Report No. 9102, Cranfield Institute of Technology, November 1990.

11. Hinds, H.A. and COOK, M.V. — A Review of the Reduced Equations of a 1/12th Scale Dynamic Wind Tunnel Model of a B.Ae.Hawk Aircraft. Unpublished College of Aeronautics Report No. NFP9014, Cranfield Institute of Technology, October 1991.

12. HINDS, H.A. and COOK, M.V. — Use of a Modified Stepwise Regression Method to Estimate Dynamic Aircraft Wind Tunnel Model Derivatives. IMA Conference on Aerospace Vehicle Dynamics and Control, Cranfield Institute of Technology, September 1992.

13. ROSS, A.J.; EDWARDS, G.F.; KLEIN, V.; BATTERSON, J.G. — Validation of Aerodynamic Parameters at High Angles of Attack for RAE High Incidence Research Models, AIAA paper 87-2558. AIAA Atmospheric Flight Conference, Monterey, CA, 1987.

14. MULKENS, M.J.M. — Measurement of Aerodynamic Stability Derivatives Using a Whirling Arm Facility. College of Aeronautics Ph.D. Thesis, Cranfield Institute of Technology, 1993.

15. MENDENHALL, W. and SINCICH, T. — A Second Course in Business Statistics: Regression Analysis. 3rd Edition, Dellen Publishing Company, 1989.

16. DRAPER, N.R. and SMITH, H. — Applied Regression Analysis. 2nd Edition. John Wiley and Sons Inc., 1966.

17. MINKOWOWYCZ, W.J. et al. Handbook of Numerical Heat Transfer. John Wiley and Sons Inc., 1988.

18. HEYDARI, F. On the Estimation of Stability and Control Characteristics of a Generalised Forward Swept Wing Aircraft. College of Aeronautics Ph.D. Thesis, Cranfield Institute of Technology, 1986.

19. GOOD, D.I. What Can Formal Methods Offer to Digital Flight Control Systems Design? Formal Methods Workshop, NASA Langley Research Center, Hampton, V.A. August 20-23, 1990.

20. STENGAL, R.F. and LINSE, D.J. System Identification for Nonlinear Control Using Neural Networks. NASA Langley Research Centre, Joint Univeristy Program for Air Transportation Research, 1989-1990, December 1990. N91-19039/GAR.

21. LINSE, D.J. Neural Networks in Nonlinear Aircraft Control. NASA Langley Research Centre, Joint Univeristy Program for Air Transportation Research, 1989-1990, December 1990. N91-19038/9/GAR.

22. MALIK, I.A. The Design, Development and Evaluation of an Active Control Aircraft Model Wind Tunnel Facility. College of Aeronautics Ph.D. Thesis, Cranfield Institute Technology, 1982.

23. WRIGHT, M.C.N. Further Development of a Dynamic Aircraft Wind Tunnel Facility. College of Aeronautics M.Sc. Thesis, Cranfield Institute of Technology, 1984.

24. FILMER, S.W. An Artificial "g" Control System for the Dynamic Wind Tunnel Facility. College of Aeronautics M.Sc. Thesis, Cranfield Institute of Technology, 1989.

25. COOK, M.V. and HEDARI, F. The Estimation of the Stability and Control Characteristics of a Canard Configured Combat Aircraft Having a Forward Swept Wing. Paper ICAS-86-5.5.1, Proc. 15th Congress of the International Council of the Aeronautical Sciences, London 1986.

26. COOK, M.V. Flight Dynamics Principles. Unpublished MSc Lecture Notes, College of Aeronautics, Cranfield Institute of Technology, 1986.

27. GOMES, S.B.V. Task 3: Measurement of Some Aerodynamic Damping Derivatives for the YEZ-2A Airship. Unpublished College of Aeronautics Report No. NFP8909, Cranfield Institute of Technology, May 1989.

28. ACSL Advanced Continuous Simulation Language (ACSL) Reference Manual. Edition 4.1, Mitchell and Gauthier Associates, 1987.

29. HAWKER SIDDELEY AVIATION LTD. Aerodynamic Data and Stability and Control Derivatives of the Hawker Siddeley H.S. 1182. Airframe Engineering Note AERO-1880, 1971.

30. CED Cambridge Electronic Design Ltd.: SPECTRUM Array Arithmetic Library for MS-DOS, 1987.

31. E.A.I. Handbook of Analogue Computation. Electronics Associates Inc., 1967.

32. JACKSON, A. S. Analog Computation. McGraw-Hill Book Co. 1960.

33. HOROWITZ, P. and HILL W. The Art of Electronics. Cambridge University Press, 1980.

34. JAMES, M.L.; SMITH, G.M; WOLFORD, J.C. Applied Numerical Methods For Digital Computation. 3rd Edition, Harper & Row Publishers Inc., 1985.

35. YAKOWITZ, S. and SZIDAROVSZKY, F. An Introduction to Numerical Computations. 2nd Edition, Macmillan Publishing Co., 1989.

36. THOMASSON, P. G. Motion of a Rigid Body in an Unsteady Non Uniform Heavy Fluid. College of Aeronautics Report No. 9501, Cranfield University, July 1995.

37. GRAMMATICAS, A. The Design and Evaluation of a Height Hold Auto Pilot for the Dynamic Wind Tunnel Test Rig. College of Aeronautics M.Sc. Thesis, Cranfield University, 1994.

38. LATHI, B.P. Modern Digital and Analogue Communication Systems. Holt-Saunders Int. Editions. 1983.

39. BETTS, J.A. Signal Processing, Modulation and Noise. Hodder and Stoughton. 1981.

APPENDIX A

SCALING LAWS

A.0 SCALING LAWS.

For geometric similarity, the model aircraft must have the same shape as the full scale aircraft with the ratio of all linear dimensions (l_m/l_a) being constant. Kinematic similarity involves the consideration of aerodynamic characteristics and the scaling of linear and angular acceleration and velocity. Dynamic similarity exists when the geometric and kinematic similarities are satisfied and the ratio of all the forces are the same.

For example, the aerodynamic forces can be represented in the following form:

$$\text{Force} = f_1(\rho, L, \upsilon, V)$$

in which f_1 is a function of density, ρ, a length , L, kinematic viscosity υ and velocity V, (Ref 38).

When comparing aircraft manoeuvring gravity, g, must be taken into account. Further, if an aircraft is moving fast enough Mach number is also included so that:

$$\text{Force} = \rho . L^2 . V^2 . f_2\left(\frac{VL}{\upsilon} , \frac{V}{a} , \frac{V^2}{Lg} \right) \qquad [A.1]$$

The terms in the brackets of [A.1] will be recognised as:

(i) Reynolds Number, $\quad R_e = \mu_1 . \frac{V}{\upsilon}$

(ii) Mach Number, $M = \frac{V}{a}$

(iii) Froude Number, $F = \frac{V^2}{gL}$

Complete dynamic simulation can only be achieved when the following dimensionless parameters are numerically equal for both the model and the full size aircraft, as shown in Ref 22.

A.1 Scale factor.

The geometric scale factor, λ, is the constant ratio which relates all aircraft lengths, l_a, and model lengths, l_m, as shown below:

$$\lambda = \frac{l_m}{l_a} \qquad [A.2]$$

For the BAe Hawk model $\lambda = 1/12$.

A.2 Mach number.

The Mach Number, M, is expressed as the ratio of fluid velocity to its local speed of sound, a. This number takes into account the compressibility effect of the airflow. The Weybridge tunnel which will be used with the Hawk model is only a low speed tunnel and as $M < 0.4$ with this facility the compressibility effects may be neglected.

$$M = \frac{V}{a} \qquad [A.3]$$

A.3 Relative density factor and mass scaling.

The relative density factor, μ_L, allows for correct mass scaling for a given set of flight conditions. It is defined as:

$$\mu_L = \frac{2m}{\rho S l_\mu} \qquad [A.4]$$

where:

m = mass;

ρ = air density;

S = wing area;

l_μ = fuselage length.

The ratio of model to aircraft mass may be expressed as:

$$m_m = m_a . (\lambda)^3 \qquad [A.5]$$

A.4 Relative radius of inertia factor.

For correct dynamic response the relative radius of inertia, K_y, must be the same for both the model and aircraft. K_y is defined by

$$K_y = \left(\frac{r_y}{l_\mu} \right) \qquad [A.6]$$

where

r_y = radius of inertia.

Furthermore, $r_{y_m} = r_{y_a} . (\lambda)$

A.5 Froude number.

The Froude Number, F_r, scales the effect of gravity on the aircraft model and can be defined as the ratio of inertia to gravitational forces as follows:

$$F_r = \frac{V}{\sqrt{l_\mu g}} \qquad [A.7]$$

where

V is the velocity of the c.g.

g = acceleration due to gravity

When the Froude Number is combined with the relative density parameter μ_L, the lift coefficient for steady flight C_{L_0} can be found using the expression:

$$C_{L_0} = \frac{\mu_L}{F_r^2} = \frac{2mg}{\rho S V^2} \qquad [A.8]$$

To ensure that the model model aircraft flies at the same reference angle of attack as the full scale aircraft, F_{r_m} should equal F_{r_a}. Correct mass scaling is also required. Froude number equality results in the following expression for the ratio of aircraft and model velocity:

$$\frac{V_m}{V_a} = \sqrt{\lambda} . \sqrt{g_m/g_a} \qquad [A.9]$$

where

g_m = model gravity

g_a = aircraft gravity.

Equation [A.9] shows that the model velocity is dependent on the scale factor, λ, and the ratio of gravitational forces. Supporting part of the model weight allows a reduction in tunnel speed to simulate similar aircraft velocities.

A.6 Reynolds number.

The Reynolds Number, R_e, is the ratio of inertia to viscous forces and is defined as:

$$R_e = \frac{\rho . l_\mu . V}{\mu} \qquad [A.10]$$

where

μ = viscosity of air.

Using the relationship $\upsilon = \mu/\rho$, where υ is the coefficient of kinematic viscosity of air, enables R_e to be expressed as:

$$R_e = \frac{l_\mu V}{\upsilon}$$

Hence

$$\frac{Re_m}{Re_a} = \frac{l_{\mu m} . V_m}{l_{\mu a} . V_a} = \frac{l_{\mu m}}{l_{\mu a}} . \left(\lambda \frac{g_m}{g_a} \right)^{1/2}$$

If g_m is assumed equal to g_a then for the same altitude conditions

$$\frac{Re_m}{Re_a} = (\lambda)^{3/2} \qquad [A.11]$$

From this last equation, [A.11], it is clear that R_e can never be the same for the full scale aircraft and the scaled model because of the scale factor $\lambda^{3/2}$. To achieve both dynamic similarity and a reasonable test Reynolds number requires the use of very large models. Therefore it is common practice to just ensure that the value of R_e in the wind tunnel is higher than 0.4×10^6, which is the critical value at which the flow becomes turbulent.

A.7 Scaling of derivatives.

In order to directly compare the magnitudes of the stability and control derivatives, the derivatives are first expressed in a non-dimensional form and then further reduced to the concise form defined overleaf, Ref 39. The non-dimensional form of the equations of motion use these concise derivatives as well as a non-dimensional time, $\hat{t}$ and non-dimensional inertia parameters.

A.7.1 Non-dimensional mass and inertia.

Non-dimensional time $\hat{t}$ is given by :

$$\hat{t} = t/\tau$$

where

$$\tau = \frac{m}{0.5\rho V S} = \frac{V_e C_L}{g.\cos(\theta_e)}$$

The *aircraft longitudinal relative density parameter* is given by

$$\mu_1 = \frac{m}{0.5\rho S\bar{\bar{c}}} = \frac{V_\tau}{\bar{\bar{c}}}$$

where $\bar{\bar{c}}$ is the mean aerodynamic chord of the wing.

The *aircraft lateral relative density parameter* is given by

$$\mu_2 = \frac{m}{0.5\rho Sb} = \frac{V_\tau}{b}$$

where b is the wing span.

The non-dimensional inertia parameters are as follows:

non-dimensional rolling moment of inertia, $i_x = \frac{I_x}{mb^2}$

non-dimensional pitching moment of inertia, $i_y = \frac{I_y}{m\bar{\bar{c}}}$

non-dimensional yawing moment of inertia, $I_z = \frac{I_z}{mb^2}$

non-dimensional product of inertia about 0_x & 0_z, $i_{zx} = \frac{I_{zx}}{mb^2}$

A.7.2 Concise longitudinal derivatives.

concise form		non-dimensional form
$x_u = X_u.(-1)$	where	$X_u = \mathring{X}_u/0.5\rho VS$
$x_w = X_w.(-1)$	where	$X_w = \mathring{X}_w/0.5\rho VS$
$x_{\dot{w}} = X_{\dot{w}}.(-1/\mu_1)$	where	$X_{\dot{w}} = \mathring{X}_{\dot{w}}/0.5\rho S\bar{\bar{c}}$
$x_q = X_q.(-1/\mu_1)$	where	$X_q = \mathring{X}_q/0.5\rho VS\bar{\bar{c}}$
$x_\eta = X_\eta.(-1)$	where	$X_\eta = \mathring{X}_\eta/0.5\rho V^2S$
$z_u = Z_u.(-1)$	where	$Z_u = \mathring{Z}_u/0.5\rho VS$
$z_w = Z_w.(-1)$	where	$Z_w = \mathring{Z}_w/0.5\rho VS$
$z_{\dot{w}} = Z_{\dot{w}}.(-1/\mu_1)$	where	$Z_{\dot{w}} = \mathring{Z}_{\dot{w}}/0.5\rho S\bar{\bar{c}}$
$z_q = Z_q.(-1/\mu_1)$	where	$Z_q = \mathring{Z}_q/0.5\rho S\bar{\bar{c}}$
$z_\eta = Z_\eta.(-1)$	where	$Z_\eta = \mathring{Z}_\eta/0.5\rho V^2S$
$m_u = M_u.(-\mu_1/i_y)$	where	$M_u = \mathring{M}_u/0.5\rho VS\bar{\bar{c}}$
$m_w = M_w.(-\mu_1/i_y)$	where	$M_w = \mathring{M}_w/0.5\rho VS\bar{\bar{c}}$
$m_{\dot{w}} = M_{\dot{w}}.(-1/i_y)$	where	$M_{\dot{w}} = \mathring{M}_{\dot{w}}/0.5\rho S\bar{\bar{c}}^2$
$m_q = M_q.(-1/i_y)$	where	$M_q = \mathring{M}_q/0.5\rho VS\bar{\bar{c}}^2$
$m_\eta = M_\eta.(-\mu_1/i_y)$	where	$M_\eta = \mathring{M}_\eta/0.5\rho V^2S\bar{\bar{c}}$

A.7.3 Concise lateral derivatives.

concise form		non-dimensional form
$y_v = Y_v.(-1)$	where	$Y_v = \mathring{Y}_v/0.5\rho VS$
$y_p = Y_p.(-1/\mu_2)$	where	$Y_p = \mathring{Y}_p/0.5\rho VSb$
$y_r = Y_r.(-1/\mu_2)$	where	$Y_r = \mathring{Y}_r/0.5\rho VSb$
$y_\xi = Y_\xi.(-1)$	where	$Y_\xi = \mathring{Y}_\xi/0.5\rho V^2S$
$y_\zeta = Y_\zeta.(-1)$	where	$Y_\zeta = \mathring{Y}_\zeta/0.5\rho V^2S$
$l_v = L_v.(-\mu_2/i_x)$	where	$L_v = \mathring{L}_v/0.5\rho VSb$
$l_p = L_p.(-1/i_x)$	where	$L_p = \mathring{L}_p/0.5\rho VSb^2$
$l_r = L_r.(-1/i_x)$	where	$L_r = \mathring{L}_r/0.5\rho VSb^2$
$l_\xi = L_\xi.(-\mu_2/i_x)$	where	$L_\xi = \mathring{L}_\xi/0.5\rho V^2Sb$
$l_\zeta = L_\zeta.(-\mu_2/i_x)$	where	$L_\zeta = \mathring{L}_\zeta/0.5\rho V^2Sb$
$n_v = N_v.(-\mu_2/i_z)$	where	$N_v = \mathring{N}_v/0.5\rho VSb$
$n_p = N_p.(-1/i_z)$	where	$N_p = \mathring{N}_p/0.5\rho VSb^2$
$n_r = N_r.(-1/i_z)$	where	$N_r = \mathring{N}_r/0.5\rho VSb^2$
$n_\xi = N_\xi.(-\mu_2/i_z)$	where	$N_\xi = \mathring{N}_\xi/0.5\rho V^2Sb$
$n_\zeta = N_\zeta.(-\mu_2/i_z)$	where	$N_\zeta = \mathring{N}_\zeta/0.5\rho V^2Sb$

APPENDIX B

EQUATIONS OF MOTION

B.0 EQUATIONS OF MOTION.

This Appendix describes the longitudinal and lateral general dimensional equations of motion for the full scale aircraft. The reduced equations which should apply for the wind tunnel model are also given. In each case, the equations describing the longitudinal motion of an aircraft will be considered first, followed by the equations describing lateral motion. Finally, a review of longitudinal equations in which the inertial and aerodynamic responses of the Hawk model are separated is presented.

B.1 Full scale longitudinal equations of motion.

The general dimensional equations of longitudinal symmetric motion for small disturbances (when referred to body axes) may be written as follows (Ref 12),

$$m\dot{u} - \mathring{X}_u.u - \mathring{X}_w.w - \mathring{X}_{\dot{w}}.\dot{w} + (mW_e - \mathring{X}_q).q + mg_1.\theta = \mathring{X}_\eta.\eta \qquad [B.1]$$

$$-\mathring{Z}_u.u - \mathring{Z}_w.w + (m - \mathring{Z}_{\dot{w}}).\dot{w} - (mU_e + \mathring{Z}_q).q + mg_2.\theta = \mathring{Z}_\eta.\eta \qquad [B.2]$$

$$-\mathring{M}_u.u - \mathring{M}_w.w - \mathring{M}_{\dot{w}}.\dot{w} - \mathring{M}_q.q + I_y.\dot{q} = \mathring{M}_\eta.\eta \qquad [B.3]$$

where "$\circ$" denotes a dimensional coefficient;

In the special case of wind axes and level flight, $\theta_e = 0$ giving

$$g_1 = g\cos\theta_e = g \; ; \qquad g_2 = g\sin\theta_e = 0;$$

$$U_e = V\cos\alpha_e = V \; ; \qquad W_e = V\sin\alpha_e = 0;$$

If small perturbations are assumed then $\dot{\theta} = q$ is considered valid.

Equations [B.1] and [B.2] may be divided through by mass m and equation [B.3] by pitch inertia I_y. Re-arranging all three equations and combining them into a single matrix equation of the form

$M\dot{\underset{\sim}{x}} = A'\underset{\sim}{x} + B'\underset{\sim}{u}$ yields:

$$\begin{pmatrix} 1 & -\mathring{X}_{\dot{w}} & 0 & 0 \\ 0 & (1-\mathring{Z}_{\dot{w}}) & 0 & 0 \\ 0 & -\mathring{M}_{\dot{w}} & 1 & 0 \\ 0 & 0 & 0 & 1 \end{pmatrix} \begin{pmatrix} \dot{u} \\ \dot{w} \\ \dot{q} \\ \dot{\theta} \end{pmatrix} = \begin{pmatrix} \mathring{X}_u & \mathring{X}_w & (\mathring{X}_q - W_e) & -g \\ \mathring{Z}_u & \mathring{Z}_w & (\mathring{Z}_q + U_e) & 0 \\ \mathring{M}_u & \mathring{M}_w & \mathring{M}_q & 0 \\ 0 & 0 & 1 & 0 \end{pmatrix} \begin{pmatrix} u \\ w \\ q \\ \theta \end{pmatrix} + \begin{pmatrix} \mathring{X}_\eta \\ \mathring{Z}_\eta \\ \mathring{M}_\eta \\ 0 \end{pmatrix} (\eta) \qquad [B.4]$$

Pre-multiplying [B.4] by the inverse mass matrix M^{-1} yields equation [B.5], in the standard state space format of $\dot{\underset{\sim}{x}} = A\underset{\sim}{x} + B\underset{\sim}{u}$. Note: In this format $\dot{\underset{\sim}{x}}$ is the response output vector, $\underset{\sim}{x}$ is the state variable vector, $\underset{\sim}{u}$ is the input variable vector, A is the state matrix and B the input matrix.

$$\begin{pmatrix} \dot{u} \\ \dot{w} \\ \dot{q} \\ \dot{\theta} \end{pmatrix} = \begin{pmatrix} X_u & X_w & X_q & -g \\ Z_u & Z_w & Z_q & 0 \\ M_u & M_w & M_q & 0 \\ 0 & 0 & 1 & 0 \end{pmatrix} \begin{pmatrix} u \\ w \\ q \\ \theta \end{pmatrix} + \begin{pmatrix} X_\eta \\ Z_\eta \\ M_\eta \\ 0 \end{pmatrix} (\eta) \qquad [B.5]$$

where the normalised aerodynamic stability and control derivatives are defined as shown overleaf,

$$\mathring{x}_u = \mathring{X}_u/m \; ; \quad \mathring{x}_w = \mathring{X}_{\dot{w}}/m \; ; \quad \mathring{x}_w = \mathring{X}_w/m \; ; \quad \mathring{x}_q = \mathring{X}_q/m \; ; \quad \mathring{x}_\eta = \mathring{X}_\eta/m \; .$$

$$\mathring{z}_u = \mathring{Z}_u/m \; ; \quad \mathring{z}_w = \mathring{Z}_{\dot{w}}/m \; ; \quad \mathring{z}_w = \mathring{Z}_w/m \; ; \quad \mathring{z}_q = \mathring{Z}_q/m \; ; \quad \mathring{z}_\eta = \mathring{Z}_\eta/m \; .$$

$$\mathring{m}_u = \mathring{M}_u/I_y \; ; \quad \mathring{m}_w = \mathring{M}_{\dot{w}}/I_y \; ; \quad \mathring{m}_w = \mathring{M}_w/I_y \; ; \quad \mathring{m}_q = \mathring{M}_q/I_y \; ; \quad \mathring{m}_\eta = \mathring{M}_\eta/I_y \; .$$

The state matrix and input matrix derivative coefficients then follow,

$$X_u = \left(\frac{\mathring{x}_{\dot{w}} \mathring{z}_u}{(1-\mathring{z}_{\dot{w}})} + \mathring{x}_u \right); \quad X_w = \left(\frac{\mathring{x}_{\dot{w}} \mathring{z}_w}{(1-\mathring{z}_{\dot{w}})} + \mathring{x}_w \right); \quad X_q = \left(\frac{(U_e + \mathring{z}_q)\mathring{x}_{\dot{w}}}{(1-\mathring{z}_{\dot{w}})} + (\mathring{x}_q - W_e) \right);$$

$$Z_u = \left(\frac{\mathring{z}_u}{1-\mathring{z}_{\dot{w}}} \right); \quad Z_w = \left(\frac{\mathring{z}_w}{1-\mathring{z}_{\dot{w}}} \right); \quad Z_q = \left(\frac{U_e + \mathring{z}_q}{1-\mathring{z}_{\dot{w}}} \right);$$

$$M_u = \left(\frac{\mathring{m}_{\dot{w}} \mathring{z}_u}{(1-\mathring{z}_{\dot{w}})} + \mathring{m}_u \right); \quad M_w = \left(\frac{\mathring{m}_{\dot{w}} \mathring{z}_w}{(1-\mathring{z}_{\dot{w}})} + \mathring{m}_w \right); \quad M_q = \left(\frac{(U_e + \mathring{z}_q)\mathring{m}_{\dot{w}}}{(1-\mathring{z}_{\dot{w}})} + \mathring{m}_q \right);$$

$$X_\eta = \left(\frac{\mathring{x}_{\dot{w}} \mathring{z}_\eta}{(1-\mathring{z}_{\dot{w}})} + \mathring{x}_\eta \right); \quad Z_\eta = \left(\frac{\mathring{z}_\eta}{1-\mathring{z}_{\dot{w}}} \right); \quad M_\eta = \left(\frac{\mathring{m}_{\dot{w}} \mathring{z}_\eta}{(1-\mathring{z}_{\dot{w}})} + \mathring{m}_\eta \right);$$

B.2 Full scale lateral equations of motion.

The general dimensional equations of lateral asymmetric motion, referred to body axes, for small disturbances may be written as follows (Ref 12):

$$m\dot{v} - \mathring{Y}_v.v - (mW_e+\mathring{Y}_p)p + (mU_e-\mathring{Y}_r)r - mg_1\phi - mg_2\psi = \mathring{Y}_\xi.\xi + \mathring{Y}_\zeta.\xi \quad [B.6]$$

$$-\mathring{L}_v.v + I_x.\dot{p} - \mathring{L}_p.p - I_{xz}.\dot{r} - \mathring{L}_r.r = \mathring{L}_\xi.\xi + \mathring{L}_\zeta.\zeta \quad [B.7]$$

$$-\mathring{N}_v.v - I_{xz}.\dot{p} - \mathring{N}_p.p + I_z.\dot{r} - \mathring{N}_r.r = \mathring{N}_\xi.\xi + \mathring{N}_\zeta.\zeta \quad [B.8]$$

In the special case of wind axes and level flight, $\Theta_e = 0$ giving

$$g_1 = g\cos\Theta_e = g; \qquad g_2 = g\sin\Theta_e = 0;$$

Furthermore, when small perturbations are assumed the relationships below, [B.9],

$$\begin{pmatrix}\dot{\phi}\\ \dot{\theta}\\ \dot{\psi}\end{pmatrix} = \begin{pmatrix}1 & \sin\phi\tan\theta & \cos\phi\tan\theta\\ 0 & \cos\phi & -\sin\phi\\ 0 & \sin\phi\sec\theta & \cos\phi\sec\theta\end{pmatrix}.\begin{pmatrix}p\\ q\\ r\end{pmatrix} \quad [B.9]$$

reduce to $\dot{\phi} = p; \qquad \dot{\theta} = q; \qquad \dot{\psi} = r.$ [B.10]

Dividing equation [B.6] through by m, [B.7] by I_x, [B.8] by I_z and re-arranging gives equation [B.11] which is of the form

$$M.\dot{\underset{\sim}{x}} = A.'\underset{\sim}{x} + B'.\underset{\sim}{u}$$

$$\begin{pmatrix} 1 & 0 & 0 & 0 & 0 \\ 0 & 1 & -e_x & 0 & 0 \\ 0 & e_z & 1 & 0 & 0 \\ 0 & 0 & 0 & 1 & 0 \\ 0 & 0 & 0 & 0 & 1 \end{pmatrix} \begin{pmatrix} \dot{v} \\ \dot{p} \\ \dot{r} \\ \dot{\phi} \\ \dot{\psi} \end{pmatrix} = \begin{pmatrix} \mathring{y}_v & (\mathring{y}_p + W_e) & (\mathring{y}_r - U_e) & g & 0 \\ \mathring{l}_v & \mathring{l}_p & \mathring{l}_r & 0 & 0 \\ \mathring{n}_v & \mathring{n}_p & \mathring{n}_r & 0 & 0 \\ 0 & 1 & 0 & 0 & 0 \\ 0 & 0 & 1 & 0 & 0 \end{pmatrix} \begin{pmatrix} v \\ p \\ r \\ \phi \\ \psi \end{pmatrix} + \begin{pmatrix} \mathring{y}_\xi & \mathring{y}_\zeta \\ \mathring{l}_\xi & \mathring{l}_\zeta \\ \mathring{n}_\xi & \mathring{n}_\zeta \\ 0 & 0 \\ 0 & 0 \end{pmatrix} \begin{pmatrix} \xi \\ \zeta \end{pmatrix} \quad [B.11]$$

where the inertia ratios are,

$$e_x = I_{xz}/I_x \; ; \qquad e_z = I_{xz}/I_z \; .$$

Pre-multiplying [B.11] by the inverse mass matrix M^{-1} yields the lateral equations of motion (in the standard state variable form):

$$\begin{pmatrix} \dot{v} \\ \dot{p} \\ \dot{r} \\ \dot{\phi} \\ \dot{\psi} \end{pmatrix} = \begin{pmatrix} y_v & y_p & y_r & g & 0 \\ l_v & l_p & l_r & 0 & 0 \\ n_v & n_p & n_r & 0 & 0 \\ 0 & 1 & 0 & 0 & 0 \\ 0 & 0 & 1 & 0 & 0 \end{pmatrix} \begin{pmatrix} v \\ p \\ r \\ \phi \\ \psi \end{pmatrix} + \begin{pmatrix} y_\xi & y_\zeta \\ l_\xi & l_\zeta \\ n_\xi & n_\zeta \\ 0 & 0 \\ 0 & 0 \end{pmatrix} \begin{pmatrix} \xi \\ \zeta \end{pmatrix} \quad [B.12]$$

where the normalised aerodynamic stability and control derivatives are given by,

$$\mathring{y}_v = \mathring{Y}_v/m \; ; \qquad \mathring{y}_p = \mathring{Y}_p/m \; ; \qquad \mathring{y}_r = \mathring{Y}_r/m \; ; \qquad \mathring{y}_\xi = \mathring{Y}_\xi/m \; ; \qquad \mathring{y}_\zeta = \mathring{Y}_\zeta/m \; ;$$

$$\mathring{l}_v = \mathring{L}_v/I_x \; ; \qquad \mathring{l}_p = \mathring{L}_p/I_x \; ; \qquad \mathring{l}_r = \mathring{L}_r/I_x \; ; \qquad \mathring{l}_\xi = \mathring{L}_\xi/I_x \; ; \qquad \mathring{l}_\zeta = \mathring{L}_\zeta/I_x \; ;$$

$$\mathring{n}_v = \mathring{N}_v/I_z \; ; \qquad \mathring{n}_p = \mathring{N}_p/I_z \; ; \qquad \mathring{n}_r = \mathring{N}_r/I_z \; ; \qquad \mathring{n}_\xi = \mathring{N}_\xi/I_z \; ; \qquad \mathring{n}_\zeta = \mathring{N}_\zeta/I_z \; ;$$

$$e_x = I_{xz}/I_x \; ; \qquad e_z = I_{xz}/I_z \; ; \qquad E_{xz} = 1 + e_x e_z \; ;$$

$$y_v = \mathring{y}_v \; ; \qquad y_p = (\mathring{y}_p + W_e) \; ; \qquad y_r = (\mathring{y}_r - U_e) \; ;$$

whence the state matrix and input matrix derivative coefficients are

$$l_v = \left\{ \frac{\mathring{l}_v}{E_{xz}} + \frac{e_x \mathring{n}_v}{E_{xz}} \right\} ; \qquad l_p = \left\{ \frac{\mathring{l}_p}{E_{xz}} + \frac{e_x \mathring{l}_p}{E_{xz}} \right\} ; \qquad l_r = \left\{ \frac{\mathring{l}_r}{E_{xz}} + \frac{e_x \mathring{l}_r}{E_{xz}} \right\} ;$$

$$n_v = \left\{ \frac{-e_z \mathring{l}_v}{E_{xz}} + \frac{\mathring{n}_v}{E_{xz}} \right\} ; \qquad n_p = \left\{ \frac{-e_z \mathring{l}_p}{E_{xz}} + \frac{\mathring{n}_p}{E_{xz}} \right\} ; \qquad n_r = \left\{ \frac{-e_z \mathring{l}_r}{E_{xz}} + \frac{\mathring{n}_r}{E_{xz}} \right\} ;$$

$$y_\xi = \mathring{y}_\xi ; \qquad l_\xi = \left\{ \frac{\mathring{l}_\xi}{E_{xz}} + \frac{e_x \mathring{n}_\xi}{E_{xz}} \right\} ; \qquad l_\zeta = \left\{ \frac{\mathring{l}_\zeta}{E_{xz}} + \frac{e_x \mathring{n}_\zeta}{E_{xz}} \right\} ;$$

$$y_\zeta = \mathring{y}_\zeta ; \qquad n_z = \left\{ \frac{-e_z \mathring{l}_\xi}{E_{xz}} + \frac{\mathring{n}_\xi}{E_{xz}} \right\} ; \qquad n_\zeta = \left\{ \frac{-e_z \mathring{l}_\zeta}{E_{xz}} + \frac{\mathring{n}_\zeta}{E_{xz}} \right\} ;$$

B.3 Hawk model reduced equations of longitudinal motion.

One method of reducing the full scale equations of motion is presented below. (Alternative methods are presented in section B.5 and Chapter 14) .Equations [B.1], [B.2] and [B.3] are for an aircraft in free flight. However, the experimental dynamic rig is such that when the Hawk model is flown in the wind tunnel longitudinal translation of the aircraft is suppressed. This means that [B.3] may be removed completely from the normal equations of motion governing free flight. Further, when considering wind axes (rather than body axes) and assuming that the wind tunnel speed remains constant

(i.e. u = 0), the following conditions may be assumed,

$$\alpha_e = W_e = 0 \qquad u = 0$$

$$U_e = V\cos 0 = V \qquad \dot{u} = 0$$

In the case of horizontal steady flight, it may also be assumed that

$$\theta_e = \alpha_e = W_e = 0$$

giving

$$g_1 = g \quad \text{and} \quad g_2 = 0.$$

Thus the reduced dimensional equations for semi-free flight are given by:

$$-\mathring{Z}_w.w + (m-\mathring{Z}_{\dot{w}}).\dot{w} - (mU_e+\mathring{Z}_q).q = \mathring{Z}_\eta.\eta \qquad [B.13]$$

$$-\mathring{M}_w.w - \mathring{M}_{\dot{w}}.\dot{w} - \mathring{M}_q.q + I_y.\dot{q} = \mathring{M}_\eta.\eta \qquad [B.14]$$

and these equations may be rearranged to give

$$(m-\mathring{Z}_{\dot{w}})\dot{w} = \mathring{Z}_w.w + (mU_e + \mathring{Z}_q).q + \mathring{Z}_\eta.\eta \qquad [B.15]$$

$$-\mathring{M}_{\dot{w}}.\dot{w} + I_y.\dot{q} = \mathring{M}_w.w + \mathring{M}_q.q + \mathring{M}_\eta.\eta \qquad [B.16]$$

It is often convenient to re-arrange these equations into a more manageable reduced form by dividing the force equation [B.15] by the aircraft mass m and the moment equation [B.16] by the pitch inertia I_y to obtain

$$(1-\mathring{Z}_{\dot{w}})\dot{w} = \mathring{z}_w.w + (U_e+\mathring{z}_q)q + \mathring{z}_\eta.\eta \qquad [B.17]$$

$$-\mathring{m}_{\dot{w}}.\dot{w} + \dot{q} = \mathring{m}_w.w + \mathring{m}_q.q + \mathring{m}_\eta.\eta \qquad [B.18]$$

where,

$$\mathring{z}_{\dot{w}} = \frac{\mathring{Z}_{\dot{w}}}{m}; \quad \mathring{z}_w = \frac{\mathring{Z}_w}{m}; \quad \text{etc.} \quad \text{and,} \quad \mathring{m}_{\dot{w}} = \frac{\mathring{M}_{\dot{w}}}{I_y}; \quad \mathring{m}_w = \frac{\mathring{M}_w}{I_y}; \quad \text{etc.}$$

Assuming small perturbations, [B.17] and [B.18] may also be expressed in the matrix form $M.\dot{\underset{\sim}{x}} = A.'\underset{\sim}{x} + B'.\underset{\sim}{u}$, as follows:

$$\begin{pmatrix} (1-\mathring{z}_{\dot{w}}) & 0 & 0 \\ -\mathring{m}_{\dot{w}} & 1 & 0 \\ 0 & 0 & 1 \end{pmatrix} . \begin{pmatrix} \dot{w} \\ \dot{q} \\ \dot{\theta} \end{pmatrix} = \begin{pmatrix} \mathring{z}_{w} & (u_e + \mathring{z}_{q}) & 0 \\ \mathring{m}_{w} & \mathring{m}_{q} & 0 \\ 0 & 1 & 0 \end{pmatrix} . \begin{pmatrix} w \\ q \\ \theta \end{pmatrix} + \begin{pmatrix} \mathring{z}_{\eta} \\ \mathring{m}_{\eta} \\ 0 \end{pmatrix} . (\eta) \qquad [B.19]$$

The inverse of the mass matrix M is given by

$$M^{-1} = \begin{pmatrix} \dfrac{1}{(1-\mathring{z}_{\dot{w}})} & 0 & 0 \\ \dfrac{\mathring{m}_{\dot{w}}}{(1-\mathring{z}_{\dot{w}})} & 1 & 0 \\ 0 & 0 & 1 \end{pmatrix}$$

Thus premultiplying [B.19] through by M^{-1} leads to the reduced order equations of longitudinal motion in a standard state variable form:

$$\begin{pmatrix} \dot{w} \\ \dot{q} \\ \dot{\theta} \end{pmatrix} = \begin{pmatrix} z_w & z_q & 0 \\ m_w & m_q & 0 \\ 0 & 1 & 0 \end{pmatrix} . \begin{pmatrix} w \\ q \\ \theta \end{pmatrix} + \begin{pmatrix} z_{\eta} \\ m_{\eta} \\ 0 \end{pmatrix} (\eta) \qquad [B.20]$$

where,

$$z_w = \left(\frac{\mathring{z}_w}{1-\mathring{z}_{\dot{w}}}\right); \qquad z_q = \left(\frac{u_e + \mathring{z}_q}{1-\mathring{z}_{\dot{w}}}\right); \qquad z_{\eta} = \left(\frac{\mathring{z}_{\eta}}{1-\mathring{z}_{\dot{w}}}\right);$$

and,

$$m_w = \left(\frac{\mathring{m}_{\dot{w}}\mathring{z}_w}{(1-\mathring{z}_{\dot{w}})} + \mathring{m}_w\right); \quad m_q = \left(\frac{(u_e + \mathring{z}_q)\mathring{m}_{\dot{w}}}{(1-\mathring{z}_{\dot{w}})} + \mathring{m}_q\right); \quad m_{\eta} = \left(\frac{\mathring{m}_{\dot{w}}\mathring{z}_{\eta}}{(1-\mathring{z}_{\dot{w}})} + \mathring{m}_{\eta}\right);$$

B.4 Hawk model reduced equations of lateral motion.

Equations [B.6], [B.7] and [B.8] are for an aircraft in free flight. However in the case of semi-free flight in the wind tunnel equation [B.6] may be removed as lateral translation of the aircraft model is suppressed, thus giving:

$$-\mathring{L}_v.v + I_x.\dot{p} - \mathring{L}_p.p - I_{xz}.\dot{r} - \mathring{L}_r.r = \mathring{L}(t) \qquad [B.21]$$

$$-\mathring{N}_v.v + I_{xz}\dot{p} - \mathring{N}_p.p - I_z.\ \dot{r} - \mathring{N}_r.r = \mathring{N}(t) \qquad [B.22]$$

Note: The terms $-\mathring{L}_v.v$ and $-\mathring{N}_v.v$ have still been retained as in this experimental work the sideslip angle and yaw angle may be taken to be equivalent.

To reduce these equations still further, [B.21] can be divided through by I_x, [B.22] divided through by I_z and both equations re-arranged to give

$$\dot{p} - e_x\dot{r} = \mathring{l}_v v + \mathring{l}_p p + \mathring{l}_r r + \mathring{l}_\xi \xi + \mathring{l}_\zeta \zeta \qquad [B.23]$$

$$e_z\dot{p} + \dot{r} = \mathring{n}_v v + \mathring{n}_p p + \mathring{n}_r r + \mathring{n}_\xi \xi + \mathring{n}_\zeta \zeta \qquad [B.24]$$

where,

$$e_x = I_{xz}/I_x; \qquad \mathring{l}_v = \mathring{L}_v/I_x; \qquad \mathring{l}_p = \mathring{L}_p/I_x; \qquad \text{etc.}$$

and,

$$e_z = I_{xz}/I_z; \qquad \mathring{n}_v = \mathring{N}_v/I_z; \qquad \mathring{n}_p = \mathring{N}_p/I_x; \qquad \text{etc.}$$

The absolute lateral acceleration of an aircraft may be expressed as follows, Ref 25:

$$a_y = \dot{v} - pW_e + rU_e$$

The dynamic model aircraft is free to rotate in yaw but there is no translation in the y-direction so that the aerodynamic sideforces and gravity components are balanced by the support system. However, the fact that dy/dt = 0 implies that the lateral acceleration is given by,

$$\dot{v} - pW_e + rU_e = 0 \qquad [B.25]$$

Hence, the lateral equations of motion, with respect to wind tunnel simulations for steady horizontal datum flight, may be incorporated together and expressed in matrix form as

$$\begin{pmatrix} 1 & 0 & 0 & 0 & 0 \\ 0 & 1 & -e_x & 0 & 0 \\ 0 & e_z & 1 & 0 & 0 \\ 0 & 0 & 0 & 1 & 0 \\ 0 & 0 & 0 & 0 & 1 \end{pmatrix} \cdot \begin{pmatrix} \dot{v} \\ \dot{p} \\ \dot{r} \\ \dot{\phi} \\ \dot{\psi} \end{pmatrix} = \begin{pmatrix} 0 & W_e & -U_e & 0 & 0 \\ \mathring{l}_v & \mathring{l}_p & \mathring{l}_r & 0 & 0 \\ \mathring{n}_v & \mathring{n}_p & \mathring{n}_r & 0 & 0 \\ 0 & 1 & 0 & 0 & 0 \\ 0 & 0 & 1 & 0 & 0 \end{pmatrix} \cdot \begin{pmatrix} v \\ p \\ r \\ \phi \\ \psi \end{pmatrix} + \begin{pmatrix} 0 & 0 \\ \mathring{l}_\xi & \mathring{l}_\zeta \\ \mathring{n}_\xi & \mathring{n}_\zeta \\ 0 & 0 \\ 0 & 0 \end{pmatrix} \cdot \begin{pmatrix} \xi \\ \zeta \end{pmatrix} \qquad [B.26]$$

This equation is of the form $M\dot{\underline{x}} = A\underline{x} + B\underline{u}$, with mass matrix M which is given by,

$$M = \begin{pmatrix} 1 & 0 & 0 & 0 & 0 \\ 0 & 1 & -e_x & 0 & 0 \\ 0 & e_z & 1 & 0 & 0 \\ 0 & 0 & 0 & 1 & 0 \\ 0 & 0 & 0 & 0 & 1 \end{pmatrix}$$

The inverse mass matrix M^{-1} is thus

$$M^{-1} = \begin{pmatrix} 1 & 0 & 0 & 0 & 0 \\ 0 & 1/(1+e_x e_z) & e_z/(1+e_x e_z) & 0 & 0 \\ 0 & -e_x/(1+e_x e_z) & 1/(1+e_x e_z) & 0 & 0 \\ 0 & 0 & 0 & 1 & 0 \\ 0 & 0 & 0 & 0 & 1 \end{pmatrix}$$

Pre-multiplying equation [B.26] by M^{-1} yields the final reduced model equations of motion in a standard state variable form:

$$\begin{pmatrix} \dot{v} \\ \dot{p} \\ \dot{r} \\ \dot{\phi} \\ \dot{\Psi} \end{pmatrix} = \begin{pmatrix} 0 & w_e & -u_e & 0 & 0 \\ l_v & l_p & l_r & 0 & 0 \\ n_v & n_p & n_r & 0 & 0 \\ 0 & 1 & 0 & 0 & 0 \\ 0 & 0 & 1 & 0 & 0 \end{pmatrix} . \begin{pmatrix} v \\ p \\ r \\ \phi \\ \Psi \end{pmatrix} + \begin{pmatrix} 0 & 0 \\ l_\xi & l_\zeta \\ n_\xi & n_\zeta \\ 0 & 0 \\ 0 & 0 \end{pmatrix} \begin{pmatrix} \xi \\ \zeta \end{pmatrix} \qquad [B.27]$$

where

$$E_{xz} = 1 + e_x e_z$$

$$l_v = \left\{ \frac{\overset{\circ}{l}_v}{E_{xz}} + \frac{e_x \overset{\circ}{n}_v}{E_{xz}} \right\} ; \quad l_p = \left\{ \frac{\overset{\circ}{l}_p}{E_{xz}} + \frac{e_x \overset{\circ}{l}_p}{E_{xz}} \right\} ; \quad l_r = \left\{ \frac{\overset{\circ}{l}_r}{E_{xz}} + \frac{e_x \overset{\circ}{l}_r}{E_{xz}} \right\} ;$$

$$n_v = \left\{ \frac{-e_z \overset{\circ}{l}_v}{E_{xz}} + \frac{\overset{\circ}{n}_v}{E_{xz}} \right\} ; \quad n_p = \left\{ \frac{-e_z \overset{\circ}{l}_p}{E_{xz}} + \frac{\overset{\circ}{n}_p}{E_{xz}} \right\} ; \quad n_r = \left\{ \frac{-e_z \overset{\circ}{l}_r}{E_{xz}} + \frac{\overset{\circ}{n}_r}{E_{xz}} \right\} ;$$

$$l_\xi = \left\{ \frac{\overset{\circ}{l}_\xi}{E_{xz}} + \frac{e_x \overset{\circ}{n}_\xi}{E_{xz}} \right\} ; \qquad l_\zeta = \left\{ \frac{\overset{\circ}{l}_\zeta}{E_{xz}} + \frac{e_x \overset{\circ}{n}_\zeta}{E_{xz}} \right\} ;$$

$$n_\xi = \left\{ \frac{-e_z \overset{\circ}{l}_\xi}{E_{xz}} + \frac{\overset{\circ}{n}_\xi}{E_{xz}} \right\} ; \qquad n_\zeta = \left\{ \frac{-e_z \overset{\circ}{l}_\zeta}{E_{xz}} + \frac{\overset{\circ}{n}_\zeta}{E_{xz}} \right\}$$

B.5 Review of model longitudinal equations of motion.

The longitudinal equations of motion [B.1 - B.3] may be expressed:

$$m.\dot{u} = \mathring{X}_u.u + \mathring{X}_w.w - (mW_e - \mathring{X}_q).q + \theta.m.g.\cos\alpha + \mathring{X}_\eta.\eta \qquad [B.28]$$

$$m.\dot{w} = \mathring{Z}_u.u + \mathring{Z}_w.w + (mU_e + \mathring{Z}_q).q - \theta.m.g.\sin\alpha + \mathring{Z}_\eta.\eta \qquad [B.29]$$

$$I_y\dot{q} = \mathring{M}_u.u + \mathring{M}_w.w + \mathring{M}_{\dot{w}}.\dot{w} + \mathring{M}_q.q \qquad + \mathring{M}_\eta.\eta \qquad [B.30]$$

In the wind tunnel, consider the case where the Hawk model is allowed some freedom in heave. It may be assumed that the velocities u and w each consist of two components, the first one being related to inertial velocity disturbances (denoted $\underline{u} = \int\dot{\underline{u}}$ and $\underline{w} = \int\dot{\underline{w}}$ in each axis) and the second being the component of wind velocity which arises from angular perturbations (denoted u_θ and w_θ in each axis). Thus the perturbed velocities may written,

$$u = \underline{u} + u_\theta \;; \qquad w = \underline{w} + w_\theta$$

It is thus necessary to define suitable expressions for the above terms. These wind tunnel perturbed velocity relationships may be derived as follows.

It may be shown that the perturbation velocity along O_x is given by

$$U = (U_e + u)$$

where

$$u = \underline{u} + u_\theta \;.$$

Hence in the wind tunnel, where $\underline{u} = 0$, this velocity can be written

$$U = U_e + u_\theta \qquad [B.31]$$

Further,

$$U_e = V_e \cos\alpha_e \qquad [B.32]$$

and

$$W_e = V_e \sin\alpha_e \qquad [B.33]$$

Thus combining B.31 and B.32 gives:

$$U_e + u_\theta = V_e \cos(\alpha_e + \theta)$$

and

$$u_\theta = V_e.\cos(\alpha_e + \theta) - V_e.\cos\alpha_e$$

or

$$u_\theta = V_e\{\cos\alpha_e.\cos\theta - \sin\alpha_e.\sin\theta - \cos\alpha_e\}$$

For small perturbations of θ, $\cos\theta \to 1$ and $\sin\theta \to \theta$, this reduces to

$$u_\theta = V_e\{\cos\alpha_e.1 - \sin\alpha_e.\theta - \cos\alpha_e\} \qquad [B.34]$$

Hence $$u_\theta = -V_e.\sin\alpha_e.\theta \qquad [B.35]$$

Vertical velocity may be expressed as $W = W_e + w$ where $w = \underline{w} + w_\theta$

Therefore if the model is restrained in height, $\underline{w}$ is equal to 0 giving:

$$W = W_e + w_\theta \qquad [B.36]$$

Thus combining [B.33] and [B.36] yields:

$$W_e + w_\theta = V_e.\sin(\alpha_e + \theta)$$

$$w_\theta = V_e\{\sin\alpha_e.\cos\theta + \cos\alpha_e.\sin\theta - \sin\alpha_e\}$$

Assuming small θ, $\cos\theta \to 1$ and $\sin\theta \to \theta$, giving:

$$w_\theta = V_e\{\sin\alpha_e.1 + \cos\alpha_e.\theta - \sin\alpha_e\}$$

and hence

$$w_\theta = V_e.\cos\alpha_e.\theta \qquad [B.37]$$

Differentiating [B.37] yields

$$\dot{w}_\theta = V_e.\cos\alpha_e.\dot{\theta} \quad \text{or} \quad \dot{w}_\theta = V_e.\cos\alpha_e.q \qquad [B.38]$$

Further, if $\alpha_e = 0$:

$$\dot{w} = q.V_e \qquad [B.39]$$

Returning to the longitudinal equations of motion [B.28, B.29, B.30], it is realised that in the wind tunnel, with longitudinal translation suppressed,equation B.28 may be removed since $u = \underline{\dot{u}} = 0$. Thus, the equations become

$$m.\underline{\dot{w}} = \mathring{Z}_u.u_\theta + \mathring{Z}_w.(\underline{w} + w_\theta) + (mU_e + \mathring{Z}_q).\underline{q} - \theta.mg\sin\alpha + \mathring{Z}_\eta.\eta \qquad [B.40]$$

$$I_y\underline{\dot{q}} = \mathring{M}_u.u_\theta + \mathring{M}_w.(\underline{w} + w_\theta) + \mathring{M}_{\dot{w}}.(\underline{\dot{w}} + \dot{w}_\theta) + \mathring{M}_q.\underline{q} + \mathring{M}_\eta.\eta \qquad [B.41]$$

Furthermore, if the Hawk model is further restrained in height, by collars above and below the gimbal, whilst on the experimental rig, equation [B.40] may also be removed and [B.41] reduced to the following expression:

$$I_y.\dot{\underline{q}} = \mathring{M}_u.u_\theta + \mathring{M}_w.w_\theta + \mathring{M}_{\dot{w}}.\dot{w}_\theta + \mathring{M}_q.\underline{q} + \mathring{M}_\eta.\eta \qquad [B.42]$$

Summarizing the wind tunnel relationships derived above, i.e.,

$$U_e = V_e\cos\alpha_e \qquad u_\theta = -V_e\sin\alpha_e.\theta$$

$$W_e = V_e\sin\alpha_e \qquad w_\theta = V_e\cos\alpha_e.\theta$$

$$\dot{w}_\theta = V_e\cos\alpha_e.\dot{\theta}$$

where V_e = tunnel speed and α_e = trim incidence

and substituting them into [B.42] leads to:

$$I_y\dot{\underline{q}} = (-\mathring{M}_u.W_e + \mathring{M}_w.U_e).\theta + (\mathring{M}_{\dot{w}}.U_e + \mathring{M}_q).\underline{q} + \mathring{M}_\eta.\eta \qquad [B.43]$$

or

$$I_y\dot{\underline{q}} = (-\mathring{M}_u V_e\sin\alpha_e + \mathring{M}_w V_e\cos\alpha_e)\theta + (\mathring{M}_{\dot{w}}.V_e\cos\alpha_e + \mathring{M}_q)\underline{q} + \mathring{M}_\eta\eta \qquad [B.44]$$

Further for wind axes where $\alpha_e = 0$, this equation may be written

$$I_y\dot{\underline{q}} = (-\mathring{M}_u.V_e).\theta + (\mathring{M}_{\dot{w}}.V_e).\underline{q} + \mathring{M}_\eta.\eta \qquad [B.45]$$

APPENDIX C

FIXED WEYBRIDGE WIND TUNNEL AND HAWK MODEL DATA

C.0 FIXED WEYBRIDGE WIND TUNNEL AND HAWK MODEL DATA

This Appendix presents various fixed parameters for the Weybridge low speed wind tunnel and the 1/12th scale BAe Hawk model. The conversion required from mm of water of the Betz manometer to the wind tunnel speed in m/s is also described.

C.1 Weybridge wind tunnel data.

Jet diameter	= 42" ≡ 1.067 m
Length of jet	= 60" ≡ 1.524 m
Collector diameter	= 50" ≡ 1.270 m
Fan diameter	= 48" ≡ 1.219 m
Maximum contraction ratio	= 4.4
Maximum H.P. of fan motor	= 35
Maximum tunnel speed	= 130 ft/sec ≡ 39.6 m/s

Wind tunnel pressure ΔP_{Betz} = 1.015 * dynamic pressure

C.2 Measurement of wind tunnel speed.

The wind tunnel speed is recorded during experiments using a Betz manometer which indicates a level of H_2O , h (mm). To convert to actual wind tunnel speed, V (in m/s) the dynamic pressure q (equal to $0.5\rho_o V^2$) is equated to the Betz water level which measures the wind tunnel pressure difference using $\Delta P_{betz} = \rho gh$. The Weybridge pressure calibration is assumed to be constant and is given by $\Delta P_{betz} = 1.015.q$.

Thus the following conversion formula may be derived:

$$V^2 = \frac{2\rho gh}{1.015\rho_o} \qquad [C.1]$$

where

ρ = water density = 1000 kg/m^3

g = gravitational acceleration = 9.81 m/s^2

ρ_o= sea level (SL) air density = 1.225 kg/m^3

Finally, substituting the appropriate values into equation C1 yields:

$$V^2 = \frac{(hx10^{-3}).(2).(1000).(9.81)}{(1.015).(1.225)}$$

Hence enabling the wind tunnel speed to calculated using the formula:

$$V^2 = (h).(15.78) \qquad [C2]$$

C.3 Fixed Hawk model aircraft data.

Gross wing area (S)	= 0.115 m^2
Root chord	= 0.221 m
Tip chord	= 0.075 m
Wing span	= 0.782 m
Mean geometric chord ($\bar{c}$)	= 0.148 m
Aerodynamic mean chord ($\bar{\bar{c}}$)	= 0.148 m
Reference MAC ($\bar{\bar{c}}_{ref}$)	= 0.148 m
Tailplane gross area (S_t)	= 0.029 m^2
Tailplane moment arm (l_t)	= 0.358 m

TEM pivot point (h_p) = $0.797\bar{c} \equiv$ 118 mm aft of reference line.

Centre of gravity (h) = $0.686\bar{c} \equiv$ 101.5 mm aft of reference line.

Note: The "reference line" mentioned above was taken from the point of intersection of the wing leading edge and fuselage.

APPENDIX D

ESTIMATION OF FULL SCALE HAWK DERIVATIVES

D.0 ESTIMATION OF FULL SCALE HAWK DERIVATIVES.

To estimate a set of stability and control derivatives for the full scale Hawk aircraft a BAe document giving graphical details of various performance and stability and control data was used, Ref 29. A flight case was chosen which fell into the limited flight envelope which can be produced by the dynamic rig in the wind tunnel. Details of the flight case chosen and the estimation of the various dimensional derivatives is presented below.

D.1 Flight case definition and Hawk design details.

A/C SPEED: M = 0.31 (i.e. V =105.5m/sec)

A/C MASS: m = 9000 lb (i.e. m = 4082.4kg)

A/C HEIGHT: Sea Level

A/C C.G. at: $h = 0.275\ \bar{\bar{c}}$

WING AREA $s = 179.635\ ft^2$ $=16.6887 m^2$

WING SPAN $b = 30.808\ ft$ $=9.3903m$

HORIZONTAL TAIL ARM $\bar{l}_T = 14.109\ ft$ $=4.299m$

INCLINATION OF FUSELAGE DATUM TO AIRSTREAM $\alpha_f = 4^\circ$

MOMENT OF INERTIA ABOUT LONGITUDINAL, LATERAL AND VERTICAL BODY AXES:

I_X $=5346.7 kg/m^2$

I_y $=19534.4 kg/m^2$

I_z $=23786.5 kg/m^2$

PRODUCT OF INERTIA I_{xz} $=816.74 kg/m^2$

D.1.1 Conversion factors.

1. ρVS = 2156.81 kgm/sec

2. $\rho VS\bar{l}_T$ = 9272.11 kgm/sec

3. ρV^2S = 227543.02 kgm/sec^2

4. $\rho S(\bar{l}_T)^2$ = 377.83 kgm

5. $\rho VS(\bar{l}_T)^2$ = 39860.79 kgm^2/sec

6. $\rho V^2S\bar{l}_T$ = 978207.43 kgm^2/sec^2

7. $(1/2)\rho VSb$ = 10126.53 kgm/sec

8. $(1/2)\rho V^2Sb$ = 1068348.60 kgm^2/sec^2

9. $(1/4)\rho VSb^2$ = 47545.56 kgm^2/sec

D.2 Longitudinal derivatives and modes of motion.

$\mathring{X}_u = X_u * \rho VS$	=	-64.71	kg/sec	$\Rightarrow$	$x_u = -0.016$
$\mathring{X}_{\dot{w}} = X_{\dot{w}} * \rho S\bar{l}_T$	=	0.0	kg	$\Rightarrow$	$x_{\dot{w}} = 0.0$
$\mathring{X}_w = X_w * \rho VS$	=	+107.841	kg/sec	$\Rightarrow$	$x_w = 0.026$
$\mathring{X}_q = X_q * \rho VS\bar{l}_T$	=	0.0	kgm/sec	$\Rightarrow$	$x_q = 0.0$
$\mathring{X}_\eta = X_\eta * \rho V^2S$	=	0.0	kgm/sec^2	$\Rightarrow$	$x_\eta = 0.0$

$\mathring{Z}_u = Z_u * \rho VS$	=	-884.37	kg/sec	$\Rightarrow$	$z_u = -0.217$
$\mathring{Z}_{\dot{w}} = Z_{\dot{w}} * \rho S\bar{l}_T$	=	0.0	kg	$\Rightarrow$	$z_{\dot{w}} = 0.0$
$\mathring{Z}_w = Z_w * \rho VS$	=	-5478.297	kg/sec	$\Rightarrow$	$z_w = -1.342$
$\mathring{Z}_q = Z_q * \rho VS\bar{l}_T$	=	-5628.104	kgm/sec	$\Rightarrow$	$z_q = -1.379$
$\mathring{Z}_\eta = Z_\eta * \rho V^2S$	=	-89196.856	kgm/sec^2	$\Rightarrow$	$z_\eta = -21.849$

$$\mathring{M}_u = M_u * \rho V S \bar{l}_T = -120.536 \text{ kgm/sec} \Rightarrow m_u = -0.005$$

$$\mathring{M}_{\dot{w}} = M_{\dot{w}} * \rho S (\bar{l}_T)^2 = -92.19 \text{ kgm} \Rightarrow m_{\dot{w}} = -0.0047$$

$$\mathring{M}_w = M_w * \rho V S \bar{l}_T = -1066.292 \text{ kgm/sec} \Rightarrow m_w = -0.048$$

$$\mathring{M}_q = M_q * \rho V S (\bar{l}_T)^2 = -23039.658 \text{ kgm}^2\text{/sec} \Rightarrow m_q = -1.669$$

$$\mathring{M}_\eta = M_\eta * \rho V^2 S \bar{l}_T = -383457.144 \text{ kgm}^2\text{/sec}^2 \Rightarrow m_\eta = -19.527$$

D.2.1 Longitudinal motion characteristic equation.

$$\Delta(s) = s^4 + 3.034s^3 + 7.876s^2 + 0.096s + 0.046 = 0$$

D.2.2 Short period pitching oscillation.

$$(s^2 + 2\rho_{sp}\omega_{sp}s + \omega_{sp}^2) = 0$$

$$\omega_{sp} = 2.8 \text{ rad/sec}$$

$$\rho_{sp} = 0.54$$

$$s = (-1.512 \pm 2.357i)$$

D.2.3 Phugoid oscillation.

$$(s^2 + 2\rho_p\omega_p s + \omega_p^2) = 0$$

$$\omega_p = 0.077 \text{ rad/sec}$$

$$\rho_p = 0.065$$

$$s = (-0.005 \pm 0.077i)$$

D.3 Lateral derivatives and modes of motion.

$\mathring{Y}_v = Y_v * \rho VS = -864.879$ kg/sec $\Rightarrow$ $y_v = -0.212$

$\mathring{Y}_p = Y_p * (1/2)\rho VSb = 0.0$ kgm/sec $\Rightarrow$ $y_p = 0.0$

$\mathring{Y}_r = Y_r * (1/2)\rho VSb = 0.0$ kgm/sec $\Rightarrow$ $y_r = 0.0$

$\mathring{Y}_\xi = Y_\xi * \rho V^2 S = 0.0$ kgm/sec^2 $\Rightarrow$ $y_\xi = 0.0$

$\mathring{Y}_\zeta = Y_\zeta * \rho V^2 S = -31173.394$ kgm/sec^2 $\Rightarrow$ $y_\zeta = +7.636$

$\mathring{L}_v = L_v * (1/2)\rho VSb = -486.073$ kgm/sec $\Rightarrow$ $l_v = -0.085$

$\mathring{L}_p = L_p * (1/4)\rho VSb^2 = -20206.865$ kgm^2/sec $\Rightarrow$ $l_p = -3.780$

$\mathring{L}_r = L_r * (1/4)\rho VSb^2 = +5943.196$ kgm^2/sec $\Rightarrow$ $l_r = +1.038$

$\mathring{L}_\xi = L_\xi * (1/2)\rho V^2 Sb = -188136.189$ kgm^2/sec^2 $\Rightarrow$ $l_\xi = -34.842$

$\mathring{L}_\zeta = L_\zeta * (1/2)\rho V^2 Sb = +30982.109$ kgm^2/sec^2 $\Rightarrow$ $l_\zeta = +5.075$

$\mathring{N}_v = N_v * (1/2)\rho VSb = +875.945$ kgm/sec $\Rightarrow$ $n_v = +0.040$

$\mathring{N}_p = N_p * (1/4)\rho VSb^2 = -3138.007$ kgm^2/sec $\Rightarrow$ $n_p = -0.002$

$\mathring{N}_r = N_r * (1/4)\rho VSb^2 = -10550.361$ kgm^2/sec $\Rightarrow$ $n_r = -0.479$

$\mathring{N}_\xi = N_\xi * (1/2)\rho V^2 Sb = +25640.366$ kgm^2/sec^2 $\Rightarrow$ $n_\xi = +2.274$

$\mathring{N}_\zeta = N_\zeta * (1/2)\rho V^2 Sb = -107903.209$ kgm^2/sec^2 $\Rightarrow$ $n_\zeta = -4.711$

D.3.1 Lateral motion characteristic equation.

$$\Delta(s) = s(s^4 + 3.753s^3 + 6.198s^2 + 12.188s + 0.132)=0$$

D.3.2 Roll subsidence mode.

$$(1 + sT_R) = 0$$

$$T_R = 0.33 \text{ sec}$$

$$s = -3.0 \text{sec}^{-1}$$

D.3.3 Spiral mode.

$$(1 + sT_S) = 0$$

$$T_S = 91.74 \text{ sec}$$

$$s = -0.0109 \text{sec}^{-1}$$

D.3.4 Dutch roll mode.

$$(s^2 + 2\rho_{dr}\omega_{dr}s + \omega_{dr}^2) = 0$$

$$\omega_{dr} = 2.0 \text{ rad/sec}$$

$$\rho_{dr} = 0.178$$

$$s = (-0.356 \pm 1.968i)$$

APPENDIX E

PREDICTION SUM OF SQUARES CRITERION.

E.0 PREDICTION SUM OF SQUARES CRITERION.

Consider the following linear regression model, which is of the form:

$$Y = Xb + \varepsilon \qquad [E.1]$$

where b is a vector of unknown parameters and ε is a random vector which is independent of X and has a zero mean and covariance $\sigma^2 I$. If the values of the estimates β are known, it is possible to predict future values of the random variable y, where y has mean xb and variance σ^2; note x is a row vector of matrix X containing the values of the independent variables associated with the future observation.

A predictor $\hat{y}$ will be considered as an optimal predictor if the expected value

$$E\{y - \hat{y}\}^2 \qquad [E.2]$$

has the minimum value, i.e. the residual sum of squares of the observed minus the predicted value is as small as possible. Equation [E.2] is known as the mean square prediction error (MSPE). It can be expressed as

$$MSPE = \sigma^2 + Var\{\hat{y}\} + [E\{\hat{y}\} - xb]^2 \qquad [E.3]$$

which means that

MSPE = Variance of the response
+ Variance of the prediction
+ Squared bias of the prediction

It may be shown that the addition of a variable to the prediction equation almost always increases (and never decreases) the variance of a predicted response. This means that for two models $\hat{y}_1 = x_1\beta_1$, and $\hat{y}_2 = x_2\beta_2$, where β_1 is an $n \times 1$ vector and β_2 is an $(n + 1) \times 1$ vector of estimated parameters

$$\text{Var}\{\hat{y}_2\} \geq \text{Var}\{\hat{y}_1\} \qquad [E.4]$$

From equations [E.3] and [E.4] it can be concluded that, for a model with a redundant number of parameters, the MSPE will increase from its minimal value because of the increase in $\text{Var}\{\hat{y}\}$. For the incomplete model, the MSPE will increase because of the bias error in prediction.

For the practical implementation of the MSPE as a measure for the selection of a parsimonious model, the prediction sum of squares (PRESS) criterion has the form

$$\text{PRESS} = \sum_{i=1}^{N} \{ y(i) - \hat{y}[i|x(1), \ldots, x(i-1), x(i+1), \ldots, x(N)] \}^2 \qquad [E.5]$$

which means that the PRESS uses (N - 1) data points for the estimation and one data point for the prediction. However, equation [E.5] is not in a very convenient format for computing the PRESS. A more efficient scheme is to use the expression

$$\text{PRESS} = \sum_{i=1}^{N} \frac{[y(i) - \hat{y}(i)]^2}{1 - \dfrac{\text{Var}\{y(i)\}}{\sigma^2}} \qquad [E.6]$$

where y(i) is now based on all the data points.

The second term in the denominator of equation [E.6] can be written as

$$\frac{\mathrm{Var}\{\hat{y}(i)\}}{\sigma^2} = x_i (X^T X)^{-1} x_i^T \qquad [E.7]$$

The behaviour of equation [E.7] with the increased number of data points can be examined from its limit as $N \to \infty$. This limit can be formulated as

$$\lim_{N\to\infty} \frac{\mathrm{Var}\{\hat{y}(i)\}}{\sigma^2} = \lim_{N\to\infty} x_i (X^T X)^{-1} x_i^T$$

$$= \lim_{N\to\infty} \frac{x_i}{N} \left(\frac{1}{N} X^T X \right)^{-1} x_i^T = 0 \qquad [E.8]$$

$$\text{if} \quad \lim_{N\to\infty} \left(\frac{1}{N} X^T X \right)^{-1} \quad \text{does exist.}$$

From equations [E.6] and [E.8] it is apparent that the PRESS approaches RSS for an increasing number of data points.

APPENDIX F

EXPERIMENTAL PATCH DIAGRAMS

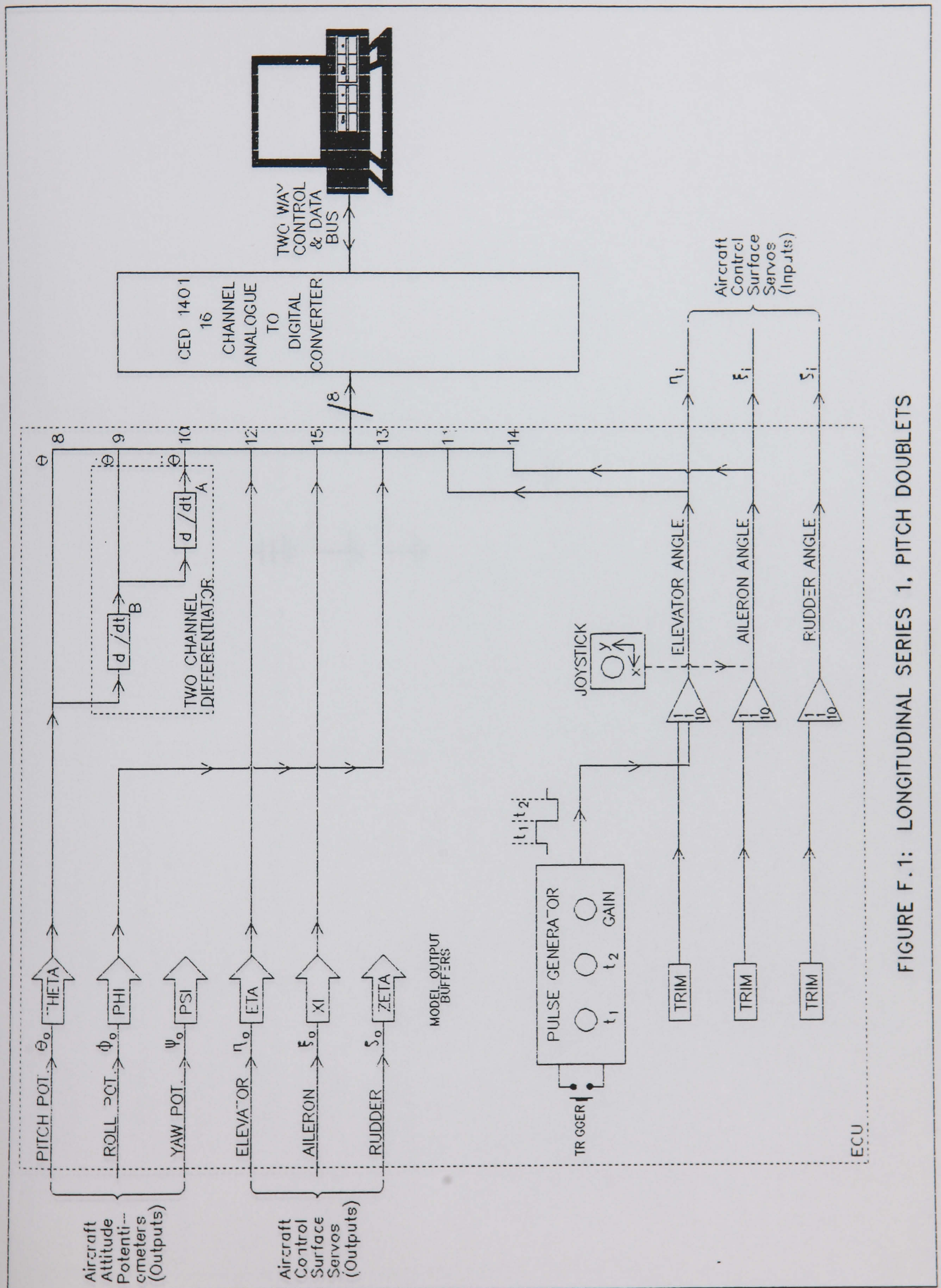

FIGURE F.1: LONGITUDINAL SERIES 1, PITCH DOUBLETS

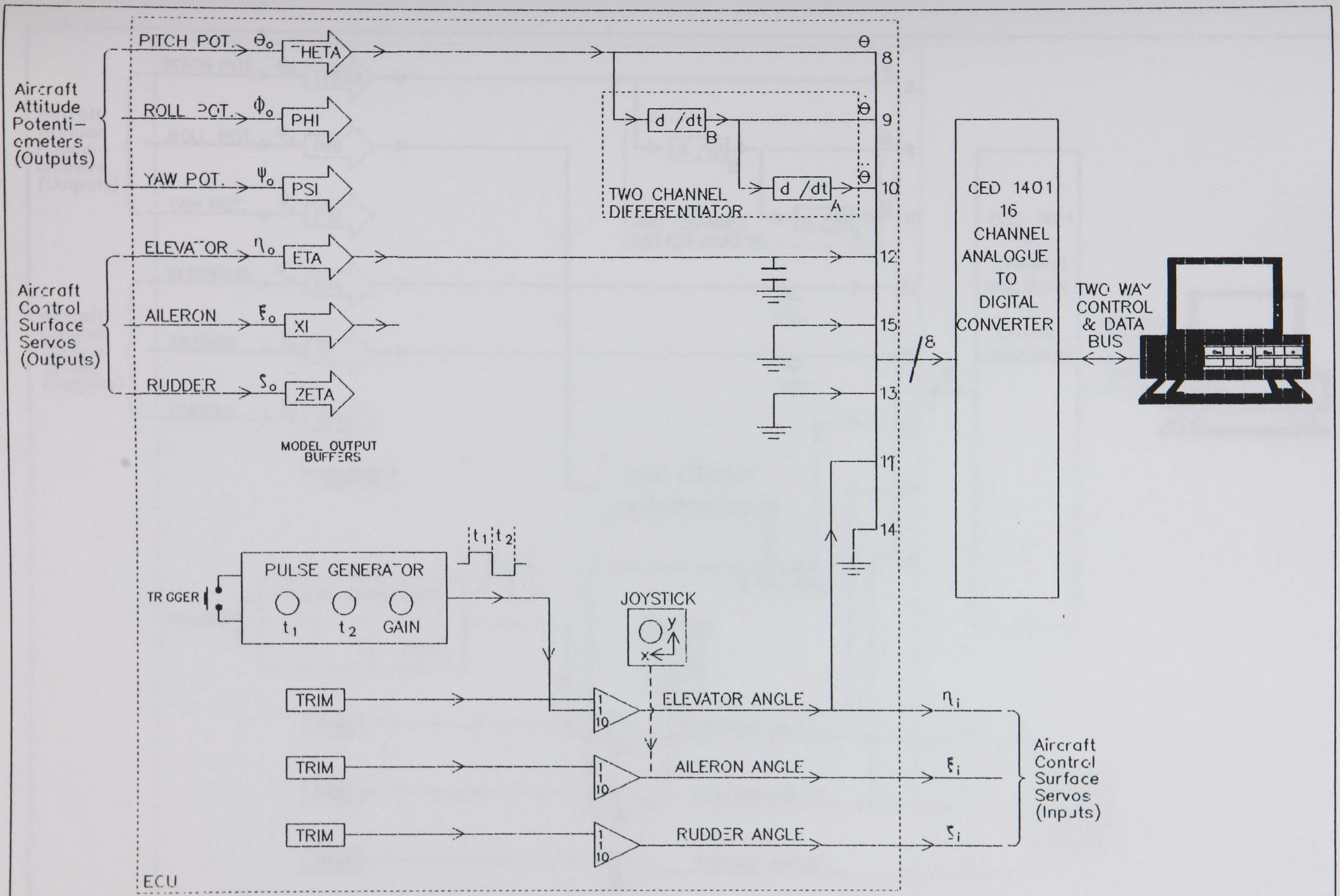

FIGURE F.2: LONGITUDINAL SERIES 2, PITCH DOUBLETS

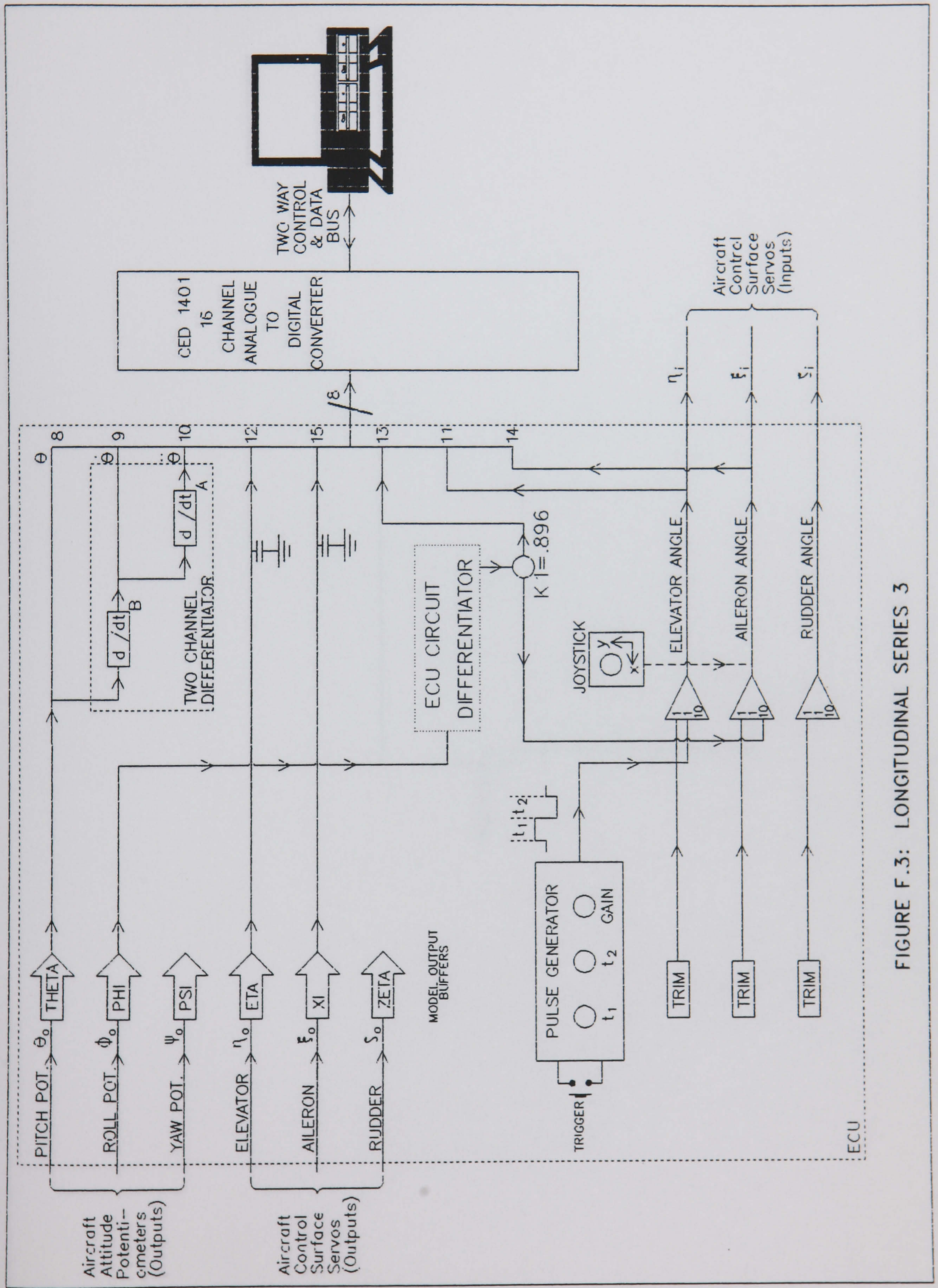

FIGURE F.3: LONGITUDINAL SERIES 3

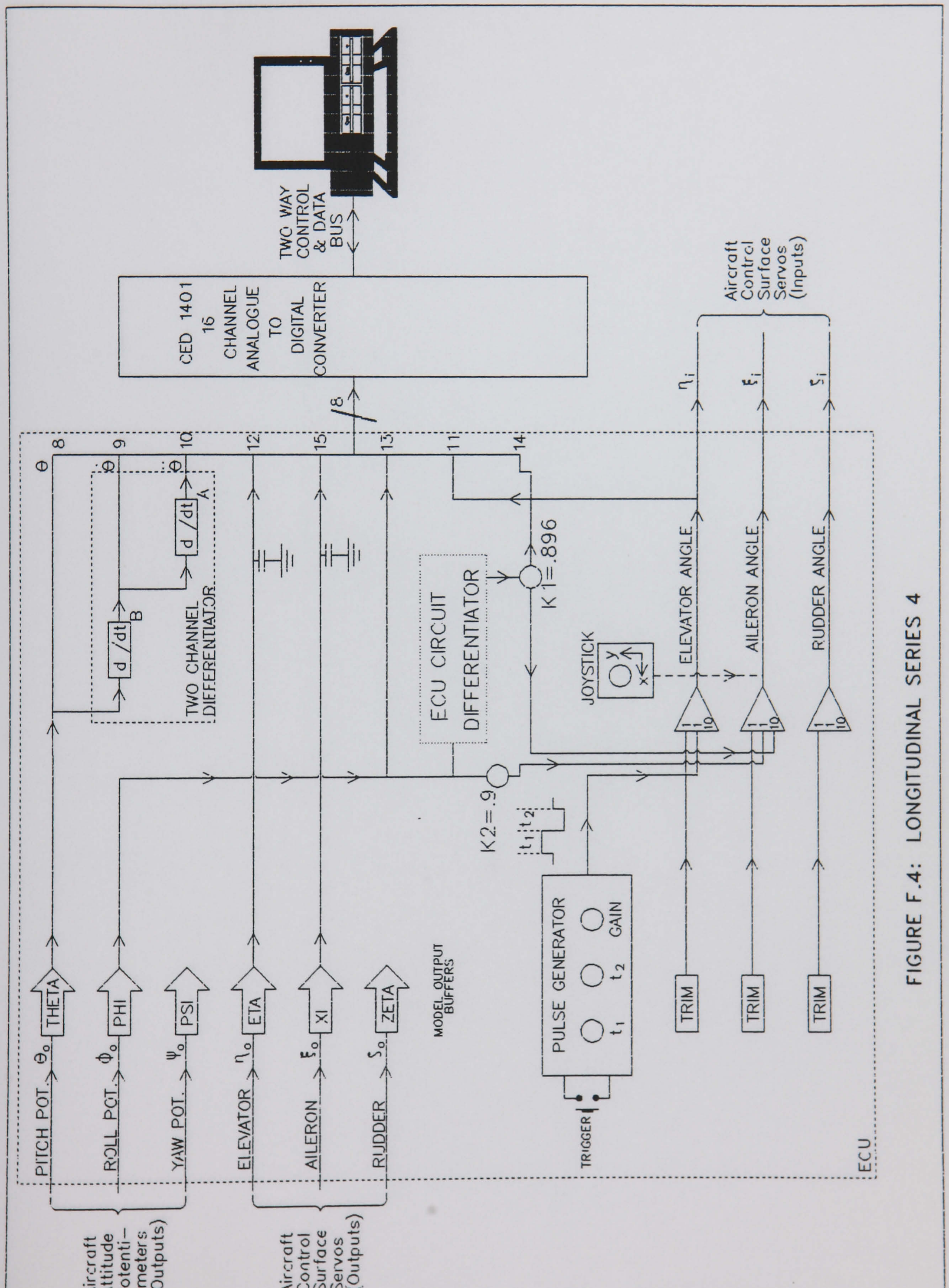

FIGURE F.4: LONGITUDINAL SERIES 4

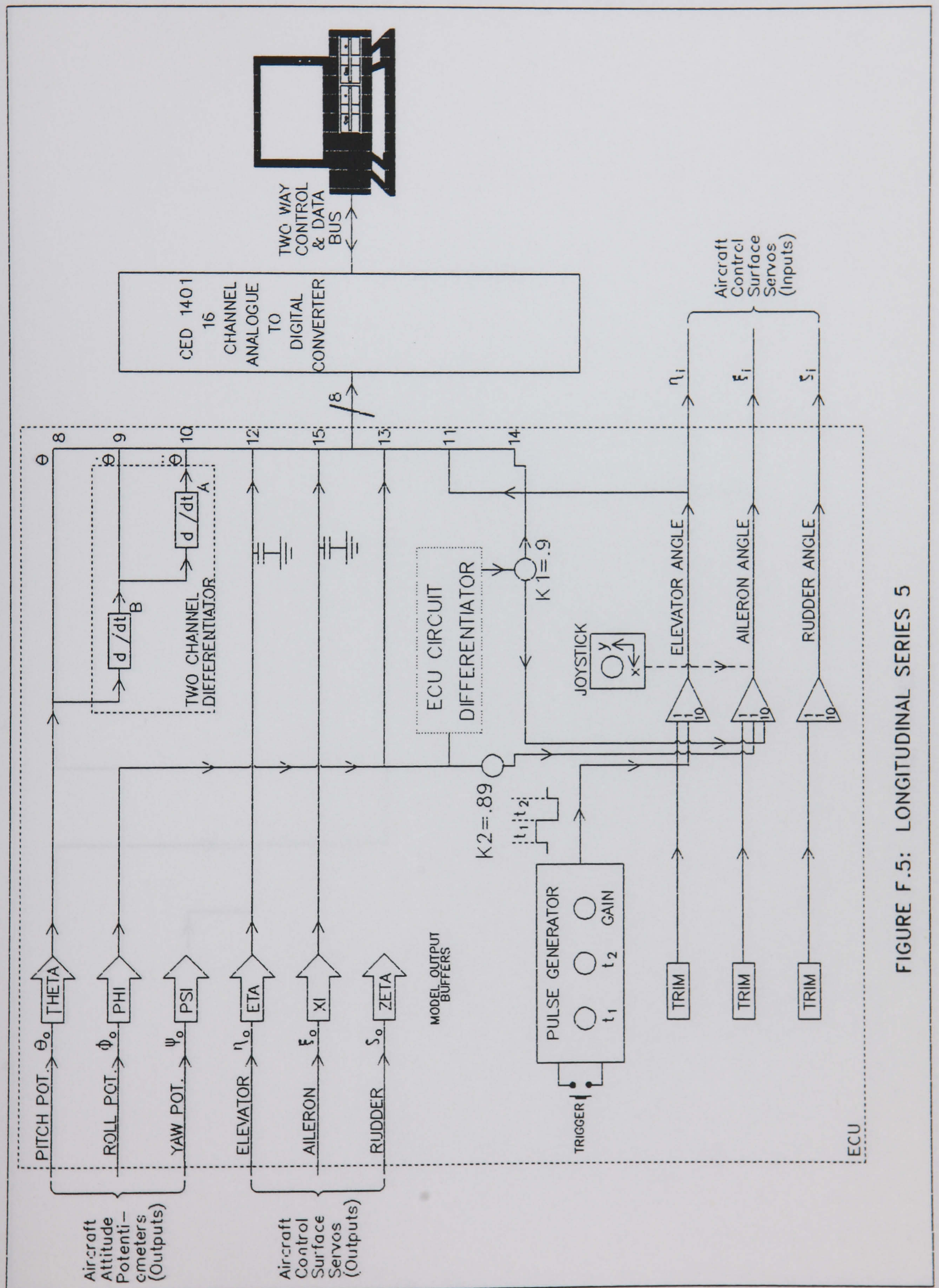

FIGURE F.5: LONGITUDINAL SERIES 5

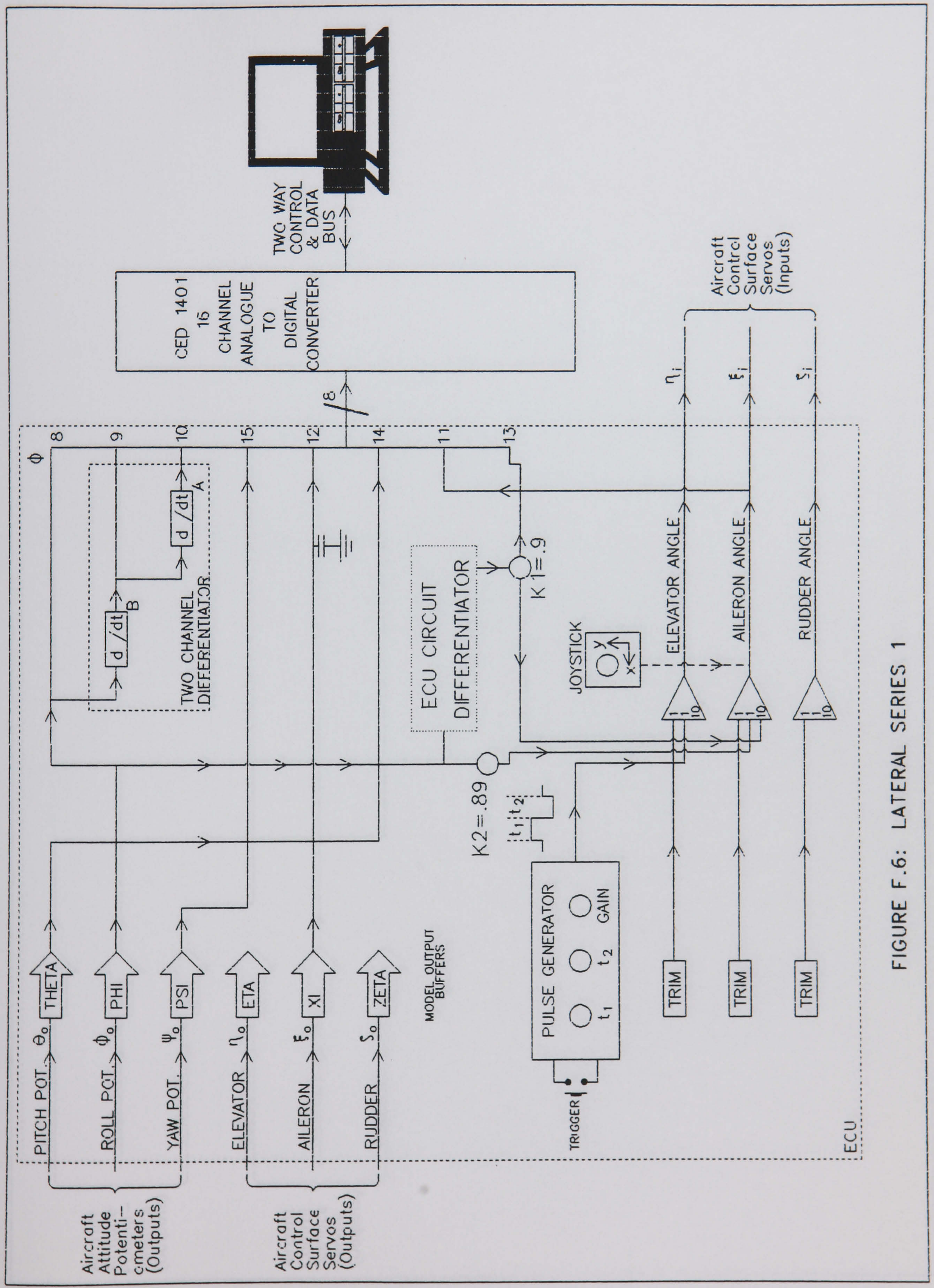

FIGURE F.6: LATERAL SERIES 1

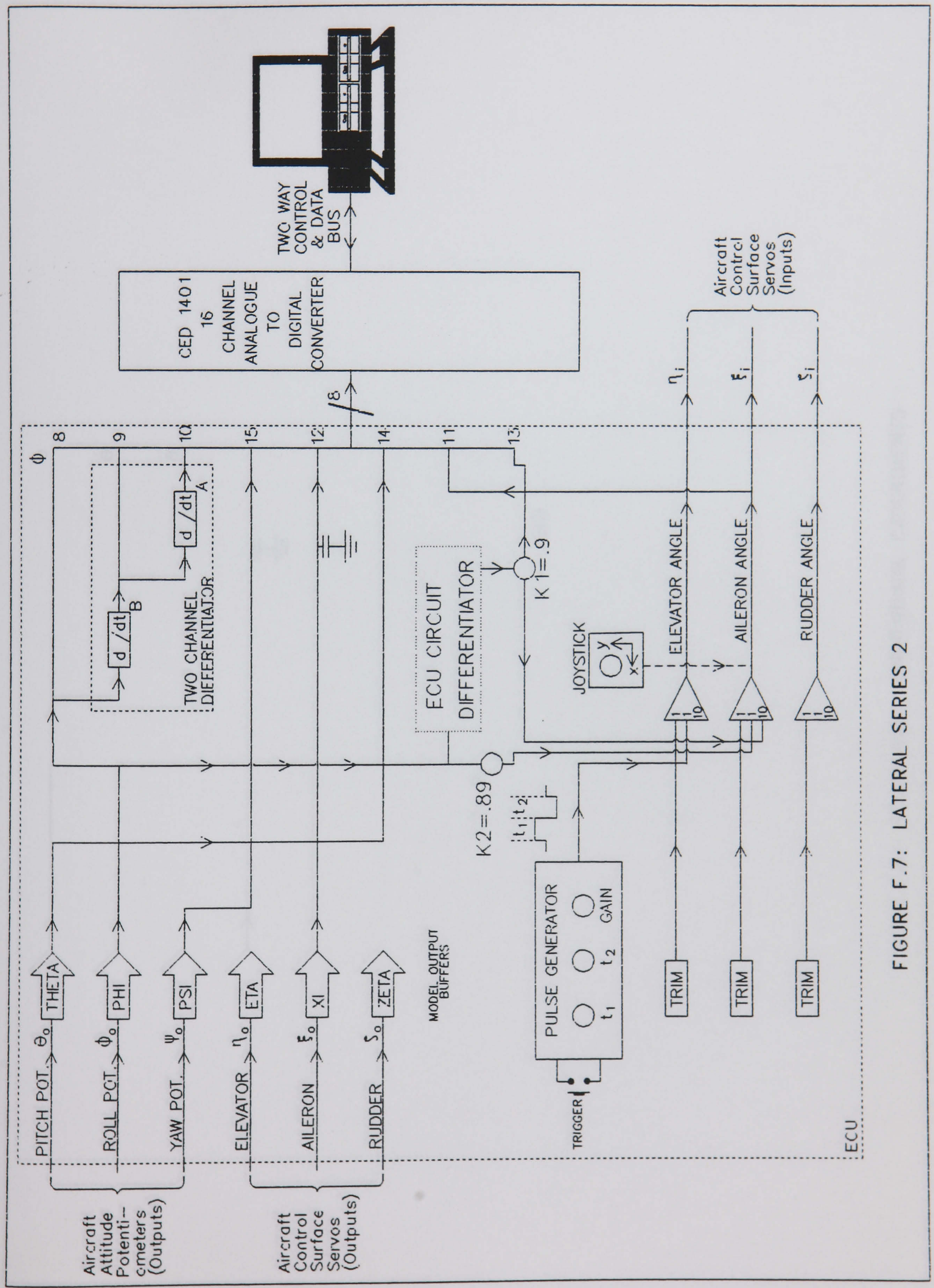

FIGURE F.7: LATERAL SERIES 2

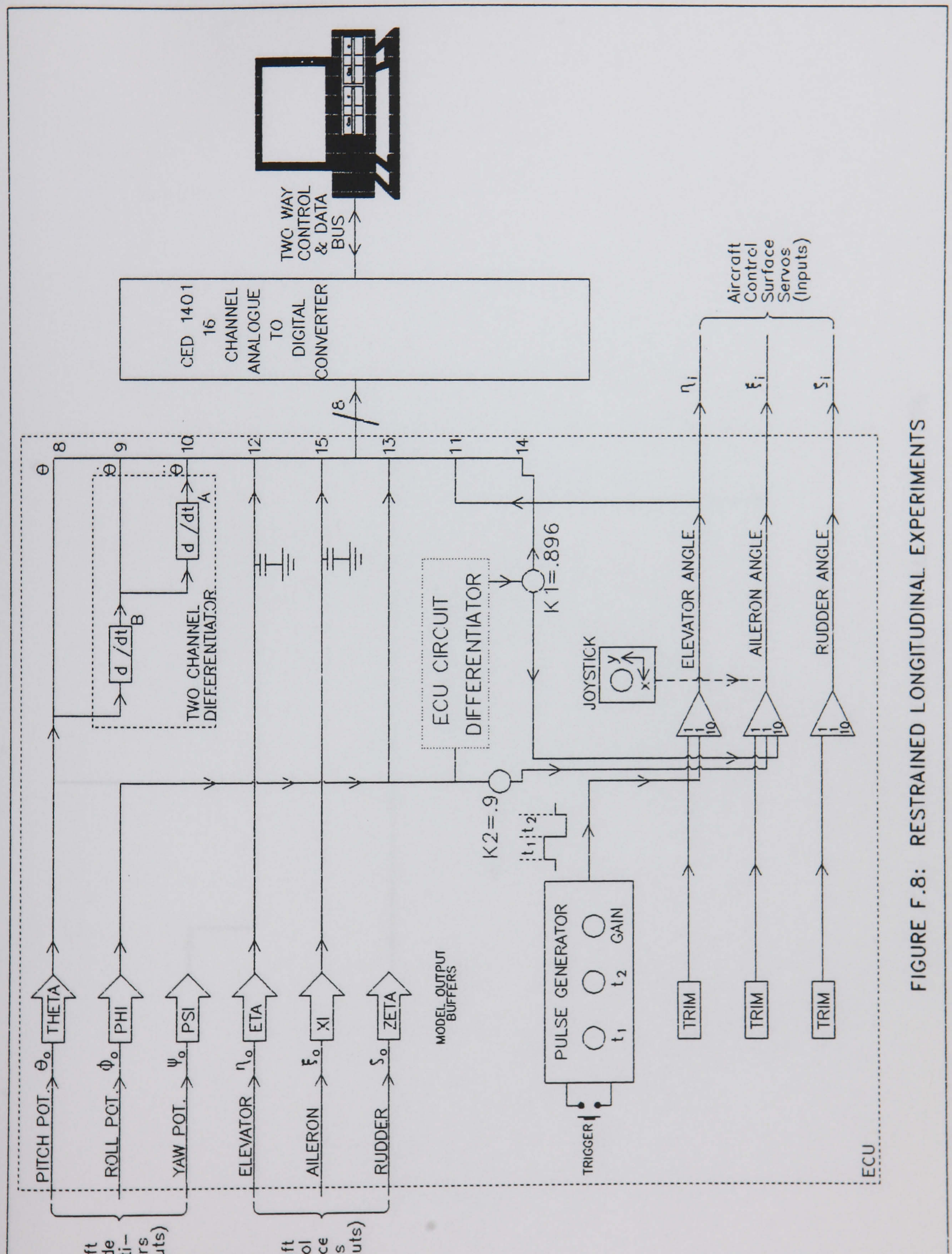

FIGURE F.8: RESTRAINED LONGITUDINAL EXPERIMENTS

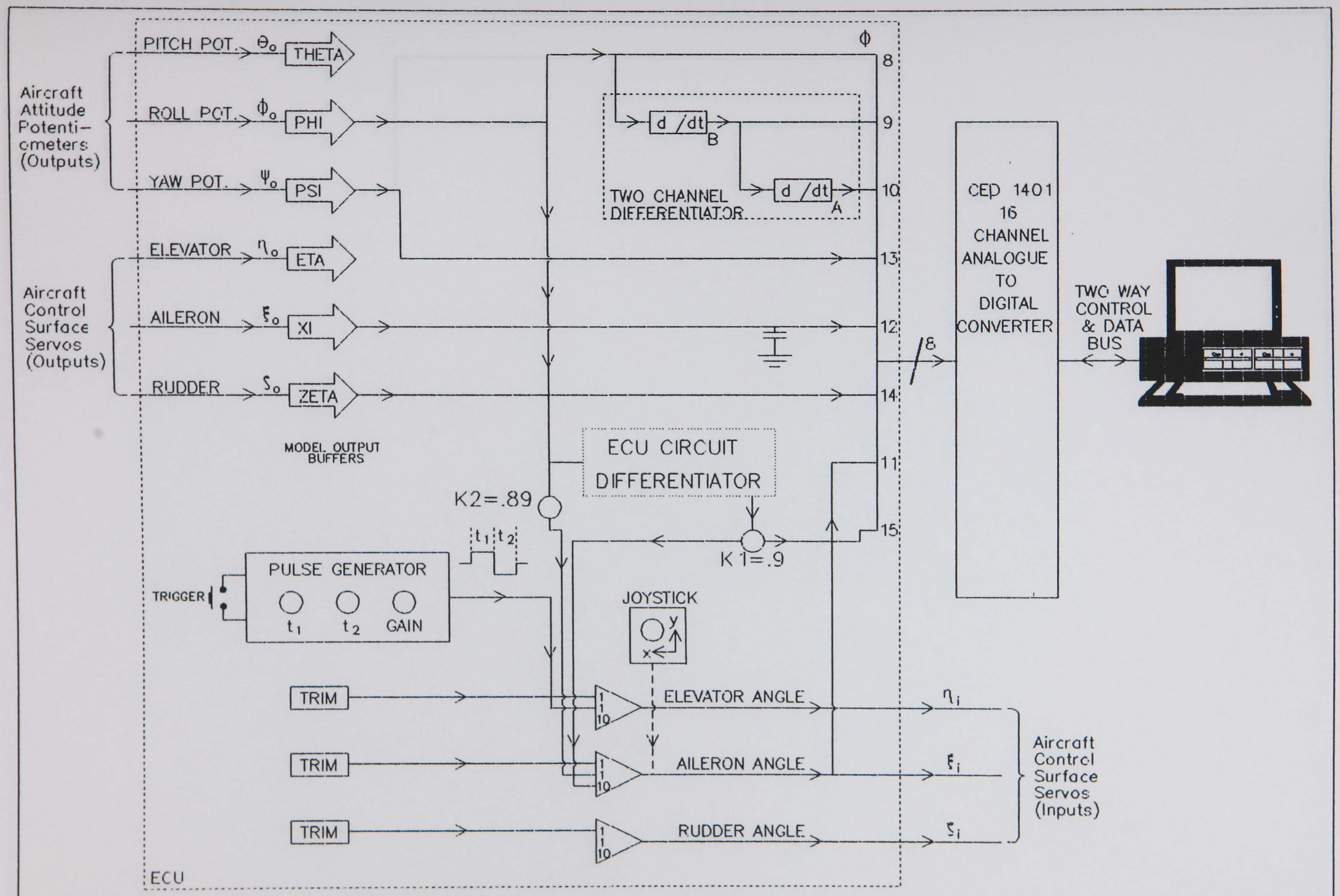

FIGURE F.9: RESTRAINED LATERAL (ROLL) EXPERIMENTS

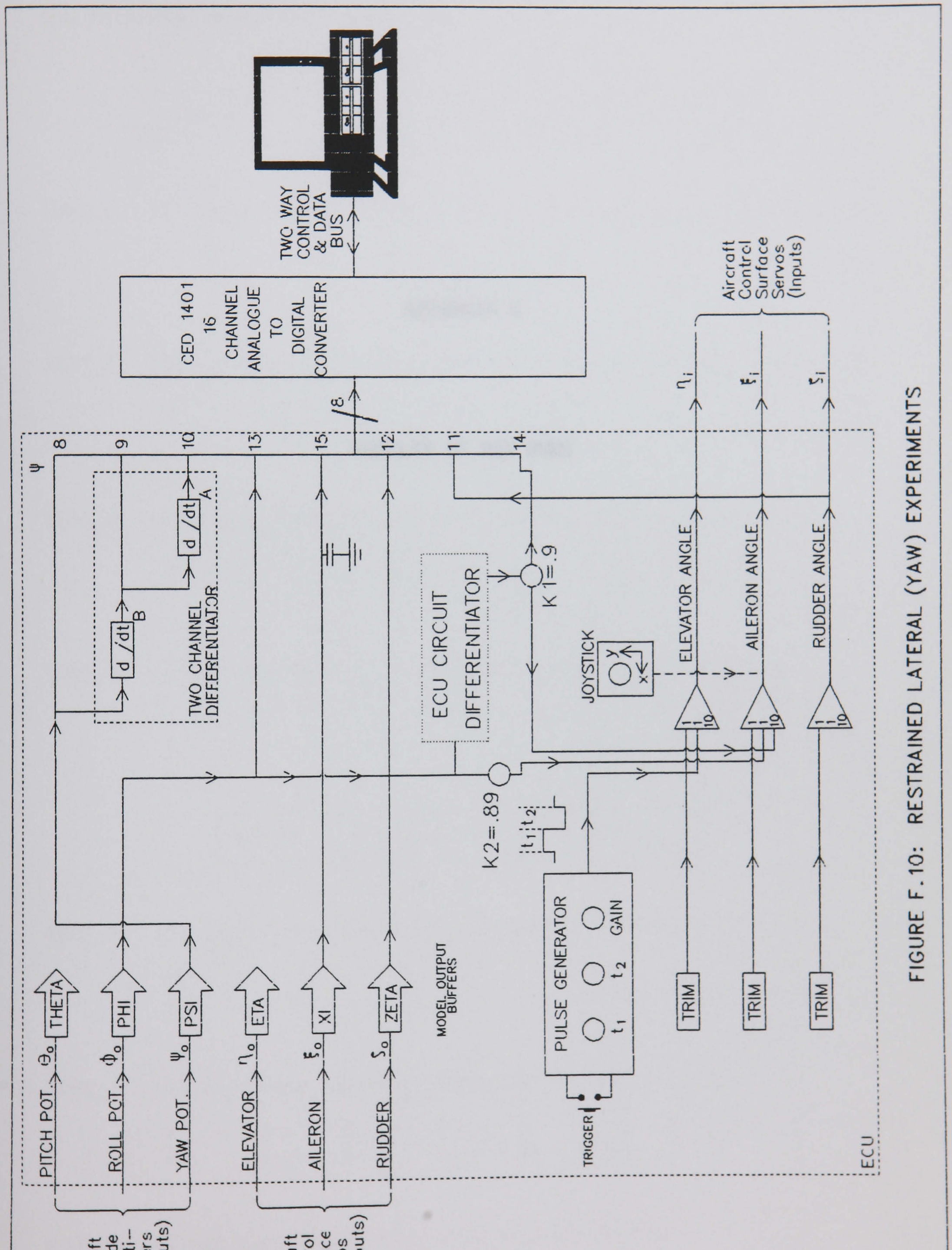

FIGURE F.10: RESTRAINED LATERAL (YAW) EXPERIMENTS

APPENDIX G

RESULTS OF MSR RUNS

This Appendix contains tables of results for MSR runs which used the following equations of motion:

EQN 1: $\dot{w} = \mathring{z}_w.w + (U_e + \mathring{z}_q).q + \mathring{z}_\eta.\eta + g.\sin\alpha_e.\theta$

EQN1_1: $(V_t\cos\alpha_e\dot{\theta}) = (g\sin\alpha_e)(\theta) + (\mathring{z}_w)(V_t\cos\alpha_e\theta) + (V_t\cos\alpha_e + \mathring{z}_q)(\dot{\theta}) + (\mathring{z}_\eta)(\eta)$

Y = B1.X1 + B2.X2 + B3.X3 + B4.X4

EQN1_2: $(\dot{\theta}) = ([g/V_t]\tan\alpha_e)(\theta) + (\mathring{z}_w)(\theta) + (1 + \mathring{z}_q/V_t\cos\alpha_e)(\dot{\theta}) + (\mathring{z}_\eta/V_t\cos\alpha_e)(\eta)$

Y = B1.X1 + B2.X2 + B3.X3 + B4.X4

EQN1_3: $(\dot{\theta}) = ([g/V_t]\tan\alpha_e + \mathring{z}_w)(\theta) + (1 + \mathring{z}_q/V_t\cos\alpha_e)(\dot{\theta}) + (\mathring{z}_\eta/V_t\cos\alpha_e)(\eta)$

Y = B1.X1 + B2.X2 + B3.X3

EQN1_4: $(0) = (g\sin\alpha_e)(\theta) + (\mathring{z}_w)(V_t\cos\alpha_e\theta) + (V_t\cos\alpha_e + \mathring{z}_q)(\dot{\theta}) + (\mathring{z}_\eta)(\eta)$

Y = B1.X1 + B2.X2 + B3.X3 + B4.X4

EQN 2: $\dot{q} = \mathring{m}_w.w + \mathring{m}_{\dot{w}}.\dot{w} + \mathring{m}_q.q + \mathring{m}_\eta.\eta$

EQN2_1: $(\ddot{\theta}) = (\mathring{m}_w)(V_t\cos\alpha_e\theta) + (\mathring{m}_{\dot{w}})(V_t\cos\alpha_e\dot{\theta}) + (\mathring{m}_q)(\dot{\theta}) + (\mathring{m}_\eta)(\eta)$

Y = B1.X1 + B2.X2 + B3.X3 + B4.X4

EQN2_2: $(\ddot{\theta}) = (\mathring{m}_w V_t\cos\alpha_e)(\theta) + (\mathring{m}_{\dot{w}} V_t\cos\alpha_e)(\dot{\theta}) + (\mathring{m}_q)(\dot{\theta}) + (\mathring{m}_\eta)(\eta)$

Y = B1.X1 + B2.X2 + B3.X3 + B4.X4

EQN2_3: $(\ddot{\theta}) = (\mathring{m}_w V_t\cos\alpha_e)(\theta) + (\mathring{m}_{\dot{w}} V_t\cos\alpha_e + \mathring{m}_q)(\dot{\theta}) + (\mathring{m}_\eta)(\eta)$

Y = B1.X1 + B2.X2 + B3.X3

E1_1.RS1

INITIAL MODEL VARIABLES: X1, X2, X3, X4

ITERATION 0

	PARAMETER:	STD. ERROR:	Fp TO REMOVE:	PARTIAL CORR.:
B0				= - 0.008867
B1 =	- 2.255	± 4.506	= 0.2504	
B2 =	0.06942	± 0.1388	= 0.2502	
B3 =	32.47	± 0.7865E-3	= 0.1704E10	
B4 =	0.002912	± 0.007259	= 0.1609	

RSS=0.452E-3; S^2=0.307E-5; F=0.5666E9; R^2=1.000; Reject X4; Add X0

ITERATION 1

	PARAMETER:	STD. ERROR:	Fp TO REMOVE:	PARTIAL CORR.:
B0 =	- 0.2654E-3	± 0.8107E-3	= 0.1072	
B1 =	- 2.236	± 4.578	= 0.2385	
B2 =	0.06883	± 0.1410	= 0.2382	
B3 =	32.47	± 0.8061E-3	= 0.1622E10	
B4				

RSS=0.467E-3; S^2=0.317E-3; F=0.5488E9; R^2=1.000; Reject X0; Add -

ITERATION 2

	PARAMETER:	STD. ERROR:	Fp TO REMOVE:	PARTIAL CORR.:
B0				
B1 =	- 2.246	± 4.514	= 0.2475	
B2 =	0.06918	± 0.1390	= 0.2476	
B3 =	32.47	± 0.7848E-3	= 0.1711E10	
B4				

RSS=0.457E-3; S^2=0.309E-5; F=0.8469E9; R^2=1.000; Reject X1; Add -

ITERATION 3

	PARAMETER:	STD. ERROR:	Fp TO REMOVE:	PARTIAL CORR.:
B0				
B1				
B2 =	0.5457E-5	± 0.3121E-4	= 0.03057	
B3 =	32.47	± 0.7739E-3	= 0.1760E10	
B4				

RSS=0.454E-3; S^2=0.304E-5; F=0.172E10; R^2=1.000; Reject X2; Add -

ITERATION 4 (CRASHED DUE TO ÷0 ERROR IN CALCULATION OF F)

	PARAMETER:	STD. ERROR:	Fp TO REMOVE:	PARTIAL CORR.:
B0				
B1				
B2				
B3 =	32.47	± 0.5783E-3		
B4				

RSS=0.454E-3; S^2=0.302E-5; F= R^2= Reject ; Add

E1_1.RS5

INITIAL MODEL VARIABLES: X1, X2, X4

ITERATION 0 (NORMAL END - ALL B(J)=0)

	PARAMETER:	STD. ERROR:	Fp TO REMOVE:	PARTIAL CORR.:
B0				
B1 =	0.2267E5	± 0.1518E5	= 2.232	
B2 =	- 697.1	± 467.4	= 2.224	
B3				
B4 =	- 26.05	± 24.54	= 1.127	

RSS=5238; S^2=35.39; F=-0.188; R^2=-0.0025; Reject - ; Add -

E1_2.RS1

INITIAL MODEL VARIABLES: X1, X2, X3, X4

ITERATION 0 (FLOATING POINT ERROR)

	PARAMETER:	STD. ERROR:	Fp TO REMOVE:	PARTIAL CORR.:
B0				=
B1 =		±	=	
B2 =		±	=	
B3 =		±	=	
B4 =		±	=	

RSS= S^2= F= R^2= Reject ; Add

E1_2.RS3

INITIAL MODEL VARIABLES: X0, X1, X4

ITERATION 0

	PARAMETER:	STD. ERROR:	Fp TO REMOVE:	PARTIAL CORR.:
B0 =	1.256	± 0.1598	= 61.79	
B1 =	- 1.117	± 0.4019	= 7.729	
B2				= - 0.0021
B3				= 1.000
B4 =	- 11.18	± 1.147	= 58.15	

RSS=3.559; S^2=0.0240 ; F=29.08; R^2=0.2821; Reject - ; Add X3

ITERATION 1 (CRASHED DUE TO TAKING SQUARE ROOT OF NEGATIVE NUMBER)

	PARAMETER:	STD. ERROR:	Fp TO REMOVE:	PARTIAL CORR.:
B0 =	0.39E-14	±	=	
B1 =	- 0.631E-15	±	=	
B2				=
B3 =	1.000	±	=	
B4 =	- 0.23E-13	±	=	

RSS=-0.46E-13; S^2=-0.27E-15; F= R^2= Reject - ; Add -

E1_3.RS1

INITIAL MODEL VARIABLES: X1, X2, X3

ITERATION 0 (CRASHED DUE TO ÷0 ERROR IN CALCULATION OF F)

	PARAMETER:	STD. ERROR:	Fp TO REMOVE:	PARTIAL CORR.:
B0				=
B1 =	- 0.1E-15	± (0)	=	
B2 =	1.000	± (0)	=	
B3 =	0.1E-14	± (0)	=	

RSS=-0.3E-14; S^2=-0.2E-16; F= R^2= Reject - ; Add -

E1_3.RS2

INITIAL MODEL VARIABLES: X0, X1, X3

ITERATION 0

	PARAMETER:	STD. ERROR:	Fp TO REMOVE:	PARTIAL CORR.:
B0 =	1.256	± 0.1598	= 61.79	
B1 =	- 1.167	± 0.4019	= 7.729	
B2				= 1.000
B3 =	- 11.18	± 0.4666	= 58.15	

RSS=3.559; S^2=0.02404; F=29.08; R^2=0.2821; Reject - ; Add X2

ITERATION 1 (CRASHED DUE TO ÷0 ERROR IN CALCULATION OF F)

	PARAMETER:	STD. ERROR:	Fp TO REMOVE:	PARTIAL CORR.:
B0 =	0.39E-14	± (0)	=	=
B1 =	- 0.63E-15	± (0)	=	=
B2 =	1.000	± (0)	=	=
B3 =	- 0.23E-13	± (0)	=	=

RSS=-0.4E-13; S^2=-0.3E-15; F= R^2= Reject - ; Add -

E1_4.RS1

INITIAL MODEL VARIABLES: X1, X2, X3, X4

ITERATION 0 (CRASHED DUE TO ÷0 IN CALCULATION OF F; S^2=0)

	PARAMETER:	STD. ERROR:	Fp TO REMOVE:	PARTIAL CORR.:
B0				=
B1 =	0.0	±	=	
B2 =	0.0	±	=	
B3 =	0.0	±	=	
B4 =	0.0	±	=	

RSS=0.0 S^2=0.0 F= R^2= Reject - ; Add -

E2_1.RS1

INITIAL MODEL VARIABLES: X1, X2, X3, X4

ITERATION 0

	PARAMETER:	STD. ERROR:	Fp TO REMOVE:	PARTIAL CORR.:
B0				= 0.8288
B1	= - 0.4477	± 0.06096	= 53.94	
B2	= 48.76	± 50.52	= 0.9314	
B3	= - 1582	± 1640	= 0.9297	
B4	= 30.79	± 4.455	= 47.75	

RSS=170.0; S^2=1.157; F=18.56; R^2=0.2747; Reject X3; Add X0

ITERATION 1

	PARAMETER:	STD. ERROR:	Fp TO REMOVE:	PARTIAL CORR.:
B0	= 13.26	± 0.7459	= 315.8	
B1	= - 1.088	± 0.04979	= 477.6	
B2	= - 0.05330	± 0.009927	= 28.82	
B3				= - 0.1521
B4	= - 81.08	± 6.787	= 142.7	

RSS=54.33; S^2=0.3696; F=162.4; R^2=0.7682; Reject - ; Add X3

ITERATION 2

	PARAMETER:	STD. ERROR:	Fp TO REMOVE:	PARTIAL CORR.:
B0	= 13.27	± 0.7398	= 321.6	
B1	= - 1.087	± 0.04938	= 484.5	
B2	= 52.63	± 28.33	= 3.453	
B3	= - 1711	± 919.6	= 3.460	
B4	= - 81.33	± 6.732	= 145.9	

RSS=53.08; S^2=0.3635; F=124.7; R^2=0.7760; Reject X3; Add -

ITERATION 3 (NORMAL END)

	PARAMETER:	STD. ERROR:	Fp TO REMOVE:	PARTIAL CORR.:
B0	= 13.26	± 0.7459	= 315.8	
B1	= - 1.088	± 0.04979	= 477.6	
B2	= - 0.05330	± 0.009927	= 28.82	
B3				
B4	= - 81.08	± 6.787	= 142.7	

RSS=54.33; S^2=0.3696; F=162.4; R^2=0.7682; Reject - ; Add -

E2_1.RS2

INITIAL MODEL VARIABLES: X0, X1, X2, X3, X4

ITERATION 0

	PARAMETER:	STD. ERROR:	Fp TO REMOVE:	PARTIAL CORR.:
B0 =	13.27	± 0.7398	= 321.6	
B1 =	- 1.087	± 0.04938	= 484.5	
B2 =	52.63	± 28.33	= 3.453	
B3 =	- 1711	± 919.6	= 3.460	
B4 =	- 81.33	± 6.732	= 145.9	

RSS=53.08; S^2=0.3635; F=124.7; R^2=0.7760; Reject X2; Add -

ITERATION 1

	PARAMETER:	STD. ERROR:	Fp TO REMOVE:	PARTIAL CORR.:
B0 =	13.26	± 0.7459	= 315.9	
B1 =	- 1.088	± 0.04979	= 477.6	
B2				= 0.1520
B3 =	- 1.731	± 0.3223	= 28.83	
B4 =	- 81.09	± 6.787	= 142.8	

RSS=54.33; S^2=0.3696; F=162.4; R^2=0.7682; Reject - ; Add X2

ITERATION 2

	PARAMETER:	STD. ERROR:	Fp TO REMOVE:	PARTIAL CORR.:
B0 =	13.27	± 0.7398	= 321.6	
B1 =	- 1.087	± 0.04938	= 484.5	
B2 =	52.63	± 28.33	= 3.453	
B3 =	- 1711	± 919.6	= 3.460	
B4 =	- 81.33	± 6.732	= 145.9	

RSS=53.08; S^2=0.3635; F=124.7; R^2=0.7760; Reject X2; Add -

ITERATION 3 (NORMAL END)

	PARAMETER:	STD. ERROR:	Fp TO REMOVE:	PARTIAL CORR.:
B0 =	13.26	± 0.7459	= 315.9	
B1 =	- 1.088	± 0.04979	= 477.6	
B2				
B3 =	- 1.731	± 0.3223	= 28.83	
B4 =	-81.09	± 6.787	= 142.8	

RSS=54.33; S^2=0.3696; F=162.4; R^2=0.7682; Reject - ; Add -

E2_1.RS3

INITIAL MODEL VARIABLES: X2, X3

ITERATION 0

	PARAMETER:	STD. ERROR:	Fp TO REMOVE:	PARTIAL CORR.:
B0 =				
B1 =				
B2 =	54.41	± 58.63	= 0.99228	
B3 =	- 1896	± 1904	= 0.99196	
B4 =				

RSS=232.4; S^2=1.5599; F=1.256; R^2=0.0084; Reject ; Add

E2_2.RS1

INITIAL MODEL VARIABLES: X1, X2, X3, X4

ITERATION 0 (CRASHED IN MINV, I.E. WHEN INVERTING MATRIX)

PARAMETER:	STD. ERROR:	Fp TO REMOVE:	PARTIAL CORR.:
B0			
B1 =	±	=	
B2 =	±	=	
B3 =	±	=	
B4 =	±	=	

RSS= S^2= F= R^2= Reject ; Add

E2_2.RS3

INITIAL MODEL VARIABLES: X1, X2, X4

ITERATION 0

	PARAMETER:	STD. ERROR:	Fp TO REMOVE:	PARTIAL CORR.:
B0				= 0.8255
B1 =	- 14.59	± 1.978	= 54.38	
B2 =	1.379	± 0.4787	= 8.295	
B3				= 0.4914
B4 =	30.93	± 4.452	= 48.26	

RSS=171.1; S^2=1.156; F=27.38; R^2=0.2701; Reject - ; Add X0

ITERATION 1

	PARAMETER:	STD. ERROR:	Fp TO REMOVE:	PARTIAL CORR.:
B0 =	13.26	± 0.7460	= 315.8	
B1 =	- 35.32	± 1.617	= 477.5	
B2 =	- 1.730	± 0.3233	= 28.80	
B3				= - 0.002678
B4 =	- 81.08	± 6.787	= 142.7	

RSS=54.34; S^2=0.3697; F=162.3; R^2=0.7681 Reject - ; Add X3

ITERATION 2 (CRASHED DUE TO PROBLEM IN INVERTING MATRIX)

	PARAMETER:	STD. ERROR:	Fp TO REMOVE:	PARTIAL CORR.:
B0 =		±	=	=
B1 =		±	=	=
B2 =		±	=	=
B3 =		±	=	=
B4 =		±	=	=

RSS= S^2= F= R^2= Reject ; Add

E2_3.RS1

INITIAL MODEL VARIABLES: X1, X2, X3

ITERATION 0

	PARAMETER:	STD. ERROR:	Fp TO REMOVE:	PARTIAL CORR.:
B0				= 0.8255
B1	= - 14.59	± 1.978	= 54.38	
B2	= 1.379	± 0.4787	= 8.295	
B3	= 30.93	± 4.452	= 48.26	

RSS=171.1; S^2=1.156; F=27.38; R^2=0.2701; Reject - ; Add X0

ITERATION 1 (NORMAL END, NOTHING TO ADD OR REJECT)

	PARAMETER:	STD. ERROR:	Fp TO REMOVE:	PARTIAL CORR.:
B0	= 13.26	± 0.7460	= 315.8	
B1	= - 35.32	± 1.617	= 477.5	
B2	= - 1.730	± 0.3223	= 28.80	
B3	= - 81.08	± 6.787	= 142.7	

RSS=54.34; S^2=0.3697; F=162.3; R^2=0.7681; Reject - ; Add X0